Mechanistic Insights into the Substrate-Mediated Regulation of p300 Autoacetylation: Implications in Tumor Suppressor/Oncogene functions

A thesis submitted for the degree of

Doctor of Philosophy

By

Stephanie Kaypee

To

Molecular Biology and Genetics Unit,

Jawaharlal Nehru Centre for Advanced Scientific Research

(A Deemed University)

Jakkur P.O., Bangalore-560064, INDIA.

JUNE 2017

Table of Contents

Chapter 1

Introduction

This chapter introduces the basic concepts of epigenetics, chromatin dynamics, and histone post-translational modification. The chapter includes a brief review on lysine acetylation and the chromatin modifying enzymes that regulate this dynamic covalent modification. The focus of the chapter will be on a specific lysine acetyltransferase, p300 (KAT3B), which is an indispensible factor in transcription and maintenance of cellular homeostasis. The chapter will give a comprehensible account of the history, evolution, functions, and regulation of this critical epigenetic enzyme.

1.1. Chromatin Dynamics

The vast eukaryotic genome is present within the confines of the nuclei as a compact nucleoprotein complex known as chromatin. Chromatin is fundamentally made up of repeating nucleosomal units which consists of 147 base pairs of DNA double helix wrapped around an octameric core of histone proteins (H3-H4 tetramer and two H2A-H2B dimers) (Luger et al., 1997). In the presence of linker histone H1, the string of nucleosomes can further fold to form higher ordered structures. In 1942, the term 'epigenetics' was coined by Conrad Waddington which described how the interaction between gene expression and the external environment could modulate cellular phenotype, a phenomenon which was not dictated by genetics alone (Waddington, 1942). Even though the term was coined in the development perspective, the understanding of epigenetics has evolved over the years to encompass several biological events. Epigenetics is defined as a heritable alteration in the gene expression or phenotype without any change in the underlying DNA sequences. In a broad sense, epigenetics is the link between the genotype and the exhibited phenotype (Goldberg et al., 2007). The molecular machinery of epigenetics incorporates several factors which modulate chromatin structural dynamicity and gene expression.

Chromatin architecture is maintained by histone, chromatin-associated proteins and non-coding RNA; and the chromatin dynamics is essential to allow the underlying DNA template to be accessed for important nuclear processes, for example, DNA replication, transcription, and DNA damage repair. Chromatin dynamicity is modulated by the concerted effort of a myriad of factors which include DNA methylation, post-translational modification of histone

and chromatin-associated proteins, chromatin remodelers and histone chaperones, incorporation of histone variants, non-histone chromatin protein complexes, and non-coding RNAs (Dulac, 2010) (Figure 1.1). The spatial organization of chromatin in the nucleus is a highly dynamic, permitting large-scale functional chromatin interactions which have been proved by chromatin conformation capture experiments (Carty et al., 2017; de Wit and de Laat, 2012). The spatial looping of chromatin results in the formation of functional compartmentalization (Nora et al., 2017). This allows for the establishment of transcription factories and repair centres, optimizing the nuclear resources for efficient responses to external and internal cues (Kulashreshtha et al., 2016; Mitchell and Fraser, 2008).

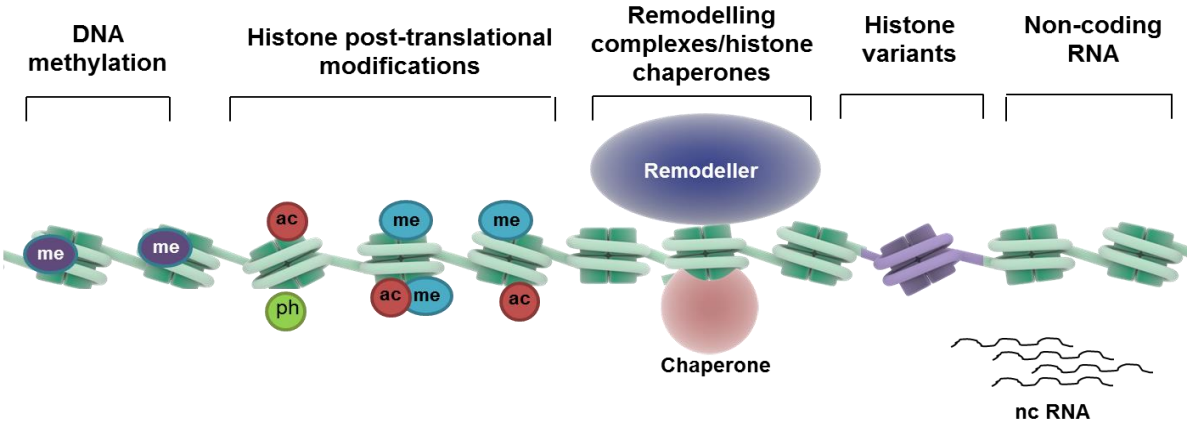

Figure 1.1: Factors regulating Chromatin Dynamics. Diagrammatic representation of factors modulating chromatin accessibility. Adapted from Dulac C, *Nature*, 2010 (Dulac, 2010).

1.2. Histone Post-Translational Modifications

At the nucleosomal level, the degree of wrapping of DNA around the histone octamer is determined by the electrostatic interaction of the negatively charged phosphate backbone of DNA with the protruding basic amino-terminal tail of histone proteins. This interaction is modulated by the multitude of post-translational modifications that the histone proteins undergo.

Internal and external signaling pathways are integrated into cellular responses via the modulation of differential gene expression. The extensive repertoire of post translational modifications (PTMs) on histone and non-histone proteins couples various stimuli to differential gene expression. These modifications often dictate important cellular events such as gene expression, replication, cell cycle, DNA damage response, cell signaling pathways, and metabolism. PTMs such as phosphorylation, N-terminal acetylation, lysine acetylation, methylation, SUMOylation, ubiquitination, propionylation, butyrylation, crotonylation,

carbonylation, neddylation, proline isomerization, and ADP ribosylation regulate the diverse protein functions (Kouzarides, 2007; Lee et al., 2010b).

Histone post translational modifications function by altering the accessibility of chromatin to different non-histone chromatin proteins. These proteins "read" the epigenetic language encoded by the combination of various histone marks and result in certain structural changes within chromatin, culminating in the regulation of important cellular processes. Histone modifications can be repressive which cause compaction of chromatin by recruiting repressive protein complexes. These marks are present on promoters of silenced or repressed genes. For example, on histone H3, the trimethylation of lysine 9 (H3K9me3) and lysine 27 (H3K27me3) are repressive marks known to be present on transcriptionally inactive genes. In contrast, active marks H3K4me3, acetylation of H3K9 and H3K27 are present on the promoters of transcriptionally active genes (Kouzarides, 2007). In embryonic stem cell, region of bivalent marks i.e. both active and repressive marks, function as signatures of poised transcription, which are observed at promoters of certain developmentally important genes (Bernstein et al., 2006). Histone PTMs are interdependent and influence each other either positively or negatively depending on the context in which they are present. This cross-talk is made possible by the interaction of effector protein or protein complexes with these PTMs through their specialized domains like bromodomain for acetylated lysine and chromodomain for methylated lysine and ubiquitin-binding domain (UBD) for ubiquitinated lysines to name a few (Arif et al., 2010a).

1.3. Lysine acetylation

Lysine acetylation is the transfer of an acetyl moeity from Acetyl Coenzyme A (acetyl-CoA) onto the ε-Nitrogen on a lysine residue (Figure 1.2A,B). It was first described as a covalent modification associated with active transcription (Allfrey et al., 1964). Further studies proposed that the lysine acetylation can neutralize the positive charge on the lysine residues. Thus, when present on histone tails, lysine acetylation can weaken the interaction between the positively charged histone tails and the negatively charged phosphodiester backbone of DNA, resulting in the loosening of chromatin. This in turn facilitates the access of protein machineries involved in replication, transcription or DNA repair, onto the DNA template (Capell and Berger, 2013; Unnikrishnan et al., 2010; Vo and Goodman, 2001). Lysine acetylation is essential for the maintenance of cellular homeostasis and is associated with chromatin architecture (Shogren-Knaak et al., 2006), DNA repair (Chatterjee et al., 2012), protein stability and protein-protein interaction (Kouzarides, 2007). It has emerged as the

ubiquitous post-translational modification that is found across the every compartment of the cell (Choudhary et al., 2009; Zhao et al., 2010). Choudhary *et al*. have reported around 3600 acetylation sites on over 1750 proteins in the first global acetylome study (Choudhary et al., 2009). Currently, over 35,000 acetylation sites exist in human cells, as shown in public repositories such as PhosphoSitePlus database, which is almost comparable to the abundance of protein phosphorylation (Hornbeck et al., 2012).

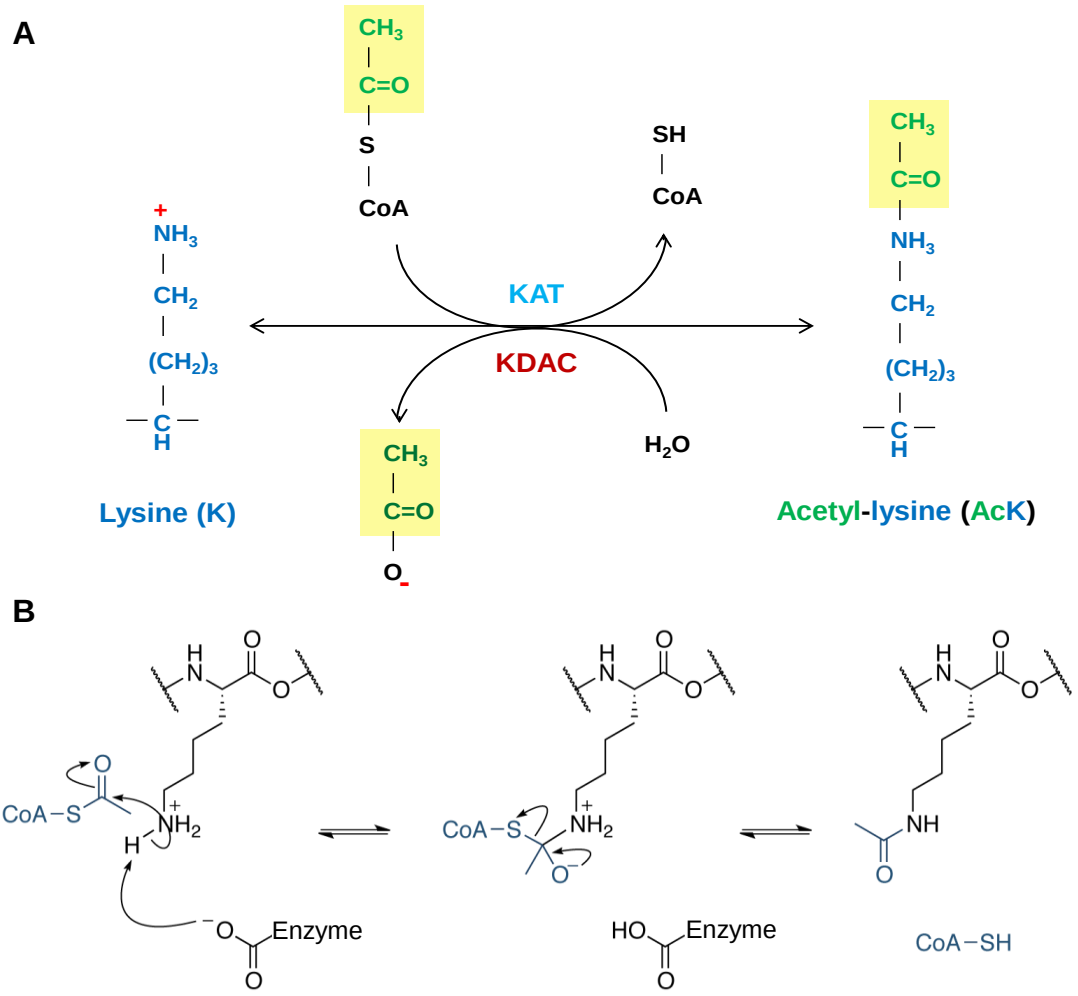

Figure 1.2: Lysine acetylation. (A) Lysine acetylation is the transfer of an acetyl moiety from Acetyl Coenzyme A (acetyl-CoA) to the ε-Nitrogen on the lysine residue. The forward reaction is catalyzed by Lysine Acetyltransferases (KAT) and the reverse reaction is catalyzed by lysine deacetylases (KDAC). (B) Detailed mechanism of the forward reaction of lysine acetylation.

1.4. The 'Writers', 'Readers' and 'Erasers' of Lysine Acetylation

Lysine acetylation is a highly dynamic, covalent modification which is reversibly modulated by lysine acetyltransferases (KATs) which are the 'writers' and lysine deacetylases (KDACs), the 'erasers' of lysine acetylation. The lysine acetylation 'code' is read by specialized group of proteins known as 'readers' which specifically recognize the acetylated lysine moiety and help relay downstream signaling pathways (Figure 1.3).

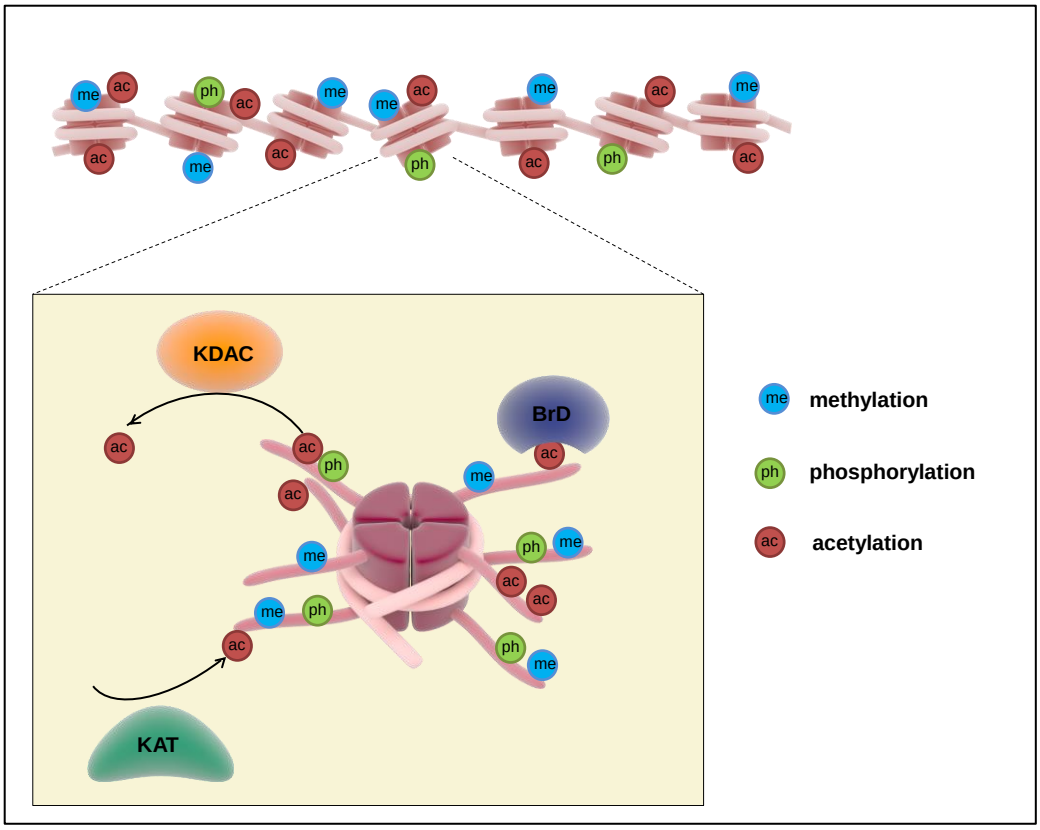

Figure 1.3: Dynamics of lysine acetylation. The dynamics of acetylation is modulated by the writers, lysine acetyltransferases (KATs), the 'erasers', lysine deacetylases (KDACs), and the 'readers' by specialized protein domains such as bromodomains (BrD) which can specifically bind to acetyl-lysine residues. Adapted from Kaypee *et al*, *Pharmacol Ther.,* 2016 (Kaypee et al., 2016).

Intrinsic lysine acetyltransferase activity has been identified in several proteins. The KATs are mainly classified into two groups based on (i) their subcellular localization and (ii) their ability to acetylate chromatinized histones. Type-A KATs consists of the nuclear KATs which can acetylate histones incorporated into chromatin. The major families are GNAT (GCN5-related N-acetylatransferase) family, p300/CBP (KAT3) family and MYST (MOZ, Ybf2, Sas2, and TIP60) family, and Transcription Factor-related KATs and KATs that cannot be classified into any specific family are grouped together (Figure 1.4). Type-B KATs are predominantly located in the cytoplasm and catalyze the acetylation on H4K5 and -K12 of

nascent histones before they are transported to the nucleus and assembled into the chromatin. HAT1 is the catalytic subunit of the Type-B KAT complex (Parthun et al., 1996). Studies in yeast have shown that the HAT1 complex is involved in nuclear functions such as telomeric silencing, mismatch repair (Kelly et al., 2000). Another cytoplasmic KAT, HAT4, has be shown to acetylate free H4 including the globular lysine sites, H4K79ac and H4K91ac (Yang et al., 2011). Type-B HATs share homology with general control non-derepressible 5 (Gcn5) and belong to the GNAT superfamily (Dutnall et al., 1998; Yang et al., 2011). In contrast to the HAT1 complex, which cannot acetylate histones assembled into chromatin, the Type-A KATs are nuclear acetyltransferases which are capable of acetylating chromatinized histones (Brownell and Allis, 1996). In the recent years, three new proteins were added to the growing list of lysine acetyltransferases: Camello, which was identified as an unrelated KAT protein essential for *Danio rario* development (Karmodiya et al., 2014), the bromodomain protein 4 (BRD4), an epigenetic reader protein which was identified as a lysine acetyltransferase required for histone eviction (Devaiah et al., 2016), and hnRNPA2, a mitochomdrial protein, recently discovered as a KAT which bears structural resemblance to p300/CBP family of KATs (Guha et al., 2016).

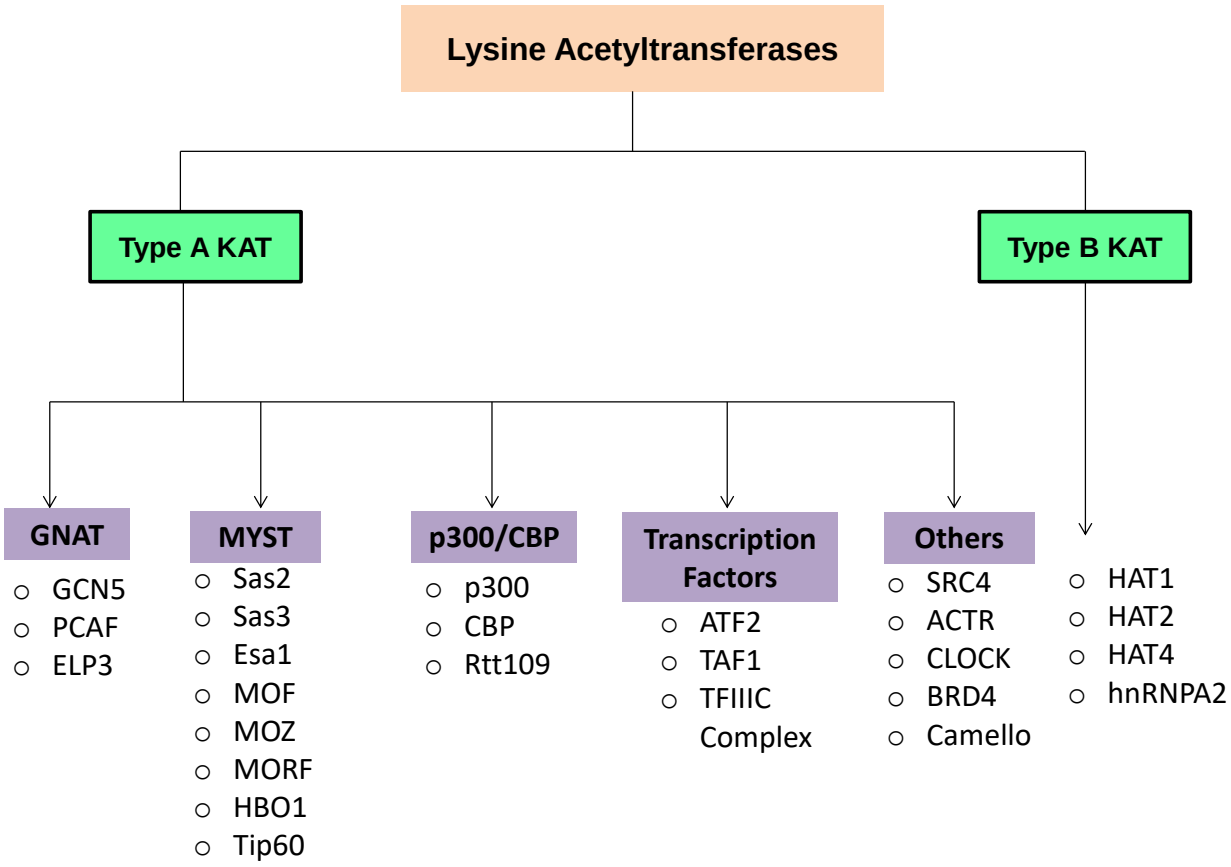

Figure 1.4: Classification of Lysine acetyltransferases. Lysine acetyltransferases (KATs) belong to two broad groups Type A and B, depending on their predominant subcellular localization. The nuclear KATs are further classified into four major families based on their structural homology, namely, GNAT, MYST, p300/CBP and Transcription factors related KAT family. Nuclear KATs that do not share homology with any of the aforementioned families are classified under 'Others'.

Proteins that can bind to acetylated lysine contain one or more of the following specialized domains: (i) bromodomains (BrD), (ii) tandem plant homeodomain (PHD) and (iii) the YEATS domain (Dhalluin et al., 1999; Li et al., 2014; Zeng et al., 2010). The bromodomain consists of an evolutionally conserved structural fold, 'BrD fold', comprising of a left-handed four-helix bundle motif that specifically recognize ε-N- lysine acetylation modification of proteins (Dhalluin et al., 1999). The tandem PHD domain has of two typical PHD fold placed in tandem, each of which consists of two-strand anti-parallel β-sheet and an α-helix stabilized by two zinc atoms (Zeng et al., 2010). The YEATS domain of AF9 protein is known to specifically recognize the H3K9 acetylation. The domain consists of an eight-strand immunoglobin fold consisting of a serine-lined aromatic cage which recognizes acetyl lysine (Li et al., 2014). The acetyl-lysine moiety on proteins serve as docking sites for proteins

possessing these ‘reader’ domains, which recognize specific acetylation codes resulting in downstream readouts.

Lysine deacetylases are classified broadly as the classical KDACs consisting of Class I which are homologs of yeast Rpd3 (HDAC 1,2,3 and 8), Class II which are homologs of yeast Hda1 (HDAC 4,5,6,7,9,10) and Class IV (HDAC 11), and NAD+ -dependent Class III HDACs or Sirtuins which resemble yeast Sir2. KDACs have been implicated in many diseases and they play an active role in the progression of cancer. KDAC inhibitors have shown efficacy in cancer treatment. Vorinostat (suberanilohydroxamic acid or SAHA) was approved by the U S Food and Drug Administration (FDA) in 2006 (Richon et al., 1998) and romidepsin was licensed by the FDA in 2009 for cutaneous T-cell lymphoma (CTCL) (Nakajima et al., 1998). Chidamide approved by China in 2015 for peripheral T-cell lymphoma (PTCL) (Liu et al., 2010). Panobinostat was licensed by FDA in 2015 for the treatment of multiple myeloma (George et al., 2005). Belinostat (PXD101) was approved in 2014 for the use against peripheral T-cell lymphoma (Plumb et al., 2003). Vorinostat, romidepsin, panobinostat, valproic acid and other KDAC inhibitors have been extensively studied in clinical trials for treatments of different hematological cancers and solid cancers such as breast cancer, pancreatic cancer and NSCLC (ClinicalTrials.gov).

1.5. p300 (KAT3B) acetyltransferase

p300 is a ubiquitously expressed, essential protein, possessing intrinsic KAT activity. Apart from its lysine acetyltransferase activity, it also has other enzymatic functions, namely, lysine acyltransferase activity (butyryl-, propionyl-, and crotonyltransferase) and E3/E4 ligase activity. Among its non-enzymatic functions, p300 is a transcription coactivator which acts as a nodal integrating point for several signaling pathways. p300 is enriched on crucial regulatory elements, such as gene promoters and enhancers, thereby directly modulating gene expression. Due these multitude of functions, p300 is a key player in several developmental and differentiation programs, which will be discussed in details in the Subsection 1.5.4 (Figure 1.5).

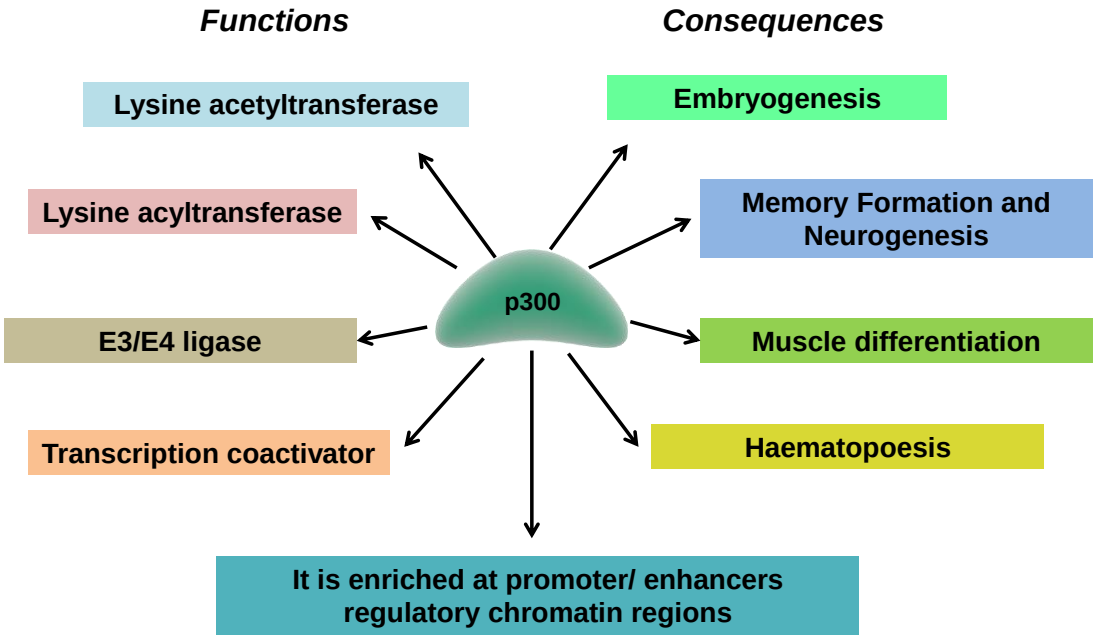

Figure 1.5: The multiple intrinsic enzymatic/non-enzymatic activities of p300. p300 is a general transcription coactivator possessing several enzymatic functions, of which its lysine acetyltransferase activity is well studied. It is an essential protein with functional consequences in numerous developmental/ differentiation programs.

1.5.1. p300: A brief history

p300 (also known as KAT3B, E1A-Binding Protein, 300kD and RSTS2) was first discovered as an adenoviral protein, E1A-interacting phophoprotein (Yee and Branton, 1985). In a follow-up study, it was found that p300 is indispensible for the transforming activity of E1A (Whyte et al., 1989). In 1994, p300 was cloned and characterized as a transcriptional adaptor protein (Eckner et al., 1994). The EP300 gene maps to chromosome 22q13, a region known to be deleted in cancers (Eckner et al., 1994). The p300 paralog, CBP was discovered in 1993 as a nuclear protein interacting specifically to phosphorylated CREB (c-AMP response element binding protein) and facilitating cAMP-regulated gene expression (Chrivia et al., 1993). In 1996, it was reported that p300/CBP possessed intrinsic HAT activity (Bannister and Kouzarides, 1996; Ogryzko et al., 1996). The discovery of intrinsic HAT activity, instilled a new dimension to the p300/CBP family in the realm of transcription regulation. Furthermore, discovery of several non-histone substrates of p300/CBP indicated the importance of these enzymes in non-chromatin-related functions which will be discussed in greater details in the following sections.

1.5.2. Evolution of the KAT3 acetyltransferase family

p300 and CBP (KAT3 family) were found to be highly homologous proteins and were predicted to be members of a family of coactivators (Arany et al., 1994; Lundblad et al., 1995). p300/CBP is conserved across higher eukaryotes from plants to metazoans. The plant *Arabidopsis* possesses four orthologs of CBP/p300 (Bordoli et al., 2001). One CBP ortholog each is present in *Drosophila* (dCBP or Nejire) and *Caenorhabditis elegans* (CBP-1) with conserved functions in transcriptional coactivation, development and differentiation (Akimaru et al., 1997a; Akimaru et al., 1997b; Shi and Mello, 1998). In vertebrates the emergence of these paralogs is said to have occurred due to a duplication event at the chromosomal location of CBP/p300 and eight surrounding genes, giving rise to p300 gene at human chromosome 22q13.2 and CBP on human chromosome 16p13 (Giles et al., 1998). EP300 (Ensembl ID: ENSG00000100393) is a vast gene spanning ~91 kb genomic region on the long arm of chromosome 22 (Chromosome 22: 41,092,610-41,180,077; + strand) (Figure 1.6A) and CBP is located on chromosome 16 (Chromosome 16: 3,725,055-3,880,120; - strand) spanning over 150 kb (Figure 1.6B). In vertebrates too, there are variations in the copies of the p300/CBP genes, zebrafish appears to have duplicated their p300 gene while in puffer-fish the CBP gene is duplicated (Dancy and Cole, 2015).

Even though p300 and CBP may have originated from a single gene, over the course of evolution these proteins have diverged considerably, acquiring unique functions which render them indispensible for the development of multicellular organisms. Interestingly, even though CBP/p300 do not have a sequence homolog in fungi, they do have a distant structural ortholog in yeast, known as Rtt109 (Dancy and Cole, 2015; Tang et al., 2008).

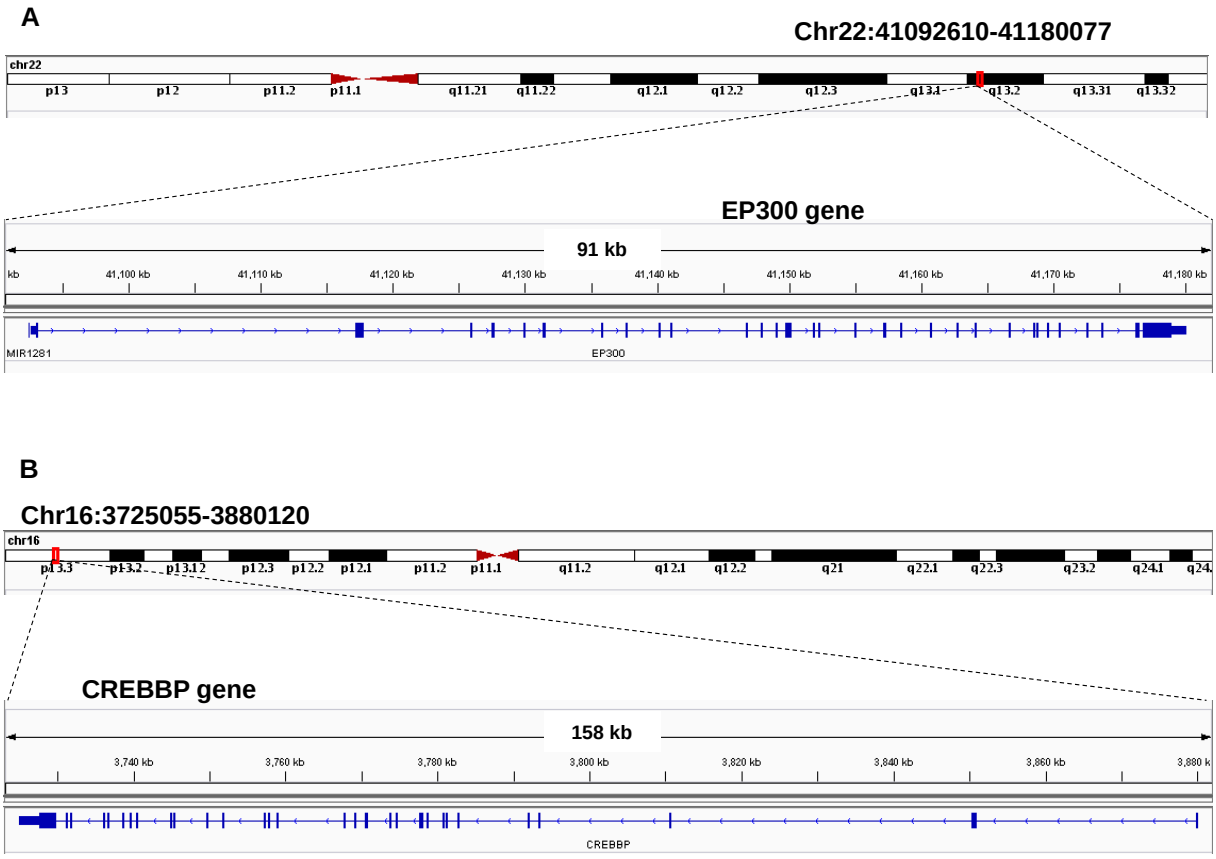

Figure 1.6: Genomic location of the EP300 gene and its homologous CREBBP gene. EP300 is located on chromosome 22:q13.2 while its homolog CREBBP is located on chromosome 16:p13.3. EP300 and CREBBP are large genes spanning approximately 90 kb and 150 kb in length respectively. Visualization of gene loci was done using the Integrative Genomics Viewer (Robinson et al., 2011).

1.5.3. Structure and Substrate specificity of p300/CBP

The EP300 gene comprises of 31 exons (Figure 1.6A) which encodes a 2414 amino acids long protein with a molecular weight of 264 kDa. The large protein consists of multiple globular domains and interspersing unstructured flexible loops, which together are important for protein interaction (Dyson and Wright, 2016). The globular domains of p300 are also conserved in the CBP protein. The N-terminal domains include the Nuclear Receptor Interacting Domain (NRID), the Cysteine/ Histidine-rich domain 1 (CH1) and KIX domain. The central catalytic core domains comprise of the Bromodomain, CH2 domain (consisting of the RING and PHD), and Lysine/histone acetyltransferase domain (KAT/HAT). The C-terminal domains are the CH3 domain and the Interferon binding domain (IBiD). The CH1 and CH3 domains contain transcriptional zinc-finger adapter motifs, TAZ1 and TAZ2 respectively. The CH3 domain also contains another zinc-finger motif known as ZZ motif. The IBiD domain comprises of Nuclear Coactivator Binding Domain (NCBD), a glutamine-

rich stretch followed by a proline-rich PxP motif (Bedford et al., 2010; Yang and Seto, 2008) (Figure 1.7).

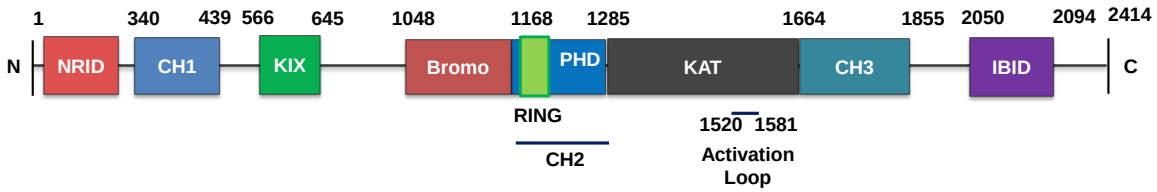

Figure 1.7: Domain Architecture of p300. p300 consists of (from N-terminal) the Nuclear Receptor Interacting Domain (NRID), Cysteine/ Histidine-rich domain (CH1), KIX, Bromodomain, CH2 (RING, PHD), Lysine/histone acetyltransferase domain KAT, CH3 and Interferon binding domain (IBiD).

The structure of full length p300 has not been solved due to the intrinsically disordered regions present in p300 protein, however crystal structures of purified p300 domains are available, such as the bromodomain spanning from amino acids 1047-1161 (PDB: 3I3J, 2.33 Å), KAT domain (amino acids 1281-1664; PDB: 3BIY, 1.7 Å), TAZ2 domain (amino acids 1723-1836; PDB: 3IO2, 2.5 Å) and the core catalytic domain (amino acids 1048-1664; PDB: 4BHW, 2.8 Å). A cryo-EM structure of p300 of a very low resolution of 42 Å is available, but the available structure will not give much information regarding the details of the p300 structure (structure is deposited in Electron Microscopy Data Bank and the accession number is EMD-6261) (Yi et al., 2015).

In 2008, Philip Cole's group reported the crystal structure of the p300 HAT domain (PDB: 3BIY) in complex with Lys-CoA bisubstrate inhibitor. The HAT domain consists of a central seven β-strands surrounded by nine α-helices and loops (Liu et al., 2008) (Figure 1.8A). The central core of the HAT domain structure is well conserved with the corresponding regions in Gcn5/PCAF (Trievel et al., 1999) and MYST family KATs (Yan et al., 2002). However the flanking regions around the core exhibit structural divergence from other KAT families. The structure revealed that the acetyl-CoA binding site is more buried than other KAT active sites. The loop L1 (Figure 1.8A) contributes to about one-third of the protein–cofactor interactions and plays an important role in p300 catalysis. Strikingly, the surface charge of p300 catalytic domain is electronegative, especially around the substrate-binding site, contrasting to the neutral surface charges of other KATs. The HAT domain harbors two distinct shallow electronegative patches, of which one (P1) makes contacts with the lysine moiety of the Lys-CoA bisubstrate while the other (P2) located ~10 Å away was shown to be important for substrate binding and catalysis (Liu et al., 2008; Wang et al., 2008) (Figure 1.8B). The presence of the P1 and P2 electronegative pockets confer substrate specificity to

p300. Typically, p300/CBP substrates have p300/CBP-acetylated lysine residues flanked by positively charged amino acid residues either three to four residues upstream or downstream (~10 Å) from the acetylation site (Thompson et al., 2001). The flexibility of the shallow substrate binding P2 groove, which governs substrate recognition, could account for the promiscuous substrate specificity of p300 in comparison to the other KATs (Wang et al., 2008). p300/CBP acetylates a wide variety of proteins, both histone as well as non-histone proteins. Histone acetylation by p300/CBP often results in transcription activation. p300-mediated histone acetylation is a mark of actively transcribing promoters (eg. H2AK5ac, H3K9ac, H3K18ac, H3K23ac, H3K27ac, H4K5ac, H4K8ac, H4K12ac) and active enhancers (H3K27ac). Furthermore, there is a growing interest in the non-histone substrates of p300/CBP. Lysine acetylation can have a profound effect on the function and stability of proteins. A brief overview of a few p300/CBP substrates and the functional consequences of p300/CBP-mediated acetylation on their functions have been listed in Table 1.1.

Protein	Lysine Residues acetylated	Enzymes Involved	Consequence/ Function	References
RelA	K218, K221, K310	p300/CBP	Increased DNA binding and recruitment of coactivators	(Chen et al., 2002; Huang et al., 2009)
RelA	K122, K123	p300/CBP	Decreased DNA binding, Increased IκB binding	(Kiernan et al., 2003)
p50	K431, K440, K441	p300/CBP	Enhanced transcriptional activation	(Deng and Wu, 2003)
STAT3	K685	p300/CBP	Increased DNA binding, transcriptional activation	(Wang et al., 2005a; Zhuang, 2013)
WNT/β-catenin	K354	p300	Transcriptional activation of WNT target genes	(Garcia-Jimenez et al., 2014; Levy et al., 2004)
c-Myc	K143, K157, K275, K317, K323, and K371	p300	Negative regulation of c-Myc induced transformation in cancer	(Wasylishen et al., 2014; Zhang et al., 2005)
c-Myc	C-terminal domain	CBP	Increases stability	(Vervoorts et al., 2003)
p53	K382	CBP	Increases p53 affinity to CBP bromodomain and interaction with tandem bromodomains of TAF1, a TFIID subunit	(Li et al., 2007; Mujtaba et al., 2004)
p53	C-Terminal	p300	Increases DNA binding and transcription	(Gu and Roeder, 1997)
p53	K117, K161, K162	p300	Essential for p53 to mediate cell cycle arrest, apoptosis and senescence	(Li et al., 2012)
PC4	Lysine-rich domain	p300	Increases double-stranded DNA binding	(Kumar et al., 2001)
ERα	K229, K299, K302 and K303	p300	Induce aberrant expression and proliferation of cells breast cancer	(Wang et al., 2001)
AR	K630, K632, K633	p300, PCAF	Enhanced transcriptional activation, promotes cancer cell growth	(Fu et al., 2003; Fu et al., 2000)
Beclin-1	K430, K437	p300	Inhibits, autophagosome maturation	(Sun et al., 2015)
MATIIα	K81	p300	Destabilizes protein, leads to repression of cell growth	(Yang et al., 2015b)
RFPL3	-	CBP	Upregulated hTERT activity and promotes cancer growth	(Qin et al., 2015)
Ku80	-	CBP	Promotes COX-2 expression and tumor growth.	(Xiao et al., 2015)
PTEN	K402	CBP	Modulates PTEN interaction with PDZ domain-containing proteins	(Ikenoue et al., 2008)
HDAC1	K218, 220, 432, 438, 439, and 441	p300	Acetylated HDAC1 shows reduced deacetylation function. Loses ability to deacetylate p53, stabilizing p53 during heat stress	(Qiu et al., 2006; Yang et al., 2015a)
Snail	K146,K187	CBP	Switches snail from being a repressor to an activator	(Hsu et al., 2014)
Smad2	K19, K20, K39	p300/CBP	Modulates TGF-B and Activin responses	(Tu and Luo, 2007)
Smad3	K378	p300/CBP	Positively regulates Smad3 mediated transcription	(Inoue et al., 2007)
Smad7	K64, K70	p300	Increase protein stability	(Grönroos et al., 2002; Simonsson et al., 2005)
HIF-1α	K709	p300	Stabilizes protein, sensitizes cells to hypoxia-induced growth arrest	(Geng et al., 2012)
pRB	K873, K874	p300, PCAF	Increased affinity to MDM2, hinders phosphorylation and cell cycle progression.	(Chan et al., 2001; Nguyen et al., 2004)
E1A	K239	p300/CBP, PCAF	Inhibits p300 activity, reduces p300 mediated transcription	(Deng et al., 2005)
p73a	K321,327,331	p300	Gets recruited to proapoptotic promoters and induces apoptosis	(Costanzo et al., 2002)
FoxO1	K242, K245 and K262	p300/CBP, PCAF	Diminishes DNA binding , reducing activity	(Calnan and Brunet, 2008)
RUNX1	K24, K43	p300	Increases DNA binding ability	(Wang et al., 2009)
NPM1	K212, K215,K229, K230, K257, K267 and K292	p300	Enhanced histone chaperone activity, relocalizes to nucleoplasm, activates NPM1 mediated transcription.	(Shandilya et al., 2009; Swaminathan et al., 2005)
HMGA1	K65, K71	CBP, PCAF	Modulates transcription of IFN-β upon viral infection	(Munshi et al., 1998)
HMGB1	K2, K11,	CBP	Acetylated upon LPS activation in monocytes and macrophages, triggers inflammation	(Pasheva et al., 2004; Sterner et al., 1979)

Table 1.1: p300/CBP-mediated non-histone protein acetylation and its consequence

Biochemical studies revealed that p300 follows the Theorell-Chance (or 'hit and run') catalytic mechanism, which implies that p300 does not form a stable ternary complex during the reaction. The enzyme rather forms a stable complex with acetyl-CoA, followed by the transient binding to the protein substrate at the P1 pocket. After acetylation of the lysine residue, the protein substrate immediately dissociates from the enzyme. This mechanism is consistent with the broad spectrum of substrate specificity observed in the case of p300/CBP. The catalytic residues are highlighted in Figure 1.8C, of which Tyr 1467 (functions as a general acid to protonate the CoA leaving group) and Trp 1436 (which helps direct the substrate to the binding site) are critical (Wang et al., 2008) (Figure 1.8C).

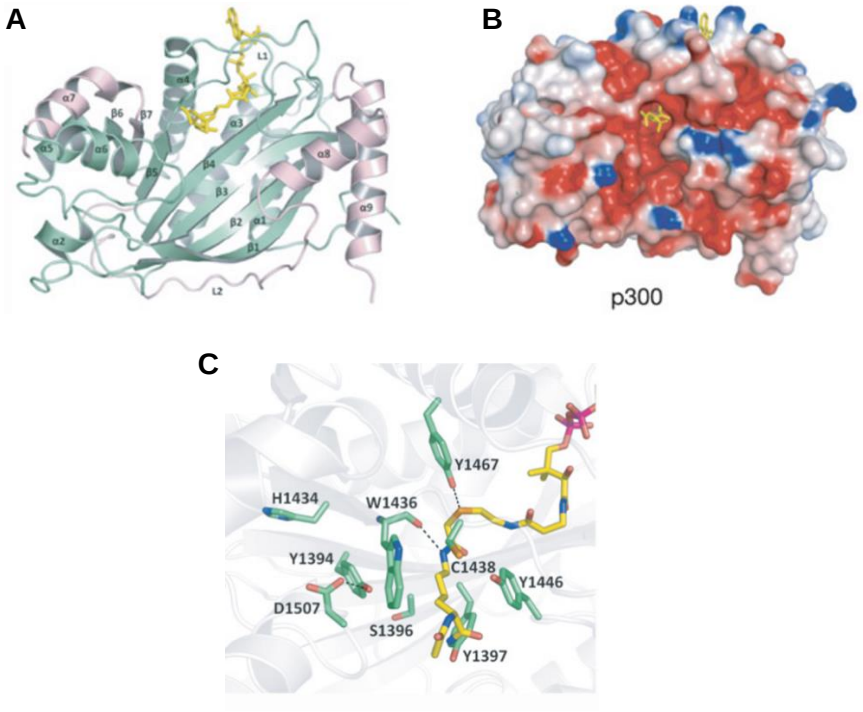

Figure 1.8: Structure of p300 HAT domain. (A) Structure of the p300 HAT domain with N and C subdomains coloured in green and pink, respectively. Lys-CoA is shown in yellow stick figure representation. (B) Electrostatic surface representations of the HAT domains of p300. (C) The active site of p300 showing residues that are in position to play potential catalytic roles (Liu et al., 2008).

To gain further insights into the molecular mechanisms of p300 function and the spatial cooperativity of the bromodomain and PHD domain involved in p300 activity, Delvecchio et al. solved the crystal structure of the core catalytic domain of p300, which consists of the bromodomain, PHD, RING and HAT domains (Delvecchio et al., 2013). The structure revealed that the four domains form a compact conformation in which the RING domain is positioned such that it occludes the substrate-binding site of the HAT domain (Figure 1.9A,B). The structure implied that the RING domain has an inhibitory function towards

p300 substrate-binding (Figure 1.9B). In congruence with this finding, it was observed that mutations that map to the RING domain resulted in an enhancement of p300 acetyltransferase activity, suggesting that the repositioning of the RING domain was essential for access to the otherwise buried substrate-binding pocket of the HAT domain (Delvecchio et al., 2013). This revelation on the essentiality of structure-function relationship in the induction of p300 acetyltransferase activity highlights that the conformational context of p300 dictates its catalytic activity, and that p300 activity may be modulated through the spatial-temporal interactions it makes with other proteins under different environmental cues.

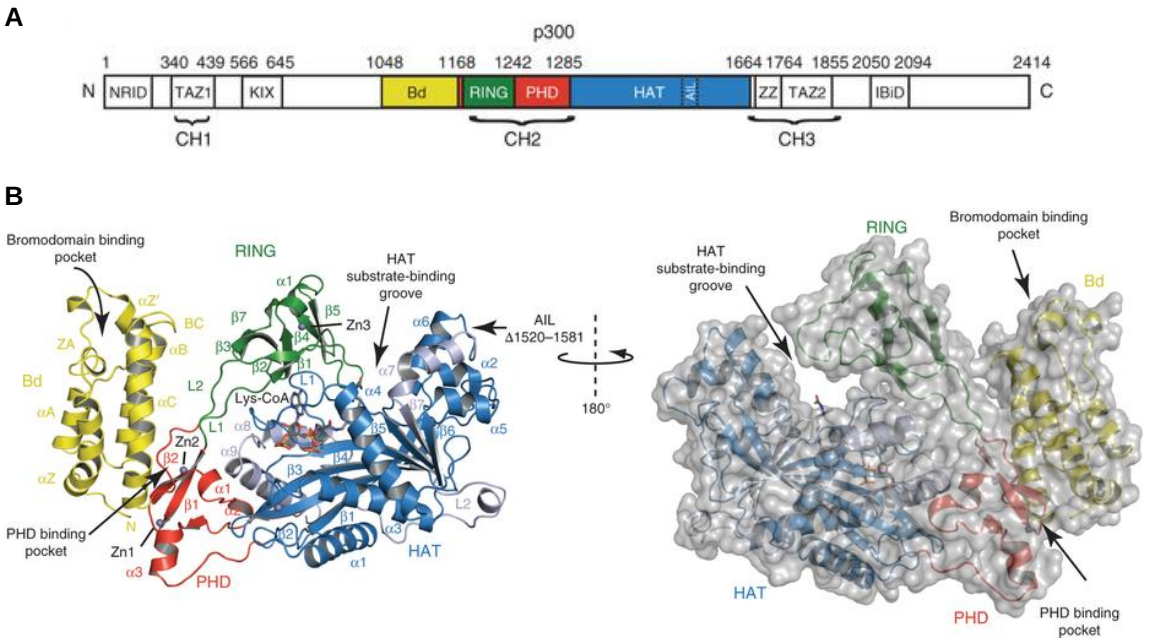

Figure 1.9: Structure of p300 catalytic core. (A) Domain architechture of p300, with the domains corresponding color-coded to the ribbon representation of the crystal structure. (B) Ribbon and surface representations of the p300 core structure with labeling of secondary-structure elements. The bromodomain (Bd), RING and PHD domains are shown in yellow, green and red, respectively. The N and C subdomains of the HAT domain are shown in blue and grey, respectively. The position of the deleted autoinhibitory loop (AIL) is indicated with an arrow. Lys-CoA is shown in stick representation (Delvecchio et al., 2013).

1.5.4. Role of p300 in development and differentiation

p300 and its paralog CBP are intimately involved in developmental pathways. Even though they share extensive homology, their functions are not entirely overlapping. Knockout studies in mice have revealed the functionally distinct nature of these proteins. Homozygous knockout mice of p300 die *in utero,* and the lethality occurs between embryonic day (E)9 and E11.5. Multiple developmental defects are observed in these embryos, such as defects in neural tube closure, cell proliferation, and heart development (Yao et al., 1998). This

indicates that p300 is essential for crucial developmental programs. Fibroblasts isolated from these mice exhibit defects in certain signaling pathways, for example, retinoic acid receptor signaling, while other pathways such as CREB signaling remain intact (Yao et al., 1998). Studies have shown that homozygous mutations in the CBP gene may also lead to a similar spectrum of embryonic defects, suggesting that the gene dosage of p300/CBP is critical for efficient execution of developmental programs (Kung et al., 2000; Oike et al., 1999). Furthermore, the double heterozygous mutants are also embryonic lethal (Yao et al., 1998).

The human developmental disorder, Rubinstein-Taybi Syndrome (RTS), caused by the heterozygous mutation in the p300 or CBP gene, is characterized by multiple abnormalities including mental retardation, cranio-facial defects, and broad digits (Blough et al., 2000; Rubinstein and Taybi, 1963). Approximately, 5% patients have germline mutations in the EP300 gene while 55% occur in the CREBBP gene (Bartholdi et al., 2007; Roelfsema and Peters, 2007). Patients diagnosed with RTS also have a higher predisposition to childhood haematological malignancies (Miller and Rubinstein, 1995). A reduction in histone acetylation is also observed in the cells isolated from RTS patients, highlighting that the loss in p300/CBP activity is involved in the disease etiology (Lopez-Atalaya et al., 2012). p300 catalytic activity is also essential for the formation of the lungs, heart and small intestine (Shikama et al., 2003).

The plethora of neural defects in p300 null mice suggests that p300 may be intimately associated with embryonic neurogenesis. Studies involving dominant negative truncated p300 mutants and brain region-specific conditional knockouts have demonstrated the importance of p300 in long-term memory formation (Oliveira et al, 2007; Oliveira et al, 2011). Intriguingly, activation of p300 using small molecule activators of p300 promotes adult neurogenesis and long term memory formation in mice (Chatterjee et al., 2013). Furthermore, chromatin immunoprecipitation studies have revealed that in a resting cell p300 is enriched over neural differentiation-related genes (Wang and Li, 2016).

The transcription factor, c-Myb, is the master regulator of haematopoiesis and is an important regulator of stemness in hematopoietic stem cells (Ramsay and Gonda, 2008). p300 is a coactivator of c-Myb-mediated transcription and the interaction between c-Myb and p300 is essential for the maintenance of hematopoietic stem cells and the induction of c-Myb-mediated leukemia (Pattabiraman et al., 2014; Sandberg et al., 2005). A small molecule inhibitor of interaction between c-Myb and the KIX domain of p300, Naphthol AS-E

phosphate, can effectively inhibit c-Myb mediated gene expression and induce myeloid differentiation (Uttarkar et al., 2015).

p300 plays an in important role in myogenesis as well. Genetic and small molecule inhibitor-based studies have shown that p300 is essential for myogenesis and the loss of p300 severely attenuates the transactivation of MyoD and Myf-5-mediated gene expression, leading to loss in myogenic differentiation (Roth et al., 2003).

1.5.5. p300/CBP: Integrators of transcriptional networks

The acetyltransferases, p300/CBP, have multifaceted roles in transcription regulation. The function mainly in the following ways: (i) transcription co-activators p300/CBP act as adaptor proteins bridging the basal transcription machinery (eg. TATA box-binding protein (TBP), TFIIB, TFIIE, TFIIF) to DNA sequence-specific transcription factors (eg. p53, NFκB, cMyc) (Bannister and Kouzarides, 1996; Chan and La Thangue, 2001; Ogryzko et al., 1996). (ii) They can act as a scaffold protein interacting with multiple transcription factors/co-factors through their multiple domains (Chan and La Thangue, 2001; Dyson and Wright, 2016). By virtue of their structural plasticity, p300/CBP can physically interact with a vast array of transcription factors thereby functioning as nodal integrators of transcription (Bedford et al., 2010; Dyson and Wright, 2016; Lee et al., 1998; Perissi et al., 1999; Ravi et al., 1998). (iii) Finally through their acyltransferase activities, p300/CBP can covalently modify histones to facilitate the loosening of chromatin resulting in enhanced transcription (Chen et al., 2007a; Sabari et al., 2015). Therefore, its recruitment via the interaction with sequence-specific transcription factors can facilitate transcription from the chromatin template partially through the acetylation of promoter-proximal histones (Kraus et al., 1999; Kundu et al., 2000).

p300 and CBP are referred to as molecular integrators owing to their complex network of protein-protein interactions. They integrate multiple transcriptional cues which are highlighted by their ability to synergize the transactivation of multiple transcription factors bound to the same promoter elements in *cis*. In contrast, the limited intracellular pool of these transcription co-activators leads to constant competition among transcription factor for the binding of p300/CBP. This could also dictate the preference of a transcription signaling pathway over another. Therefore, it is evident that p300/CBP play a pivotal role in the decision of transcriptional outcomes. This function of p300/CBP is endowed by their ability to interact with a multitude of cellular proteins. It is estimated that p300 can interact with over 400 proteins in the cell, most of which are related to transcription regulation. Figure 1.17 represents the top 100 experimentally proven, high confidence protein interactions of p300

and Table 1.2 enlist the top 10 GO pathways that these proteins are involved in. It is quite clear from this interactome analysis that p300 is functionally entwined in the transcription machinery (Figure 1.10; Table 1.2)

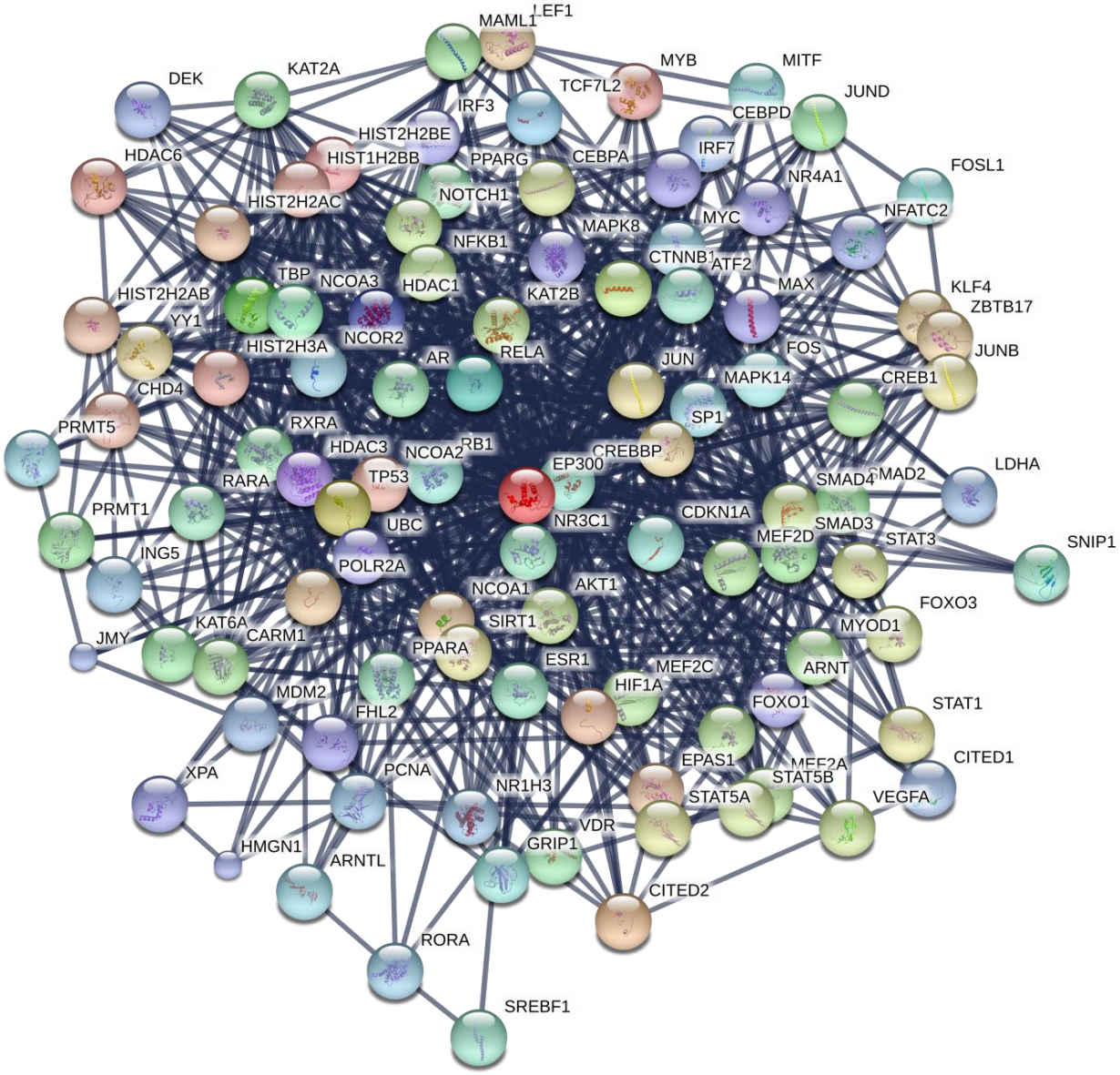

Figure 1.10: p300 Interactome. Top 100 protein-protein interactions of p300 based on experimental evidences with highest confidence (0.900) using the STRING database (https://string-db.org/) v10.5 (Szklarczyk et al., 2015).

Pathway ID	Pathway Description	No. of genes	False Discovery Rate (FDR)
GO:0010557	positive regulation of macromolecule biosynthetic process	70	1.24e-52
GO:1902680	positive regulation of RNA biosynthetic process	68	1.24e-52
GO:0045935	positive regulation of nucleobase-containing compound metabolic process	70	7.93e-52
GO:0045893	positive regulation of transcription, DNA-templated	66	6.93e-51
GO:0010628	positive regulation of gene expression	69	1.41e-50
GO:0009891	positive regulation of biosynthetic process	69	3.4e-49
GO:0031328	positive regulation of cellular biosynthetic process	68	1.96e-48
GO:0045944	positive regulation of transcription from RNA polymerase II promoter	57	7.43e-47
GO:0000122	negative regulation of transcription from RNA polymerase II promoter	51	2.27e-44
GO:0010604	positive regulation of macromolecule metabolic process	74	4.19e-44

Table 1.2: The top 10 GO pathways of the p300 interactome

1.5.6. Role of PTMs in the regulation of p300/CBP

These homologous enzymes undergo a vast array of post-translational modifications. Since CBP and p300 share conserved domains, the PTMs they undergo also appear to be conserved in both proteins (Figure 1.11). Several *in vitro* studies use both proteins in an interchangeable manner, and thus it may be presumed that these PTMs and their consequences may also be shared by both proteins even though the studies majorly involve either p300 or CBP. The reported PTMs such as phosphorylation, arginine methylation, SUMOylation and acetylation have varying consequences on their enzymatic activity, transactivation potential, protein stability and interactome, which will be further discussed in details.

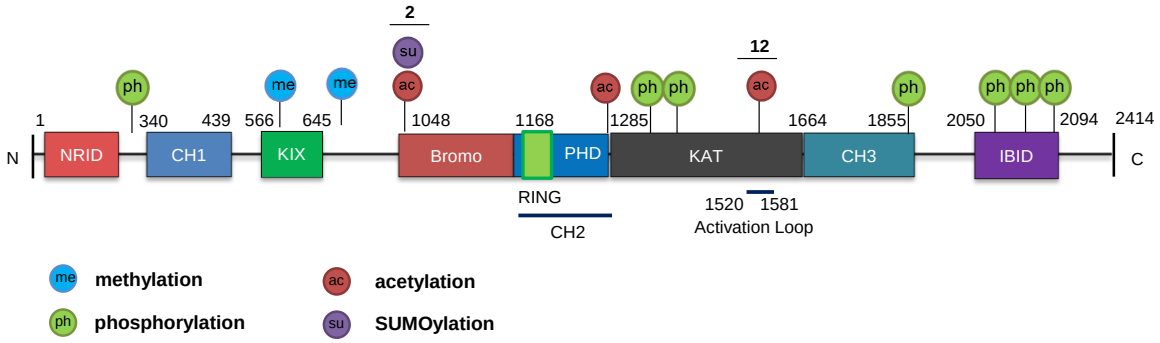

Figure 1.11: Post translational modifications of p300. Domain organization of human p300 protein. Acetylation, phosphorylation, methylation, and sumoylation sites are denoted by circles containing the letters ac, ph, me, and su, respectively.

1.5.6.1. Phosphorylation

p300 was first discovered as a highly phosphorylated nuclear protein (Yee and Branton, 1985). p300 is the substrate of several kinases including, protein kinase A (PKA), PKC, Akt, ERK1/2, salt-inducible kinase 2(SIK2), p38 MAPK and cyclin-dependent kinase 1 (CDK1). The phophsorylation of p300 on different sites have differential effects on its catalytic activity and stability. Phosphorylation of p300 at specific sites can stimulate p300 acetyltransferase activity, for example, ERK1/2-mediated phosphorylation of p300 on S2279, S2315 and S2366 (Chen et al., 2007b), and Akt-mediated phosphorylation on S1834 increase the KAT activity of p300 (Huang and Chen, 2005), while phosphorylation on S89 by SIK2 and PKC kinase inhibits its catalytic activity (Bricambert et al., 2010; Yuan et al., 2002). Phosphorylation may also have contrasting roles on p300 protein stability as well; in response to double-strand breaks (DSB) induced by etoposide or ionizing radiation (IR), ataxia-telangiectasia mutated (ATM) kinase phosphorylates p300 on S106 which results in p300 stabilization (Jang et al., 2010; Jang et al., 2011). Contrastingly, p38 MAPK-mediated

phosphorylation on S1834 induces p300 degradation following DNA damage response (Poizat et al., 2005; Wang et al., 2013). In lung cancer, p300 is phosphorylated on S1038 and S2039 by CDK1 and ERK1/2 leading to its degradation, resulting in increased cell proliferation and metastasis (Wang et al., 2014).

1.5.6.2. Arginine Methylation

p300/CBP are important non-histone substrates of the protein arginine methyltrasferase CARM1 (Bedford and Clarke, 2009). Arginine methylation on p300 can result in differential signaling pathways depending on the domains methylated. Arginine methylation of p300 within the KIX domain, on R580, abrogates its interaction with the transcription factor CREB thereby selectively switching off cAMP-induced transcription (Xu et al., 2001), while methylation further down (towards the C-terminal) on R754 does not affect CREB binding but is essential for steroid hormone receptor-mediated transcription (Chevillard-Briet et al., 2002). Notably, methylation of p300 in this region is also important of BRCA1 recruitment to the p21 promoter in response to DNA damage (Lee et al., 2011).The methylation and demethylimination of p300 by CARM1 and peptidyl deiminase 4 (PAD4), respectively, on the sites R2088 and R 2142 are important for the interaction of p300 with the coactivator GRIP-1 (Lee et al., 2005). Arginine methylation on these sites regulate the assembly and disassembly of p300 coactivator complexes, thus modulating transcriptional outcomes (Lee et al., 2005). In a subsequent study, the role of CBP methylation by CARM1 was investigated for ligand-induced CBP recruitment to ER-responsive target genes. Comparative genome-wide chromatin immunoprecipitation coupled with sequencing (ChIP-seq), for specific methyl-CBP (meCBP) species (sites R742, R768, and R2151 on CBP), demonstrated the existence of distinct but overlapping binding site repertoires in response to ER-signaling, suggesting that CARM1-mediated CBP methylation specifies estrogen-induced subprograms (Ceschin et al., 2011).

1.5.6.3. SUMOylation

p300 is SUMOylated on the Cell Cycle Regulatory domain 1 (CRD1) which is located within the bromodomain between the residues 1017 and 1029. SUMOylation occurs on the two copies of the sequence ψKxE present in this region. SUMOylated p300 is involved in transcriptional repression which is mediated by the specific recruitment of the histone deacetylase, HDAC6 (Girdwood et al., 2003). Interestingly the cell cycle regulatory protein, p21 can ablate the effect of SUMOylation-mediated repression by competing for the CRD1 domain on p300 (Garcia-Wilson and Perkins, 2005).

1.5.6.4. Autoacetylation

Thompson *et al* have proposed that the significance of an auto-inhibitory loop residing in the HAT domain is to modulate the catalytic activity of p300 (Thompson et al., 2004). The model suggests that this lysine-rich loop interacts with the electronegative patch present in the catalytic site, inhibiting efficient substrate binding by acting as a pseudosubstrate. When this loop is in the unacetylated form, it hinders the optimal binding of substrates. Upon *trans*-autoacetylation, the positive charges on the loop are neutralized, allowing it to be displaced from its active site, consequently leading to the activation of the enzyme (Karanam et al., 2006; Thompson et al., 2004) (Figure 1.12).

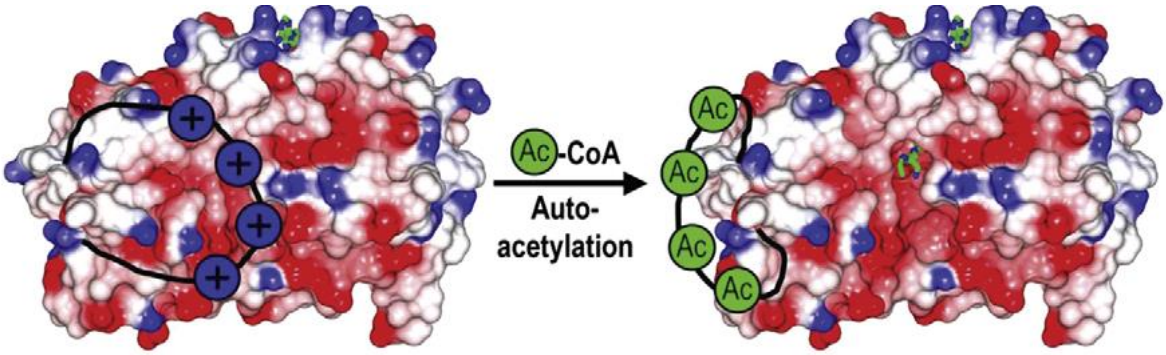

Figure 1.12: Modulation of p300 catalytic activity through autoacetylation. A model for the regulation of p300/CBP by autoacetylation is shown where it is proposed that the lysine-rich basic activation loop blocks the substrate-binding site when unacetylated but is displaced upon autoacetylation (Wang et al., 2008).

This model has been revised by Delvecchio *et al*, who proposed that the additional effect of the domains flanking the catalytic domain play an important role in the regulation of p300 acetyltransferase activity. Their study revealed the inhibitory effect of a non-canonical RING domain on the activity of p300, which appears to occlude the HAT domain. This reveals that the relative arrangement of the p300 protein in three-dimensional space may reveal insights about its mode of regulation. The study also proposed the existence of a "active" conformation of p300, but experimental evidence of this conformation of p300 was still elusive (Delvecchio et al., 2013) (Figure 1.13).

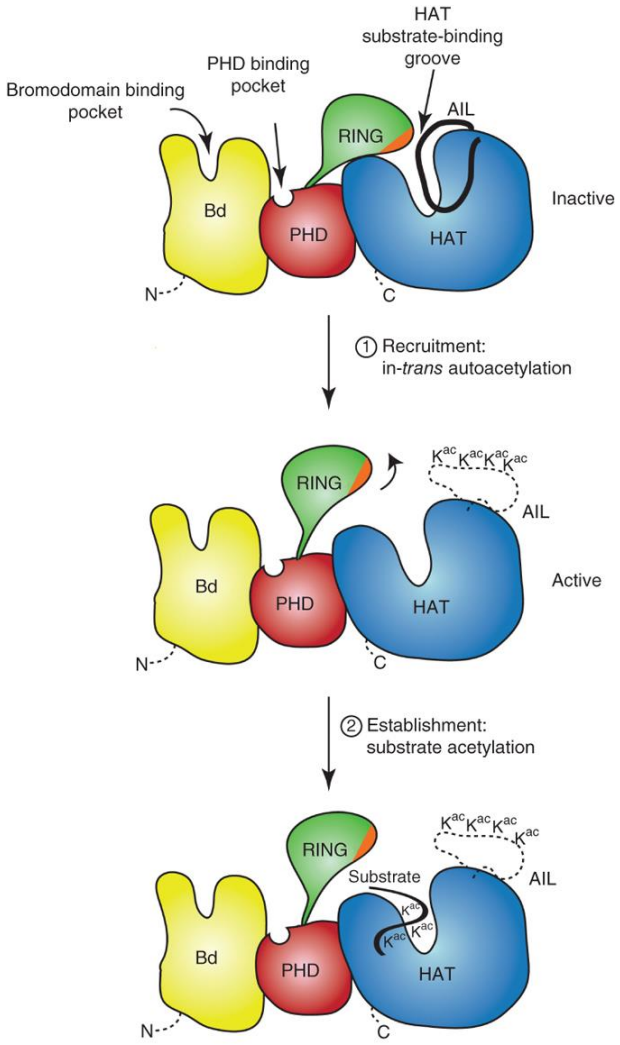

Figure 1.13: Model for p300 autoregulation. In the inactive state (top), the RING domain occludes the catalytic domain (substrate-binding groove in the HAT domain). The model proposes that p300 activation will be initiated by the recruitment of at least two copies of p300 resulting in autoacetylation in *trans* of the autoinhibitory loop (AIL) and displacement of the RING domain. Rearrangement of the core catalytic domains exposes the HAT active site, resulting in substrate acetylation. Yellow, bromodomain (Bd); green, RING; red, PHD; blue, HAT; Kac, acetyl-lysine; X, any amino acid (Delvecchio et al., 2013).

1.6. Factors modulating p300/CBP autoacetylation

The event of trans-autoacetylation of p300 can be modulated by several factors, such as proteins (for example, MAML1, GAPDH, NPM1) (Arif et al., 2010b; Hansson et al., 2009; Sen et al., 2008), post-translational modifications (for example, CARM1-mediated arginine methylation of p300/CBP) (Ceschin et al., 2011), small molecule activators such as TTK21 (Chatterjee et al., 2013), and most recent addition to the list of autoacetylation modulators, enhancer RNAs (Bose et al., 2017) (Figure 1.14). The following subsections will give a brief

overview of how p300/CBP catalytic activity can be regulated through factor-induced enhancement of p300/CBP autoacetylation.

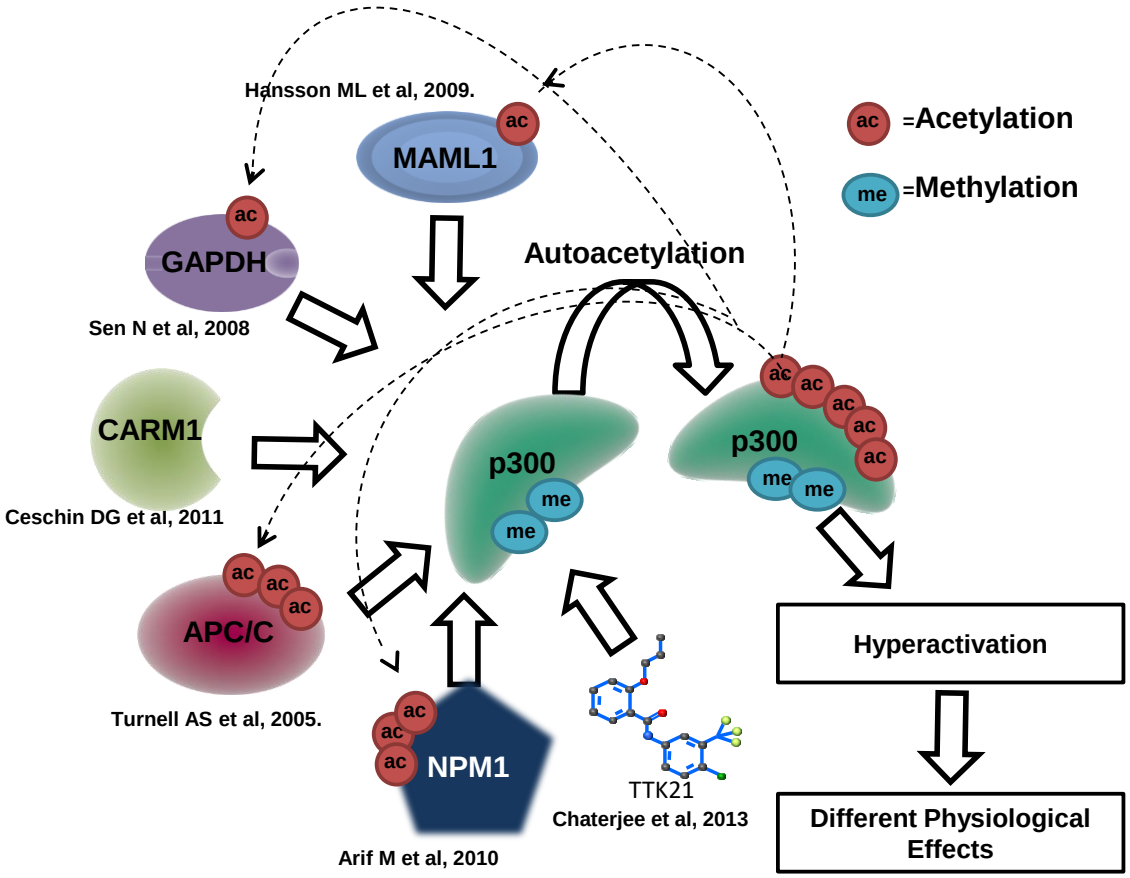

Figure 1.14: Factor-mediated induction of p300 autoacetylation. A few examples of the factors that induce p300 autoacetylation and acetyltransferase activity, under different physiological contexts. The bold arrows indicate the process of p300 autoacetylation. The dotted-lines indicate factor acetylation by activated p300.

1.6.1. GAPDH

Glyceraldehyde-3-phosphate dehydrogenase (GAPDH) is an enzyme which catalyzes the conversion of glyceraldehyde-3-phosphate to D-glycerate-1,3-bisphosphate in glycolysis. In addition to its role in metabolism, it has also been shown to play a role in initiating apoptosis (Hara et al., 2005). In this study, authors demonstrated that under inflammatory signals such as lipopolysaccharide (LPS) or interferon γ treatment, GAPDH translocates into the nucleus by associating with the E3 ligase SIAH1 in a nitric oxide(NO)-signaling dependent manner (Hara et al., 2006; Hara and Snyder, 2006). Subsequent studies have shown that in the nucleus, GAPDH is acetylated on K160 by p300/CBP, and in turn GAPDH stimulated the catalytic activity of these enzymes by inducing the levels autoacetylation. As a consequence of activation, p300/CBP acetylate their downstream targets, eg. p53, to elicit the cell death

cascade (Sen et al., 2008). The study also highlighted that the direct interaction of p300/CBP with their inducer was essential for the induction of autoacetylation.

1.6.2. MAML1

Mastermind-like protein 1 (MAML1) is a transcription coactivator of the NOTCH pathway. MAML1 directly interacts with p300 and recruits it to chromatin and is in turn acetylated by p300 on its proline-rich motif (Saint Just Ribeiro et al., 2007). Hannson *et al*. demonstrated that MAML1 enhances p300 autoacetylation and potentiates p300-driven transcription co-activation. Mechanistically, they proposed that the CH3 domain of p300 had an inhibitory effect on p300 HAT activity. Upon MAML1 binding to this domain, its inhibitory effect is abrogated, thereby facilitating intermolecular autoacetylation and enhancement in activity (Hansson et al., 2009).

1.6.3. Histone Chaperone NPM1

The histone chaperone NPM1 is a substrate of p300. Acetylated NPM1 translocates to the nucleoplasm from the nucleolus, where it associates the with RNA polymerase II transcription machinery. In oral squamous cell carcinoma (OSCC) the levels of NPM1 acetylation correlates positively with the increase in OSCC tumor grade (Shandilya et al., 2009). OSCC patient samples also exhibit global hyperacetylation of histones correlating with the concomitant increase in the levels of NPM1 and GAPDH, which translocate to the nucleus under chronic inflammatory signals, a hallmark of cancer. The global histone hyperacetylation is a consequence of the enhanced p300 autoacetylation, induced by NPM1 and nuclear GAPDH in a nitric oxide (NO) signaling-dependent manner. The autoacetylated p300 may be the driving force causing the alteration in the epigenetic landscape and resultant deregulation in global gene expression, required for the manifestation of oral cancer (Arif et al., 2010b). Interestingly, inhibiting p300 activity with a small molecule inhibitor, CTK7A, reduced tumor volume in xenografted mice, proving that p300 is a potential epigenetic target (Arif et al., 2010b) (Figure 1.15).

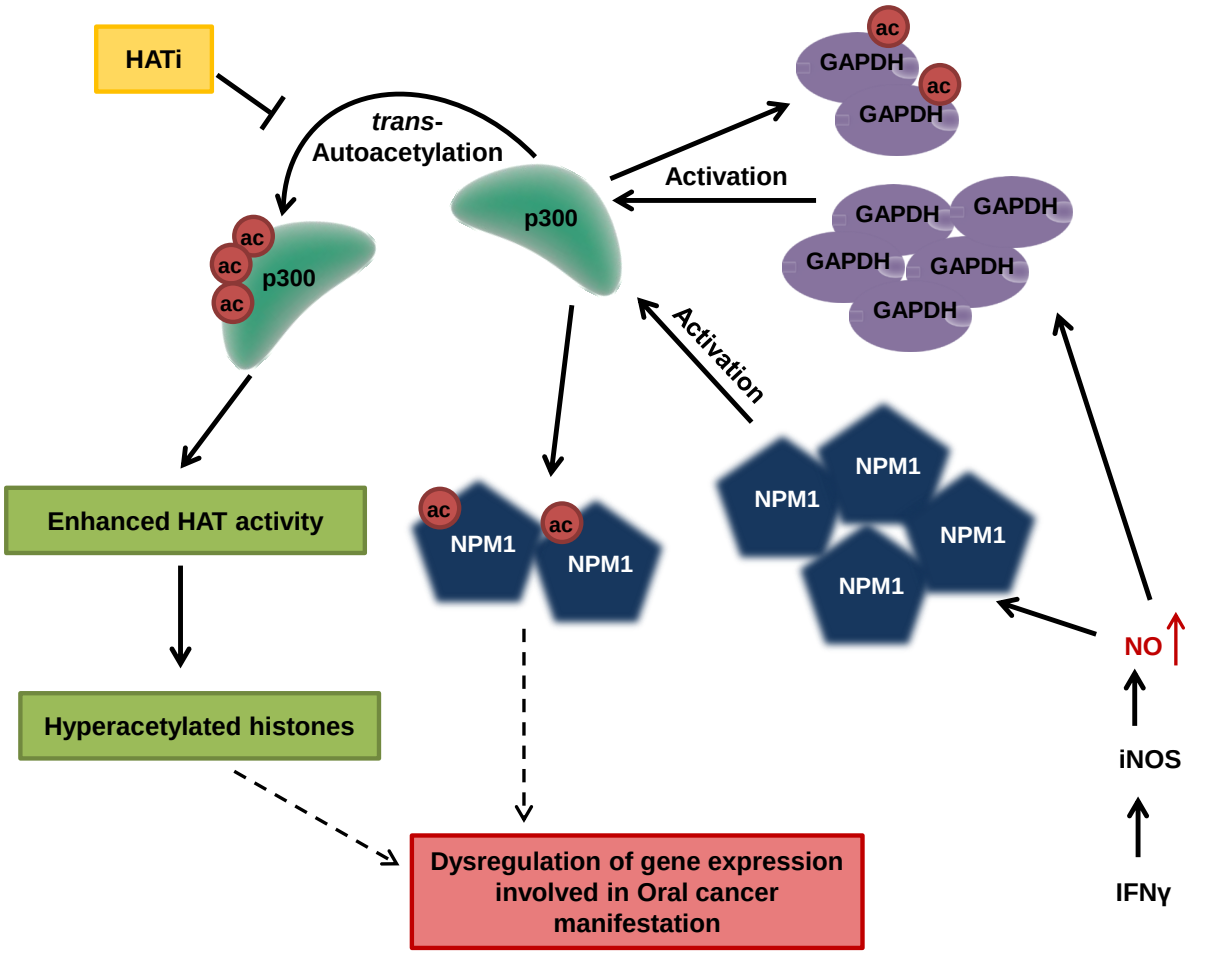

Figure 1.15: Model for the pathways involved in p300 hyperactivation in Human Oral Cancer. Nitric Oxide **(**NO) triggers the upregulation of NPM1 and GAPDH, which in turn enhance the autoacetylation of p300. Highly active p300 acetylates histones and histone chaperone NPM1, which presumably enhances gene expression for oral cancer manifestation. Adapted from Arif et al, *Chem Biol*. 2010 (Arif et al., 2010b).

To delve deeper into the understanding of NPM1-mediated induction of p300 autoacetylation, an in-depth understanding of NPM1 protein structure and function is requisite. Therefore, this section will include a detailed description of the NPM1 protein and its functions.

The human NPM1 (nucleophosmin, B23, NO38, numatrin) gene maps to chromosome 5q35, consisting of 12 exons which gives rise to two transcripts, a long transcript encoding a protein of 294 amino acids known as B23.1 or NPM1.1, the canonical isoform, and a shorter transcript encoding a truncated protein of 259 amino acids (B23.2 or NPM1.3). B23.1 is ubiquitously expressed and is the characterized canonical isoform while not much is known about the other isoform B23.2 (Wang et al., 1993). The NPM1 protein have three distinct domains, the N-terminal oligomerization domain, the unstructured central domain containing the acidic residue stretches, and the unique C-terminal domain containing a basic stretch

followed by an aromatic amino acid stretch (Hingorani et al., 2000). The N-terminal core domain of NPM1 is conserved through the Nucleophosmin/ Nucleoplasmin family. The crystal structure of the oligomerization domain (PDB: 2P1B, 2.75 Å) reveals that the domain is organized into eight β-barrels forming a jelly roll barrel. The monomers are arranged into a pentamer. Two pentamers of NPM1 interact head-to-head with an offset of 20° to form a decamer (Lee et al., 2007). The N-terminal domain also contains two leucine-rich nuclear exit signals (NES) through which NPM1 can interact with the nuclear export receptor CRM1 (Wang et al., 2005b; Yu et al., 2006). The nuclear-cytoplasmic shuttling of NPM1 is regulated by the two NES located in the N-terminal and the nuclear localization signal (NLS) located between the acidic stretches in the central domain. Being a shuttling protein, NPM1 has been functionally implicated in the transport of pre-ribosomal subunits from the nucleus to the cytoplasm (Borer et al., 1989) (Figure 1.16). NPM1 is a nucleolar protein. This is due to a nucleolar localization signal (NoLS) present in its C-terminal domain which consists of the aromatic amino acids, W288 and W290 (Nishimura et al., 2002). Interestingly these residues are often mutated in acute myeloid leukemia (AML) leading to aberrant localization of NPM1 to the cytoplasm in AML patients. NMR studies have revealed that these aromatic residues are essential for the formation of a well-defined right-handed 3-helix bundle in the C-terminal, which plays an important role in the nucleolar retention of NPM1 (Grummitt et al., 2008). The C-terminal domain is functionally important and is implicated in ATP binding (Chang et al., 1998), nucleic acid binding (Dumbar et al., 1989; Hingorani et al., 2000), histone transfer (Okuwaki et al., 2001b), and ribonuclease activity (Hingorani et al., 2000), apart from its role in nucleolar localization.

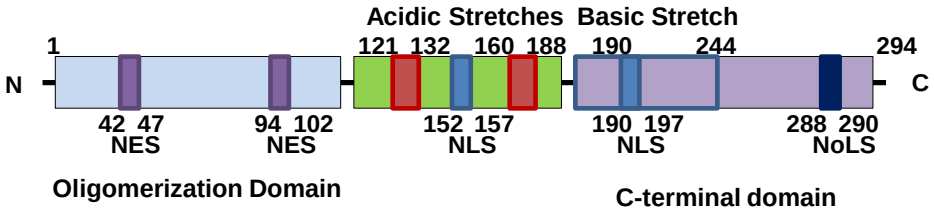

Figure 1.16: Domain Architecture of NPM1. NPM1 protein consists of an N-terminal oligomerization domain, a central acidic domain, and a unique C-terminal domain. NES: nuclear exit signal; NLS: Nuclear localization signal; and NoLS: nucleolar localization signal.

NPM1 was first identified as a nucleolar phosphoprotein which could stimulate replication from adenoviral chromatin (Okuwaki et al., 2001a). The same group later characterized NPM1 as a histone chaperone which can preferentially bind to histones to mediated nucleosome formation and decondense sperm chromatin. It was also noted that the acidic

stretches present in the unstructured central domain of NPM1 were essential for its activity as a histone chaperone (Okuwaki et al., 2001b). NPM1 is critical for embryogenesis. NPM1 knockout mice die between E11.5 and E16.E. The loss of NPM1 results in aberrant centrosome duplication, impaired ribosome biogenesis, and genomic instability. The $NPM1^{-/-}$ knockout have characteristic defects in organogenesis, especially in the forebrain development. The embryos also exhibit severe defects in haematopoiesis (Grisendi et al., 2005). It is evident from the knockout studies that NPM1 is intimately involved in ribosome biogenesis. NPM1 is known to associate with preribosomal subunits and is functionally implicated in ribosome assembly as a ribosome chaperone (Yu et al., 2006). NPM1 possesses intrinsic endoribonuclease activity which facilitates the cleavage of ribosomal RNA to mature rRNA transcripts (Hingorani et al., 2000). NPM1 directly interacts with ribosomal proteins and aid in their shuttling to the cytoplasm (Maggi et al., 2008). Therefore, NPM1 promotes cell proliferation through the facilitation of ribosome biogenesis.

Stress conditions triggers the rapid translocation of NPM1 out of the nucleolus where it can interact with components of stress-response pathways. Phosphorylated NPM1 accumulates around IR-induced DNA damage foci. NPM1 is also involved in transcription. NPM1 is known to interact with c-Myc and is important for c-Myc driven Pol II transcription (Li et al., 2008). NPM1 also promotes Pol II-mediated transcription from a chromatin template in an acetylation-dependent manner (Swaminathan et al., 2005). Moreover, acetylated NPM1 shuttles into the nucleoplasm where it associates with Pol II-driven transcription (Shandilya et al., 2009). Furthermore, NPM1 can act as a co-repressor or co-activator of transcription by interacting with several transcription factors (Lindström, 2011). NPM1 also binds to nucleolar rDNA chromatin and enhances Pol I transcription (Murano et al., 2008) (Figure 1.17).

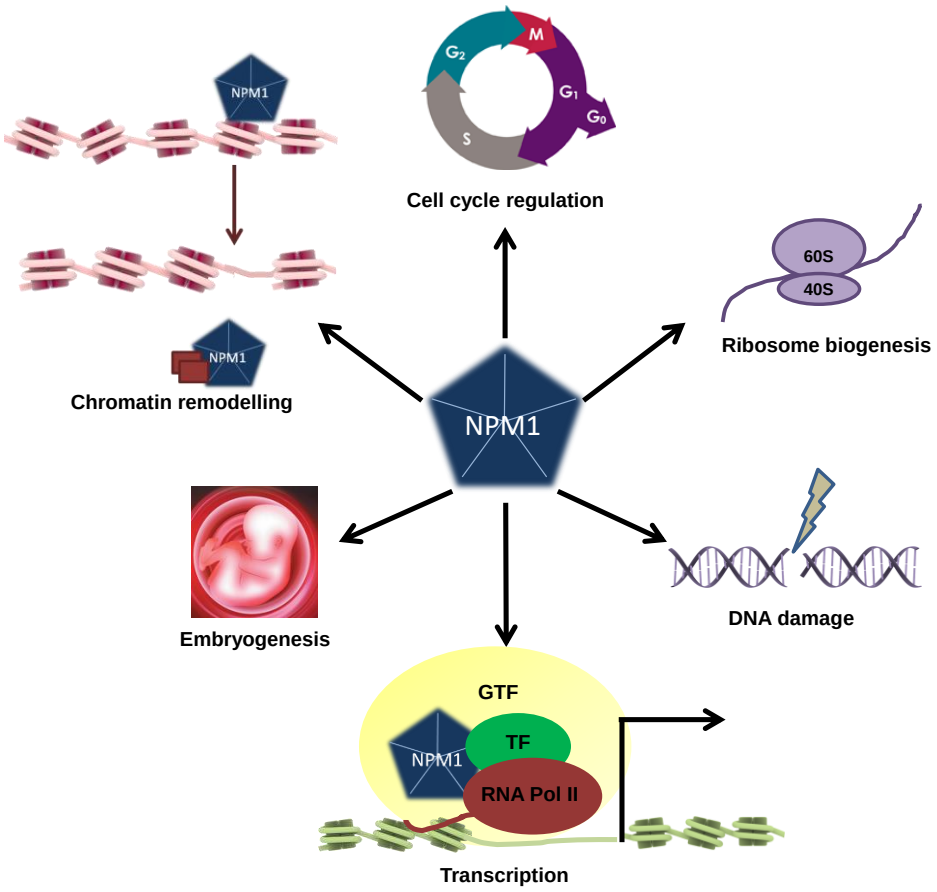

Figure 1.17: The multiple functions of the histone chaperone Nucleophosmin. NPM1 is multifunctional protein involved in chromatin remodeling, cell cycle regulation, ribosome biogenesis, DNA damage, transcription, and embryogenesis.

1.6.4. Other known inducers of p300/CBP function

As p300 is involved in diverse physiological roles, the precise regulation of its function is essential. It has been demonstrated that many various factors affect the levels of p300 autoacetylation in the cell. Intriguingly, each of these factors has distinct cellular functions and can induce p300 autoacetylation under different cellular events. The Anaphase Promoting Complex/Cyclosomes (APC/C) subunits APC5 and APC7 are capable of enhancing p300 autoacetylation which is required for proper cell cycle progression (Turnell et al., 2005). p300 autoacetylation is negatively regulated by the Class III lysine deacetylase, SIRT2 and as expected, the suppression of p300 autoacetylation leads to the reduction of its enzymatic activity (Black et al., 2008). In a recent study, Bose *et al* have demonstrated that CBP contains a unique RNA-binding motif in its HAT domain which can bind eRNAs. This leads to the induction of CBP autoacetylation and activity, resulting in histone acetylation at active enhancers and subsequent gene expression alteration (Bose et al., 2017). PTMs can also

regulate the catalytic activity of p300 and CBP. Arginine methylation on R742 and R768 residues of the KIX domain by CARM1 increases CBP activity and autoacetylation, whereas phosphorylation may have contrasting effects on p300 activity, depending on the kinase and sites that are phosphorylated (Ait-Si-Ali et al., 1998; Ceschin et al., 2011; Huang and Chen, 2005; Schwartz et al., 2003; Zhang et al., 2011). These PTMs may alter p300 activity by differentially regulating the protein CBP and p300 can associate with, at a given cellular context. The cascade of molecular events that culminate in factor-induced p300 autoacetylation is still not clearly understood.

1.6.5. Small Molecule Activators

The autoacetylation of p300/CBP can be enhanced by certain small molecules as well. The first reported activator of p300 activity is N-(4-chloro-3-trifluoromethyl-phenyl)-2-ethoxy-6-pentadecyl-benzamide (CTPB), an anacardic acid derivative (Balasubramanyam et al., 2003). Since this molecule is cell impermeable, a carbon nanoshere (CSP) was used as a carrier (Selvi et al., 2008). Further derivatization of CTPB molecule led to the synthesis of TTK21 (N-(4-chloro-3-trifluoromethyl-phenyl)-2-N-propoxy-benzamide), another potent KAT3 activator *in vitro* and *in vivo.* TTK21, when conjugated to CSP, could effectively cross the blood brain barrier and enhance neurogenesis and long-term memory formation in adult mice (Chatterjee et al., 2013). These small molecule activators of p300/CBP appear to be promising therapeutics in diseases where CBP or p300 proteins are down-regulated or inactivated.

1.7. Tumor Suppressor p53

The functional association between p300 and p53 is well established. Besides being a coactivator of p53, p300 also acetylates p53 on 7 lysine residues present in the DNA binding domain (Gu and Roeder, 1997; Lill et al., 1997), though contradictory findings have shown that p53 C-terminal acetylation may not have a profound effect on its promoter binding (Barlev et al., 2001; Espinosa and Emerson, 2001). Nevertheless, accumulation of acetylated p53 has been observed during cellular stresses (Reed and Quelle, 2014; Sakaguchi et al., 1998) and p53 acetylation has been studied extensively with respect to cell cycle arrest, apoptosis, senescence, and ferroptosis (Bieging et al., 2014; Jiang et al., 2015). Moreover, studies using the acetylation-defective mutants of p53 have shown that the acetylation of p53 is not required for its DNA binding, rather it is crucial for the recruitment of co-activators such as p300 which are essential for p53 transactivation function (Barlev et al., 2001).

Thereby, reiterating the fact that the interaction between p300 and p53 is functionally important. p53 interacts with p300 in its tetrameric conformation, through its bipartite transactivation domain AD1 and AD2, while p300 interacts through several domains namely, TAZ1, KIX, TAZ2 and IBiD (Krois et al., 2016; Teufel et al., 2007). Intriguingly, numerous factors such as E1A, DDX24, WTX, MYBB1A, Skp2, can regulate p53 tumor suppressive functions *in vivo* by dictating its association with p300, thereby proving that the p300-p53 axis is an important cell fate determinant in stress responses (Kim et al., 2012; Kitagawa et al., 2008; Kumazawa et al., 2011; Lill et al., 1997; Shi et al., 2016).

In the pursuit of elucidating the mechanistic details of effector-mediated enhancement of p300 autoacetylation, certain proteins which are functionally closely related to p300 were screened (Discussed in Chapter 4). Based on the evidences discussed, the tumor suppressor protein, p53, appeared to be a promising candidate as an inducer of p300 function.

The TP53 gene maps to the chromosome 17p13.1 and encodes the p53 protein. The p53 protein was first identified as an simian virus 40 (SV40) large T-antigen interacting protein (Lane and Crawford, 1979). It was also observed that p53 expression levels were more abundant in tumor tissue, suggesting that it may have a role in oncogenesis (DeLeo et al., 1979; Rotter, 1983). Through the first decade since its discovery, p53 was regarded as a proto-oncogene. However, there were several experimental evidences that challenged its status as an oncogene. For example, in several tumor models, the mouse Tp53 gene was shown to be inactivated through retroviral insertions (Ben David et al., 1988; Wolf and Rotter, 1984). Furthermore, the different reports using p53 cDNAs in cellular transformation differed in sequences from each other (Levine and Oren, 2009). In 1989, Vogelstein and his group demonstrated that the p53 gene exhibited >50% Loss of Heterozygosity in tumors, which was a hallmark of tumor suppressor (Baker et al., 1989). This seminal study caused a paradigm shift in the field of p53 biology. Later studies corroborated these findings, thereby establishing that p53 was indeed a tumor suppressor protein. The forms of p53 used in the earlier experiments were the mutant form of p53 which will be discussed in the following Subsection 1.7.3. The germline mutation in p53 causes a familial cancer syndrome known as Li-Fraumeni syndrome (LFS). This rare autosomal-dominant disorder predisposes individuals to higher frequency of malignancies of various origins (Li and Fraumeni, 1969a, b; Malkin et al., 1990; Srivastava et al., 1990). p53 knockout studies have revealed that even though $p53^{-/-}$ do not exhibit obvious developmental defects, these mice are highly prone to cancers (Attardi and Jacks, 1999; Donehower et al., 1992).

Structurally, p53 is a 393 amino acid long protein which forms tetramers. The N-terminal domain of p53 is intrinsically disordered. It contains the bipartite transactivation domain and the proline-rich region. The central portion of the protein is the DNA binding domain (DBD), which is responsible for sequence-specific DNA binding. Wild-type p53 functions as a homo-tetramer in cells, binding to p53 response elements which is composed of two decamers separated by a spacer of 0–14 nucleotides (-RRRCWWGYYYn0–14RRRCWWGYYY-) (A: adenine; T: thymine; C: cytosine; G: guanine; R and Y are purine and pyrimidine respectively, W: A or T; and n: any nucleotide (el-Deiry et al. 1992; Funk et al. 1992; Riley et al. 2008). The DBD is followed by a short oligomerization domain, which is important for tetramer formation. The C-terminal domain is the regulatory domain of p53. It is an unstructured region, rich in basic amino acids which can bind to DNA non-specifically (Figure 1.18).

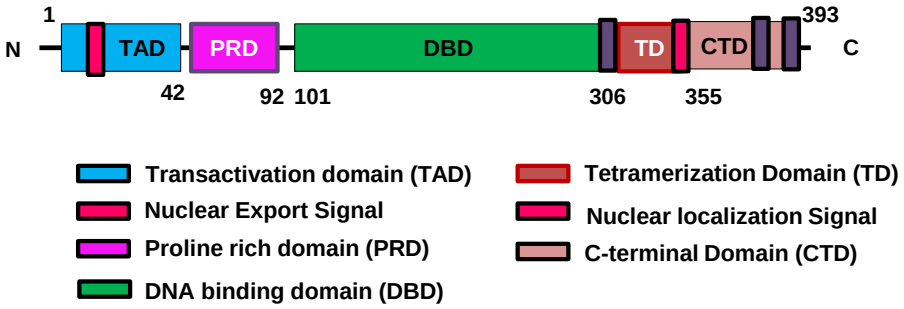

Figure 1.18: Domain Architecture of tumor suppressor p53. p53 is a transcription factor possessing a N-terminal transactivation domain, a proline-rich domain, a DNA binding domain, tetramerization domain and a regulatory C-terminal domain.

Functionally, the wildtype protein is a sequence-specific transcription factor, which mediates gene expression pathways in response to cellular stresses. In a resting cell, the p53 protein is maintained at low levels by the concerted action of several E3 ligases, especially MDM2, which is also a target gene of p53 creating a negative feedback loop. p53 is activated upon various cellular stresses including DNA damage, oxidative stresses, nutrient deprivation, hypoxia, oncogenic stress, ribosomal stress and telomere attrition (Figure 1.19). Following activation, p53 exhibits its tumor suppressive functions through the transcriptional activation of its downstream effector proteins, resulting in DNA damage repair, cell cycle arrest, apoptosis, senescence, autophagy and alteration in metabolic pathways (Kruse and Gu, 2009; Vousden and Prives, 2009).

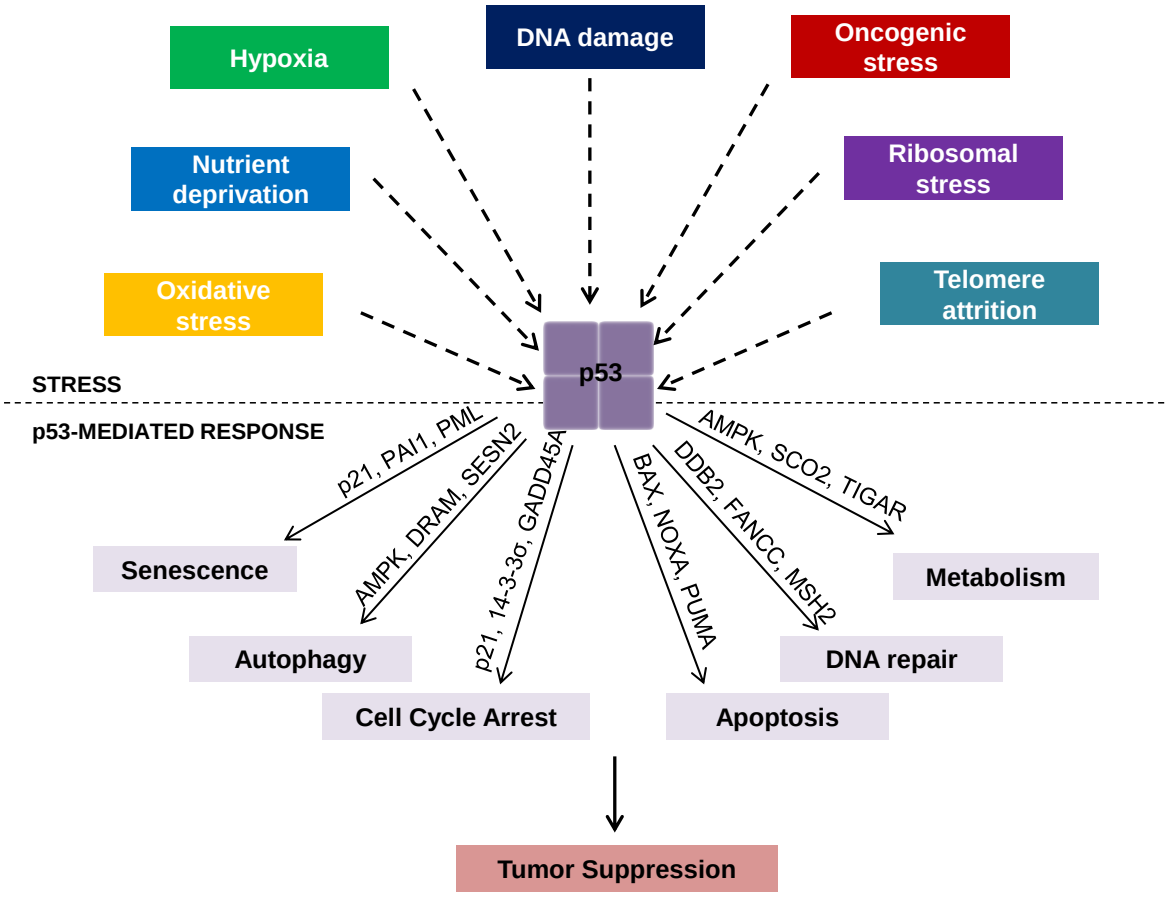

Figure 1.19: p53-mediated stress response pathways. Schematic depicting the myriad of stresses which activate the tumor suppressor p53- driven stress response pathways. Each response is executed by p53-target effector proteins (indicated on the arrows).

1.8. Mutant p53

As described earlier, p53 was first described as a proto-oncogene, but later found to be an important tumor suppressor protein, often dubbed as the 'guardian of the genome' (Lane, 1992). But unlike other tumor suppressor proteins which are predominantly inactivated (Weinberg, 1991), p53 exhibited a unique characteristic of acquiring GOF properties upon mutation which are predominantly missense mutations (~75%) resulting in amino acid substitutions, apart from the LOH and inactivating mutations. Approximately 97% of the missense mutants map to the DBD of which a small number mutants occur in high frequency in cancers (Residues: 248 (7%), 273 (6.7%), 175 (5.1%), 245 (3.3%), 249 (2.9%), 282 (2.9%)), which are termed as "hot spot" mutants (Freed-Pastor and Prives, 2012).

The p53 protein has a pivotal role in regulating the manifestation of cancers. The wildtype p53 protein is often lost or inactivated in cancers. A subset of missense mutants can act as inactivating dominant negative p53 proteins by binding and inactivating the wildtype copy.

These mutants can also inactivate the other p53 family members such as p63 and p73 by forming hetero-tetramers. These mutants lose their tumor suppressive properties and are known as the loss-of-function mutants. But the more intriguing missense mutants are the p53 mutant which not only lose their tumor suppressive functions but also acquire additional tumorigenic properties which promote carcinogenesis (Freed-Pastor and Prives, 2012). The mutants may function in the following ways:

1. They may bind directly to DNA other than the p53 cognate site and stimulate transcription of pro-survival and cell cycle genes.
2. They may bind and recruit other transcription factors causing deregulation of transcriptional programs.
3. They may bind and alter the functions of proteins (Figure 1.20).

Recent studies have also implicated the role of mutant p53 in altering the epigenetic landscape. The study showed that mutant p53 can upregulate the expression of certain epigenetic modifying enzymes which lead to the alteration in global histone acetylation and methylation levels contributing to cancer progression (Zhu et al., 2015). In this study, the role of p300 autoacetylation in disease conditions has been explored. A screen for different p53 missense mutants in the context of factor-induced p300 autoacetylation has been investigated.

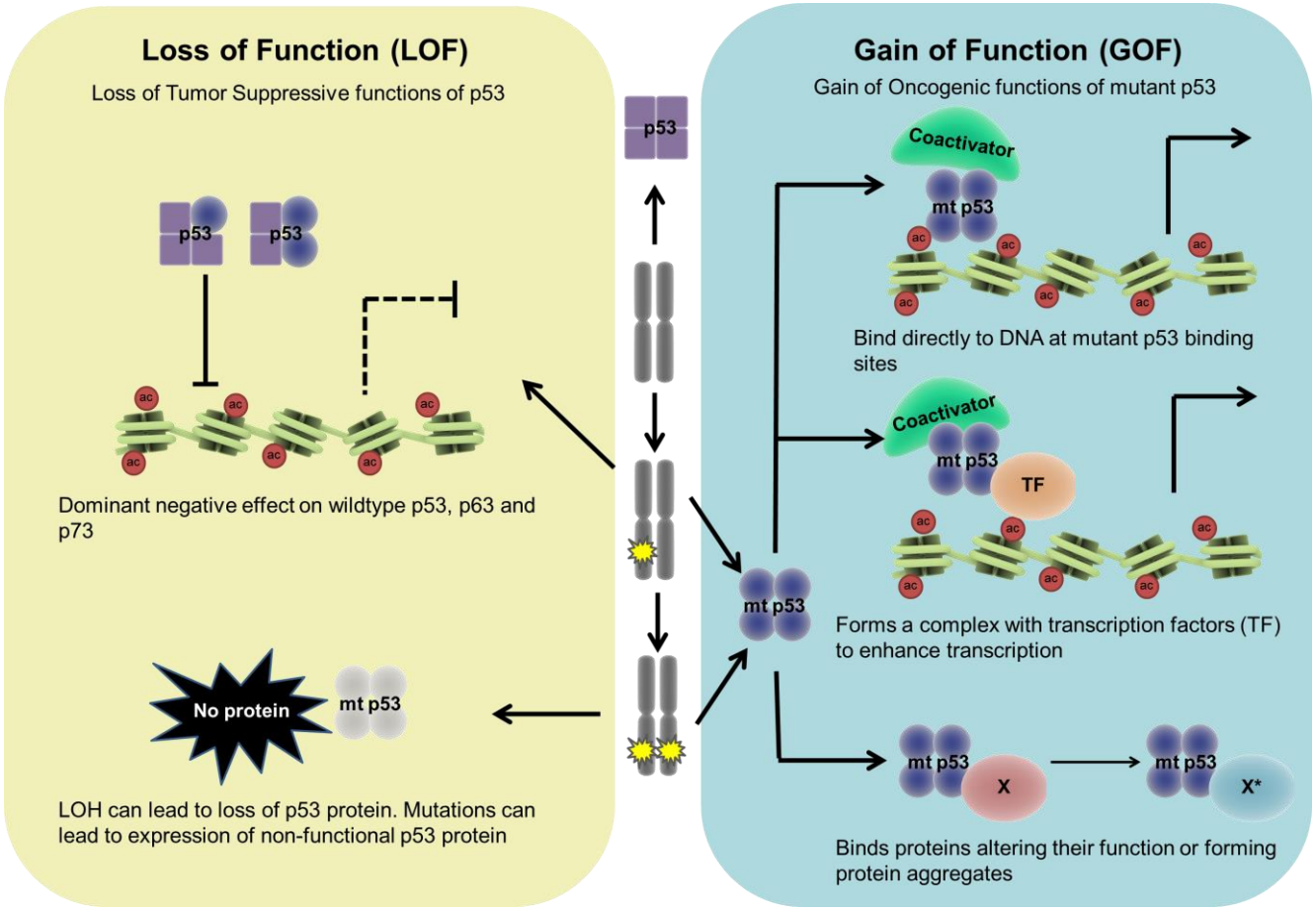

Figure 1.20: Roles of mutant p53 in tumorigenesis. Missense mutants of p53 are classified mainly into two groups: Loss of Function (LOF) mutants and Gain of Function (GOF) mutants. The illustration depicts the different modes of action through which missense mutant p53 proteins can disrupt the tumor suppressive functions of the wildtype p53 leading to the manifestation of cancer.

1.9. Deregulation of p300

The transcription co-activator p300 is required for faithful cell cycle progression and cell proliferation. Disruption of p300 activity either by chemical inhibition or by microinjection of specific antibodies leads to G1/S arrest (Ait-Si-Ali et al., 2000) and an increase in senescence (Yan et al., 2013). Moreover, fibroblasts isolated from p300 null embryos have severe cell proliferation defects (Yao et al., 1998).

p300/CBP, both play an important role in DNA damage response and apoptosis, especially through the modulation of the p53 pathway. Surprisingly, even though both p300 and CBP are homologs, their functions *in vivo* are relatively distinct, which is evident due to the haplo-insufficiency observed in Rubinstein-Taybi syndrome (RTS) caused by germline mutations either in EP300 or CREBBP gene allele (Roelfsema and Peters, 2007; Rubinstein and Taybi, 1963). Predisposition towards childhood malignancies is characteristic in RTS patients (Iyer

et al., 2004; Miller and Rubinstein, 1995). There is also a higher incidence of hematological malignancies in mice heterozygous for CBP (Ghizzoni et al., 2010). Moreover, chimeric mice of CBP-/- and p300-/- null cells are observed to have tumors arising from the null cells (Rebel et al., 2002). Since both p300 and CBP are important for maintenance of cellular homeostasis, perturbation in their functions can lead to severe pathological consequences. In cancers, p300 and CBP can function either as oncogenes or tumor suppressors, depending on the context which govern their cellular functions.

Somatic mutations in the EP300 or CREBBP gene loci have been observed in many malignancies. The loss of heterozygosity (LOH) in cell lines and primary tumors at the EP300 or CREBBP gene loci due to chromosomal loss or inactivating mutations such as missense mutations, frameshift or truncations, have indicated a probable tumor suppressive role of these enzymes. LOH at the EP300 locus (22q13) has been observed in numerous cancers including oral, breast, ovarian, hepatocellular, colorectal, gastric cancers and glioblastomas (Iyer et al., 2004). The biallelic loss and inactivating mutations are relatively rarer at the CREBBP locus (16p13). CREBBP gene mutations have been observed in colon, breast, lung, and ovarian cancers (Kishimoto et al., 2005; Ozdağ et al., 2002; Tillinghast et al., 2003). In hematological malignancies, chromosomal instability at the CREBBP or EP300 loci leads to translocation events. Although, the events of translocations occur at a low frequency, they are often associated with poor prognosis of the disease (Diab et al., 2013). Chromosomal translocations often result in fusion KAT proteins which retain the functional HAT and bromodomains. In-frame translocations confer oncogenic potential to these chimeric proteins, such as in the case of mixed lineage leukemia (MLL)-CBP t[11;16](q23;p13) or in MLL-p300 t[11;22](q23;q13) fusions (Krivtsov and Armstrong, 2007).

Through the vast interactome of p300 and CBP, these enzymes can modulate cellular events in normal and pathological conditions. p300/CBP proteins can promote malignancies by interacting with oncoproteins such as c-Myc, c-Myb, HIF1α, β-catenin, and androgen receptor (AR), which are often associated with tumorigenesis (Bannister and Kouzarides, 1995; Bannister et al., 1995; Dai et al., 1996; Hecht et al., 2000; Liu et al., 2008; Sobulo et al., 1997). The expression levels of p300/CBP are dysregulated in malignancies. Moreover, the overexpression of p300 strongly correlates with aggressiveness of hepatocellular carcinoma (HCC) and is a predictive marker for the poor prognosis of the disease (Li et al., 2011; Yokomizo et al., 2011). In prostate cancer, p300 levels correlate with the grade and

tumor size and the higher p300 expression increases the risk of recurrence among patients (Debes et al., 2003; Isharwal et al., 2008). p300 expression is also correlates with the aggressiveness of cutaneous squamous cell carcinoma (CSCC) and nasopharyngeal carcinoma (Chen et al., 2015; Liao et al., 2012). In colorectal adenocarcinomas, p300 and CBP appear to have contrasting roles in disease outcome. The higher expression of p300 is predictive of poor prognosis while higher CBP expression correlates with longer survival in patients (Ishihama et al., 2007). Upregulation in p300 expression is also linked to recurrence and poor prognosis in breast cancer and non-small cell lung carcinoma, while in the case of bladder cancer cells the high expression of p300 may confer doxorubicin-resistance (Hou et al., 2012; Takeuchi et al., 2012; Xiao et al., 2011).

As discussed previously, post-translational modifications play a major role in the modulation of p300/CBP function. Phosphorylation of p300 on S1038 and S2039, by CDK1 and ERK1/2, results in its degradation which promotes the progression of lung cancer (Wang et al., 2014). In oral cancer p300 activity is dysregulated due to the enhancement in its autoacetylation by NPM1 and GAPDH (Arif et al., 2010b). Overall, it is apparent that the regulation of p300/CBP expression and activity is important for the normal functioning of the cell. In circumstances where the precise regulation of p300 or CBP is lost may lead to disorders such as cancers, neurodegenerative disorders, and metabolic diseases (Figure 1.21).

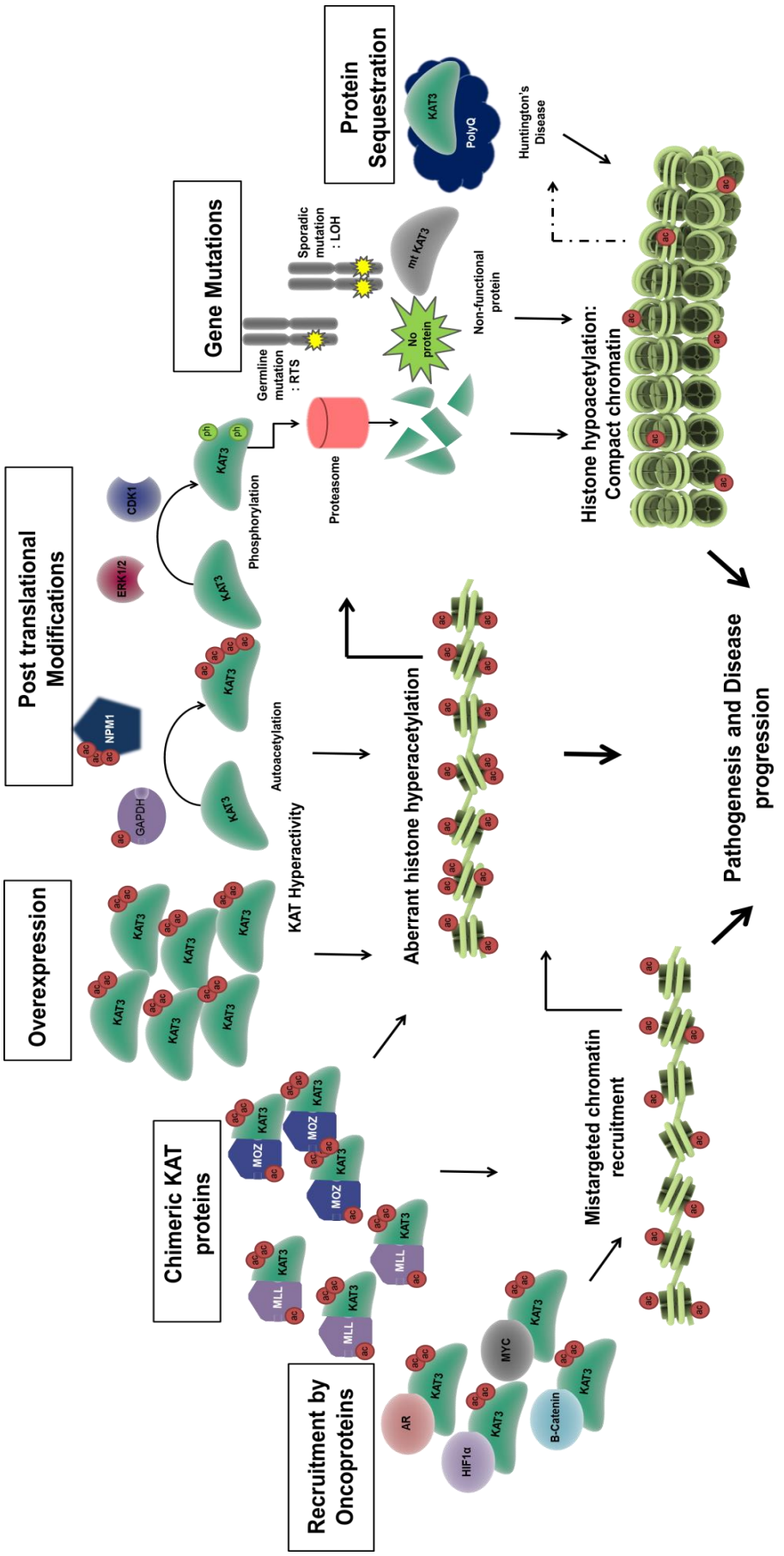
Protein Sequestration
KAT3
PolyQ
Huntington's Disease
Gene Mutations
Sporadic mutation : LOH
mt KAT3
No protein
Non-functional protein
Germline mutation : RTS
Post translational Modifications
CDK1
ERK1/2
KAT3
ph
Phosphorylation
Proteasome
Histone hypoacetylation: Compact chromatin
NPM1
GAPDH
Autoacetylation
KAT Hyperactivity
Overexpression
Aberrant histone hyperacetylation
Pathogenesis and Disease progression
Chimeric KAT proteins
MOZ
MLL
Mistargeted chromatin recruitment
Recruitment by Oncoproteins
AR
HIF1α
MYC
B-Catenin

Figure 1.21: Multiple modes of KAT3 deregulation. Three scenarios of CBP/p300 (KAT3 proteins) deregulation have been illustrated: first, the mistargeted chromatin recruitment of CBP/p300 by oncoproteins and fusion proteins; second, the aberrant histone acetylation by hyperactive CBP/p300 due to in-frame MOZ-CBP/p300 chimeric protein, p300/CBP overexpression and enhancement of autoacetylation by NPM1and GAPDH; third, loss of KAT activity by degradation, gene mutations in the case of Rubinstein-Tyabi Syndrome (RTS) or Loss of Heterozygosity (LOH) in different malignancies and the sequestration of CBP by poly(Q) proteins in Huntington Disease. Adapted from Kaypee et al, Emerging Epigenetic Therapies, Academic Press, 2015 (Kaypee et al., 2015).

1.10. Rational of the study

Auto-regulation in enzymes is an evolutionary conserved phenomenon, observed in several classes of enzymes, including kinases, methyltransferases and acetyltransferases. Autoacetylation is essential for the optimal catalytic activity of p300. Interestingly, the phenomenon of autoacetylation has been observed in other KATs as well, such as PCAF (Santos-Rosa et al., 2003) and members of the MYST family such as Esa1, Tip60 (Creaven et al., 1999; Wang and Chen, 2010) and MOF (Sun et al., 2011; Yang et al., 2012). The yeast homolog of p300/CBP, Rtt109 has also been shown to undergo autoacetylation which indicates that the phenomenon of autoacetylation is well conserved (Albaugh et al., 2011).

Earlier structural studies have revealed that p300 alone has a compact spatial conformation, where the substrate-binding groove in the HAT domain is partially obstructed. The induction of autoacetylation in *trans* is possible only when the auto-inhibitory loop is exposed for acetylation. The model proposed by Delvecchio *et al*, predicted that p300 must be present in an active conformation, in which the RING domain is repositioned, to allow efficient substrate-binding to the HAT domain. But the mechanisms governing the conformational switch from an inactive to an active conformation are still unknown (Delvecchio et al., 2013). In a simplistic view, it may be speculated that the modulation of p300 conformation is critical for regulation of its cellular functions. But in the cellular context, p300 can associate with a wide number of proteins, many of which are its substrates. Since p300/CBP play a major role in transcription as transcriptional integrators, it is expected that several proteins may possess the ability to influence their activity, either positively or negatively. To add complexity to this, many previous studies have shown that p300 and its homolog CBP are present in limiting amounts in the cells. Therefore, the importance to optimize the activity of p300/CBP is more relevant under cellular cues which require rapid tuning in transcriptional programs. It is known that p300 and CBP are present in multiprotein complexes in cells therefore their interaction with different factors can modulate the enzymes in terms of both substrate-

specificity as well as activity (Bedford et al., 2010; Dyson and Wright, 2016; Perissi et al., 1999). Thus, the availability of an 'active' or 'inactive' conformation of p300 could be highly dependent on the factors it associates with, which may skew the kinetics of p300 autoacetylation in the cellular context.

Based on the available data, it may be proposed that the activation of p300 catalytic activity is fundamentally a two-step process, wherein the first step involves the switch in conformation from an inactive to an active 'open' conformation and the second step is the *trans*-autoacetylation of the 'exposed' autoinhibitory loop at the substrate-binding groove. Once the substrate-binding pocket is unhindered, p300 can efficiently acetylate its substrate (Figure 1.13). As discussed in the earlier sections, there are many protein factors, which can enhance the levels of p300 autoacetylation. It is intriguing that each of these factors can modulate the autoacetylation and activity of p300 under specific physiological contexts. The contextual modulation of p300 activity is plausibly an efficient optimization of the limited availability of this enzyme in the cell.

Based on the surveyed reports on p300 autoacetylation, the following are the lacunae in the understanding of the phenomenon of p300 autoacetylation:

Existence of the 'active' conformation of p300.

Structural studies have indirectly hinted towards the existence of an 'active' state in p300 conformation, but so far no study has been able to experimentally prove the actuality of this conformation.

The mechanism of factor-induced enhancement of p300 autoacetylation.

Since the reaction of p300 autoacetylation is highly cooperative, following 4th order kinetics, it is evident that two or more molecules of p300 are required to induce autoacetylation. Nature has devised a method to allow other proteins to act as modulator of this process of p300 autoacetylation. But it is unclear whether these 'inducers' act at the stage of conformational switching, or are capable of bringing to two or more molecules of p300 in close vicinity to enhance intermolecular autoacetylation, or are capable of both.

The importance of p300 autoacetylation in terms of transcriptional outcome and chromatin occupancy

To understand the true physiological significance of factor-induced p300 autoacetylation, it is important to decipher the consequences of p300 autoacetylation in the context of

transcriptional networks and chromatin occupancy. A previous study predicted that upon autoacetylation, p300 undergoes substantial conformational alteration which leads to its eviction from the Pre-Initiation Complex (PIC). The authors showed that the dissociation of autoacetylated p300 from the PIC was essential for transcription initiation (Black et al., 2006). This study suggests that p300 is recruited to the chromatin in its unacetylated state, but the experimental data provided in the study was entirely *in vitro*, giving a very limited insight into the occurrence in the cell. The dynamics of p300 autoacetylation in the cellular context is still unknown.

Is the modulation of p300 autoacetylation relevant in the disease scenario?

p300 is important for the maintenance of cell homeostasis, therefore its dysfunction is witnessed in several disease conditions including malignancies, neurodegenerative diseases and metabolic diseases. Under various disease conditions, the expression and function of p300/CBP have been shown to be deregulated, skewing the balance between acetylation and deacetylation. In prostate cancer, hepatocellular carcinoma, and oral cancer, p300 has been shown to be overexpressed, which has been correlated with the aggressiveness and poor prognosis of the disease. But it is clear from the aforementioned studies that merely the control of the stoichiometry of p300 is not enough, rather the catalytic modulation of p300 may also play a pivotal role in its cellular deregulation. Deregulation of p300 autoacetylation is responsible for the global hyperacetylation of histone observed in OSCC. Mechanistically, it is the enhanced autoacetylation of p300, induced by NPM1 and GAPDH in a NO signal-dependent manner, which leads to the alteration of epigenetic landscapes required for the manifestation and progression of qral cancer (Arif et al., 2010b). The study established that p300 is an important epigenetic target for oral cancer. The results demonstrated that inhibition of p300 activity with a small molecule inhibitor (KATi) CTK7A, substantially regressed tumor volume in mouse oral tumor xenografts. Conversely, in the case of neurodegenerative disorders, where there is a loss in CBP/p300 activity due to protein sequestration, small molecule activators (KATa) of p300/CBP autoacetylation and activity such as CSP-TTK21 have immense therapeutic potential. Moreover, specific interaction inhibitors of p300 and its inducers may also serve as a novel therapeutic strategy to disrupt specific p300 autoacetylation-driven pathways without affecting the other functions of this critical epigenetic enzyme.

1.11. Objectives of the study

The overall objective of this study is to decipher the regulation of p300 catalytic activity by various effectors. The study has been divided into three comprehensive parts, each investigating the molecular and functional aspects of factor-mediated p300 autoacetylation.

Earlier observations have suggested that the alteration of acetylation landscape in cancers is closely related to the autoacetylated, hyperactive form of p300. Thus, the current study includes proteins which have important roles in cancer manifestation, have a functional interaction with p300 and are substrates of p300. Based on the available literature and data, the following objectives of this study have been laid:

I. Understanding the mechanisms of NPM1-mediated enhanced p300 autoacetylation.

The first objective is to decipher the mechanism, specificity, and physiological relevance of the histone chaperone NPM1-mediated enhancement of p300 autoacetylation.

II. To characterize a newly identified inducer of p300 autoacetylation: To decipher the mode of mechanism and functional consequences.

Proteins belonging to the tumor suppressors or onco-proteins class, which can either interact with or are substrates of p300 and are closely related to cancer manifestation, were screened for their ability to induce p300 autoacetylation. p53, a key regulator of cell fate, was discovered as a potent inducer of p300 autoacetylation. The study aims to elucidate the molecular mechanisms and physiological relevance of factor-induced p300 autoacetylation.

III. Role of mutant p53 in the induction of p300 autoacetylation.

Interestingly, when p53 is mutated in cancers, it loses its tumor suppressive functions and acquires additional properties which aid in cancer manifestation. Several mutants of p53 were screened for their ability to induce p300 autoacetylation and to investigate the importance of mutant p53-mediated p300 autoacetylation in cancer progression.

Chapter 2

Materials and Methods

This chapter presents a brief overview of the materials and experimental procedures used in this study.

2.1. General Methods

2.1.1. Preparation of competent cells

The bacterial *E. coli* strains: BL21 (DE3), Rosetta(DE3)pLysS, DH5α, XL1-Blue, XL10-Gold cells were streaked on Luria broth (10 gm/l tryptone, 5 gm/l yeast extract, and 10 gm/l NaCl) + 1.5% agar culture plates from respective frozen glycerol stocks. The streaked plates were incubated ~12 hours at 37 °C. A single colony was inoculated into 10 ml Luria Broth (LB) containing 10 mM $MgCl_2$ and 10 mM $MgSO_4$. The culture was grown at 37 °C in an incubator shaker for 12-16 hours. From this primary culture, 1% inoculum was then inoculated into 100 ml of LB. The secondary culture was grown 37 °C in an incubator shaker till the OD_{600} reached 0.35-0.4 (mid log phase). The culture was chilled to 4 °C and pelleted at 3000g for 10 minutes at 4 °C. The pellet was then resuspended in 12 ml TFB1 (30 mM potassium acetate pH 7.5, 100 mM KCl, 10 mM $CaCl_2$, 15% glycerol) and incubated for 60-90 min at 4 °C. After the incubation, the cells were pelleted at 3000g for 10 minutes at 4 °C. The pellet was resuspended in TFB2 (10 mM Na-MOPS, pH 6.8, 10 mM KCl, 75 mM CaCl2, 15% glycerol), made aliquots and flash-frozen in liquid nitrogen.

2.1.2. Transformation of competent cells

An aliquot of *E. coli* competent cells were thawed on ice and ~50 ng of purified plasmid DNA was added. The competent cells in the presence of DNA were incubated for 25 minutes on ice, following which a heat shock at 42 °C was given for 90 seconds. The cells were immediately chilled on ice for around 5 minutes. LB was added to the cells and the cells were allowed to recover at 37 °C in and incubator shaker for around 45 minutes. The transformed cells were subsequently spread over an LB-agar plate containing the appropriate selection antibiotic. The plated cells were then incubated at 37 °C for 12-16 hours.

2.1.3. DNA purification

Plasmids amplified in DH5α, XL10-Gold or XL1-Blue, were isolated using the QIAprep Spin Miniprep Kit (Qiagen) as per the manufacturer's protocol. The quality and quanty of the DNA purified was checked on agarose gels and the NanoDrop 1000 (Thermo Scientific). PCR amplicons and restriction enzyme digested products were purified from agarose gels using the Sigma GenElute Gel Extraction Kit following the manufacturer's protocol. The purified DNA was quality check and quantification was done on the NanoDrop 1000 (Thermo Scientific) by measuring the absorbance at 260 nm of 1 µl of the DNA sample. A_{260} of the value 1 corresponds to 50 ng/µl.

2.1.4. Agarose gel electrophoresis

Agarose (Sigma) gels of the percentage 0.8-1.5% were prepared in 1X TBE (90 mM Tris-Borate and 2mM EDTA, pH 8.3), to separate nucleic acids (DNA/RNA) by size. The nucleic acid samples were prepared in 6X loading buffer (0.25% bromophenol blue, 0.25% xylene cyanol, 30 % glycerol) to a final concentration of 1X. The samples were loaded into the gel wells submerged in 1X TBE buffer. The gel was run at 5V/cm. The agarose gel was stained in 0.5 mg/ml Ethidium Bromide (EtBr) solution and destained in water. The EtBr stained DNA/RNA samples were visualized and imaged under a UV illuminator in the BIO-RAD Gel Documentation System.

2.1.5. SDS-polyacrylamide gel electrophoresis (SDS-PAGE)

Proteins, either recombinant or cell lysates, were resolved on 8-15% SDS-PAGE, depending on their molecular weight. The resolving portion of the gel was made by adding the required volume (depending on the desired gel %) of 30% solution of acrylamide/ bisacrylamide (29% acrylamide, 1% bisacrylamide), 0.375 M Tris-HCl pH 8.8, 0.1% sodium dodecyl sulphate (SDS), 0.1% ammonium persulphate (APS) and 0.04% TEMED (N,N,N',N'-tetramethylethylenediamine). The stacking portion of the gel was made by adding 5% acrylamide, 0.125 M Tris-HCl pH 6.8, 0.1% SDS, 0.1% APS and 0.1% TEMED. The protein samples were prepared in 5X SDS gel loading buffer (50 mM Tris-HCl pH 6.8, 2% SDS, 0.1% bromophenol blue, 10% glycerol, 1% β-mercaptoethanol) to a final concentration of 1X. The samples were boiled at 90 °C for 5-10 minutes and loaded into the wells of the gel, mounted on a vertical electrophoresis system (Mini-PROTEAN® Tetra Vertical Electrophoresis Cell, BIO-RAD). The gels were run electrophoresis buffer consisting of 25 mM Tris, 250 mM glycine pH 8.3, 0.1% SDS, at a constant voltage of 150V. The protein

bands were stained with Coomassie Brilliant Blue (CBB) staining solution (40% methanol, 10% acetic acid, 0.25% CBB). Once the gels were stained the excess background staining was removed using destaining solution consisting of 40% methanol and 10% acetic acid. The gels were imaged and dried for storage.

2.1.6. Silver Staining

To detect proteins on a polyacrylamide gel with high sensitivity (in the nanogram range), silver staining of gels is preferred over CBB staining. The proteins are electrophoresed on a polyacrylamide gel followed by fixing in 40% methanol and 10% glacial acetic acid in water. The gel was allowed to fix for 2 hours to overnight. The gel was then rinsed thrice in 50% ethanol in water. The proteins were sensitized with 0.02% sodium thiosulfate for 2 minutes then rinsed in deionized water for a minute. The gel was then incubated with 0.1% silver nitrate for 20 minutes at room temperature. The gels were then rinsed thrice with deionized water. The gel was developed in freshly prepared 0.04% formalin/2% sodium carbonate (~4-20 minutes). The reaction was stopped in 1% glacial acetic acid. The gel was imaged and then stored in 1% glacial acetic acid.

2.2. Cloning

2.2.1. Sub-cloning of p53 wildtype and hot-spot mutants into pCMV2

The untagged wildtype p53 and missense mutant p53 constructs were amplified from the mammalian expression vector pCMV-Neo-Bam p53 plasmids (Table 2.1). The PCR amplified genes and pFLAG-CMV™-2 Mammalian Expression Vector were double digested by BamHI-HF and HindIII-HF restriction enzymes (New England Biolabs) and ligated by T4 DNA Ligase enzyme (New England Biolabs). The clones were confirmed by insert release upon double digestion with BamHI-HF and HindIII-HF restriction enzymes (Figure 2.1). The positive clones were further confirmed by sequencing.

Gene Name	Forward (5'-3')	Reverse (5'-3')
p53	CCCAAGCTTATGGAGGAGCCGCAGTC	CGCGGATCCTCAGTCTGAGTCAGGC

Table 2.1: Primers used in the subcloning of p53 construct into pFLAG-CMV™-2 Mammalian Expression Vector.

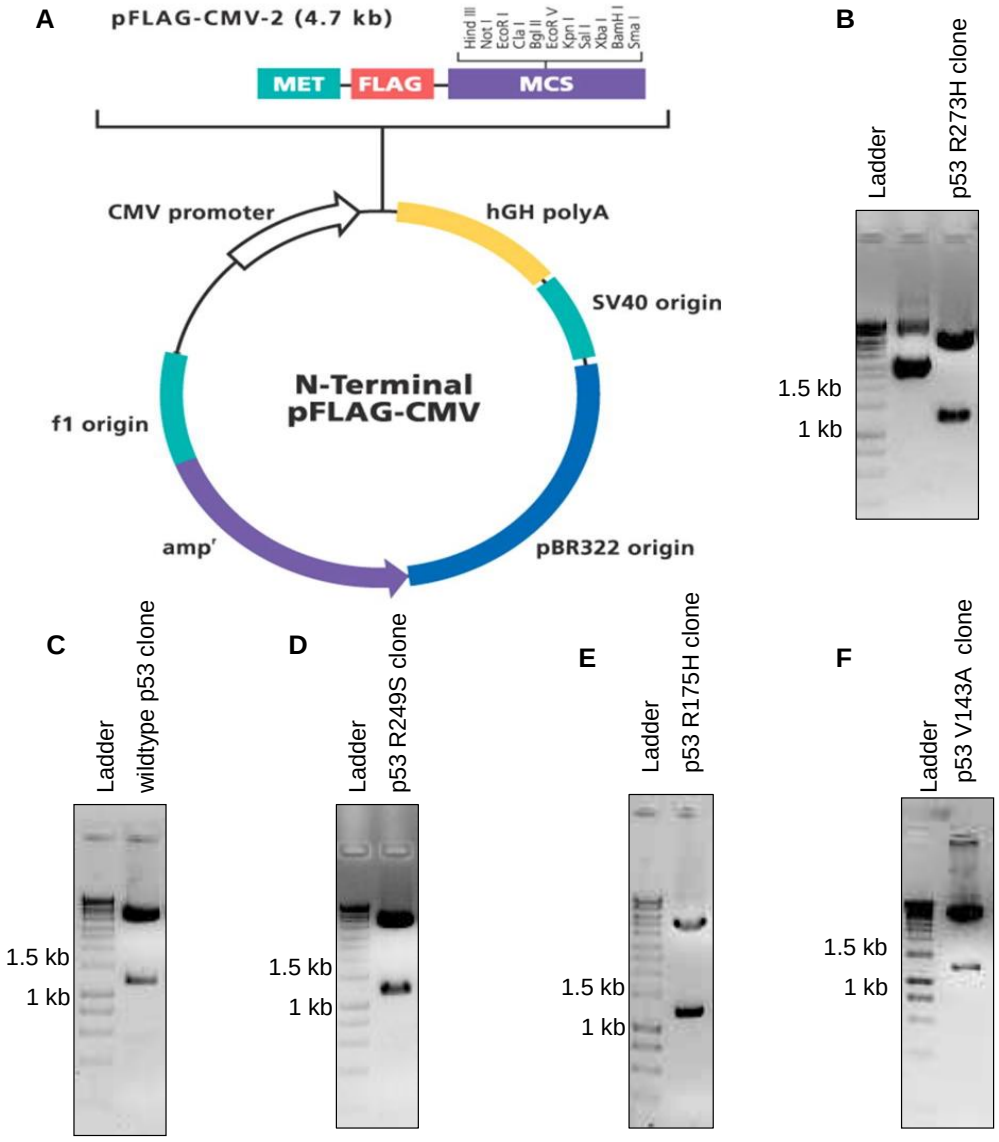

Figure 2.1: Subcloning p53 construct (wildtype/mutant) into pFLAG-CMV™-2 Mammalian Expression Vector. (A) Vector Map of pFLAG-CMV™-2 Mammalian Expression Vector. Subcloning of (B) R273H p53, (C) wildtype p53, (D) R249S p53, (E) R175H p53, (F) V143A p53, into the pFLAG-CMV™-2 Mammalian Expression Vector. Clones were confirmed by double digestion with HindIII-HF and BamHI-HF restriction enzymes (New England Biolabs) with an insert release of 1.3 kb.

2.2.2. Site-directed Mutagenesis

Point mutants were generated using Site Directed Mutagenesis (SDM) method. The point mutants were created by using primers harboring the necessary nucleotide(s) change. Pfu-Ultra polymerase was used for the SDM PCR reaction. Following the PCR, the reaction was treated with DpnI restriction enzyme, for 2 hours at 37 °C, to cleave the methylated parental plasmid, such that only the mutated plasmids remain. A portion of the reaction mixture was transformed into XL1-BLUE super-competent cells. The point mutants were confirmed by

sequencing. Single point mutants of p53 were generated using Site Directed Mutagenesis (SDM) method. pFLAG-CMV™-2-p53 wildtype or pET22b-p53 wildtype plasmids were used as the template for the SDM. Sequences of the primers used are listed in Table 2.2. Chromatograms confirming the incorporation of the point mutation are presented in Figure 2.2.

Gene Name	Forward (5'-3')	Reverse (5'-3')
L344A p53	CGAGATGTTCCGAGAGGCGAATGAGGCCTTGG	CCAAGGCCTCATTCGCCTCTCGGAACATCTCG
G334V p53	CACCCTTCAGATCCGTGTGCGTGAGCGCTTCGAG	CTCGAAGCGCTCACGCACACGGATCTGAAGGGTG
R337H p53	GATCCGTGGGCGTGAGCACTTCGAGATGTTCCGAG	CTCGGAACATCTCGAAGTGCTCACGCCCACGGATC
R175H p53	GACGGAGGTTGTGAGGCACTGCCCCCACCATGAG	CTCATGGTGGGGGCAGTGCCTCACAACCTCCGTC
R249S p53	GGGCGGCATGAACCGGAGCCCCATCCTCACCATC	GATGGTGAGGATGGGGCTCCGGTTCATGCCGCCC
V143A p53	GCCAAGACCTGCCCTGCGCAGCTGTGGGTTGATTC	GAATCAACCCACAGCTGCGCAGGGCAGGTCTTGGC
R248W p53	GCATGGGCGGCATGAACTGGCGCCCCATCCTCACCATC	GATGGTGAGGATGGGGCGCCAGTTCATGCCGCCCATGC
R273H p53	GGAACAGCTTTGAGGTGCATGTTTGTGCCTGTCCTGGG	CCCAGGACAGGCACAAACATGCACCTCAAAGCTGTTCC
R280K p53	GTTTGTGCCTGTCCTGGGAAAGACCGGCGCACAGAGG	CCTCTGTGCGCCGGTCTTTCCCAGGACAGGCACAAAC
D281G p53	GCCTGTCCTGGGAGAGGCCGGCGCACAGAGG	CCTCTGTGCGCCGGCCTCTCCCAGGACAGGC
L194F p53	GCCCCTCCTCAGCATTTTATCCGAGTGGAAG	CCTCCGGTTCATGCTGCCCATGCAGGAAC

Table 2.2: List of Primers used in creating Site Directed Mutants of p53.

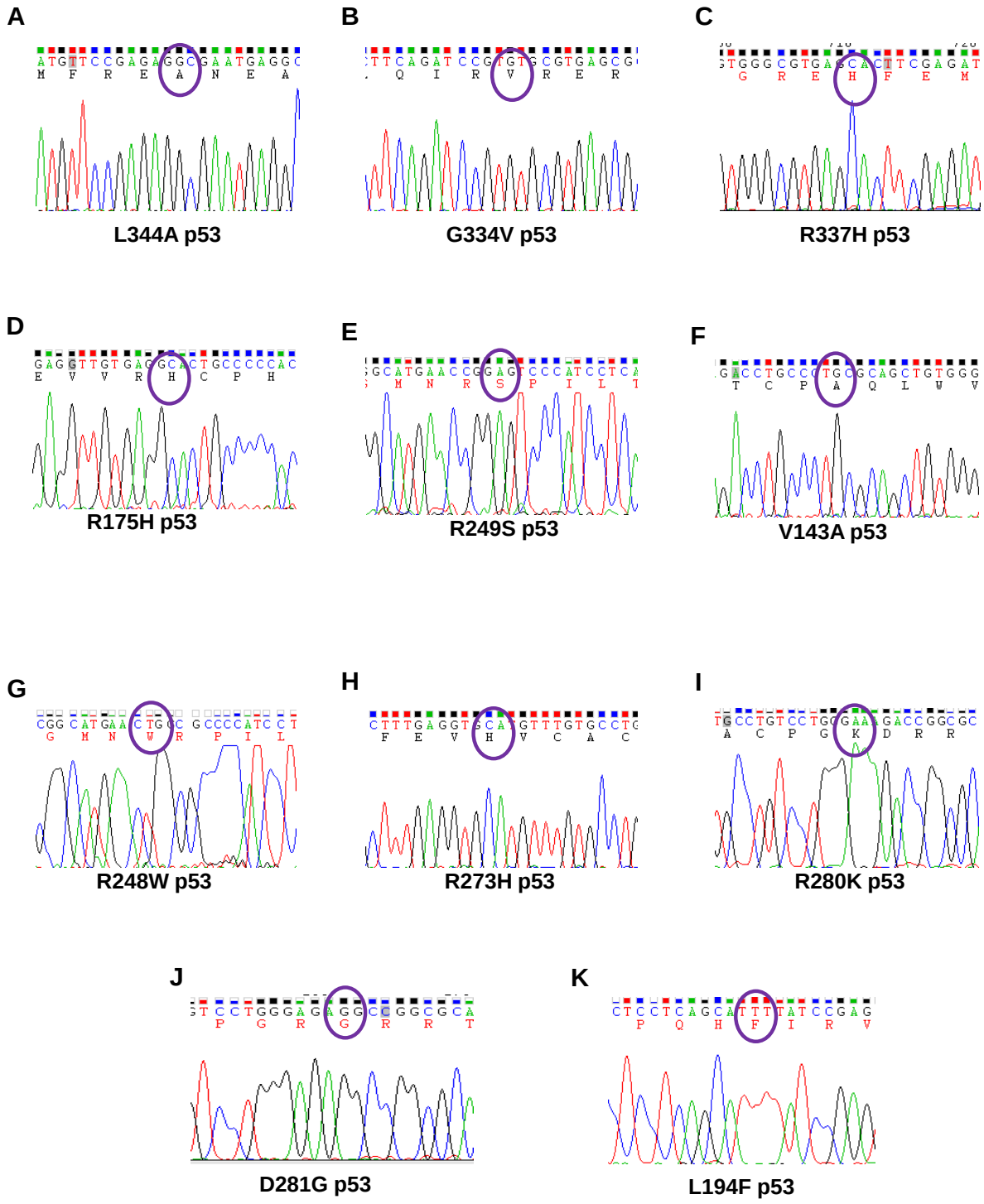

Figure 2.2: Introduction of single amino acid changes into wildtype p53 construct in the pFLAG-CMV™-2 Mammalian Expression Vector and in the pET22b bacterial expression plasmid. The chromatograms confirming the introduction of the single site mutations creating the following p53 mutants: (A) L344A p53, (B) G334V p53, (C) R337H p53, (D) R175H p53, (E) R249S p53, (F) V143A p53, (G) R248W p53, (H) R273H p53, (I) R280K p53, (J) D281G p53 and (K) L194F p53.

Double mutant of NPM1 were generated using the SDM method. pET28b-NPM1 wildtype plasmids were used as the template for the SDM. Sequences of the primers used are listed in Table 2.3. Chromatogram confirming the incorporation of the point mutation is presented in Figure 2.3.

Gene Name	Forward (5'-3')	Reverse (5'-3')
NPM1 WW288, 290FF	GGCTATTCAAGATCTCTTTCA GTTTAGGAAGTCTCTT	AAGAGACTTCCTAAACTGAAAGAGATCTT GAATAGCCCGCGGATCCTCAGTCTGAGT CAGGC

Table 2.3: Primers used in creating Site Directed Mutants of NPM1.

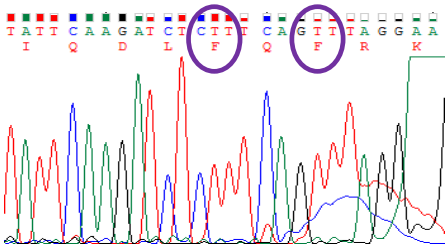

WW288,290FF NPM1

Figure 2.3: Introduction of double amino acid changes into wildtype NPM1 construct in the pET28b bacterial expression plasmid. The chromatogram confirming the introduction of the double site amino acid mutations creating the NPM1 Trp mutant, WW288,290FF NPM1.

2.2.3. Sub-cloning of p53 wildtype and hot-spot mutants into pEBTetD vector

The FLAG-tagged p53 construct was subcloned into the Tet-ON mammalian expression plasmid pEBTetD (a kind gift from Prof. Gründemann, University of Cologne, Germany (Bach et al., 2007)). The construct was amplified using a forward primer designed against the FLAG-tag containing a KpnI restriction site and a reverse primer specific to the 3' end of p53 containing a XhoI restriction site (Table 2.4). The PCR amplified p53 construct and pEBTetD mammalian expression vector were double digested by KpnI-HF and XhoI restriction enzymes (New England Biolabs) and ligated by T4 DNA Ligase enzyme (New England Biolabs). The clones were confirmed by insert release upon double digestion with KpnI-HF and XhoI restriction enzymes (Figure 2.4). The positive clones were further confirmed by sequencing.

Gene Name	Forward (5'-3')	Reverse (5'-3')
p53	CGGGGTACCATGGACTACAAAGACGATG (FLAG-KpnI Forward primer)	CCGCTCGAGTCAGTCTGAGTCAGGCCC

Table 2.4: List of Primers used in subcloning p53 constructs into the pEBTetD Tet-ON mammalian expression plasmid.

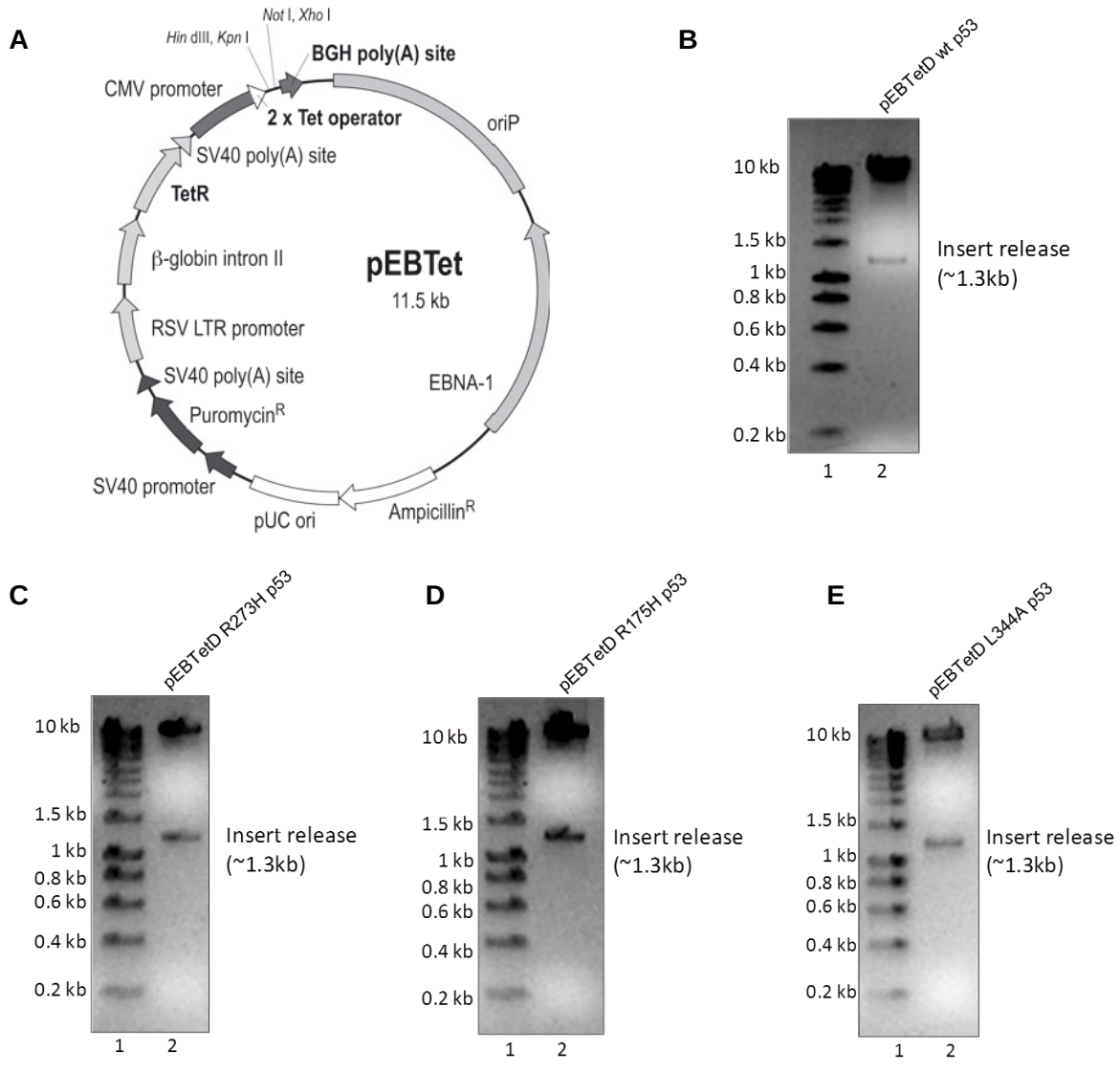

Figure 2.4: Subcloning p53 construct (wildtype/mutant) into pEBTetD Tet-ON Inducible Mammalian Expression Vector. (A) Vector Map of pEBTetD Mammalian Expression Vector. Subcloning of (B) wildtype p53, (C) R273H p53, (D) R175H p53, and (E) L344A p53, into the pEBTetD Mammalian Expression Vector. Clones were confirmed by double digestion with KpnI-HF and XhoI restriction enzymes (New England Biolabs) with an insert release of 1.3 kb.

2.3. Cell culture

2.3.1. Mammalian cell culture

H1299 (human non-small cell lung carcinoma), HepG2 (hepatocellular carcinoma), MCF7 (mammary gland carcinoma cells isolated from metastatic site) and HEK293 (human embryonic kidney) cells were procured from American Type Culture Collection (ATCC) (Figure 2.6B-E). AW13516 cells, a human cell line derived from the Oral cavity squamous cell carcinoma, was a kind gift from Dr. Amit Dutt (ACTREC, Mumbai, India) (Figure 2.6A). H1299 cells were grown in RPMI-1640 media, HepG2, MCF7 and AW13516 cells were grown in Minimum Essential Media (MEM) and HEK293 cells in Dulbecco's Modified Eagle's Media. Each of these media was supplemented with 2 mM glutamine, antibiotic solution (penicillin, streptomycin, amphotericin) and 10% fetal bovine serum (FBS). The cell stocks were stored in liquid nitrogen. The growth medium for MCF7 cells was also supplemented with 0.01 mg/ml human recombinant insulin in addition to the basic media requirements. To revive the cell lines, the stocks were quickly thawed in 37 °C waterbath, then the stocks were diluted 10 times in supplemented media containing 10% FBS (complete media). The cells were pelleted at 1000 rpm for 3 minutes at room temperature. The pelleted cells were resuspended in 5 ml of fresh complete media and seeded into a T25 flask (eppendorf). The cells were grown in a monolayer in complete media, with fresh media supplemented every 2-3 days. The cells were grown at 37 °C, 5% CO2 in a humidified incubator. When the cells reached a confluency of 80-90%, they were passaged by removing the spent media. The cells were gently washed with 1X PBS (Hi-Media, cell culture grade) to ensure all the media was removed, following which 1 ml of 0.25% Trypsin-0.53 mM EDTA was added to the cells and incubated at 37 °C in the CO_2 incubator till the cells detached from the flask polystyrene growth surface. The trypsinization process was stopped in fresh complete media. The cells were collected and pelleted at 1000 rpm for 3 minutes. The cells were pelleted in complete media, counted using a hemocytometer (Neubauer's Chamber) and seeded for experiments in the desired numbers. For cell stock preparation, the cells were trypsinized and collected as mentioned before. The cells were then resuspended in freezing mixture (40% incomplete media, 50% FBS and 10% DMSO), distributed into cryovials and stored in -80 °C, in cell freezing containers where the cell stocks freeze slowly (-1 °C/ min). After 24 hours the frozen stocks were then transferred to liquid nitrogen storage cylinders.

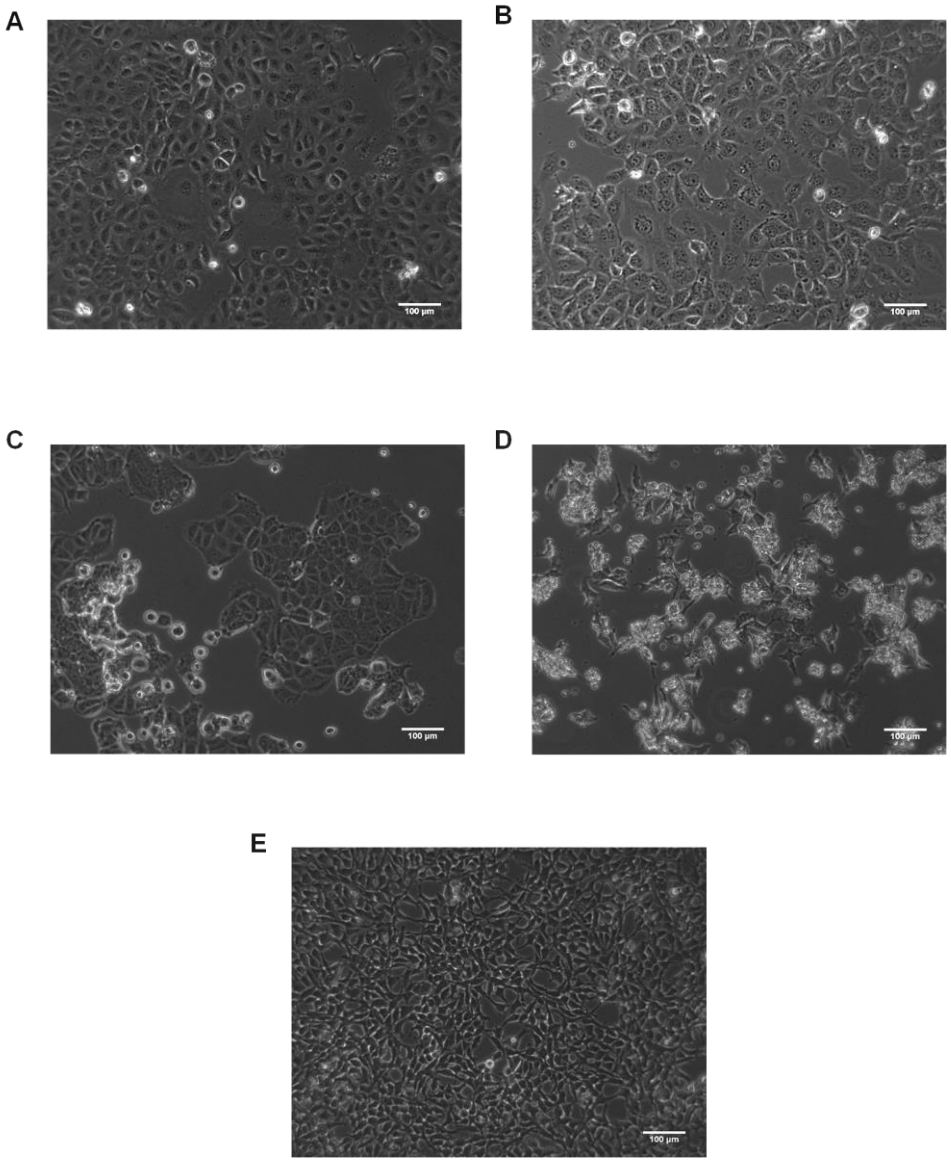

Figure 2.5: Morphological characteristics of mammalian cells grown in a monolayer. (A) AW13516, (B) H1299, (C) MCF7, (D) HepG2, and (E) HEK293 cells, imaged at 10X magnification. Scale bar represents 100 µm.

2.3.2. Insect cell culture

The insect ovarian cell line sf21 derived from *Spodoptera frugiperda* was procured from Invitrogen (ThermoScientific) (Figure 2.6A). The frozen cell stock was thawed quickly at 37 °C and diluted 10 times in Grace's media supplemented with antibiotics and 10% FBS. The cells were seeded into a T75 flask and allowed to adhere to the polystyrene growth surface for about 45 minutes- 1 hour. The media was changed to remove the DMSO from the freezing mixture and any unattached cells. The cells were incubated at 27 °C in a BOD incubator. Once the cells reached 70% confluency, the spent media was removed, fresh media

was added to the flask and the adherent cells were gently scraped off with a cell scraper. The cells were sub-cultured and cell number was expanded till there were sufficient cells to set up baculo-virus transfection-based recombinant protein expression. Stocks were made by scraping off the adherent cells, pelleting at 700g for 5 mins. The pelleted cells were then resuspended in freezing mixture (40% Grace's, 50% FBS and 10% DMSO), distributed into cryovials and stored in -80 °C, in cell freezing containers. The cell stocks were transferred into liquid nitrogen storage cylinders after 24 hours.

2.3.3. Baculovirus amplification

The sf21 cells were infected with high titre recombinant protein baculovirus stock (~ 2 x 10^8pfu/ml). Around 6-9 x 10^6 cells were used per flask for the amplification of recombinant virus. The flask was wrapped in Aluminium foil to protect the virus from direct light. The cells were observed after 48 hours for traces of virus infection. Deformed nuclei, elongated and floating cells are hallmarks of a successful infection (Figure 2.6B). The baculovirus was harvested once the cells had burst or exhibited severe features of infection (around 5-7 days post infection). The cell debris was pelleted at 4000 rpm for 5 minutes. The supernatant containing the amplified virus was collected and filter sterilized through a 0.22 µ filter. For regular usage the virus was stored at 4 °C, for storage the virus was frozen at -80 °C.

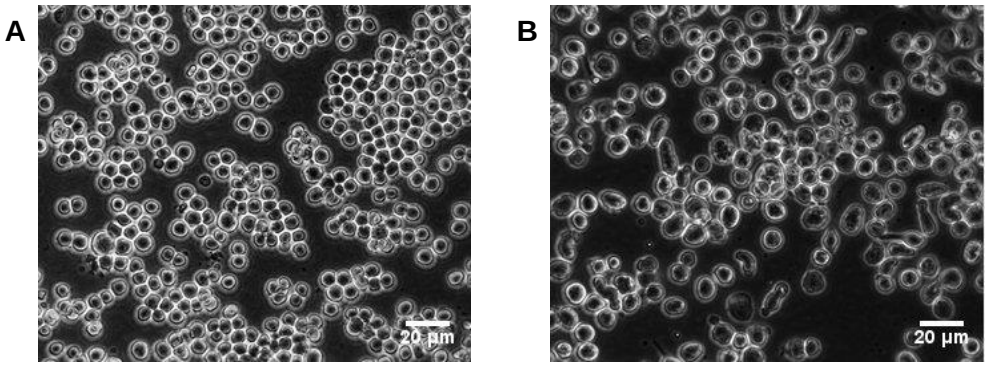

Figure 2.6: Morphological characteristics of the insect cell line sf21. (A) uninfected sf21 insect cells, (B) sf21 cells infected with recombinant baculovirus. Scale bar represents 20 µm.

2.3.4. Transfection

H1299 cells were transfected with purified mammalian expression plasmids using the Lipofectamine2000 reagent (Invitrogen) as per the manufacturer's protocol. The DNA dissolved in incomplete media and Lipofectamine2000 in incomplete media were mixed in a 1:1 (v:v) ratio. The DNA-Lipofectamine complex was allowed to stand for 5 minutes before

adding it to the cells in incomplete media. The incomplete media was replaced with fresh complete media after 4-6 hours post transfection.

2.3.5. Generation of stable cell lines

A doxycycline-inducible expression system for p53 and p53 mutants were made in H1299 cell line. The p53 GOI was cloned into the pEBTetD vector backbone. The plasmid harboured puromycin-resistance gene, thus a kill-curve was performed on the H1299 cell line to determine the lowest concentration of puromycin at which all the cells died (1.2 µg/ml puromycin). The cells were then transfected with 1.5 µg p53/ p53 mutant pEBTetD plasmid. The cells harbouring the episomal plasmids were selected under 1.2 µg/ml puromycin selection. The cells were characterized by western and qPCR. Once the cells were characterized, cell stocks were prepared and transferred from -80 °C to liquid nitrogen for long-term storage.

2.4. Cell-based assays

2.4.1. Immunofluorescence

H1299, HepG2, AW13516, and HEK293 cells were grown on poly-lysine coated cover slips at 37 °C in a 5% CO_2 incubator. The media was removed and the cell layer was washed in PBS to ensure all the media was removed. The cells were fixed in 4% para-formaldehyde for 10 minutes at room temperature. The cells were washed with PBS to remove the remnant PFA. The cells were then permeabilized in 5% Triton X-100. Cells were washed in PBS to remove the residual TritonX-100. The cells were blocked in blocking solution (5% FBS in PBS) at 37 °C for 45 minutes. The blocked cells were then incubated in primary antibody at the indicated dilution for 1 hour at room temperature on a reciprocal shaker. The cells were washed in washing buffer (1% FBS in PBS). The number of washes is standardized to remove any background (usually 2-3 washes). The cells were then incubated in Alexa-fluor conjugated secondary antibody corresponding to the primary antibody used, incubated at room temperature for 1 hour. Cells were washed in washing buffer. The nucleus was counter-stained with Hoechst 33258 (bis-benzamide (Sigma)), a fluorescent dye which emits blue fluorescence for 5 minutes at room temperature (in the dark). Excess Hoechst stain was washed off with PBS. The cover slips were mounted (inverted) in 70% glycerol onto a microscope glass slide. The stained cells were visualized using Carl Zeiss confocal microscopes LSM 510 META or the LSM 880 with Airyscan.

2.4.2. RNA isolation

Total RNA was isolated from different cell lines using TRIzol reagent (Invitrogen) according to the manufacturer's protocol. To lyse the cells, appropriate volume of TRIzol is added to the cells (1ml TRIzol per 10 cm^2 growth area = 1 ml TRIzol per ~10^6 cells), incubated at room temperature for 2 minutes. The TRIzol lysate was collected in a DEPC-treated microfuge tube and chloroform was added (0.2 ml per 1 ml of TRIzol), mixed thoroughly and incubated at room temperature for 2-3 minutes. The lysate was centrifuged at 12000g for 10 minutes at 4 °C and the aqueous phase containing the RNA was collected. The RNA was precipitated with equal volumes of isopropanol incubated at room temperature for 10 minutes. The RNA was pelleted at 12000g for 10 minutes at 4 °C. The pellet was washed with 75% ethanol and centrifuged at 12000g for 5 minutes. The wash was discarded and the pellet was allowed to air-dry. Once the pellet was dried, it was dissolved in nuclease-free water. The RNA was quantified on a Nanodrop1000 Spectrophotometer wherein the A260 value for 1 corresponds to 40 ng/µl of RNA. The quality of the RNA was determined by the A260/A280 ratio, where a ratio of 2 is indicative of pure RNA. The integrity of the RNA was further checked on a 0.8 % non-denaturing agarose gel. Distinct bands corresponding to the 28S and 18S rRNA indicated that the RNA was not denatured (Figure 2.7). The purified RNA was stored at -80 °C.

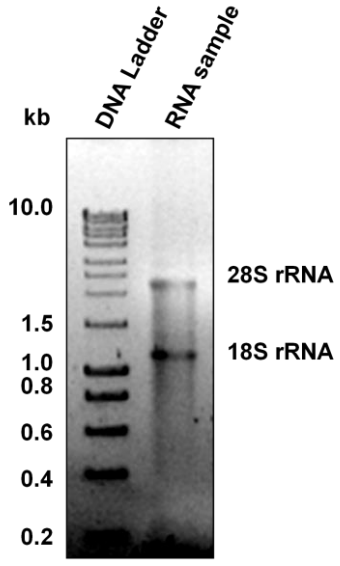

Figure 2.7: RNA profile. RNA purification profile on a 1% non-denaturing agarose gel.

2.4.3. Small Molecule Inhibitor or Peptide treatment

HepG2 cell line was treated with small molecule inhibitor Nutlin3a (5 µM, 10 µM or 20 µM) for 24 hours. Stabilization of p53 and status of p300 autoacetylation and acetylation of p300-substrates were determined by western blotting analysis and immunofluoorescence.

For the p53-p300 interfering peptides, HepG2 cells and H1299 p53 inducible expression lines were treated with the indicated concentrations of peptides for 24 hours. Induction of wildtype p53 or mutant p53 protein levels were achieved by treating the cells with either nutlin3 or doxycycline (for the Tet-ON p53 expression stable lines) for 24 hours, post peptide treatment. To study the effects of the peptides on p53-mediated modulation of p300 activity, western blotting analysis and wound healing assays were performed.

2.4.4. Wound Healing Assay

Cells were grown in a 30 mm dish or a 6-well plate. When the cells reach ~90% confluency, a scratch was created with a 0.5 µl tip held at a 45° angle. The cells were given a media change to remove all the floating cells. The wound created was monitored over a period of 24 hours to 48 hours till the wound closed. Images of the progress were taken at regular intervals.

2.4.5. Chromatin Immunoprecipitation (ChIP)

Around 10 million cells were used for each ChIP. The cells are crosslinked in 1% formaldehyde. The crosslinking was quenched in 0.125M glycine. The cells were lysed in SDS buffer and the chromatin was sheared using Diagenode ChIP sonicator (Figure 2.8). 10% of the total lysate volume was kept aside as the input. The lysates were pre-cleared with BSA-blocked protein-G sepharose beads. 5-10 µg antibody was used in each ChIP. The antibody and BSA-blocked protein G sepharose beads were added the cleared lysates and incubated at 4 °C overnight. The beads were then washed to remove non-specific binding with buffers containing different salt concentrations. The DNA-protein complexes were eluted from the washed beads using SDS-sodium bicarbonate elution buffer. The eluates and input were decrosslinked at 65 °C for 4 hours. Proteinase K and RNase H were added to the decross-linked lysates to remove the proteins and RNA. The DNA was extracted using phenol:chloroform:isoamyl alcohol method. The DNA was precipitated at -20 °C, overnight, using sodium acetate, glycogen in 100% ethanol. The DNA pellet was washed in 70% ethanol and dissolved in nuclease-free water.

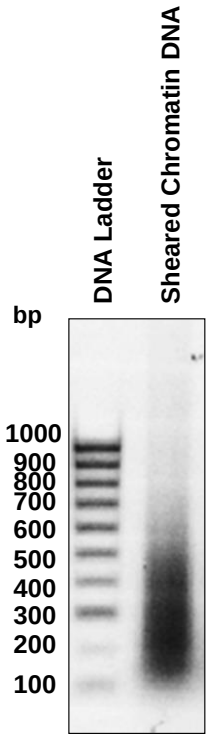

Figure 2.8: Sheared Chromatin profile for ChIP. Sonication of crosslinked chromatin was done in the Diagenode ChIP Sonicator for 15 minutes (3 cycles of 5 x 30 second pulses).

2.5. Recombinant Protein Purification

2.5.1. p300

His_6-tagged full length p300 protein was expressed by transfection of the recombinant baculovirus into Sf21 (*Spodoptera frugiperda*) insect ovary cells. 72 hours post infection the cells were harvested by scraping and were pelleted at 2000 rpm for 10 minutes at 4 °C. The cells were resuspended in chilled homogenization buffer (20 mM Tris-HCl pH 7.4, 10% glycerol, 2 mM β-mercaptoethanol, 0.2 mM EDTA, 2 mM PMSF, 0.1% NP-40, 50 µg/ml leupeptin and 50 µg/ml aprotinin, 15 mM imidazole and 500 mM NaCl). The cells were lysed on ice in the Dounce's Homogenizer (Wheaton) in 5 rounds of 7 strokes each using the tight pestle. The cell debris was then pelleted from the lysed cell suspension at 16,000 rpm for 30 minutes at 4 °C. The supernatant was then allowed to bind to the Ni-NTA beads at 4 °C on an end-to-end rotor for 2 hours and 30 minutes. The bound resin was washed eight times in wash buffer containg 20 mM Tris-HCl pH 7.4, 10% glycerol, 2 mM β-mercaptoethanol, 0.2 mM EDTA, 2 mM PMSF, 0.1% NP-40, 15 mM imidazole and 300 mM NaCl. The protein was eluted in buffer (20 mM Tris-HCl pH 7.4, 10% glycerol, 2 mM β-mercaptoethanol, 0.2 mM EDTA, 2 mM PMSF, 0.1% NP-40) containing 100 mM NaCl and 250 mM imidazole. The

integrity of the protein was examined on an 8% SDS-PAGE. The protein samples were prepared in 1X SDS loading buffer containing β-mercaptoethanol followed by denaturation at 90 °C for 5 minutes. The protein bands were visualized by staining the gel in Coomassie Brilliant Blue (Figure 2.9A) and the acetyltransferase activity of the enzyme was checked in a gel assay (Figure 2.9B). The purified protein was flashed-frozen in liquid nitrogen and stored at -80 °C.

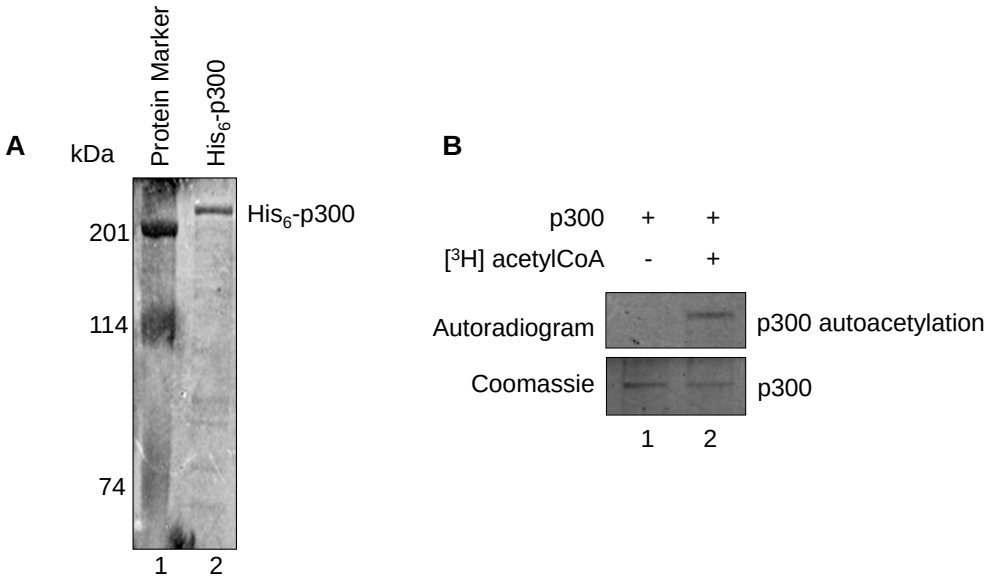

Figure 2.9: Protein purification profile of His_6-tagged-p300. (A) Protein purification profile of recombinant baculovirus expressed His_6-tagged-p300 protein on an 8% SDS-PAGE. (B) The activity of the purified p300 enzyme was determined by its ability to autoacetylate itself, as shown in the autoradiogram (upper panel). The lower panel is the CBB stained protein loading control.

2.5.2. PCAF

For the purification of FLAG-tagged PCAF protein, the Sf21 cells were harvested 60 hours post infection the cells were harvested by scraping and were pelleted at 2000 rpm for 10 minutes at 4 °C. The cells were resuspended in 10 ml of chilled homogenization buffer (20 mM Tris-HCl pH 7.4, 20% glycerol, 4 mM MgCl2, 2 mM DTT, 0.4 mM EDTA, 20 mM β-glycerophosphate, 0.4 mM PMSF, 0.1% NP-40, 50 µg/ml leupeptin and 50 µg/ml aprotinin and 500 mM NaCl) and 5 ml of chilled dilution buffer (20 mM Tris-HCl pH 7.4, 10% glycerol and 0.02% NP-40). The cells were lysed on ice in the Dounce's Homogenizer (Wheaton) in 6 rounds of 6 strokes each using the tight pestle. The cell debris was then pelleted from the lysed cell suspension at 16,000 rpm for 30 minutes at 4 °C. The supernatant was then allowed to bind to the M2-agarose beads at 4 °C on an end-to-end rotor for 3 hours.

The bound resin was washed eight times in wash buffer containing 20 mM Tris-HCl pH 7.4, 15% glycerol, 2 mM MgCl2 10 mM β-glycerophosphate, 0.2 mM EDTA, 0.2 mM PMSF, 0.1% NP-40 and 150 mM NaCl. The protein was eluted in BC-100 buffer (20 mM Tris-HCl pH 7.4, 10% glycerol, 2 mM β-mercaptoethanol, 0.2 mM EDTA, 2 mM PMSF, 0.1% NP-40) containing 100 mM NaCl and 200 ng/µl 3X FLAG peptide. The integrity of the protein was examined on a 12% SDS-PAGE. The protein samples were prepared in 1X SDS loading buffer containing β-mercaptoethanol followed by denaturation at 90 °C for 5 minutes. The protein bands were visualized by staining the gel in Coomassie Brilliant Blue (Figure 2.10A) and the acetyltransferase activity of the enzyme was checked in a gel assay (Figure 2.10B). The purified protein was flashed-frozen in liquid nitrogen and stored at -80 °C.

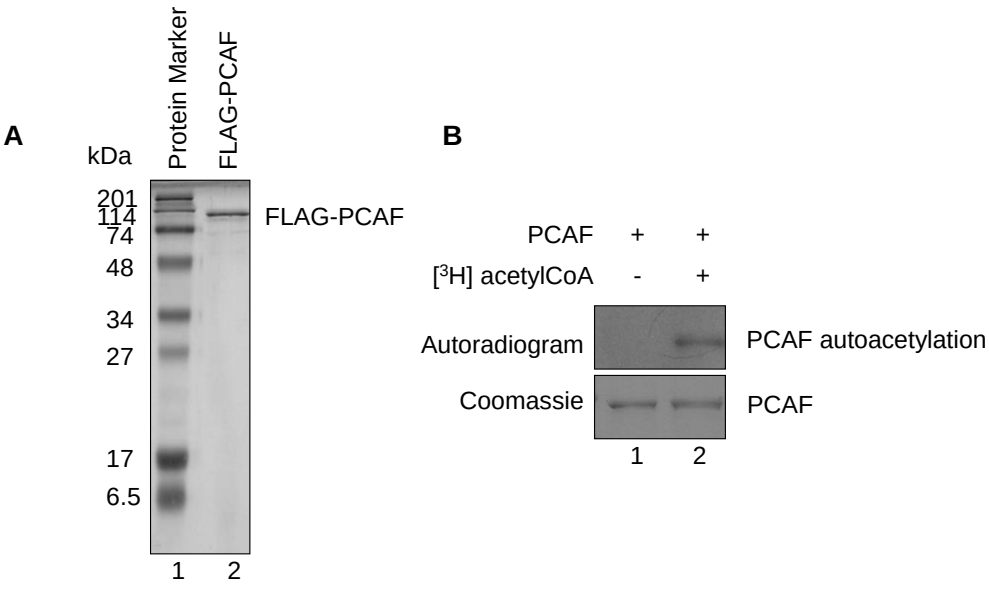

Figure 2.10: Protein purification profile of FLAG-tagged-PCAF. (A) Protein purification profile of recombinant baculovirus expressed FLAG-PCAF protein on a 12% SDS-PAGE. (B) The activity of the purified PCAF enzyme was determined by its ability to autoacetylate itself, as shown in the autoradiogram (upper panel). The lower panel is the CBB stained protein loading control.

2.5.3. Tip60

His6-tagged full length Tip60 protein was expressed by transfection of the respective recombinant baculovirus into Sf21 (*Spodoptera frugiperda*) insect ovary cells. 66 hours post infection the cells were harvested by scraping and were pelleted at 2000 rpm for 10 minutes at 4 °C. The cells were resuspended in chilled homogenization buffer (20 mM Tris-HCl pH 7.4, 10% glycerol, 2 mM β-mercaptoethanol, 0.2 mM EDTA, 2 mM PMSF, 0.1% NP-40, 50 µg/ml leupeptin and 50 µg/ml aprotinin, 15 mM imidazole, and 500 mM NaCl). The cells

were lysed on ice in the Dounce's Homogenizer (Wheaton) in 5 rounds of 7 strokes each using the tight pestle. The cell debris was then pelleted from the lysed cell suspension at 16,000 rpm for 30 minutes at 4 °C. The supernatant was then allowed to bind to the Ni-NTA beads at 4 °C on an end-to-end rotor for 2 hours and 30 minutes. The bound resin was washed eight times in wash buffer containg 20 mM Tris-HCl pH 7.4, 10% glycerol, 2 mM β-mercaptoethanol, 0.2 mM EDTA, 2 mM PMSF, 0.1% NP-40, 15 mM imidazole and 300 mM NaCl. The protein was eluted in buffer (20 mM Tris-HCl pH 7.4, 10% glycerol, 2 mM β-mercaptoethanol, 0.2 mM EDTA, 2 mM PMSF, 0.1% NP-40) containing 100 mM NaCl and 250 mM imidazole. The integrity of the protein was examined on a 12% SDS-PAGE. The protein samples were prepared in 1X SDS loading buffer containing β-mercaptoethanol followed by denaturation at 90 °C for 5 minutes. The protein bands were visualized by staining the gel in Coomassie Brilliant Blue (Figure 2.11A) and the acetyltransferase activity of the enzyme was checked in a gel assay (Figure 2.11B). The purified protein was flashed-frozen in liquid nitrogen and stored at -80 °C.

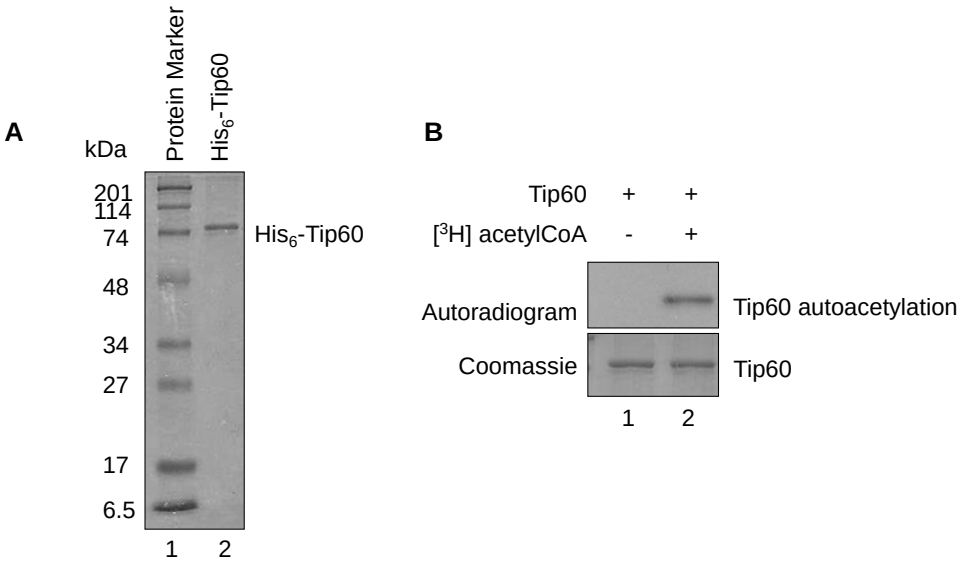

Figure 2.11: Protein purification profile of His_6-tagged-Tip60. (A) Protein purification profile of recombinant baculovirus expressed His_6-tagged-Tip60 protein on a 12% SDS-PAGE. (B) The activity of the purified Tip60 enzyme was determined by its ability to autoacetylate itself, as shown in the autoradiogram (upper panel). The lower panel is the CBB stained protein loading control.

2.5.4. p53 wildtype and mutants

FLAG-p53 and FLAG-p53 were expressed and purified from BL21 (DE3) E. coli strain. The proteins of interest were expressed by inoculating primary culture with a single colony which was allowed to grow over-night at 37 °C in LB medium under ampicillin selection (100

µg/ml) in a shaker incubator (180 rpm). The over-night culture was inoculated into a secondary culture (10% inoculum) which was then allowed to grow at 37 °C in LB medium under ampicillin selection till the OD600 reached 0.4. The bacterial culture was then induced with 0.4 mM IPTG, and grown at 37 °C for 3 hours. The cells were harvested by centrifugation at 6000 rpm for 10 mins at 4 °C. The pelleted cells were then lysed in BC-300 lysis buffer (20 mM Tris-HCl pH 7.4, 20% glycerol, 2mM β-mercaptoethanol, 0.2 mM EDTA, 2 mM PMSF, 0.1% NP-40) containing 300 mM KCl. The resuspended pellet was sonicated with 3-4 bursts of 1 minute each (Sonics-Vibra cell). The cell debris was then pelleted from the lysed cell suspension at 16,000 rpm for 30 minutes at 4 °C. The cleared supernatant containing the FLAG-tagged protein was then allowed to bind to the equilibtated M2 agarose beads at 4 °C on an end-to-end rotor for 3 hours. The Ni-NTA resin was washed five times with BC-300 buffer (20 mM Tris-HCl pH 7.4, 10% glycerol, 2 mM β-mercaptoethanol, 0.2 mM EDTA, 2 mM PMSF, 0.1% NP-40) containing 300 mM KCl, followed by 5 washes in BC-100 buffer (same composition as BC-300 containing 100 mM KCl). The bound protein was then eluted from the resin in BC-100 buffer containing 150 ng/µl 3X FLAG peptide. The integrity of the protein was examined on a 12% SDS-PAGE. The protein samples were prepared in 1X SDS loading buffer containing β-mercaptoethanol followed by denaturation at 90 °C for 5 minutes. The protein bands were visualized by staining the gel in Coomassie Brilliant Blue (Figure 2.12). The purified protein was flashed-frozen in liquid nitrogen and stored at -80 °C.

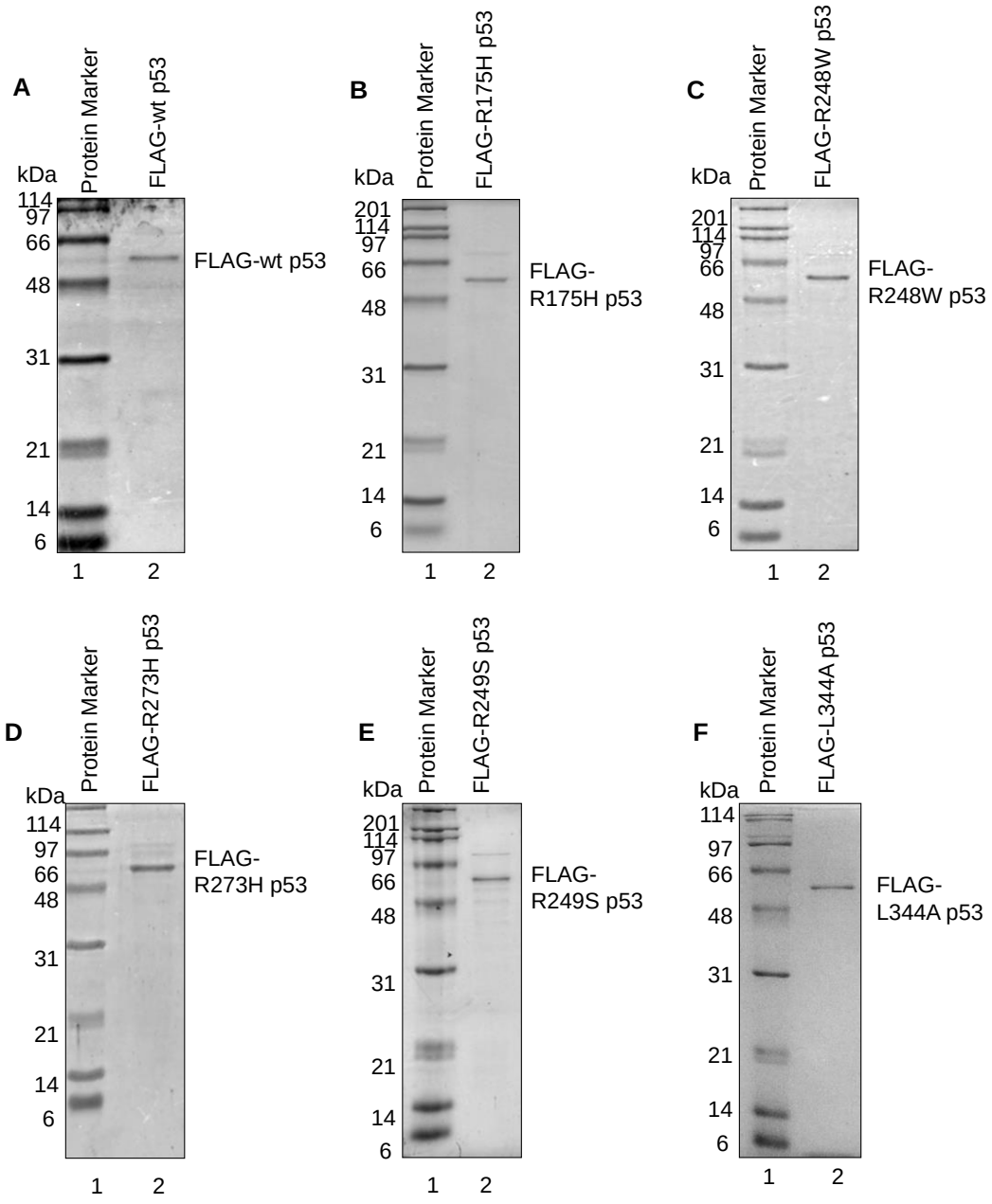

Figure 2.12: Protein purification profiles of FLAG-tagged p53 proteins. 12% SDS-PAGE purification profiles of (A) wildtype p53, (B) R175H p53, (C) R248W p53, (D) R273H p53, (E) R249S p53, and (F) L344A p53.

2.5.5. NPM1 wildtype and mutants

His_6-tagged NPM1, NPM1 point mutants and NPM1 deletion mutants which were cloned into the bacterial expression pET28b plasmid were transformed into BL21 (DE3) E. coli strain. The proteins of interest were expressed by inoculating primary culture which was allowed to grow over-night at 37 °C in LB medium under kanamycin selection (50 µg/ml) in a shaker incubator (180 rpm). The over-night culture was inoculated into a secondary culture

(10% inoculum) which was then allowed to grow at 37 °C in LB medium under kanamycin selection till the OD600 reached 0.5. The bacterial culture was then induced with 0.5 mM IPTG, and grown at 37 °C for 3 hours. The cells were harvested by centrifugation at 6000 rpm for 10 mins at 4 °C. The pelleted cells were then lysed in lysis buffer (20 mM Tris-HCl pH 7.4, 10% glycerol, 2mM β-mercaptoethanol, 0.2 mM EDTA, 2 mM PMSF, 0.1% NP-40 and 30 mM imidazole) containing 300 mM KCl. The resuspended pellet was sonicated with 4-5 bursts of 1 minute each (Sonics-Vibra cell). The cell debris was then pelleted from the lysed cell suspension at 16,000 rpm for 30 minutes at 4 °C. The cleared supernatant containing the His6-tagged protein was then allowed to bind to the Ni-NTA beads at 4 °C on an end-to-end rotor for 3 hours. The Ni-NTA resin was washed eight times with wash buffer (20 mM Tris-HCl pH 7.4, 10% glycerol, 2 mM β-mercaptoethanol, 0.2 mM EDTA, 2 mM PMSF, 0.1% NP-40 and 30 mM imidazole) containing 300 mM KCl. The bound protein was then eluted from the resin in buffer (20 mM Tris-HCl pH 7.4, 10% glycerol, 2 mM β-mercaptoethanol, 0.2 mM EDTA, 2 mM PMSF, 0.1% NP-40) containing 100 mM KCl and 250 mM imidazole. The eluted protein was dialyzed against the elution buffer containing no imidazole. The integrity of the dialyzed protein was examined on a 12% SDS-PAGE. The protein samples were prepared in 1X SDS loading buffer containing β-mercaptoethanol followed by denaturation at 90 °C for 10 minutes. The protein bands were visualized by staining the gel in Coomassie Brilliant Blue (Figure 2.13). The purified protein was flashed-frozen in liquid nitrogen and stored at -80 °C.

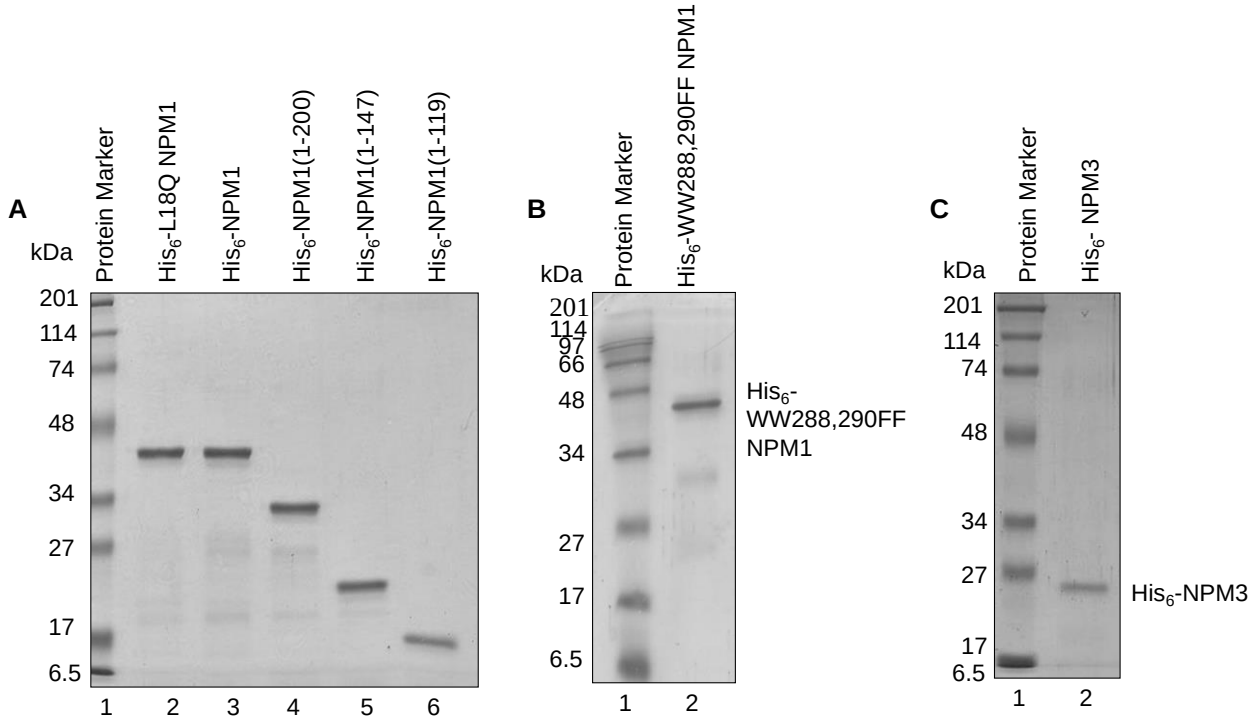

Figure 2.13: Protein purification profiles of His_6-tagged Nucleophosmin proteins. 12% SDS-PAGE purification profiles of (A) L18Q NPM1 (lane 1), wildtype NPM1 (lane 2), NPM1(1-200) (lane 3), NPM1(1-147) (lane 4), NPM1(1-119) (lane 5), (B) WW288,290FF NPM1, and (C) NPM3. The NPM1 wildtype and mutants were boiled at 90 °C for 15 minutes to disrupt the oligomers.

2.6. Structural and Biophysical analysis

2.6.1. Intrinsic Tryptophan Fluorescence

Spectra were recorded on a FluoroMax-3 spectrofluorimeter (Jobin Yvon Horiba) using a 1 cm path length cuvette and 2 nm excitation and 2 nm emission slit widths. Following excitation at 295 nm, baseline emission spectra of NPM1 wildtype, NPM1 tryptophan mutant (NPM1Trp mut), and p300 or in combinations as indicated present in 2% glycerol, 0.02M Tris-Cl, 100mM KCl and 1mM DTT were recorded from 300 to 500 nm at 2 nm/s increment.

2.6.2. Dynamic Light Scattering

DLS measurements were performed on a Nano-S Zetaseizer (Malvern Instruments, U.K.), using a helium-neon laser (632.8 nm), at room temperature, in 25 mM Tris-HCl and 100 mM NaCl buffer, pH 7.5. The intensity-weighed mean hydrodynamic diameter or the Z_{av} diameter of the samples (NPM1 and NPM1 mutants) was found from the cumulative analysis of the correlation curve. 10 runs for each measurement were recorded for each sample at 25 °C.

2.6.3. Cryo-Electron Microscopy

Sample for cryo-grid preparation:

T18E p53, prepared in a buffer containing 10 mM Tris-Cl, 150 mM NaCl, 5 mM MgCl2, 20 µM ZnCl2, 2 mM PMSF, 1mM DTT, pH-7.5, was mixed with 200 nM p300 at a molar ratio and incubated at room temperature for 5 min. For cryo-EM, 4 µl homogeneous p53-p300 complex was applied on glow-discharged Quantifoil® holey carbon TEM grids (R2/2, Quantifoil, Micro Tools GmbH, Jena, Germany) coated with a home-made continuous thin layer of carbon followed by blotting and vitrification with a Vitrobot™ (FEI Inc, Hillsboro, Or, USA) and grids were frozen in liquid ethane. Purified p300, diluted to a final concentration of 200 nM in a buffer containing 10 mM Tris-Cl, 150 mM NaCl, 1 mM DTT, 2 mM PMSF pH 8.0, was used for sample preparation. Grids were prepared and sample imaged similarly as p53-p300 complex.

Cryo-EM data collection and 3D image processing:

Data collection was performed on a Tecnai Polara microscope (FEI, USA) equipped with a FEG (Field Emission Gun) operating at 300 kV. Images were collected with 4K X 4K 'Eagle' charge-coupled device (CCD) camera (FEI, USA) at 78894/79000 X magnification, resulting in a pixel size 1.89 Å at the specimen level with defocus values ranging from 2.0 to 4.5 µm. All images were acquired using low-dose procedures with an estimated dose of ~20 electrons per $Å^2$.

Micrographs screening, particle picking were done separately with EMAN2 software (Tang et al., 2007) and SPIDER (Shaikh et al., 2008). Micrographs are selected on the basis of their visual quality, Thon rings in the power spectra and defocus values. Initially, 5400 particle were picked manually according to their sizes using the BOXER program from the EMAN2 package with a pixel size of 1.89Å/pixel. Particle screening was done by visual inspection with utmost care so that only complex particles (~ 10-12 nm) were kept and particles of smaller sizes were rejected. 2D, 3D classification and refinement were performed using EMAN2. The raw particle images were first subjected to multivariate statistical analysis and classification. The starting model was generated by the common line technique from selected 2D class averages.

In SPIDER, defocus of each micrograph was estimated on the basis of its 2D power spectrum and then micrographs were divided into groups of similar defocus. Image processing was done using the reference based alignment method, where the final refined volume of p53-p300complex obtained from EMAN2 was used as the reference. Using projections of this model as a template, total 10,088 particles of were selected semi automatically from all the micrographs. The 3D reconstruction was then done following the standard SPIDER protocols for reference-based reconstruction (Shaikh et al., 2008). The overall resolution, estimated by comparing the FSC of the two half maps, was 15.7 Å using the 0.5 cutoff criteria and 10.7Å using the 0.143 cutoff criteria**.**

Data were processed essentially as for the complex described above. Briefly, micrograph screening, particle selection, 3D reconstruction, and refinement were done in EMAN2 to generate an initial model of ~ 15 Å resolution. Coordinates of total 16,152 particles, picked manually in EMAN2, were imported in SPIDER for further reference based particle alignment and classification. After aligning imported particles with 83 two dimensional reference projections of initial model by translation and rotation, averages were calculated for each projection class. Finally, a 3D map was generated by Fourier back-projection methods and subjected to subsequent rounds of refinement. The resolution of the final map was 13.5 Å using the 0.5 cutoff criteria and 9.8 Å using the 0.143 cutoff criteria.

2.6.4. Circular Dichroism (CD) Spectroscopy

Far-UV CD spectra were recorded on a Jasco J-810 spectropolarimeter (JASCO Corp) in the wavelength interval 195–260 nm. For each spectrum the signal was converted to mean residue ellipticity in units of deg cm2 dmol1 res1. Experiments were performed employing protein concentrations of 16 uM in 50 mM phosphate buffer at pH 7.0, 1 mM DTT using a 0.1 cm path-length quartz cuvette.

2.7. Biochemical assays

2.7.1. Acetyltransferase assay

For p300 and PCAF autoacetylation assay, reactions of p300/PCAF full-length (100 ng) were carried out in HAT assay buffer (50 mM Tris–HCl, pH 7.5, 1 mM PMSF, 0.1 mM EDTA, and 10% v/v glycerol) and 100 mM Sodium butyrate at 30°C for 30 min with or without the proteins (NPM1/P53/GAPDH/p50) in the presence of 0.5µl of 4.7 Ci/mmol [^{3}H]acetyl-CoA (NEN-PerkinElmer) or 1 µl of 1.2 mM acetyl-CoA (non-radiolabeled).

For p300 and PCAF activity assay, reactions of p300/PCAF full-length (1 µl) were carried out in HAT assay buffer (50 mM Tris–HCl, pH 7.5, 1 mM PMSF, 0.1 mM EDTA, and 10 % v/v glycerol) and 100 mM sodium butyrate at 30°C for 30 min with 1 µg of histone H3 or higly purified core histones in the presence of 1 µl of 4.7 Ci/mmol [^{3}H]acetyl-CoA (NEN-PerkinElmer).

Following HAT assay, the radiolabeled proteins were processed by fluorography: the SDS-PAGE gels were incubated in DMSO for 30 mins followed by incubation in 22.5 % PPO solution in DMSO for 30 mins. The processed gel was dried at 80°C for 1 hour. The radiolabeled gels were exposed to X-ray films at -80 °C.

Following HAT activity assay, the reaction mix was spotted on p81 phosphocellulose paper which was washed in wash buffer (0.05 M sodium bicarbonate and 5 mM sodium carbonate). The spotted paper was dried and incubated in scintillation fluid (0.005% PPO and 5x10-4% POPOP in Toluene). The scintillation counts were measured in the scintillation counter (Wallac 1409).

2.7.2. Chaperone assays

2.7.2.1. Heat Protection Assay

The enzyme p300 was incubated in the presence of indicated concentrations of NPM1 in HAT buffer either at non-denaturating (30 °C) or at denaturating conditions (45 °C) for 30 minutes. The substrate (core histones or Histone H3) and [^{3}H]acetyl-CoA were added to the reaction, which was continued at 30 °C for 15 minutes. The reaction was stopped on ice followed by filter binding assay as described earlier. The activity of p300 at non-denaturing conditions (30 °C) in the absence of NPM1 was considered as 100% activity.

2.7.2.2. Activity Rescue Assay

The KAT enzyme (either p300 or Tip60) was incubated in HAT buffer either at non-denaturating (30 °C, control) or at denaturating conditions (45 °C) for 15 minutes. After the denaturation step, the enzyme was incubated in the presence of indicated concentrations of NPM1 for 30 °C for 30 minutes. The substrate (core histones or histone H3) and [^{3}H]acetyl-CoA were added and the HAT reaction was continued at 30 °C for 15 minutes. The reaction was stopped on ice followed by filter binding assay as described earlier. The activity of p300 at non-denaturing conditions (30 °C) in the absence of NPM1 was considered as 100% activity.

2.7.3. *In vitro* interaction

FLAG-tagged NPM1 and His6-tagged p300 was incubated together in interaction buffer (0.2 mM EDTA pH 8.0, 0.1% NP-40, 2 mM PMSF and 150 mM KCl) to a final volume of 300 µl along with M2 agarose slurry. The mixture was incubated at 4 °C for 3 hours on an end-to-end rotor. The beads were washed thrice with the interaction buffer. The proteins were eluted by boiling the beads in 1X SDS loading buffer. The supernatant was resolved on a 10% SDS-PAGE and the interaction was analyzed by western.

2.8. General Molecular Biology techniques

2.8.1. Western Blotting Analysis

Proteins electrophoresed on an SDS-PAGE were transferred onto nitrocellulose or PVDF membrane in transfer buffer (25 mM Tris, 192 mM glycine , 0.036 % SDS in 20 % methanol) by Semi-dry or Wet transfer method, followed by blocking in 5 % skimmed milk, the proteins of interest were detected with their corresponding primary antibodies. HRP-conjugated secondary antibodies (Genei) were used against the primary antibodies to give a chemiluminescent signal in the presence of SuperSignal West Pico Chemiluminescent Substrate (Thermo Scientific), which was captured on an X-ray film.

2.8.2. Dot-Blot/ Slot Blot Analysis

Proteins or 50ng of peptides were spotted onto nitrocellulose paper directly or using the BioRad Slot Blot apparatus. Following blocking in 5% skimmed milk, the proteins of interest were detected with their respective primary antibodies. HRP-conjugated secondary antibodies (Genei) were used against the primary antibodies to give a chemiluminescent signal in the presence of SuperSignal West Pico Chemiluminescent Substrate (Thermo Scientific), which was captured on an X-ray film.

2.8.3. Polymerase chain reaction

Polymerase chain reaction (PCR) was to amplify desired stretches of DNA from a DNA template. The reaction was set up by adding the following components, 1X Phusion HF buffer, 0.2 mM dNTPs, 0.5 µM specific primers (forward and reverse), template DNA, nuclease-free water and Phusion DNA polymerase in a thin-walled PCR tube. The reaction was carried out in a BioRAD thermocycler. The integrity of the amplicon was checked on an agarose gel (of desired concentration according to the size of the amplicon) and quantified on a NanoDrop1000.

2.8.4. cDNA Synthesis

Before cDNA synthesis from the isolated total RNA, the RNA was treated with DNase I to eliminate any genomic DNA contamination. Approximately 10 µg RNA was added to 1X DNase I Reaction Buffer made up to a final volume of 100 µl. 2 U of RNase-free DNase I was added to the reaction and incubated at 37 °C for 20 minutes. 5 mM EDTA was added to stop the reaction. The DNase I was heat inactivated at 75 °C for 10 minutes. 2 µg DNase I-treated RNA was used for the subsequent steps of cDNA synthesis and the remaining RNA was stored at 80 °C. For first strand cDNA synthesis, the RNA was added to a 10 µl reaction containing 1 mM dNTPs and 7 µM Oligo dT (Sigma, Catalog No. 04387). The reaction mixture was incubated for 10 minutes at 70 °C. The first strand cDNA synthesis was initiated by adding 2 µl of 10X M-MLV Reverse Transcriptase, 20 U of RNaseOUT (Invitrogen Catalog No. 10777019). The reaction was allowed to continue for another 50 minutes at 37 °C, followed by heat inactivation at 94 °C for 10 minutes. The cDNA synthesized was stored at -20 °C.

2.8.5. Real-time PCR

The first strand cDNA synthesized was used for Real-Time/ quantitative PCR (RT-PCR/ qPCR). To the 2X SYBR Green mastermix, specific primers (forward and reverse), cDNA and high ROX (for normalization) were added. The reaction was carried out in the StepOnePlus Real time PCR system. The data was analysed in StepOne software v2.3.

2.9. Immunohistochemistry Analysis

The oral cancer patient samples used in the study were collected from Sri Devaraj Urs Academy of Higher Education and Research (SDUAHER) after obtaining Bioethics clearances from both institutes (SDUAHER and JNCASR). The samples were collected with prior consent from the patients. The tumor and adjacent normal tissue (2 cm away from the resected tumor margin) samples were fixed in 10% formalin for 24-48 hours. Then the tissue samples were dehydrated and embedded in paraffin blocks. 5 µ sections of the samples were made using a microtome (Leica). The tissue samples were stained with haematoxylin and counterstained with eosin. The regions with higher density of cells were marked and those regions where punctured from the tissue blocks with a 1 mm puncturing tool. The 1 mm sections were placed onto a tissue microarray precast block. One array can hold 20 pairs of tissue (normal and tumor) samples. Once the tissue microarray paraffin blocks were prepared, 5 µ sections of the samples were made and collected on silane-coated glass slides. The

sections were fixed on the slides by incubating the slides at 45 °C on a hot plate for 24 hours. Before processing the samples for staining, the slides were kept at 65 °C to melt the paraffin. The paraffin was then removed in xylene, followed by dehydration of the samples in 100% alcohol and rehydration in water. Epitope retrieval was done in sodium citrate buffer by boiling for 10 minutes. Once cooled to room temperature, the sample slides were transferred to 0.9% H_2O_2 in methanol for 15 minutes to quench the endogenous peroxidases. The samples were blocked in 5% skimmed milk for 45 minutes and probed with primary antibody of interest. The Strept-Avidin Biotin (biotinylated secondary antibodies (anti-rabbit + anti-mouse) and HRP-conjugated streptavidin) kit from Dako was used. The immune-reactivity of the antigen was measured by intensity of the brown precipitate formed in the presence of the chromogen di-aminobenzidine tetrahydrochloride (DAB, Sigma) followed by counter staining with haemotoxylin. The staining was examined and imaged. Semi-quantitative analysis of the staining (H-scoring) was performed by assigning values between 0-3 (0 = no stain to 3= strong stain) per cell in a field (3 fields per sample) using the ImageJ add-on IHC profiler (ref). H-score is calculated by the following formula:

H-score= 0x % cells with no stain+ 1x % cells (low stain) + 2x % cells (moderate stain) + 3x % cells (strong stain), which can range from 0 to 300. Therefore higher the H-score corresponds to higher levels of protein.

2.10. Generation of Polyclonal Antibodies

Polyclonal antibodies were generated by injecting the Keyhole Limpet Hemocyanin (KLH) coupled peptides in rabbits. New Zealand strain of rabbits were primed with an emulsion of the peptide-KLH conjugate in complete adjuvant. Before the priming, a few ml of blood was collected from the rabbit (control serum). Booster doses were given every 2-3 weeks till the serum showed sufficient strength and specificity against the target protein or modification. Major bleed of 15-20 ml was collected twice in the course of raising the antibody. Serum was separated from the collected blood and IgG was purified using Protein G sepharose beads. The IgG was eluted from the beads using 100 mM glycine, pH 3.0 and collected into tubes containing Tris-Cl buffer to neutralize the acidic pH of the elution buffer. The IgG purified was then dialyzed against 50% glycerol in PBS. The IgG purified from the pre-immune serum was used as a control for immunoprecipitation and ChIP.

2.10.1. Generation of Rabbit Polyclonal anti-H2AK5ac antibody

Rabbit polyclonal antibodies against H2AK5Ac synthetic peptide SGRG(Ac-LYS)QGGKYC coupled to KLH. The antibody was raised in rabbit as described earlier. The antibody was further affinity purified (Abexome) to ensure specificity of the antibody. The antibody was characterized by dot blot, slot blot and western blotting analysis (Figure 2.14). The antibody was found to be specific to the H2AK5 acetylated peptide while it did not detect the other histone acetylation peptides (Figure 2.14A). The anti-H2AK5ac antibody could distinguish between mock- and p300- acetylated full length histone H3 while it did not cross-react with other acetylated histones (Figure 2.14B). The antibody could also effectively detect acetylated H2AK5 in cell lysates (Figure 2.14C).

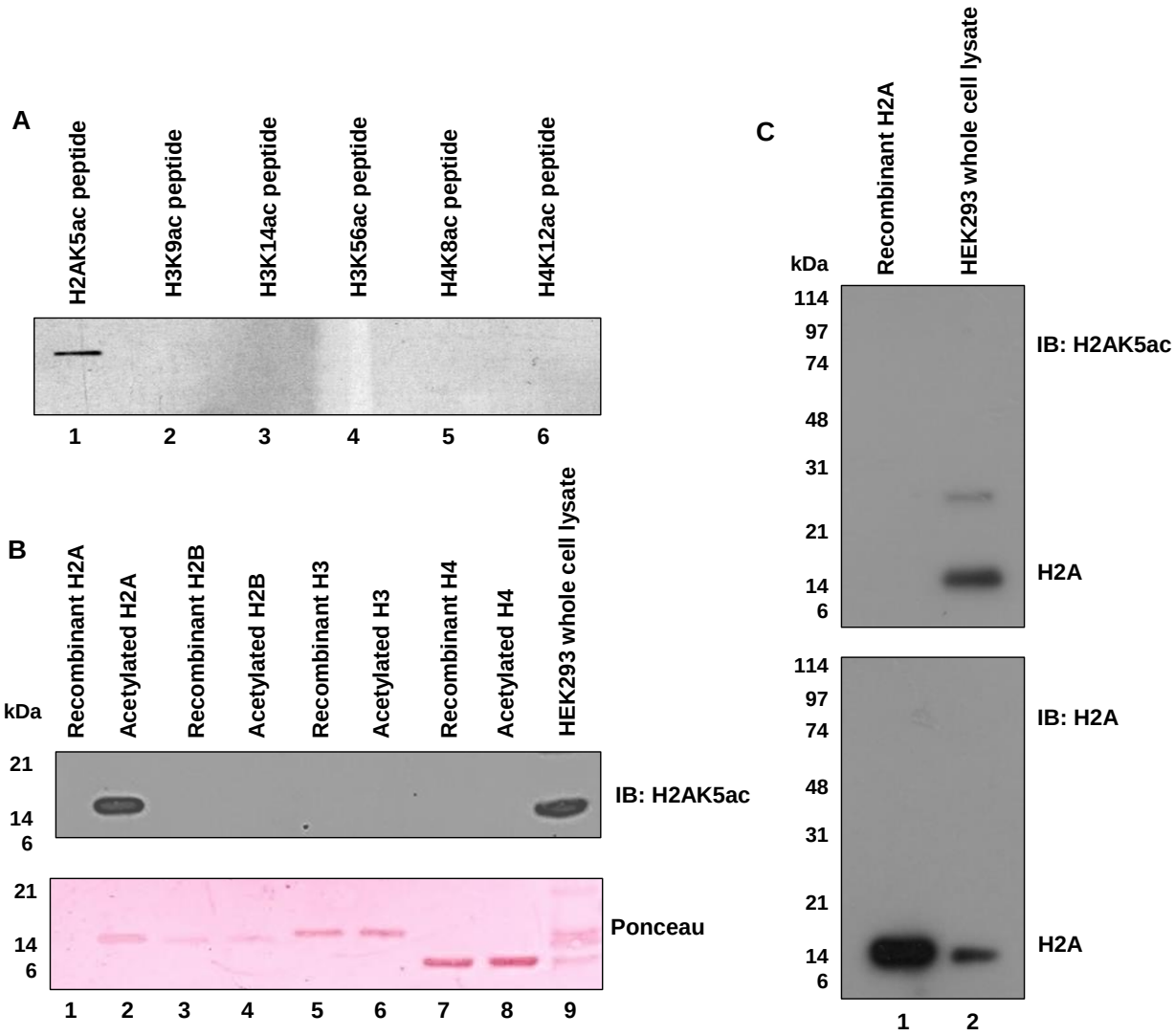

Figure 2.14: Characterization of anti-H2AKac antibody. (A) Slot blot to determine the cross-reactivity of the antibody with other acetylated histone peptides (50 ng) as indicated. (B) Western to determine the specificity of the antibody to detect only p300-mediated

acetylated H2A. Lower panel is the Ponceau stained loading control. (C) Western to determine the abiity of the antibody to specifically recognize acetylated histone in whole cell laemmli lysates over unacetylated recombinant histone H3.

2.10.2. Generation of Rabbit Polyclonal anti-H3K56ac antibody

Rabbit polyclonal antibodies against H3K56Ac synthetic IRRYQ(Ac-LYS)STELC-KLH conjugate. The antibody was raised in rabbit as described earlier. The antibody was further affinity purified (Abexome) to ensure specificity of the antibody. The antibody was characterized by dot blot, slot blot and western blotting analysis (Figure 2.15). The antibody could effectively detect as low as 10 ng of H3K56ac peptide while not recognizing 250 ng of recombinant histone H3 (Figure 2.15A). The antibody was specific towards the H3K56ac peptide and did not cross-react with other acetylated histone peptides (Figure 2.15B). To confirm this, histone H3 and core histones were acetylated by p300 and PCAF (which share many common histone acetylation sites with p300). Since H3K56 acetylation is a p300-specific site, the histones and core histones acetylated by PCAF were not recognized by the H3K56ac antibody (Figure 2.15C).

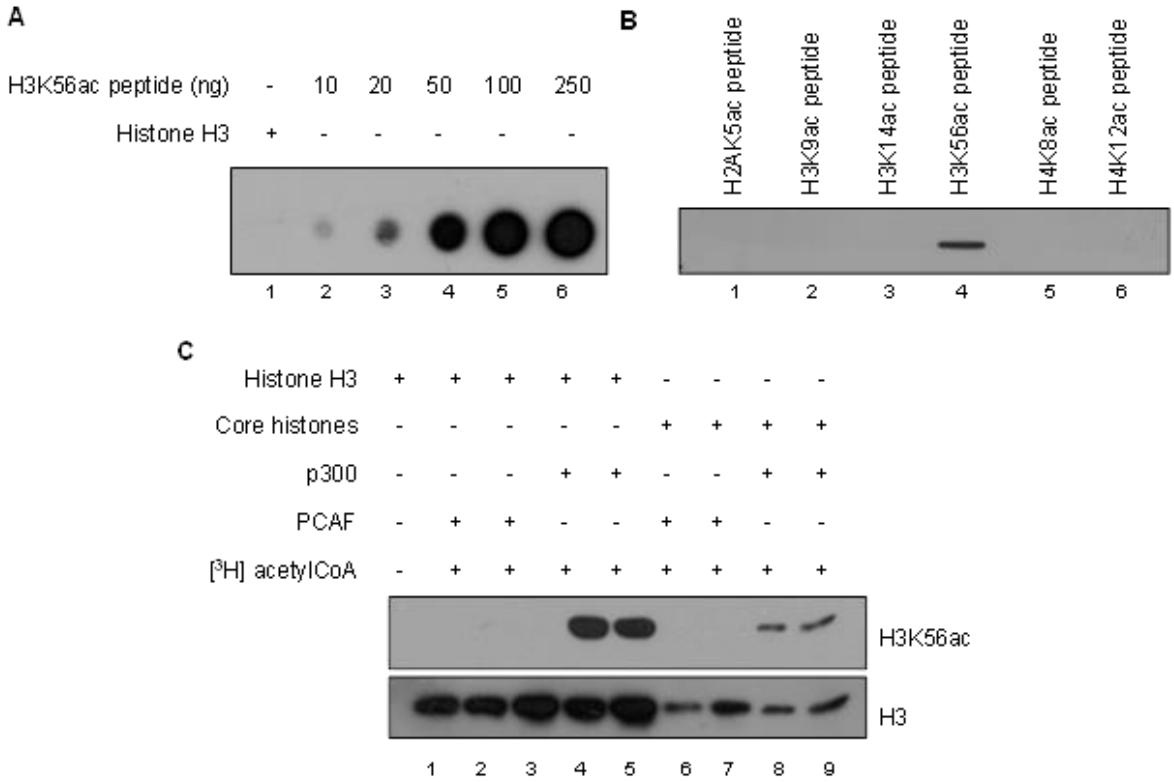

Figure 2.15: Characterization of anti-H3K56ac antibody. (A) Dot blot to determine the specificity and sensitivity of the polyclonal anti-H3K56ac antibody. (B) Slot blot to determine the cross-reactivity of the antibody with other acetylated histone peptides (50 ng) as indicated. (C) Western to determine the specificity of the antibody to detect only p300-mediated acetylation of H3. Lower panel is the H3 loading control.

2.10.3. Generation of Rabbit Polyclonal anti-K1499ac p300 antibody

Rabbit polyclonal antibodies against K1499ac p300 by using a synthetic acetylated K1499 p300 heptapeptide -KLH conjugate. The antibody was raised in rabbit as described earlier. The antibody was characterized by western blotting analysis and immunofluorescence (Figure 2.16-2.18). The K1499 site is located on the end of the lysine-rich loop residing in the p300 HAT domain (Figure 2.16A). Acetylation of the site serves as a measure of p300 autoacetylation. The antibody immuno-reacts strongly with the acetylated p300 (Figure 2.16B). Since the recombinant p300 enzyme is purified from the baculo-expression insect cell system, the p300 purified is possibly in a hypoacetylated form which could explain the detection (though faintly) of the mock acetylated p300 by the acetylation specific K1499 p300 antibody (Figure 2.16B).

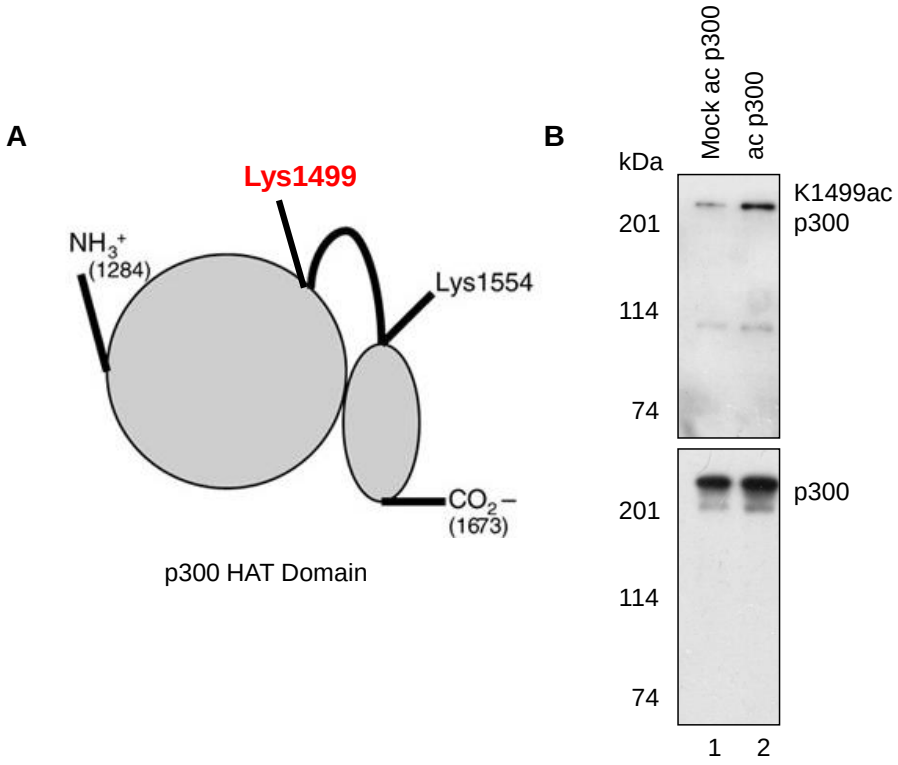

Figure 2.16: Characterization of anti-K1499ac p300 antibody. (A) Schematic to show the location of the K1499 residue in the p300 HAT domain. (B) Western to determine the specificity of the antibody to recognize the acetylated recombinant p300 over the mock-acetylated p300. Lower panel is the p300 loading control.

The antibody detects endogenous levels of p300 autoacetylation in cells (Figure 2.17). p300 autoacetylation is reversed by the deacetylase SIRT2 (Black et al., 2008), therefore to prove that the antibody is specific to p300 autoacetylation, HepG2 cells were treated with 5 nm of a Sirtuin-inhibitor, nicotinamide (NAM). Upon treatment, the intensity of anti-K1499ac p300

antibody staining increases, indicating that the antibody is specific to p300 autoacetylation (Figure 2.18).

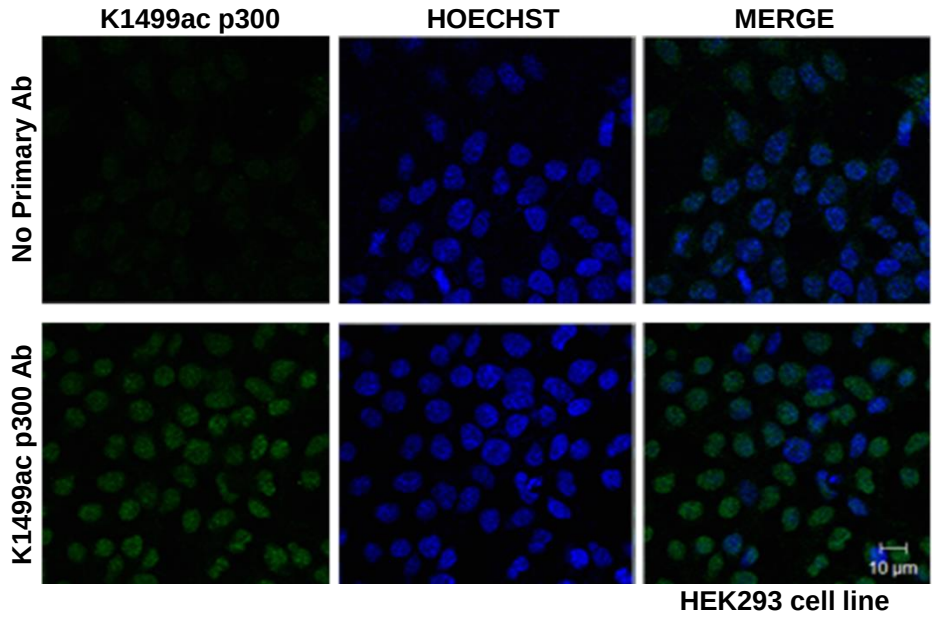

Figure 2.17: Characterization of anti-K1499ac p300 antibody in cells. Immunofluorescence to detect the levels of autoacetylated p300 using the anti-K1499ac p300 antibody.

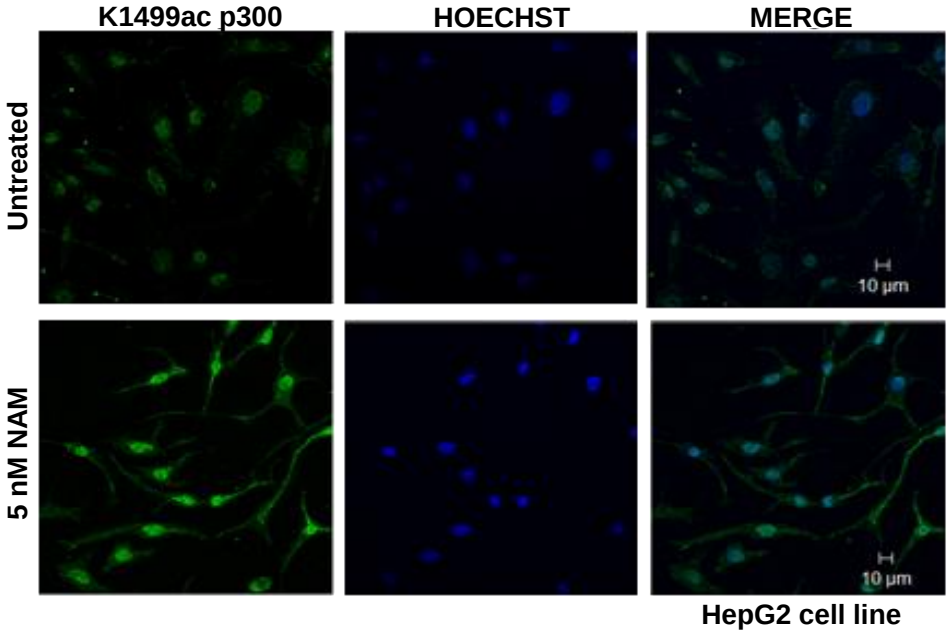

Figure 2.18: Specificity of anti-K1499ac p300 antibody in cells. Immunofluorescence to detect the levels of autoacetylated p300 using the anti-K1499ac p300 antibody in untreated and 5 nM Nicotinamide (NAM) treatment (Sirtuin inhibitor).

2.11. Microarray Analysis

The quality of the RNA samples was checked on an Agilent 2100 Bioanalyzer. The samples with a RNA integrity number (RIN) > 7.0 proceeded for further processing. Illumina expression bead array platform HumanHT-12 v4.0 was used for the expression microarray following the manufacturer's protocol.

2.12. Autoacetylated p300 and p300 ChIP-seq

To determine the global occupancy of p300 and autoacetylated p300 under the induction of p53 expression, ChIP was carried out as described before. Tet-ON inducible p53 expression H1299 cells were treated with doxycycline for 24 hours to induce the expression of wildtype p53. Each ChIP was done in duplicates under two conditions: untreated and 1 μg/ml doxycycline treatment. For the acp300 ChIP, 5 μg K1499ac p300 antibody was used whereas for the p300 ChIP, 10 μg of N-15 p300 antibody from Santa Cruz was used. Chromatin shearing was standardize to 4 cycles, 5 minutes each (20 minutes sonication), 30 seconds pulses (Diagenode) to achieve a fragment length between 100-300 bp (Figure 2.19). The ChIP was validated by qPCR using primers scoring for enrichment at the p53 responsive gene promoters. The double stranded ChIP DNA was quantified using Quant-iT PicoGreen dsDNA Assay Kit (Thermofisher Scientific).

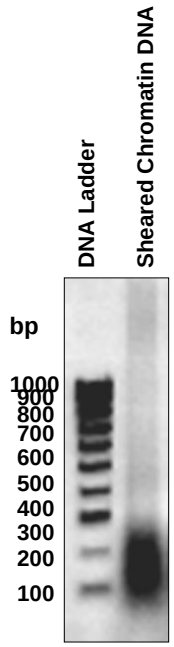

Figure 2.19: Sheared Chromatin profile for ChIP. Sonication of crosslinked chromatin was done in the Diagenode ChIP Sonicator for 20 minutes (4 cycles of 5 x 30 second pulses).

The ChIP samples DNA were sent to Quick Biology (Pasadena, USA) for sequencing. Libraries for ChIP-seq were prepared with KAPA Hyper Prep Kits. The workflow consists of end repair to generate blunt ends, A-tailing, adaptor ligation and PCR amplification. Different adaptors were used for multiplexing samples in one lane. Sequencing was performed on Illumina Hiseq3000/4000 for a pair-end 150 run. Data quality check was done on Illumina SAV for the base composition per position of the reads to rule out any base bias during sequencing (Figure 2.20), the average base quality score per position (should be >30) of all the reads (Figure 2.21), the average base score per read (Figure 2.22) and the distribution of read lengths per sample (Figure 2.23).

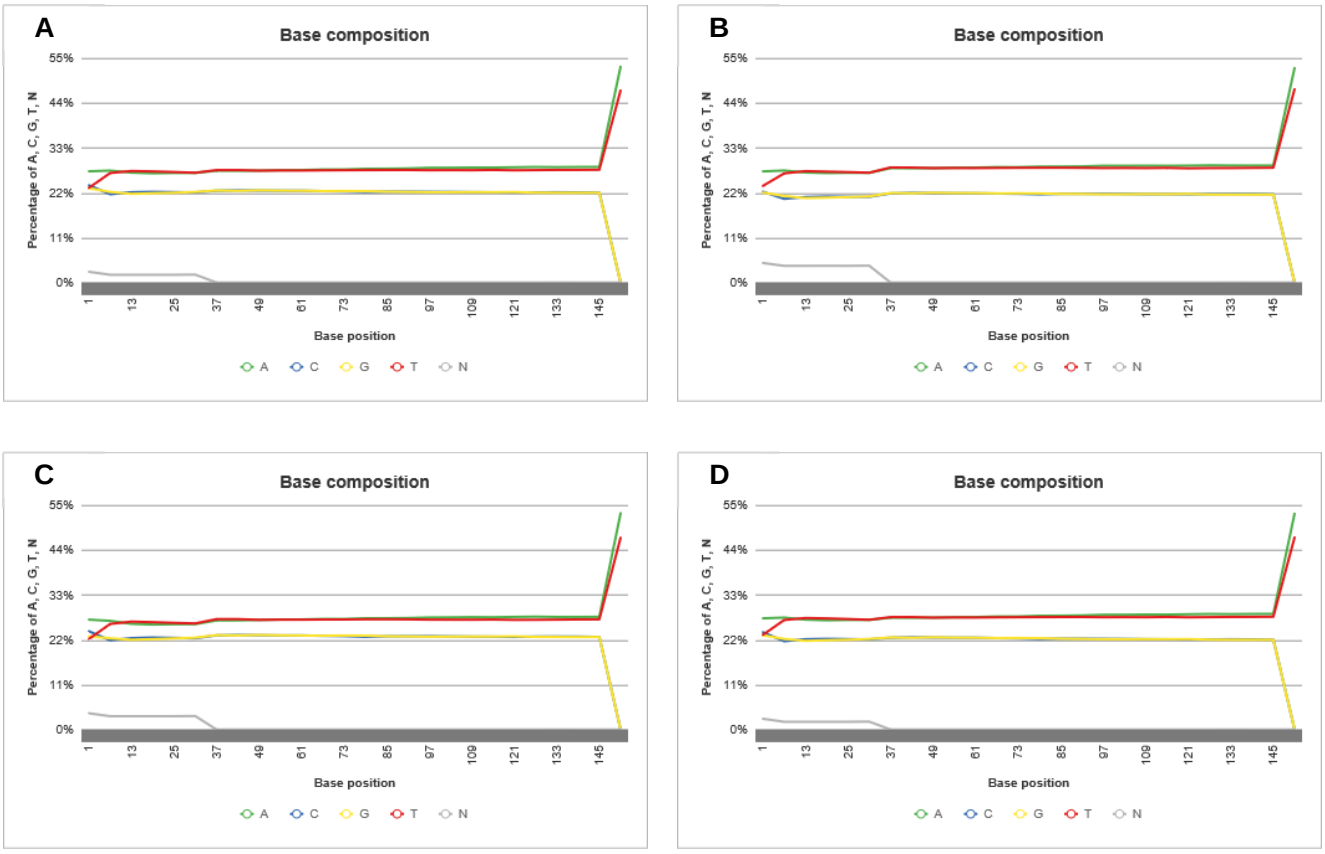

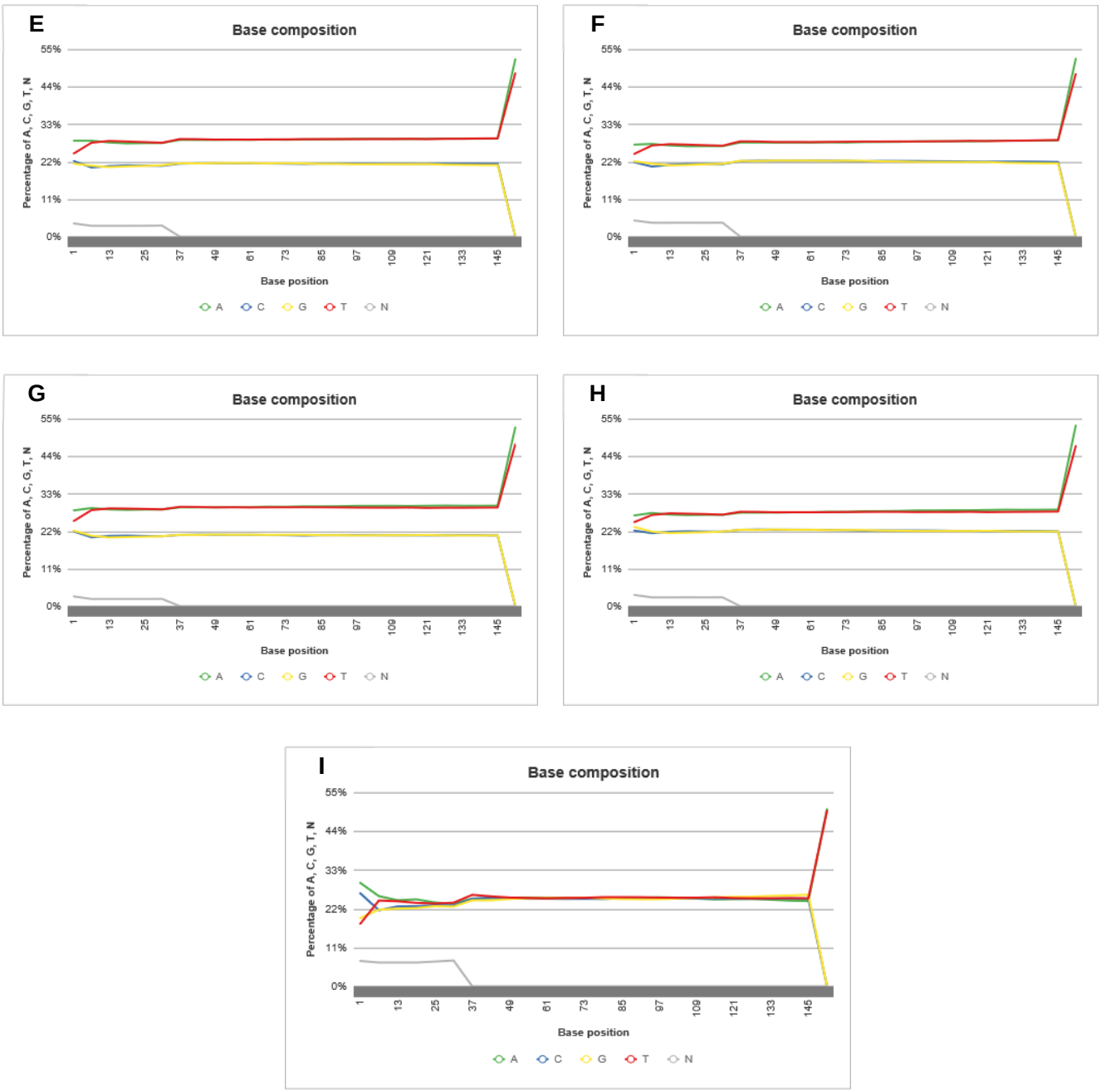

Figure 2.20: Base composition per position in the sequence read. Percentage of each nucleotide (%A (green), %C (blue), %G (yellow), %T (red)), as well as the percentage of ambiguous nucleotide (%N (grey)) at each position of all the reads for each sample (A) acp300 – dox Rep1, (B) acp300 + dox Rep1, (C) acp300 – dox Rep2, (D) acp300 + dox Rep2, (E) p300 – dox Rep1, (F) p300 + dox Rep1, (G) p300 – dox Rep2, (H) p300 + dox Rep2, and (I) Input.

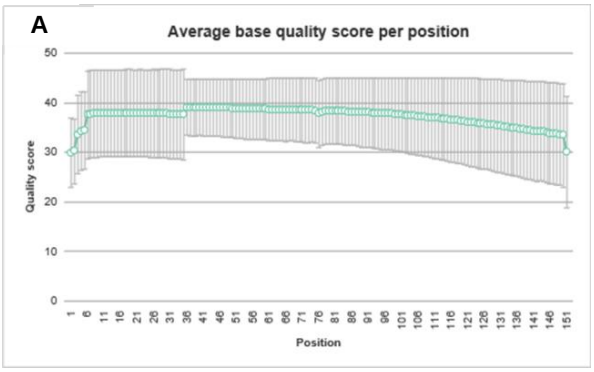
A
Average base quality score per position
Quality score
Position


B
Average base quality score per position
Quality score
Position


C
Average base quality score per position
Quality score
Position


D
Average base quality score per position
Quality score
Position


E
Average base quality score per position
Quality score
Position


F
Average base quality score per position
Quality score
Position

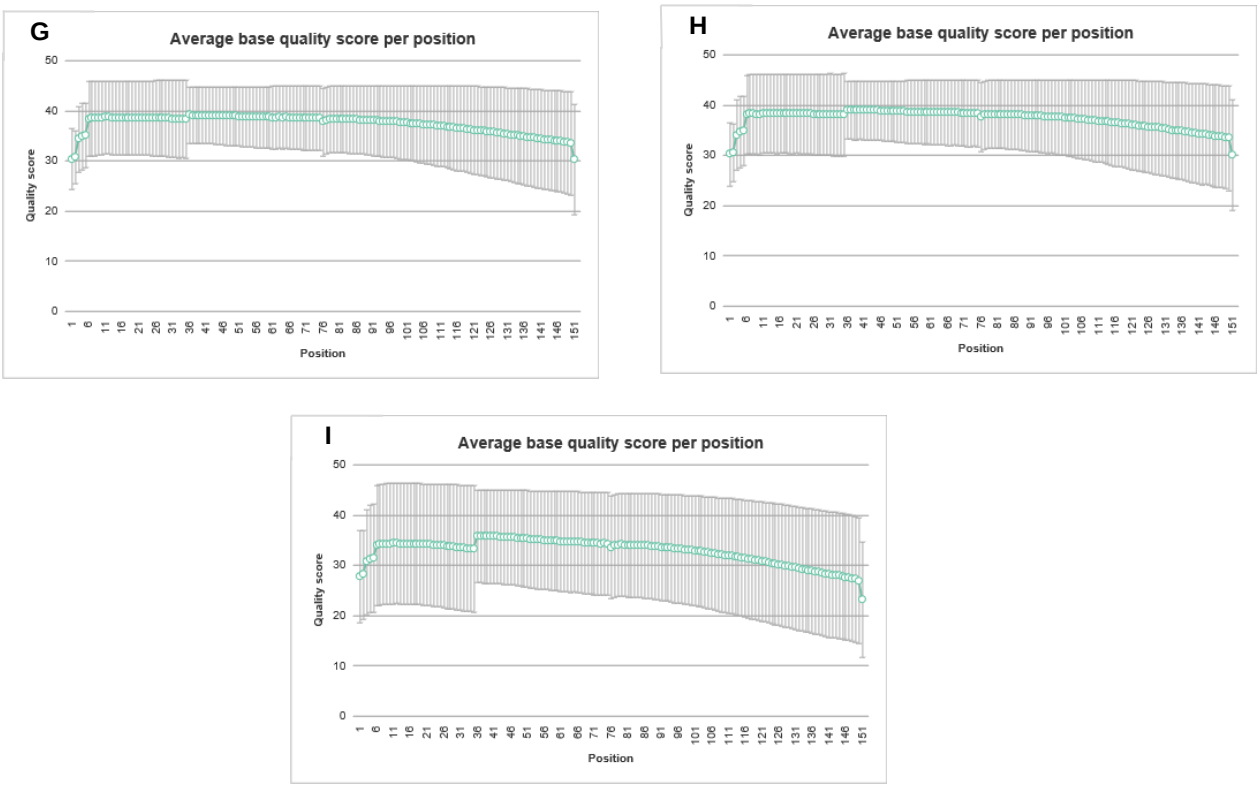

Figure 2.21: Average Phred base quality score per position in the sequence read. Average base quality at each position of all the reads for each sample (A) acp300 – dox Rep1, (B) acp300 + dox Rep1, (C) acp300 – dox Rep2, (D) acp300 + dox Rep2, (E) p300 – dox Rep1, (F) p300 + dox Rep1, (G) p300 – dox Rep2, (H) p300 + dox Rep2, and (I) Input.

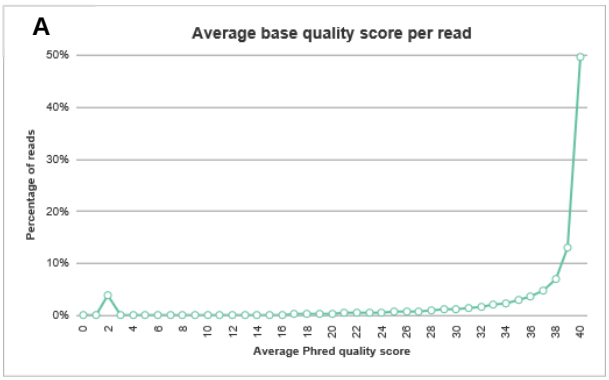
A
Average base quality score per read
Percentage of reads
50%
40%
30%
20%
10%
0%
0 2 4 6 8 10 12 14 16 18 20 22 24 26 28 30 32 34 36 38 40
Average Phred quality score

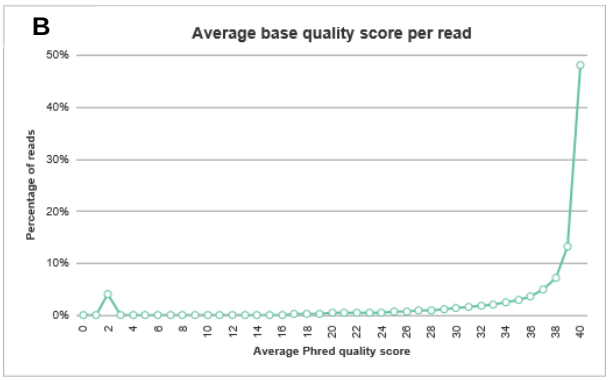
B
Average base quality score per read
Percentage of reads
50%
40%
30%
20%
10%
0%
0 2 4 6 8 10 12 14 16 18 20 22 24 26 28 30 32 34 36 38 40
Average Phred quality score

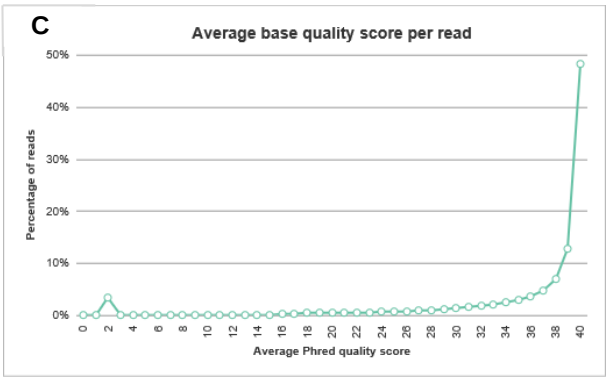
C
Average base quality score per read
Percentage of reads
50%
40%
30%
20%
10%
0%
0 2 4 6 8 10 12 14 16 18 20 22 24 26 28 30 32 34 36 38 40
Average Phred quality score

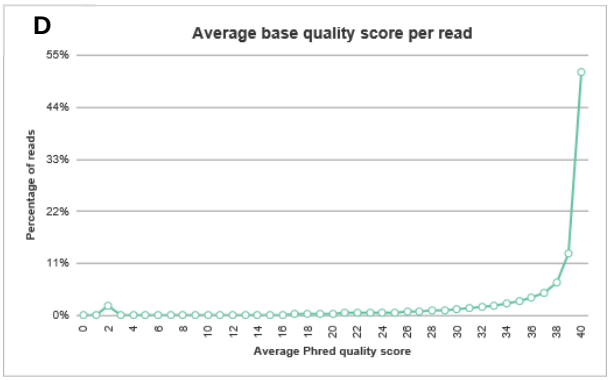
D
Average base quality score per read
Percentage of reads
55%
44%
33%
22%
11%
0%
0 2 4 6 8 10 12 14 16 18 20 22 24 26 28 30 32 34 36 38 40
Average Phred quality score

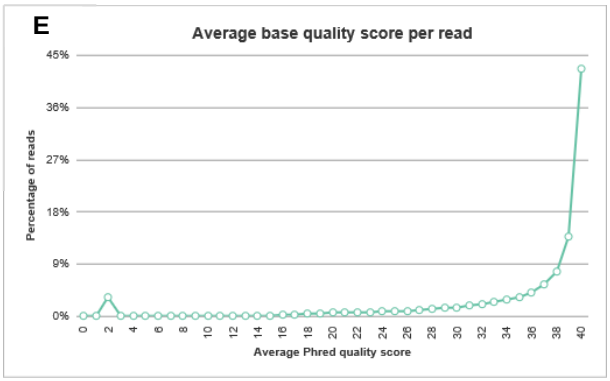
E
Average base quality score per read
Percentage of reads
45%
36%
27%
18%
9%
0%
0 2 4 6 8 10 12 14 16 18 20 22 24 26 28 30 32 34 36 38 40
Average Phred quality score

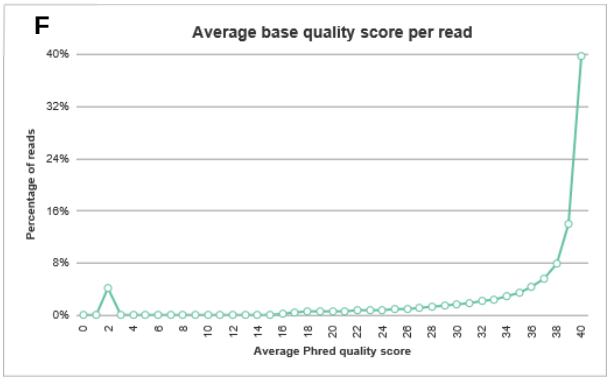
F
Average base quality score per read
Percentage of reads
40%
32%
24%
16%
8%
0%
0 2 4 6 8 10 12 14 16 18 20 22 24 26 28 30 32 34 36 38 40
Average Phred quality score

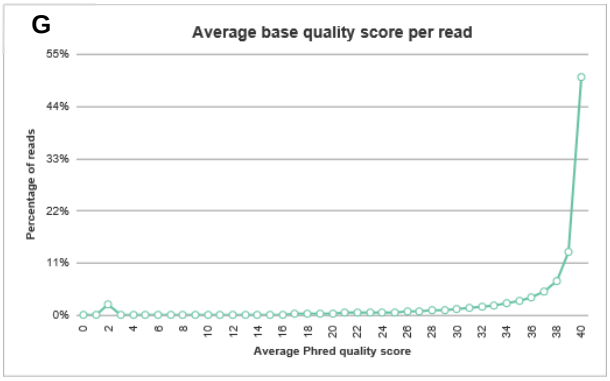
G
Average base quality score per read
Percentage of reads
55%
44%
33%
22%
11%
0%
0 2 4 6 8 10 12 14 16 18 20 22 24 26 28 30 32 34 36 38 40
Average Phred quality score

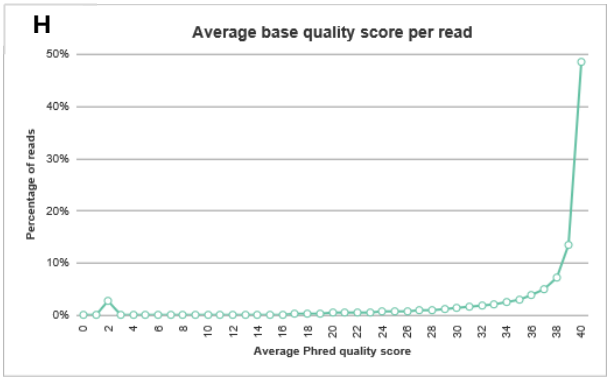
H
Average base quality score per read
Percentage of reads
50%
40%
30%
20%
10%
0%
0 2 4 6 8 10 12 14 16 18 20 22 24 26 28 30 32 34 36 38 40
Average Phred quality score

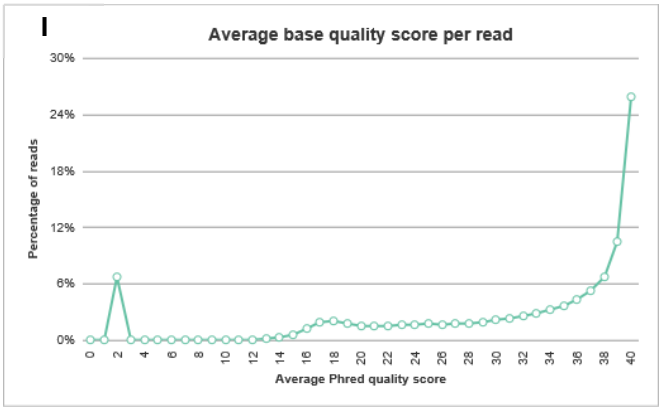

Figure 2.22: Average base quality score per read. Average base quality at of all the reads for each sample (A) acp300 – dox Rep1, (B) acp300 + dox Rep1, (C) acp300 – dox Rep2, (D) acp300 + dox Rep2, (E) p300 – dox Rep1, (F) p300 + dox Rep1, (G) p300 – dox Rep2, (H) p300 + dox Rep2, and (I) Input.

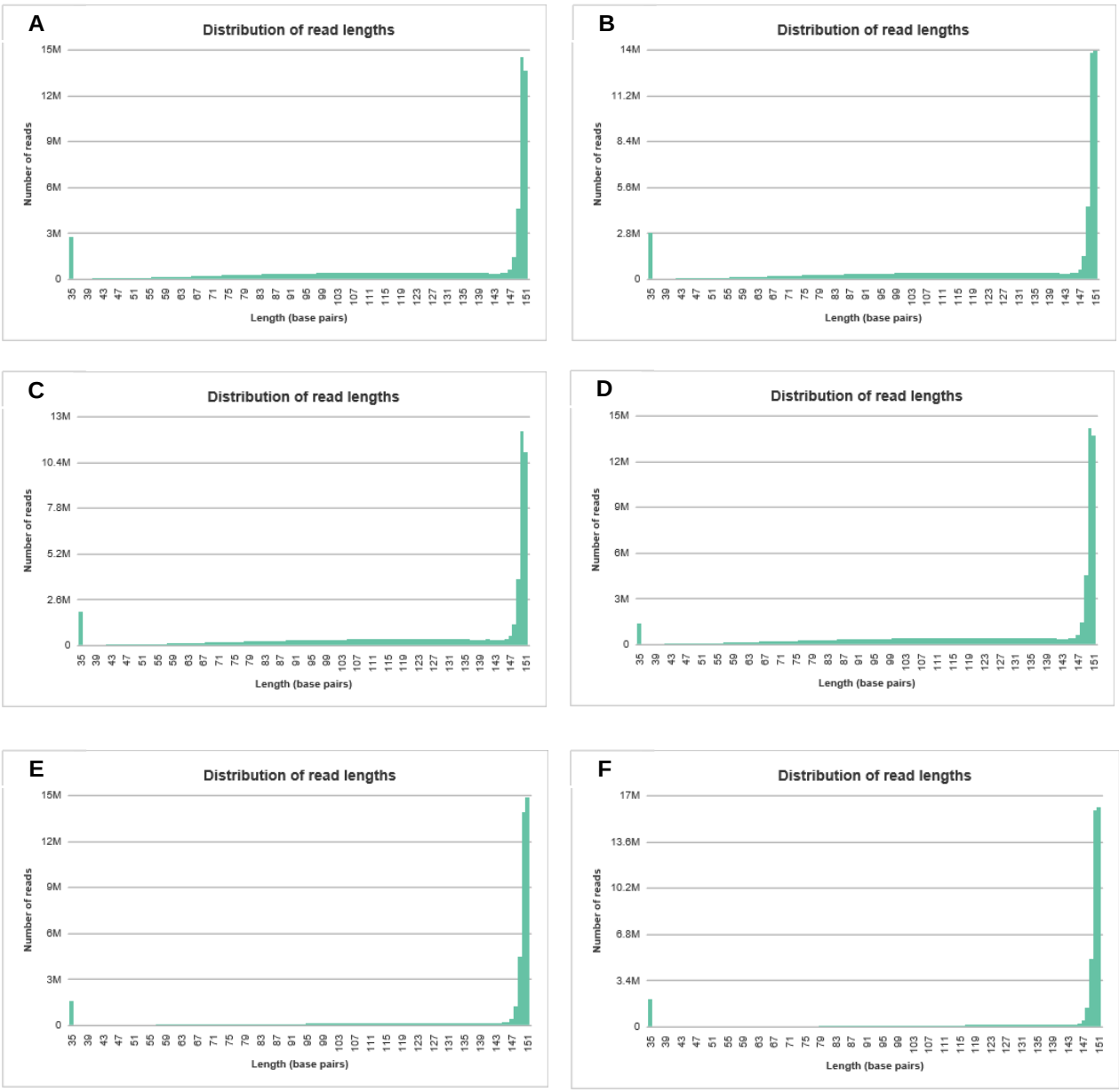

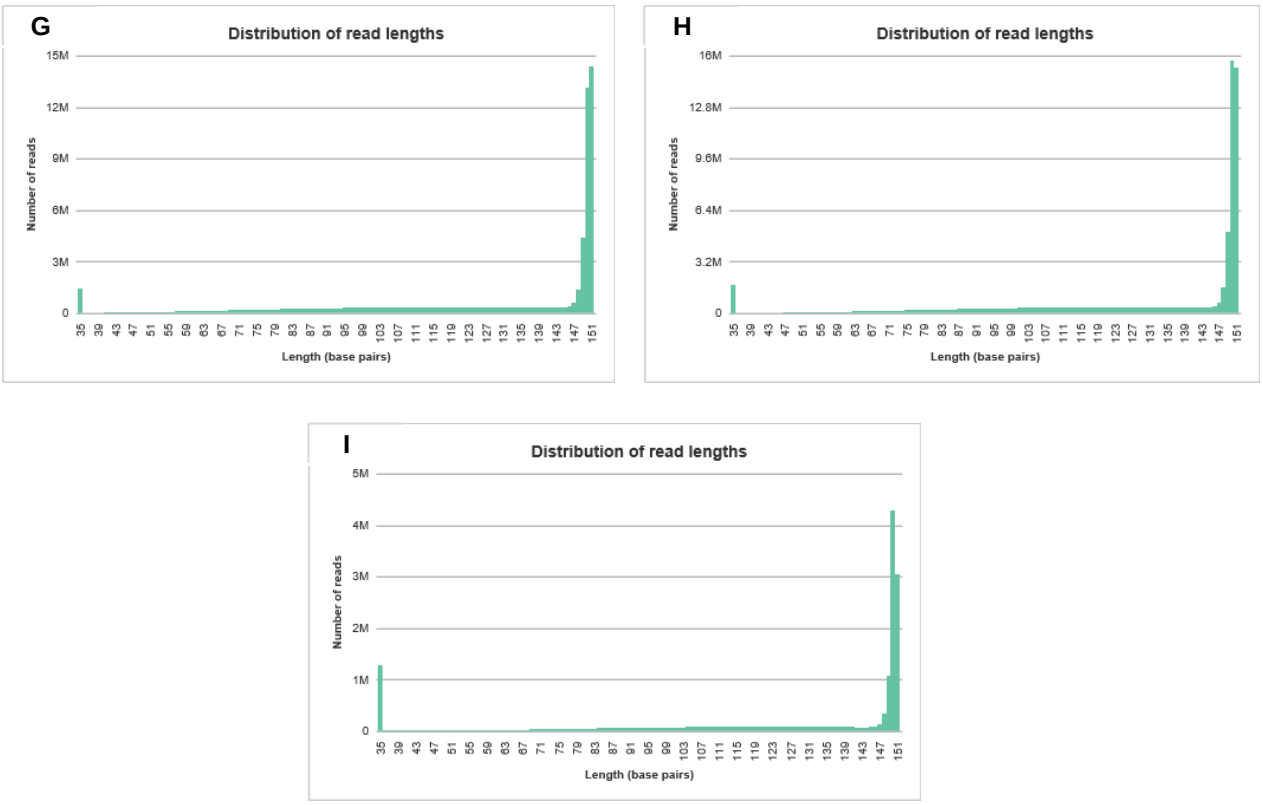

Figure 2.23: Distribution of read lengths. Distribution of read lengths for each sample (A) acp300 – dox Rep1, (B) acp300 + dox Rep1, (C) acp300 – dox Rep2, (D) acp300 + dox Rep2, (E) p300 – dox Rep1, (F) p300 + dox Rep1, (G) p300 – dox Rep2, (H) p300 + dox Rep2, and (I) Input.

Demultiplexing was performed with Illumina Bcl2fastq2 v 2.17 program. Single end reads were considered from 150bp PE data. The reads having sequences of length >75bp and quality score <=20 were trimmed using NGS QC ToolKit. The trimmed reads were aligned against the reference genome, human genome Hg19 build (Ensembl build GRCh37 build) using the alignment tool Bowtie (Langmead et al, 2009). The prealignment QC results and alignment statistics (Table 2.4) for all the IP samples were satisfactory but the input sample did not appear to meet the QC standards and was omitted from further analysis. The alignment files merged for Dox- and Dox+ replicates of acp300 and p300 using SAMTOOLS to have the single dataset of Input and IP respectively, for both the samples.

Sample Name	Filtered reads (q20,n75)	Reads aligned	Reads aligned (%)	Reads unaligned	Reads unaligned (%)
acp300 – dox Rep1	30902981	26237366	84.90	4665615	15.10
acp300 + dox Rep1	29549416	25309367	85.65	4240049	14.35
acp300 – dox Rep2	25364252	21387138	84.32	3977114	15.68
acp300 + dox Rep2	30556435	26115979	85.47	4440456	14.53
p300 – dox Rep1	21896192	1899740	86.7 6	2898772	13.24
p300 + dox Rep1	23127179	19993354	86.45	3133825	13.55
p300 – dox Rep2	28687640	25237788	87.97	3449852	12.03
p300 + dox Rep2	31150245	27665660	88.81	3484585	11.19
Input	28559960	18137372	63.51	10422588	36.49

Table 2.4: Alignment Statistics of the ChIP-seq samples.

The control ChIP which is the Dox- sample was used as the input dataset for normalization and peak calling for both p300 and acp300 ChIP-seq. MACS14 was used for Differential Peak calling with model building ratio of 3:10 with shift size of 50 bp and --keep-dup (keeping duplicates).

HOMER tool was used for finding overlapping genes within distance of 100 bp overlap within acp300 and p300 and to find unique genes specific to acp300 and p300. Unique and overlapping genes were annotated with respect to Nearest Downstream Genes (NDG) and Transcription Start Site (TSS) using the tool PeakAnalyzer.

Following are the details of the identified peaks:

1) Total no. of peaks identified in sample acp300 = 34,141

2) Total no. of peaks identified in sample p300 = 27,338

3) Common peaks between acp300 and p300 = 2044

4) Peaks unique to sample acp300 = 32,097

5) Peaks unique to p300 = 25,294

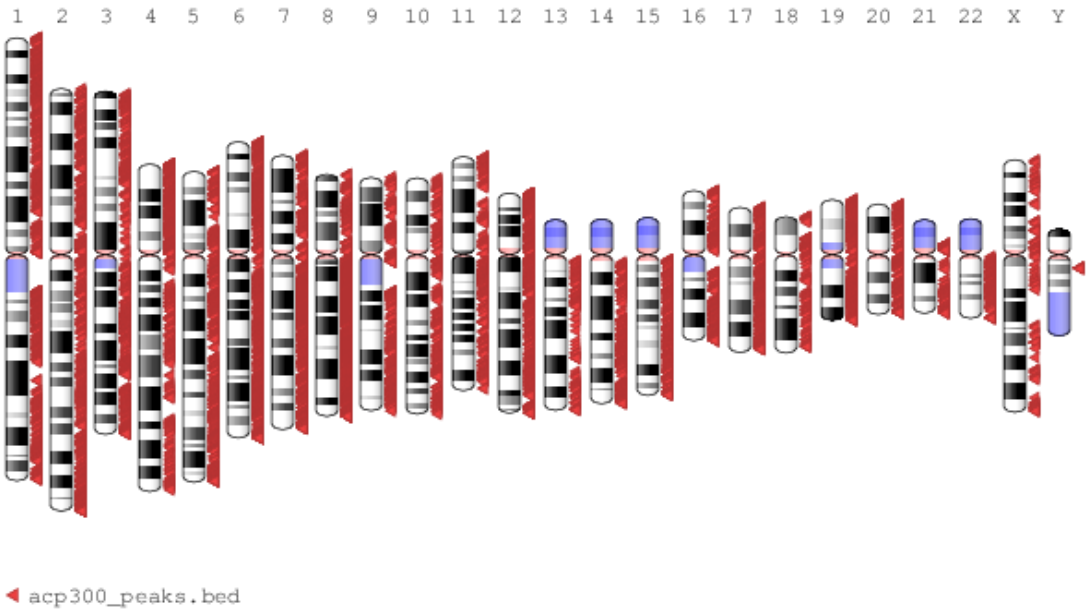

Figure 2.24: Distribution of acp300 peaks (red triangles) over chromosomes. Ideogram depicting the acp300 enrichment over chromosomes.

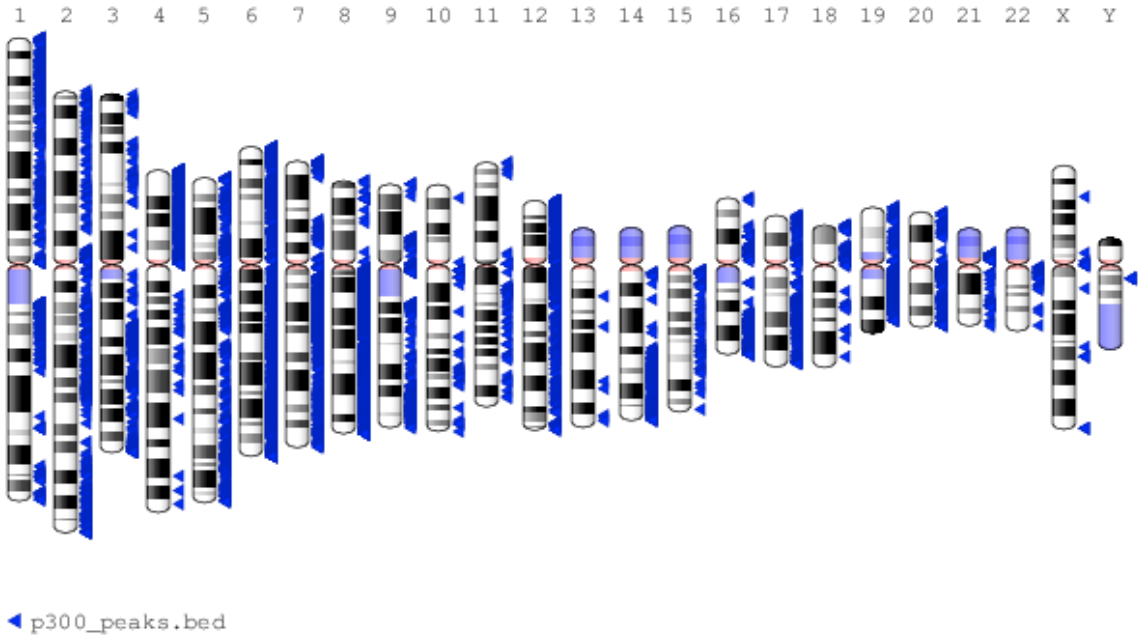

Figure 2.25: Distribution of p300 peaks (blue triangles) over chromosomes. Ideogram depicting the p300 enrichment over chromosomes.

Genome wide occupancy of acp300 (Figure 2.24) and p300 (Figure 2.25) was represented in an ideogram of identified and annotated peaks on each chromosome. This was done using NCBI Genome Decoration Page (https://www.ncbi.nlm.nih.gov/genome/tools/gdp). Integration of ChIP-seq and Microarray data was done to establish the correlation between the chromatin occupancy of p300/acp300 and the gene expression alteration upon p53 induction.

Chapter 3

Mechanisms of Histone Chaperone NPM1-induced autoacetylation of p300

This chapter presents evidence that elucidates the role of NPM1 in modulating p300 activity through the induction of p300 autoacetylation. The chapter begins with correlative data linking the overexpression of NPM1 in Oral cancer with the enhancement of p300 autoacetylation in tumor tissue. Further biochemical, biophysical and cellular evidence are provided to give insights into the molecular mechanisms that may be involved in the NPM1-mediated enhancement of p300 autoacetylation. The results suggest that NPM1 is a novel molecular chaperone for p300. It appears that NPM1 chaperone activity is essential for the stabilization of the intrinsically disordered structure of p300. Furthermore, it can be conjectured that the oligomeric form of NPM1 can interact with two or more molecules of p300 to facilitate intermolecular autoacetylation.

3.1. Correlation between NPM1 expression and autoacetylated p300 in Oral cancer.

NPM1 has been associated with cancer manifestation and progression. Overexpression of NPM1 has been reported in several solid tumors such as oral, prostate, ovarian, colon and bladder cancers (Chan et al., 1989; Colombo et al., 2011; Grisendi et al., 2006; Shandilya et al., 2009; Yung, 2007). Being an important component of ribosome biogenesis, protein synthesis, and centrosome duplication, the overexpression of NPM1 in cancers is associated with high mitotic index and proliferation (Chan et al., 1989; Feuerstein et al., 1988; Roussel and Hernandez-Verdun, 1994). NPM1 is also a transcription co-activator and can enhance RNA polymerase II transcription from a chromatin template in an acetylation dependent manner (Swaminathan et al., 2005). NPM1 is a bona fide substrate of p300. Interestingly, acetylated NPM1 shuttles into the nucleoplasm from the nucleolus and co-occupies RNA Pol II binding sites on chromatin (Shandilya et al., 2009). The data suggests that NPM1 plays an important role in RNA pol II-driven transcription. Moreover, acetylated NPM1 was observed to be upregulated in oral cancer and the increase in acetylated NPM1 levels appeared to correlate with the progressive higher grades of oral cancer (Shandilya et al., 2009). As

described earlier, NPM1 was subsequently characterized as an inducer of p300 autoacetylation. It was observed that histones were hyper-acetylated in oral tumor samples in comparison to their adjacent normal tissue. This alteration in the acetylation landscape in oral cancer was linked to the ability of NPM1 to induce the activity of p300 through the induction of p300 autoacetylation (Arif et al., 2010b).

To directly correlate the overexpression of NPM1 to the hyperactivity of p300, immunohistochemistry (IHC) was performed on oral cancer tissue microarrays consisting of 1 mm diameter punctures of tumor tissue and their adjacent normal tissue. In these arrays, the levels of NPM1, p300, autoacetylated p300 (K1499ac p300) and a p300-specific histone H3 acetylation mark, H3K18 acetylation were assessed by IHC in tumor samples versus the adjacent normal oral tissue. In conjunction with the previous study, a distinct increase was observed in NPM1, autoacetylated p300, and H3K18 acetylation (Figure 3.1). The study also revealed that p300 protein was also overexpressed in the tumor samples, albeit lower in comparison to the autoacetylated form of p300 (Figure 3.1). This significant observation suggested that it is the activated form of p300 (autoacetylated p300) which may influence the manifestation of oral cancer through the alteration in the acetylation landscape and deregulation of gene expression.

To determine whether the expression of NPM1 was indeed positively correlating with autoacetylated p300 levels, the H-scores of NPM1 and autoacetylated p300 in the same OSCC tumor samples were compared. A significant positive correlation was observed in the tumor tissues with a Pearson’s coefficient of 0.6201 (p-value= 0.0238; n=13), suggesting that higher levels of NPM1 protein expression positively correlated with enhanced levels of autoacetylated p300 (Figure 3.2A and B).

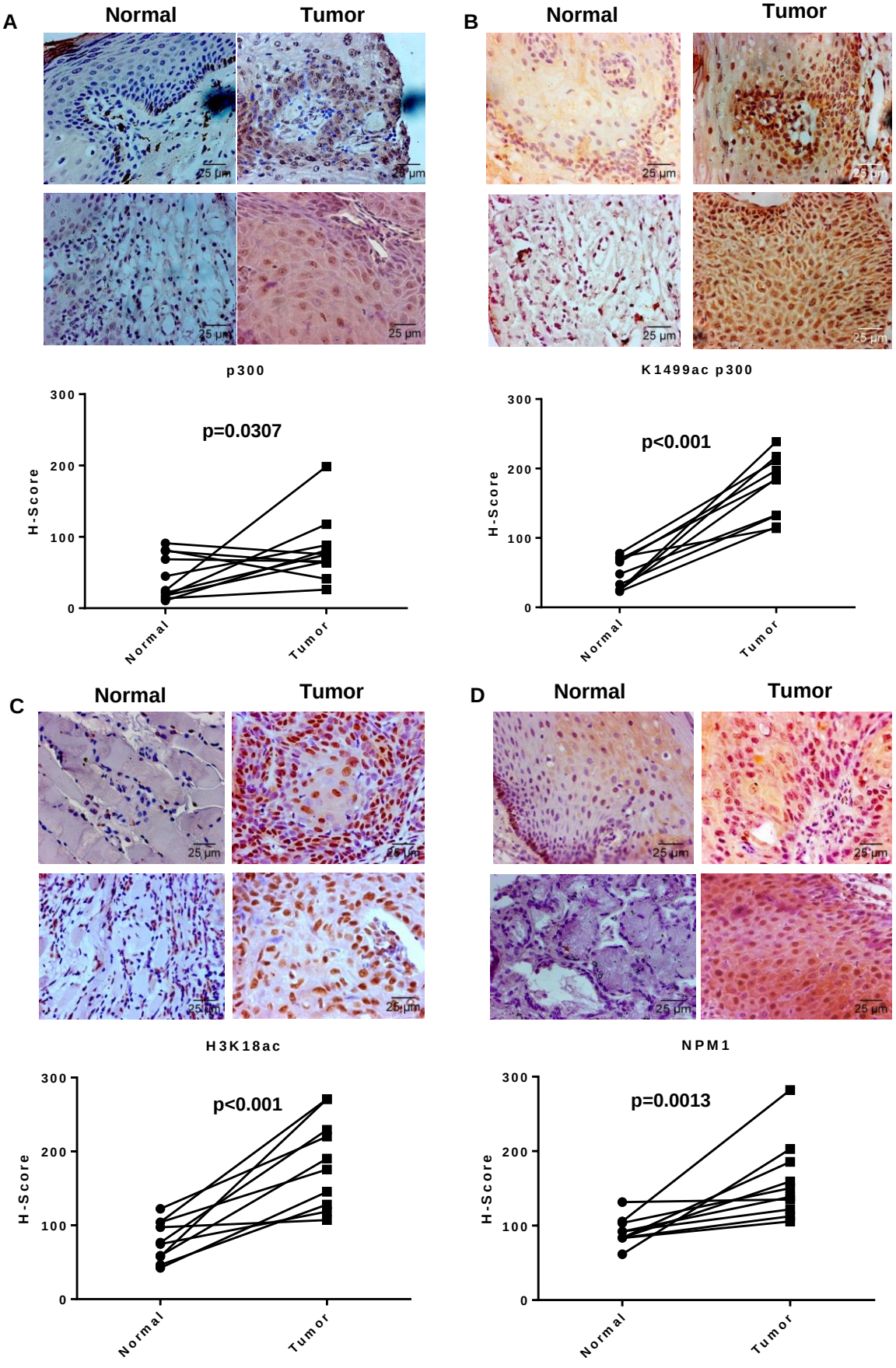
A
Normal
Tumor
25 µm
p300
300
200
100
0
H-Score
p=0.0307
Normal
Tumor
B
Normal
Tumor
25 µm
K1499ac p300
300
200
100
0
H-Score
p<0.001
Normal
Tumor
C
Normal
Tumor
25 µm
H3K18ac
300
200
100
0
H-Score
p<0.001
Normal
Tumor
D
Normal
Tumor
25 µm
NPM1
300
200
100
0
H-Score
p=0.0013
Normal
Tumor

Figure 3.1: Immunohistochemistry (IHC) in OSCC patient samples. IHC to assess the levels of (A) p300, (B) autoacetylated (K1499ac) p300, (C) H3K18ac and (D) NPM1 in OSCC tumor tissue versus the adjacent normal tissue. The intensity of the IHC staining was quantified by H-scoring which is graphically represented below the representative IHC images. The mean H-score was plotted of adjacent Normal and Tumor samples (n=10), statistical analysis was performed using unpaired two-tailed t-test.

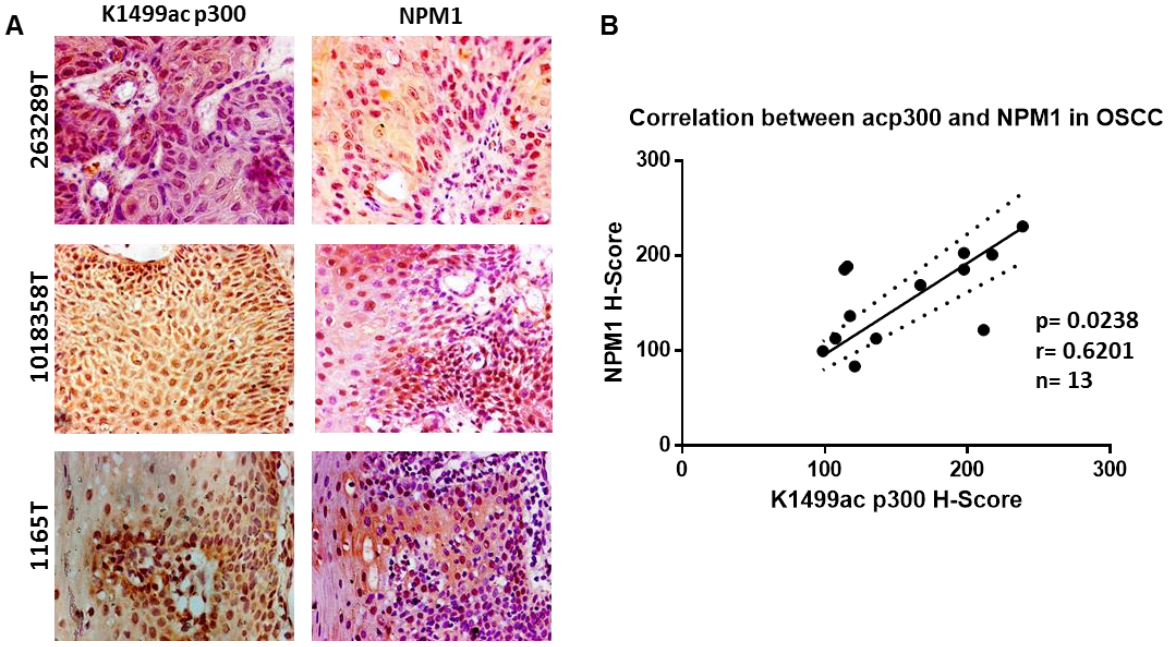

Figure 3.2: Immunohistochemistry to access the correlation between the expression levels of NPM1 and autoacetylated (K1499ac) p300 in OSCC tumor tissues. (A) Representative IHC images of K1499ac p300 and corresponding NPM1 staining in OSCC tumor tissues (patient ID given alongside). The scatter plot represents the mean H-score of NPM1 (y-axis) and K1499ac p300 (x-axis) was fitted with a linear regression line ± 95% confidence interval (CI) (slope= 0.9621 ± 0.07042, 95% CI= 0.8087 to 1.116). A significant correlation was observed (Pearson's coefficient (two-tailed), r= 0.6201; p-value= 0.0238; n=13) between the levels of NPM1 and K1499ac p300.

3.2. NPM1 regulates p300 autoacetylation in cells.

To consolidate the link between p300 autoacetylation and the histone chaperone, NPM1, the direct interaction was determined through the physical association between them and was examined by means of FLAG pull down assay (Figure 3.3A). The influence of NPM1 on p300 autoacetylation was then established by creating a doxycycline-inducible shRNA-based NPM1 knockdown in an oral cancer cell line (AW13516) and human embryonic kidney cells (HEK293). Upon silencing of NPM1 expression, a modest reduction was observed in p300 autoacetylation levels which were determined both by immunoblotting analysis as well as by immunofluorescence studies (Figure 3.3B and D). The NPM1 protein contains two nuclear localization signals (NLS) and nuclear exit signals (NES) and a nucleolar localization signal

(NoLS) (Hingorani et al., 2000; Nishimura et al., 2002; Yu et al., 2006). NPM1 is a known shuttling protein, predominantly present in the nucleolus, but it can exist in smaller fractions in the nucleoplasm and cytoplasm. Therefore to understand which fraction of NPM1 directly interacts and influences p300 function, it is important to understand its sub-cellular localization. It is also noteworthy that NPM1 subcellular localization may be affected by several factors. Interestingly, its sub-cellular localization can be influenced by the PTMs it harbors. NPM1 was discovered as a nucleolar phosphoprotein and phosphorylation is essential for its function in mitotic spindle localization and mitotic regulation, centriole accumulation and centrosome duplication (Okuwaki, 2008; Shandilya et al., 2014; Spector et al., 1984). SUMOylation of NPM1 is critical for its nucleolar localization and its function in cell proliferation (Liu et al., 2007). Acetylation of NPM1 by p300 results in the retention of NPM1 in the nucleoplasm. In the nucleus, acetylated NPM1 associates with the transcriptionally active RNA Pol II. In OSCC, enhanced levels of acetylated NPM1 correlated with higher tumor grades, suggesting that the acetylated form of NPM1 may assert its oncogenic function through the modulation of RNA pol II transcription (Shandilya et al., 2009). Moreover, under stress conditions, NPM1 is seen to translocate to the nucleus from the nucleolus, which may indicate that NPM1 exhibits important extra-nucleolar functions under stress and pathological conditions (Yao et al., 2010). It is possible that under these conditions, NPM1 interacts with p300 in the nucleoplasm, resulting in NPM1 acetylation and nucleoplasm retention, and also the induction of p300 autoacetylation and activity. This may also explain why only a modest decrease in p300 autoacetylation is observed upon NPM1 knockdown, since only a small fraction of acetylated NPM1 is present in the nucleoplasm in a resting cell (Figure 3.3B and D). Whereas, in the tumor samples higher levels of acetylated NPM1 is present, thus exhibiting a profound effect on p300 autoacetylation and p300-mediated acetylation (H3K18ac) (Figure 3.1). Quantitative PCR was performed to assess the relative transcript levels of p300 upon NPM1 silencing, to ascertain whether NPM1 regulates p300 only at the post-translationally and not at the transcriptional level. As expected, it was found that p300 transcription was not altered by the presence or absence of NPM1 (Figure 3.3C), while the status of NPM1 expression appeared to modulate p300 autoacetylation in cells (Figure 3.3B and D).

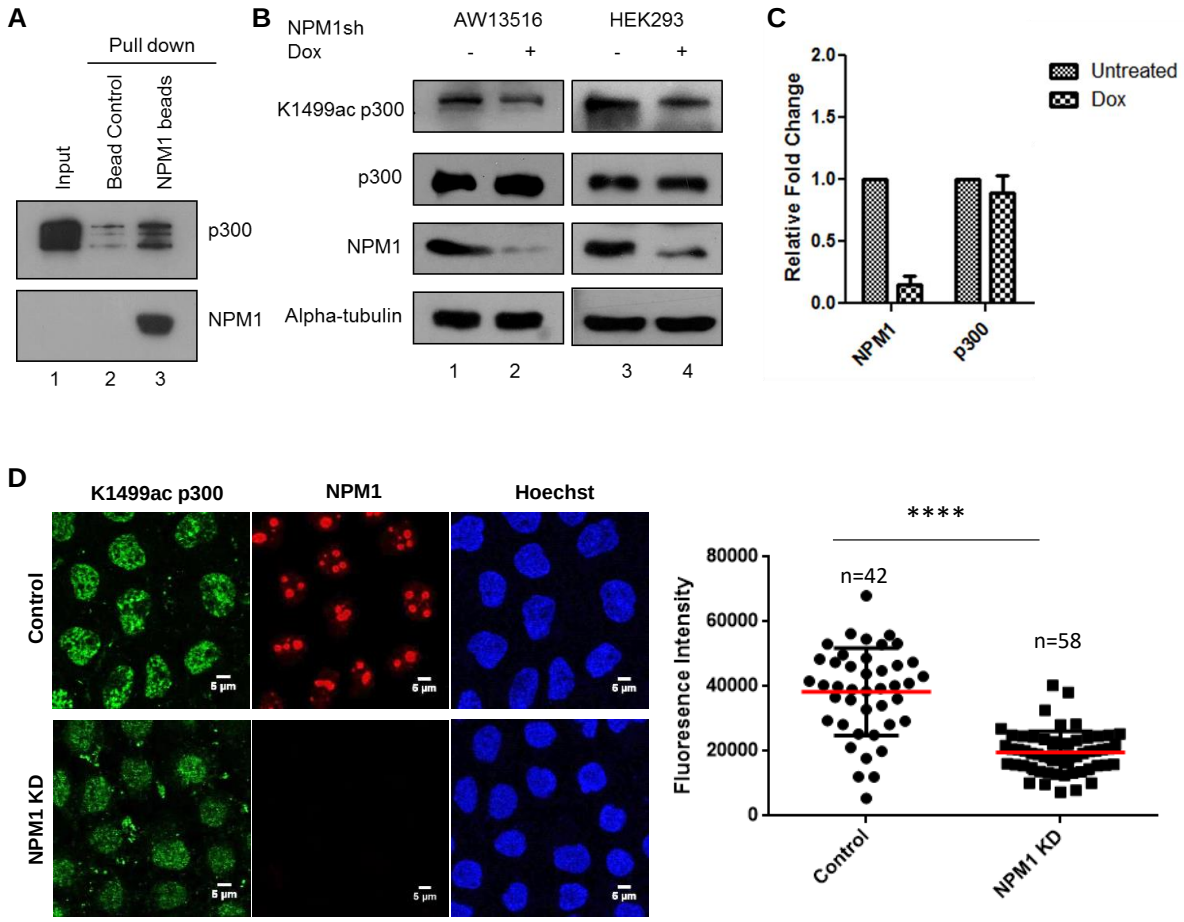

Figure 3.3: NPM1 interacts with p300 and regulates p300 autoacetylation in cells. (A) FLAG pull down assay to detect the interaction between FLAG-tagged NPM1 and p300. The co-immunoprecipitated p300 was detected by western using p300 antibody (top panel) and the immunoprecipitated NPM1 was detected using an antibody against NPM1 (bottom panel). (B) Dox-inducible knockdown of NPM1 protein expression in stably transfected AW13516 and HEK293 cell lines. The levels of NPM1, autoacetylated (K1499ac) p300 and p300 were probed by immunoblotting analysis in lysates from cells with (lanes 2, 4) and without (lanes 1, 3) doxycycline treatment (2µg/ml). Alpha-tubulin served as the loading control. (C) The relative transcript levels of p300 and NPM1 in AW13516 cells were determined by qRT-PCR (mean ± SD, n=3). (D) The levels of K1499ac p300 and NPM1 were accessed in control versus NPM1 knockdown cell line by immunofluorescence. Fluorescence intensity of K1499ac (autoacetylated) p300 in control versus NPM1 KD cells has been quantified (represented as mean ± SD).

3.3. Specificity of NPM1-mediated induction of p300 autoacetylation and activity.

NPM1 is specifically acetylated by p300, indicating that there is specificity even at the level of enzyme-substrate interaction (Shandilya et al., 2009). Acetylated NPM1 also enhances transcription from the chromatin template, revealing that p300-mediated acetylation of NPM1

is crucial for its function as a transcriptional co-activator (Shandilya et al., 2009; Swaminathan et al., 2005). Once it was revealed that NPM1 can modulate the autoacetylation status of p300 without affecting p300 protein or transcript levels, biochemical evidence was required to directly couple the specificity of NPM1 to the induction of p300 autoacetylation. The effect of NPM1 on three different families of KATs (p300, PCAF, and Tip60) was determined by an *in vitro* autoacetylation assay wherein the alteration in autoacetylated KAT was measured by the incorporation of [^{3}H]acetyl groups onto the KAT proteins' lysine residues, which was detected by autoradiography. Here, the KAT protein is both the enzyme and substrate, thereby allowing an effective measure of the influence of NPM1 on the auto-modification of these enzymes. It was observed that NPM1 could effectively enhance the levels of p300 autoacetylation (Figure 3.4A, lanes 3 and 4) over the basal autoacetylation (lane 2). In the case of PCAF (GNAT family acetyltransferase) and Tip60 (MYST family acetyltransferase), the presence of NPM1 in the reaction did not alter the levels of autoacetylation. These data suggest that NPM1 specifically enhances p300 autoacetylation levels without exhibiting much effect on PCAF or Tip60 autoacetylation.

Enhanced autoacetylation of p300 is a measure of enhanced catalytic activity (Thompson et al., 2004). Thus, to confirm that NPM1 can activate p300 catalytic activity through the enhancement of its autoacetylation, a filter binding assay was performed to measure the activity of p300 in the absence and presence of NPM1. The p300-mediated acetylation of core histones was proportional to the levels of [^{3}H]acetyl groups incorporated onto core histones bound to the p81 phosphocellulose-filter paper. The levels of [^{3}H]acetylated core histones were measured in a scintillation counter. Interestingly, in the presence of NPM1 enhanced the activity of p300 by approximately 3-fold. In this assay, the concentration of p300 used was 1 nM and NPM1 was used at concentrations 5, 15 and 25 nM. If so, then NPM1 at 15-25 nM concentrations appears to saturate all the available p300 molecules.

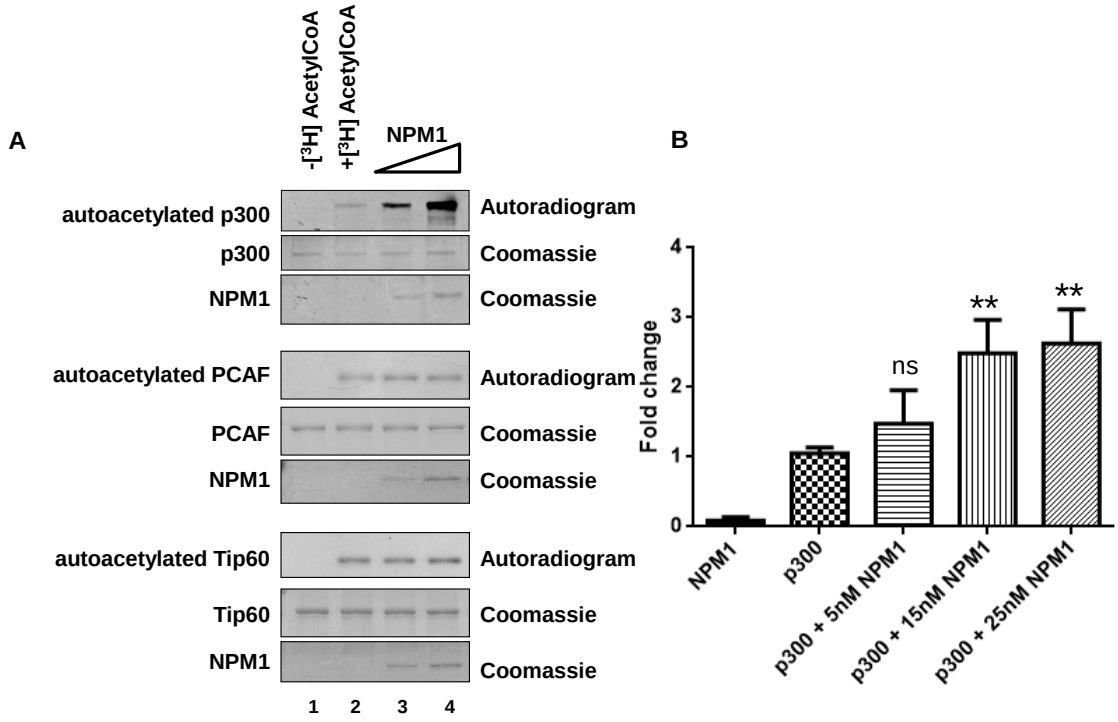

Figure 3.4: NPM1 is a specific inducer of p300 autoacetylation. (A) An *in vitro* acetyltransferase assay was performed to determine the levels of autoacetylation of different KAT enzymes in the presence of recombinant NPM1 (lanes 3 and 4, 50 nM and 100 nM, respectively). The autoradiograms indicate the levels of p300, PCAF, and Tip60 autoacetylation respectively; while the Coomassie Brilliant Blue stained protein panels serve as the loading. (B) Enhancement of p300 (1 nM) activity in the presence of increasing concentrations of NPM1, determined by filter binding assay. The mean fold change was plotted ± SEM; n=3, statistical analysis was performed using two-tailed unpaired t-test (**, $p<0.01$).

3.4. NPM1 is a molecular chaperone for p300.

NPM1 belongs to the nucleoplasmin family of histone chaperones (Okuwaki et al., 2001b). The crystal structure of the nucleoplasmin core revealed that the nucleoplasmin family proteins can form a pentamer which can be packed one over the other to form a decamer. The lateral interface formed can interact with five H2A-H2B dimers or five octamers (Dutta et al., 2001; Lee et al., 2007). NPM1 can preferentially bind to H3-H4 tetramers and can assemble nucleosomes onto a chromatin template (Okuwaki et al., 2001b; Swaminathan et al., 2005). NPM1 is also a ribosome chaperone or a ribosome assembly factor and associates with preribosome particles (Yu et al., 2006). Previous reports have indicated that NPM1 may harbor molecular chaperone activity which is distinct from its histone chaperone activity (Szebeni and Olson, 1999). It was reported that NPM1 can prevent thermal denaturation and aggregation of protein and can preferentially bind to denatured proteins (Szebeni and Olson,

1999). Since p300 is an intrinsically disordered protein, it can be speculated that the chaperone activity of NPM1 may be involved in the stabilization of p300 structure and thus contributing to the NPM1-mediated enhancement of p300 autoacetylation.

To assess whether NPM1 is a molecular chaperone for p300 the following hallmarks of a molecular chaperone activity were tested:

a. A chaperone should be able to prevent aggregation and/or denaturation of its substrate.
b. A chaperone should possess the ability to refold or rescue its substrate from a denatured conformation.

To test both possibilities, *in vitro* biochemical assays were designed.

First, to determine the role of NPM1 in preventing aggregation and denaturation of p300, p300 was thermally denatured at 45 °C either alone or in the presence of NPM1. After the thermal denaturation step, p300 activity was scored by its ability to acetylate core histone substrates. It was observed that when p300 was denatured in the absence of NPM1 (control) it loses its catalytic activity by 75%, whereas when p300 is heated in the presence of NPM1, it was found that 65% of p300 activity was retained (35% loss in activity) (Figure 3.5A). This indicated that the presence of NPM1 could prevent p300 activity loss possibly by inhibiting p300 denaturation. Independent control studies show that NPM1 does not undergo thermal denaturation at 45 °C.

Next to check whether NPM1 can rescue the activity of denatured p300, the assay was designed such that p300 was first thermally denature at 45 °C, then the reaction was incubated at 30 °C in the absence or presence of NPM1. Histone acetylation was used as a measure of the rescue of p300 activity. Interestingly, NPM1 could effectively rescue the activity of denature p300 in a concentration-dependent manner (Figure 3.5B). To rule out the possibility that the observation is due to molecular crowding, BSA, a known molecular crowding agent was used in a similar assay at equal molar concentrations to NPM1. BSA failed to rescue the enzymatic activity of p300, suggesting that the activity rescue by NPM1 is not a non-specific event (Figure 3.5C). p300 is an important KAT which can acetylate several substrates within the cell. Therefore, to ascertain that the rescue of p300 activity was not merely due to an enzyme-substrate interaction, another substrate of p300 was used in the similar assay. PC4, a substrate of p300, was used in equal molar concentrations as NPM1 in the activity rescue assay, but it was observed that PC4 failed to rescue p300 activity (Figure 3.5D). This proved that NPM1 possibly makes more stable contacts with p300 in contrast to

the transient substrate-enzyme interactions p300 is known to make with its substrates (hit-and-run (*Theorell–Chance*) mechanism). Finally, to establish that the NPM1 chaperone activity is specific to p300 among other KAT enzymes, the MYST family KAT, Tip60 was denatured followed by the addition of NPM1 to the reaction. It was found that NPM1 appeared to specifically rescue p300 activity while exhibiting little or no effect on Tip60 activity. These finding were congruent with the autoacetylation KAT assay results (Figure 3.4A), suggesting that the chaperone activity of NPM1 may be a mechanism via which it alters p300 structure to promote efficient *trans*-autoacetylation.

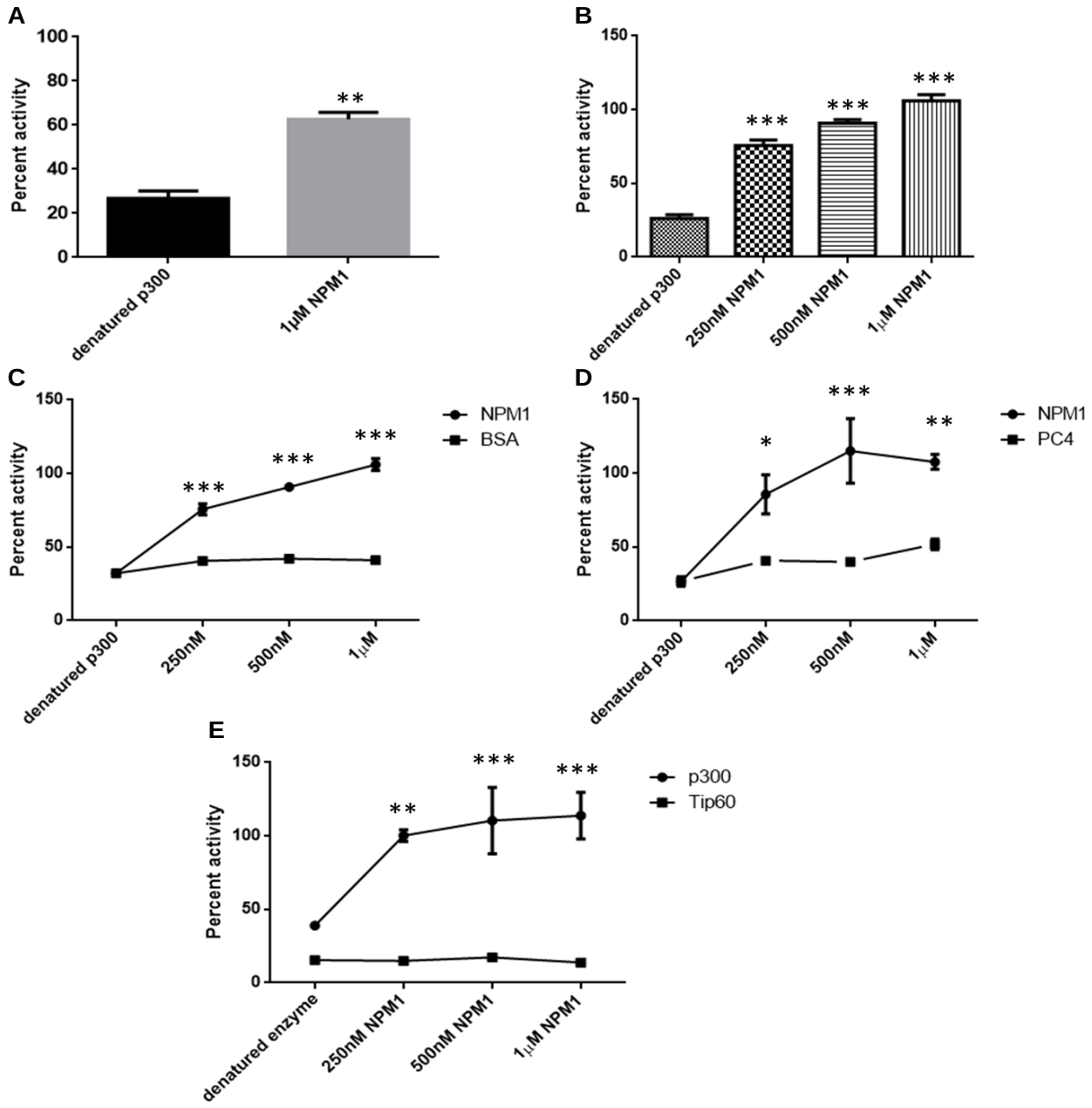

Figure 3.5: NPM1 is a novel molecular chaperone of p300. (A) Thermal protection assay was performed with and without NPM1. The rescue of heat denatured p300, upon addition of NPM1 (B), BSA (C), and PC4 (D), in the indicated concentrations, was determined by filter binding assay. (D) To determine whether NPM1 can rescue the activity of Tip60 in comparison to p300 a similar filter binding assay was carried out using the indicated concentrations of NPM1 after thermal denaturation of the two enzymes. The mean percent activity was plotted ± SEM, statistical analysis was performed using unpaired two-tailed t-test (***, p<0.001; **, p<0.01; *, p<0.05).

3.5. Intrinsic tryptophan fluorescence to detect the structural alteration of p300.

In the previous set of experiments, the rescue of denatured p300 by NPM1 was an indirect indication that NPM1 can refold p300 protein by physically binding and altering its structure. The fluorescence properties of the protein(s) due to intrinsic tryptophan fluorescence were employed as additional evidence for the physical association between the two proteins and potential of NPM1 to induce conformational alteration in p300 as a basic requirement for its chaperone activity. Tryptophan (Trp/W), Tyrosine (Tyr/Y), and Phenylalanine (Phe/F) have fluorescence properties among all the canonical amino acids. Of the three, tryptophan and tyrosine have high quantum yields (emitted photons/excited photons), in comparison to phenylalanine, which can be detected as a fluorescence signal; therefore, can be used experimentally. The excitation wavelength of 280 nm (λ_{ex}= 280 nm) can excite both tryptophan and tyrosine, while λ_{ex}= 295 nm can selectively excite only tryptophan.

The fluorescence properties (quantum yield) of a fluorophore are sensitive to the environment it is present in and in the case of tryptophan and tyrosine it depends on the folded state of the proteins. In a native protein conformation, these residues are buried with the hydrophobic core of the protein and have a high quantum yield resulting in higher fluorescence emission intensities. In a denatured or unfolded (partially or fully unfolded) state, the tryptophan residues are exposed to the surrounding hydrophilic solvent environment reducing the quantum yield and fluorescence emission intensities (Figure 3.6). Given the sensitivity of the technique, the dynamics of the 3-dimensional state of a protein can be followed from the alteration of the intensity of protein emission spectrum and the shift in the emission spectral peak relative to the unfolded state or native state. The unfolding of a protein can be achieved by disrupting the weak interactions (hydrogen bonding, electrostatic interactions, and hydrophobic interactions) that stabilize the protein in a native conformation. This is done by several methods such as the use of chaotropic agents (urea, guanidium hydrochloride), change in pH,

and thermal denaturation (heat) (Figure 3.6). The kinetics of folding/unfolding can be traced by the intrinsic fluorescence intensities of tryptophan or tyrosine residues.

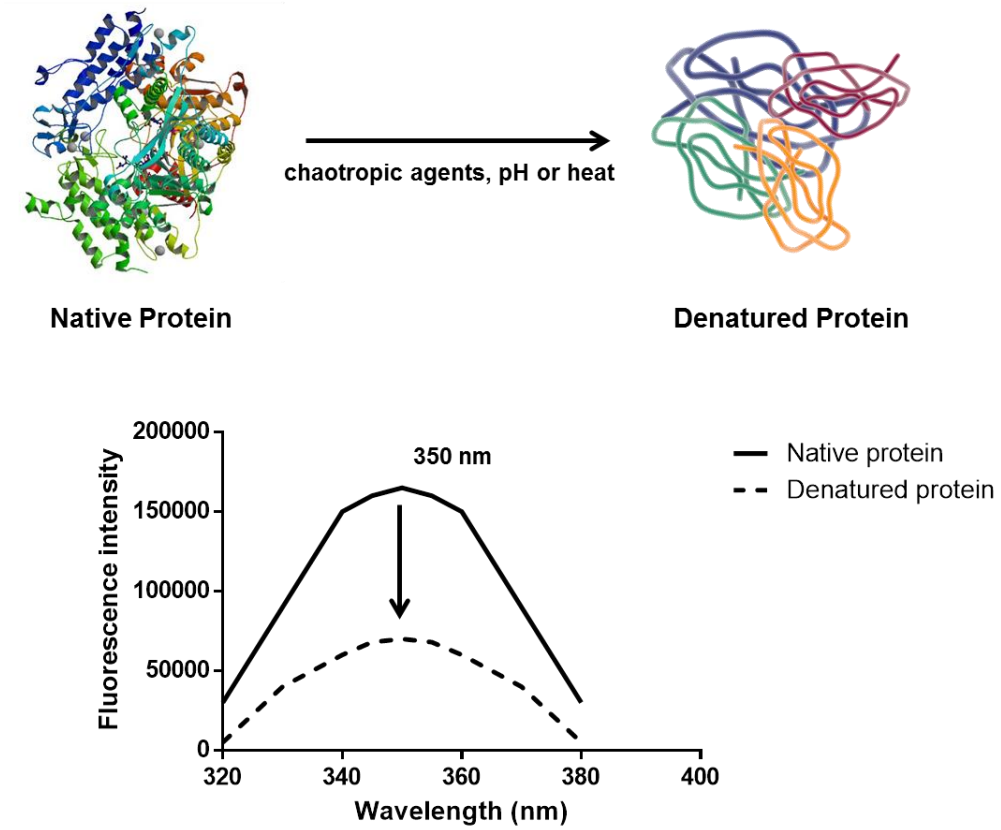

Figure 3.6: Intrinsic tryptophan fluorescence intensity alteration with protein unfolding. Protein unfolding from a native 3-dimensional conformation (native protein, (eg. p300 core domain PDB: 4BHW)) to a random unfolded state (denatured protein) upon denaturation. An example of emission scans arising from tryptophan residue(s) when the protein is in the native state and when it is denatured.

Two methods were adopted to establish the aforementioned points. The p300 protein contains 12 tryptophan residues, of which 11 residues (W403, W571, W1115, W1122, W1129, W1266, W1466, W1509, W1649, W1681) reside in globular domains and 1 tryptophan residue is present on an unstructured loop region (W1995). Interestingly, NPM1 contains only 2 tryptophan residues (W288, W290), present on the far end of the C-terminal domain (Figure 3.7 A,B).

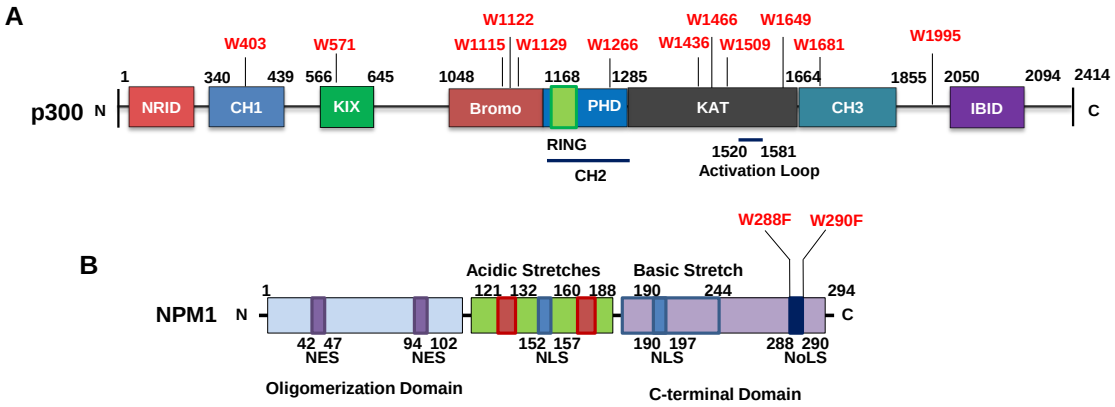

Figure 3.7: Domain architecture of p300 and NPM1. Schematic showing the domain architecture and location of the tryptophan residues on (A) p300 and (B) NPM1. The two tryptophan residues (W288 and W290) on the C-terminal of NPM1 are mutated to Phenylalanine [F] as indicated.

Since both proteins have tryptophan residue(s), in the first set of experiments the fluorescence emission spectra of each protein and their mixture were recorded. The concentrations were so chosen that most of the p300 molecules are complexed with NPM1, as indicated from the biochemical assays. The emission spectra of both proteins were summed up. The theoretical spectrum thus obtained was compared with the observed spectrum of the mixture. The non-overlap of the two spectra (Figure 3.8) suggested that there is an association between the two proteins. As a sequel to the association, the simulated spectrum and the observed spectra differed. Since the absorbance of the protein samples at λ_{ex}= 295 nm was less than 0.05, no inner filter correction was done. However, this initial result was confirmed from a second set of confirmatory fluorescence studies.

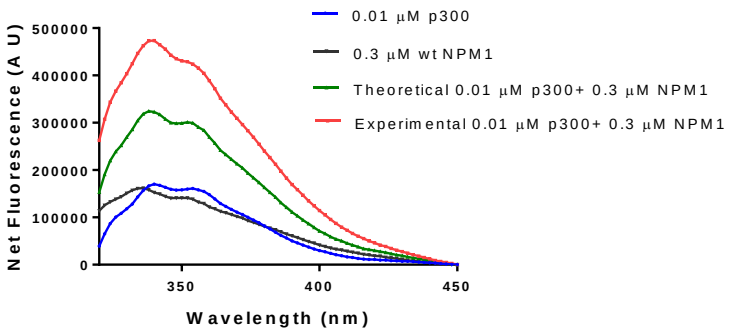

Figure 3.8: NPM1 alters the intrinsically disordered p300 structure. Graphical representation of the fluorescence spectra of p300 and wildtype NPM1 present either alone or together and the theoretical addition of the p300 and NPM1 spectra as mentioned. (λ_{ex}=295 nm, slitwidth=2 nm, representative graph of 3 independent experiments).

In the second set of experiments, mutant NPM1 lacking the two tryptophan residues was employed and the change in the fluorescence emission spectrum of p300 at λ_{ex}=295 nm was monitored as a function of the input concentrations of mutant NPM1. Appropriate controls were done to confirm the absence of fluorescence emission intensity of mutant NPM1 at λ_{ex}=295 nm. In the previous experiment, the NPM1+p300 observed spectra only gave information regarding the formation of a complex, but little information regarding the structural alteration of p300. To eliminate the contribution of NPM1 from the complex fluorescence spectra, the two tryptophan residues were substituted with phenylalanine, so that the absorbance at 295 nm is negligible, without hindering the overall amino acid side-chain properties. To test whether the mutant retained the structural integrity of wildtype NPM1, CD-spectrometry was performed. The CD spectra of the two proteins were identical, suggesting that the overall structure of the NPM1 Trp mut was unaltered. Another interesting observation in the spectra was the dip in the spectra around 210 nm implying that both proteins were predominantly composed of β-sheets, which is consistent with the crystal structure of the NPM1 core oligomerization domain (Lee et al., 2007), indicating that both the proteins are present in the oligomer conformation (Figure 3.9A). Next to assess whether the Trp mut still retained its chaperone activity, an activity rescue assay was performed as described earlier. The results of this assay indicate that the chaperone activity of the Trp mut was equivalent to the wildtype NPM1 (Figure 3.9B).

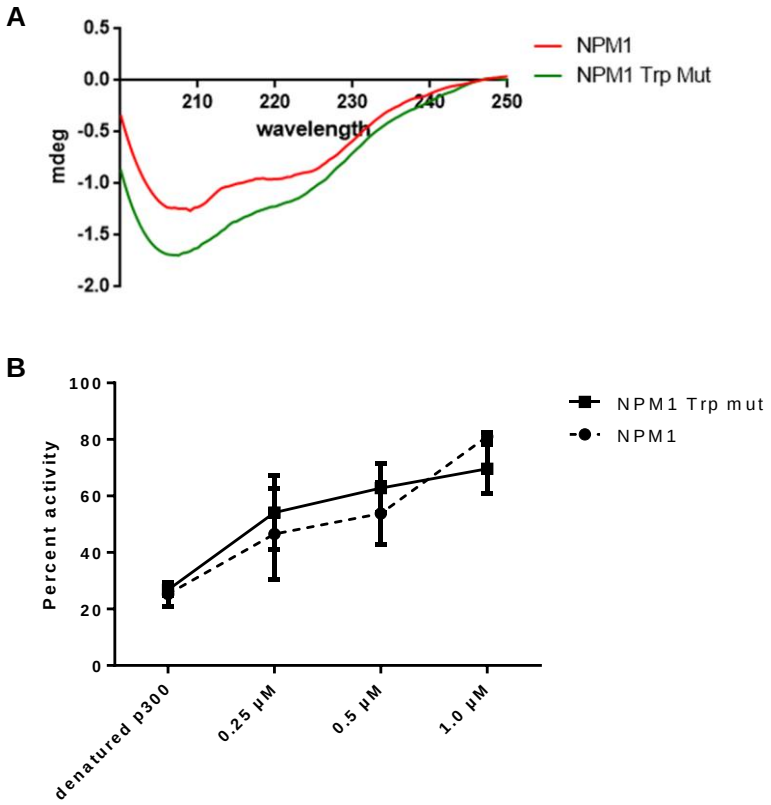

Figure 3.9: Structural and functional characterization of the Tryptophan mutant of NPM1. (A) Circular Dichroism spectra of NPM1 wildtype protein (red) and NPM1 Trp mut (green). 1.4 µM molar concentration of protein was used. (B) Activity rescue assay of heat denatured p300 in the presence of NPM1 Trp mut and wildtype NPM1.

To further characterize the NPM1 tryptophan mutant (NPM1 Trp mut), the concentration-dependent fluorescence intensities at λ_{em}= 350 nm were plotted and fitted with linear regression line with a confidence interval of 95%. For p300 and wildtype NPM1, a significant (p=0.0033 and 0.0032 respectively) concentration-dependent deviation from origin was observed, while for the NPM1 Trp mut a concentration-dependent alteration in fluorescence intensities at λ_{em}= 350 nm was not observed, thus proving the mutations had effectively nullified the absorbance λ_{ex}= 295 nm (Figure 3.10 A-C). The linear nature of the plot for wildtype NPM1 as a function of the input concentration suggests that there is no change in the state of aggregation of NPM1. Therefore, at the concentration range used in these experiments, the form of NPM1 (either monomeric or multimeric) remains constant.

The fluorescence spectra of p300 alone and in the presence of increasing concentrations of NPM1 Trp mutant are shown in Figure 3.11A and B. The following observations were made from Figure 3.11A and B.

1. There is an increase in the fluorescence emission with the increase in the input concentration of NPM1 Trp mutant.
2. There is a visible alteration in the shape of the spectra of p300. For example, the shoulders at λ= 340 nm and λ= 355 nm (indicated by dotted lines) become more prominent with increase in the concentration of NPM1 Trp mut (Figure 3.11A).
3. In order to establish the nature of binding, the emission λ= 350 nm is plotted as a function of NPM1 Trp mutant concentration. The resulting curve shown in Figure 3.11B originates from a linear binding isotherm, thereby suggesting a reversible association between the two proteins. The equation is represented as follows:

$$\mathbf{p300 + n(NPM1) \rightleftharpoons \{p300.\ (NPM1)_n\}}$$

The above equilibrium takes into account the oligomeric form of NPM1. The apparent K_d was estimated from the concentration of NPM1 corresponding to 50% of change in fluorescence intensity of p300 (as shown in Figure 3.11B).

Apparent Dissociation Constant (K_d),

$$\mathbf{K_d = \frac{[p300]\,[NPM1]^n}{[p300.(NPM1)_n]}}$$

From the fluorescence experiments the K_d was calculated to be ~150 nM.

The enhancement of fluorescence intensity of p300 in presence of NPM1 can be ascribed to alteration in the environment of the tryptophan residue(s) as a result of complex formation with NPM1. Such alteration could arise from the NPM1 induced changes in the secondary/tertiary structure of p300. The increase implies that the tryptophan residue(s) is/are in a hydrophobic environment. The increase in the hydrophobicity could in principle occur due to refolding of the p300 as a consequence of the complex formation with NPM1. However, no significant red shift was observed in the fluorescence emission spectra of p300 upon complex formation with NPM1. The plausible explanation is as follows: the tryptophan residue W1995 in p300 is the only tryptophan residue located on an unstructured loop. Upon the binding of NPM1, the disordered nature of p300 is stabilized thereby allowing the tryptophan residue W1995 to be buried into the hydrophobic core of p300, resulting in the increase in fluorescence intensity. But the absence of red shift may be due to the effect of the other 11 tryptophan residues present in the globular domains of p300 which may mask the effect of the lone W1995 residue. These observations correlate with the results obtained from

the biochemical activity rescue assays, suggesting that the ability of NPM1 to refold p300 structure is essential for its ability to activate p300 acetyltransferase activity. From the aforementioned features, it may be conjectured that NPM1 act as a chaperone for p300.

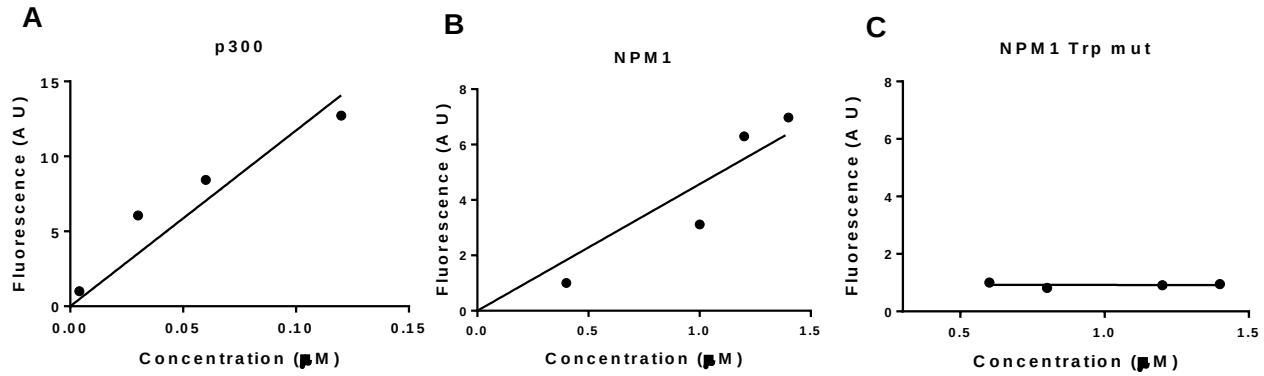

Figure 3.10: Creating a tryptophan fluorescence-defective mutant of NPM1. Graphical representation of the concentration-dependent alteration in relative fluorescence intensities (in arbitrary units) at λ_{em}=350 nm of (A) p300, (B) NPM1 and (C) NPM1 Tryptophan mutant (NPM1 Trp mut).

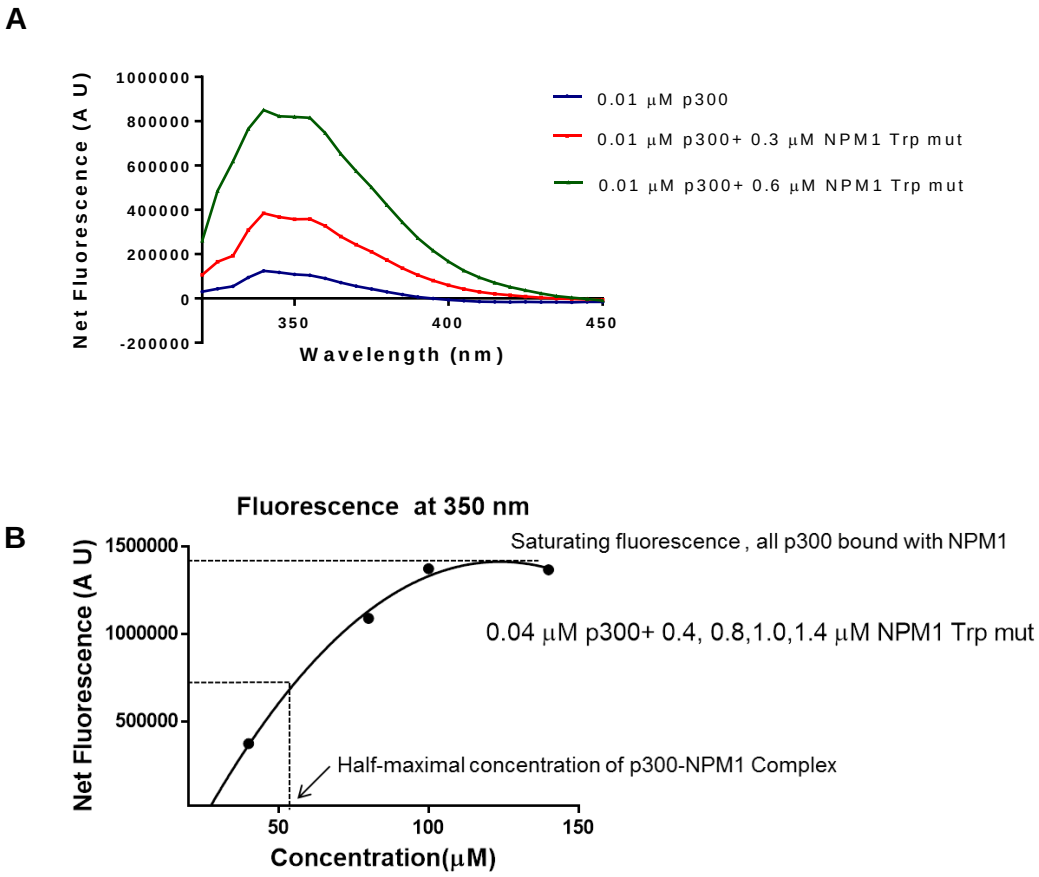

Figure 3.11: NPM1 refolds the intrinsically disordered protein, p300. (A) Fluorescence spectra of p300 and NPM1 tryptophan mutant at the indicated concentrations present either alone or together as mentioned. (B) Fluorescence intensities at λ_{em}=350 nm of p300 and

NPM1 tryptophan mutant together present at the indicated concentrations. (λ_{ex}=295 nm, slitwidth=2 nm, representative graphs of 4 independent experiments).

3.6. NPM1 domains which are essential for the enhancement of p300 autoacetylation

To map the specific domain(s) in NPM1 that may play a major role in the induction of p300 autoacetylation, a set of different deletion mutants were tested for their ability to enhance p300 autoacetylation (Figure 3.12A). These mutants were tested earlier for their ability to perform the NPM1 canonical functions of histone chaperone activity and transcription co-activation function which have been tabulated in Figure 3.12B (Swaminathan et al., 2005). An *in vitro* KAT assay was performed with the deletion mutants to determine whether the p300 autoacetylation levels were affected in comparison to the full length NPM1. A negligible reduction in p300 autoacetylation was observed upon the deletion of 94 C-terminal amino acids (1-200aa NPM1) in comparison to the full length NPM1. Further deletion of 147 amino acids from the C-terminal residues (1-147aa NPM1) drastically reduced the ability to induce p300 autoacetylation. The NPM1 deletion mutant containing only the oligomerization domain (1-119aa NPM1) did not possess the ability to induce the p300 autoacetylation and is comparable to the negative control. Consistent with the earlier histone chaperone experiments, the C-terminal domain of NPM1 appears to be important for its activity as an inducer of autoacetylation (Figure 3.12B, C). To determine whether the C-terminal domain is indeed important for NPM1 molecular chaperone activity, the activity rescue assays were performed with the deletion mutants. In congruence with the autoacetylation HAT assays, it was observed that the deletion of 94 C-terminal amino acids (1-200aa NPM1) was enough to reduce the molecular chaperone activity by approximately 50%. With progressive deletion of the domains from the C-terminal abrogated the molecular chaperone activity of the NPM1, re-enforcing the fact that the C-terminal domain may be essential for the activity of NPM1 as a chaperone (Figure 3.12D). The features of the C-terminal domain reveals that there are two distinct patches in the C-terminal domain: the basic amino acid stretch and the aromatic amino acid stretch. In the deletion mutant which encompasses the first 200 amino acids (1-200aa NPM1), the major portion of the basic patch, extending from 190-244 amino acids, and the entire aromatic stretch is missing, suggesting that these stretches may be important for the interaction with p300. Interestingly, the basic region in the C-terminal domain of NPM1 is also instrinsically disordered in nature, which could contribute significantly to the interaction with p300 (Demarest et al., 2002; Hisaoka et al., 2014). But the gradual reduction in the

activity also indicates that NPM1 may actually make more contacts with p300 through its other domains.

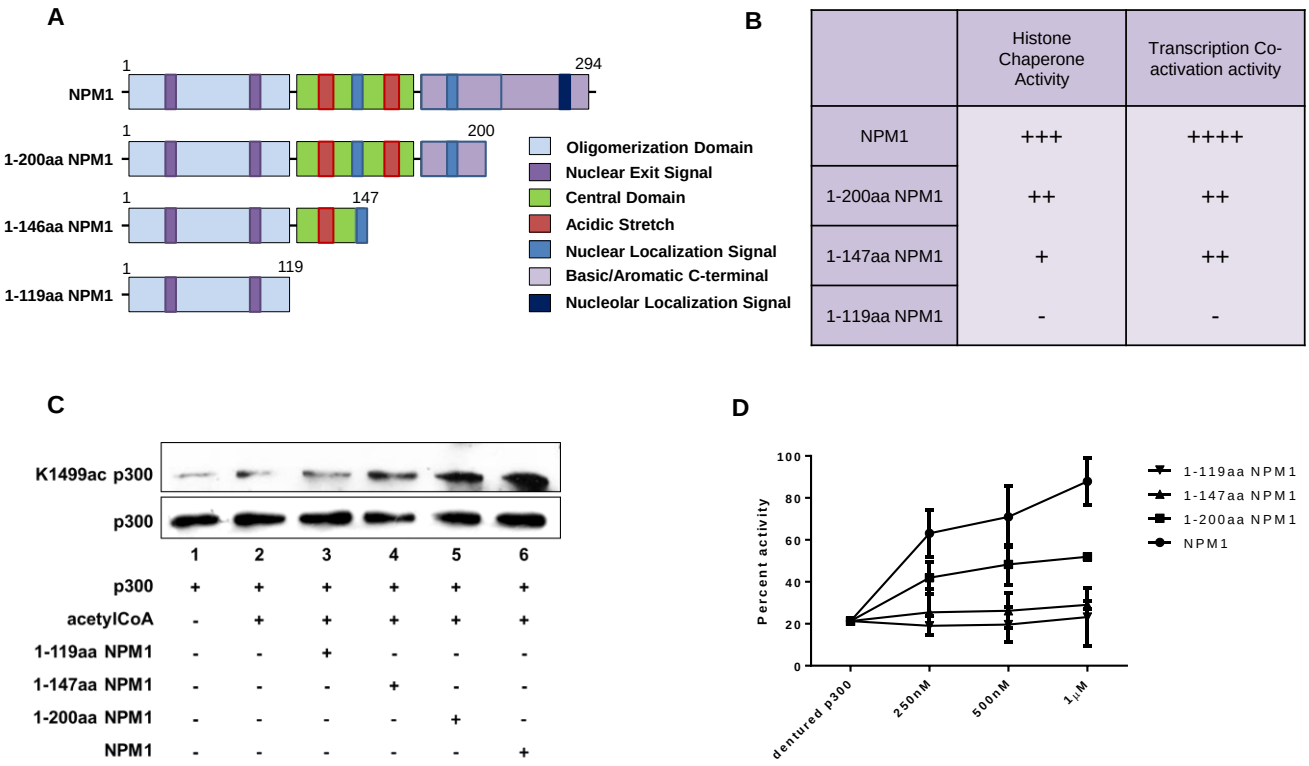

	Histone Chaperone Activity	Transcription Co-activation activity
NPM1	+++	++++
1-200aa NPM1	++	++
1-147aa NPM1	+	++
1-119aa NPM1	-	-

Figure 3.12: NPM1 domain(s) important for the induction of p300 autoacetylation. (A) Schematic showing the domain architecture of full length NPM1 and domain deletion mutant of NPM1. (B) Tabular representation of the histone chaperone activity and transactivation function of NPM1 and NPM1 domain deletions (-, no activity, + to ++++, representing lowest activity to highest activity, respectively), (C) an acetyltransferase assay followed by western using K1499ac p300 and p300 antibodies, to determine the levels of autoacetylation in the presence of 50 nM NPM1 and NPM1 deletion mutants. (D) A radioactive filter binding assay to determine whether the NPM1 deletion mutants could rescue heat denatured p300 at the indicated concentrations in comparison to NPM1.

3.7. Oligomeric form of NPM1 is essential for the enhancement of p300 autoacetylation

The core domain (containing the conserved oligomerization domain and the acidic stretches in the central domain) is an 8-stranded β- barrel forms stable pentamer-on-pentamer structure which is conserved through the three branches of the nucleoplasmin family, including the nucleophosmin, nucleoplasmin and nucleoplasmin-like proteins. This oligomeric conformation is stabilized through the hydrophobic-aromatic interactions present at the dimer-dimer interface. The interface formed on the lateral surface of the decamer is the surface which interacts with nucleosomes, therefore the oligomeric form of NPM1 is

essential for its histone chaperone activity. Small molecule inhibitors that target NPM1 oligomerization can effectively ablated the oncogenic properties of NPM1 (Qi et al., 2008).

NPM1 is a marker for several malignancies and the oligomeric form of NPM1 appeared to be critical for its function. The earlier experiments have established a correlation between NPM1 overexpression and p300 autoacetylation levels and the *in vitro* experiments have indicated that NPM1 is a molecular chaperone for p300. Therefore, to link the importance of oligomeric NPM1 to p300 autoacetylation several oligomerization-defective mutants were created by site directed mutagenesis at the dimer interface to destabilize the NPM1 pentamer (*Dr. Parijat Senapati's Thesis*). The Y17T,C21F NPM1 and L18Q NPM1 oligomerization-defective mutants were created based on the contact sites NSC348884, a small molecule inhibitor of NPM1 oligomerization, binds to at the dimer interface (Qi et al., 2008). The mutations abrogated the ability of NPM1 to enhance p300 activity in comparison to the wildtype NPM1 (Figure 3.13A). Another reported oligomerization-defective mutant of NPM1, C21F NPM1, was earlier reported to be deficient in the molecular chaperone activity of NPM1 (Prinos et al., 2011). This mutant also showed a trend similar to the other oligomerization-defective mutants, as it could not enhance p300 autoacetylation *in vitro* (Figure 3.13B). To attribute the observed lack of induction of autoacetylation to the oligomeric status of nucleophosmin, a monomeric nucleophosmin family protein, NPM3 was used. NPM3 cannot form stable homo-oligomers *in vitro*, but can form hereto-oligomers with NPM1 (Okuwaki et al., 2012). When NPM3 was tested in the *in vitro* p300 autoacetylation assay, it failed to induce autoacetylation, suggesting that the multimeric form of NPM1 is critical for the induction of p300 autoacetylation (Figure 3.13C).

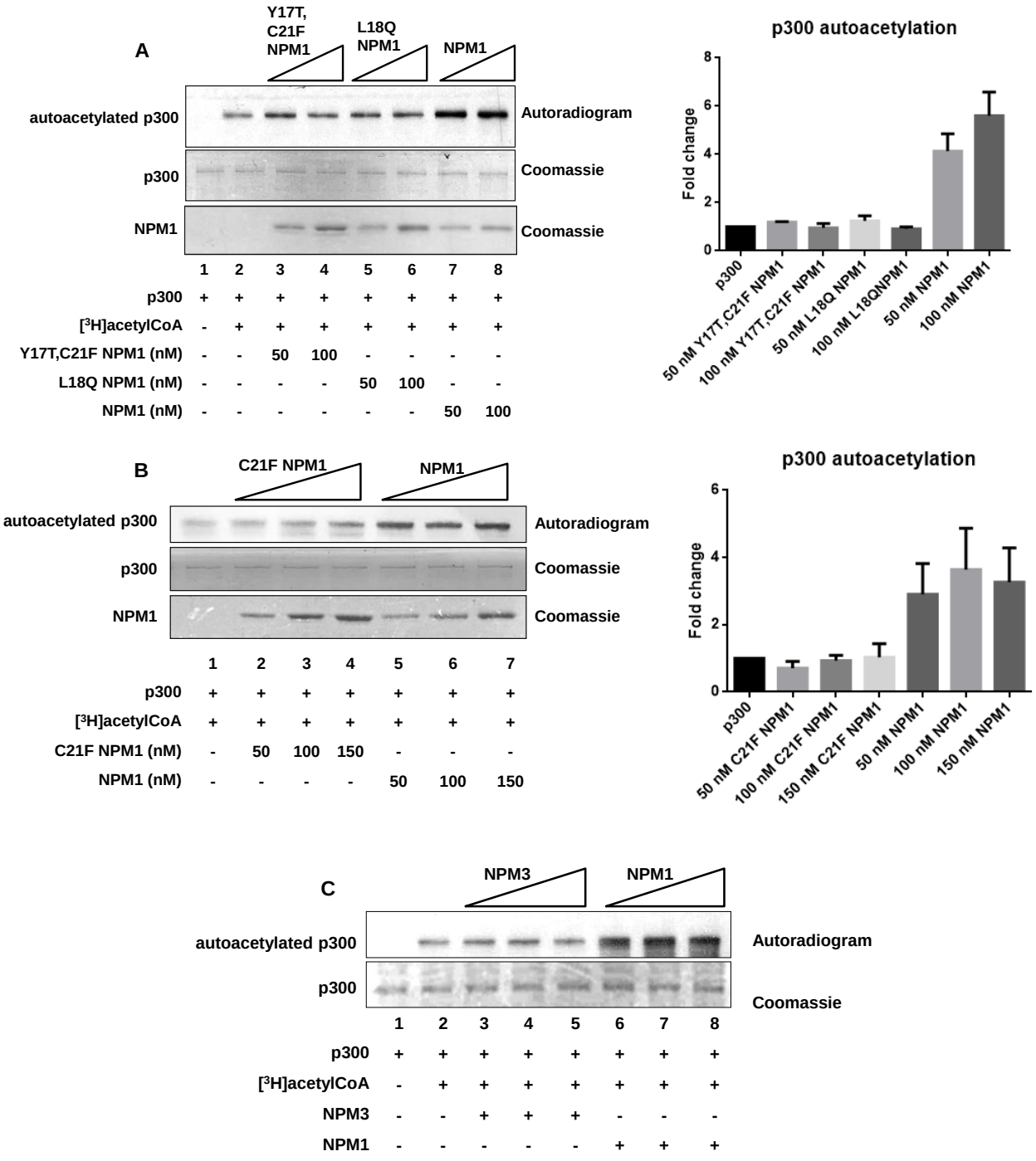

Figure 3.13: Oligomerization defective mutants NPM1 and monomeric NPM3 cannot induce p300 autoacetylation. An *in vitro* acetyltransfeerase assay was performed to determine the levels of autoacetylation of p300 in the presence of oligomerization-defective NPM1 mutants (A) Y17T, C21F and L18Q; (B) C21F and monomeric Nucleophosmin protein family member (C) NPM3 in comparison to wildtype NPM1 at concentrations indicated. The autoradiograms indicate the levels of autoacetylated p300. The graphical representation indicates the relative intensities of autoacetylated p300 bands on the autoradiogram normalized against the total protein levels on the coomassie stained SDS-PAGE. Intensities were measured using ImageJ software and the mean ± SD were plotted.

The oligomerization-defective mutants are deficient in the ability to induce p300 autoacetylation (Figure 3.13 and 3.14B) but when they were tested in the activity rescue assay, they could rescue the activity of heat denatured p300 as efficiently as wildtype NPM1 (Figure 3.14C). It is important to note that in the activity rescue experiments the concentration of NPM1 is almost 10 times more than what is required in the *in vitro* autoacetylation assay. Therefore, it was important to determine the aggregation or oligomerization status of NPM1 at higher concentrations. Through dynamic light scattering (DLS) experiments, it was revealed that at higher concentrations the mutants could exist in multimeric aggregates, thus explaining their ability to rescue heat denatured p300 as efficiently as the wildtype NPM1 (Figure 3.14A). At concentrations below 1 μM, the noise to signal ratio increased dramatically, therefore lower concentrations of NPM1 could not be tested. Due to these experimental constraints, all the concentrations used in the refolding assay could not be checked, but the results are indicative of the formation of multimeric species of NPM1. This could be explained by the fact that the monomeric form of NPM1 exhibits a conformational plasticity and the hydrophobic patches which are generally buried at the dimer interface are exposed to the solvent environment, whereas NPM1 forms a structurally stable conformation when present as a pentamer. Therefore, it can be speculated that at lower concentrations (50-100 nM) used in the autoacetylation assays, the oligomerization-defective mutants (L18Q, C21F, Y17T/C21F) cannot form stable oligomers due to the presence of bulky or charged amino acid side groups present at the dimer interface, but at higher concentrations of the protein (0.25-1.0 μM), the mutant proteins may be able to overcome the steric hindrances or charged hindrances to form higher order aggregates, albeit the nature of these aggregates are unknown under these experimental conditions.

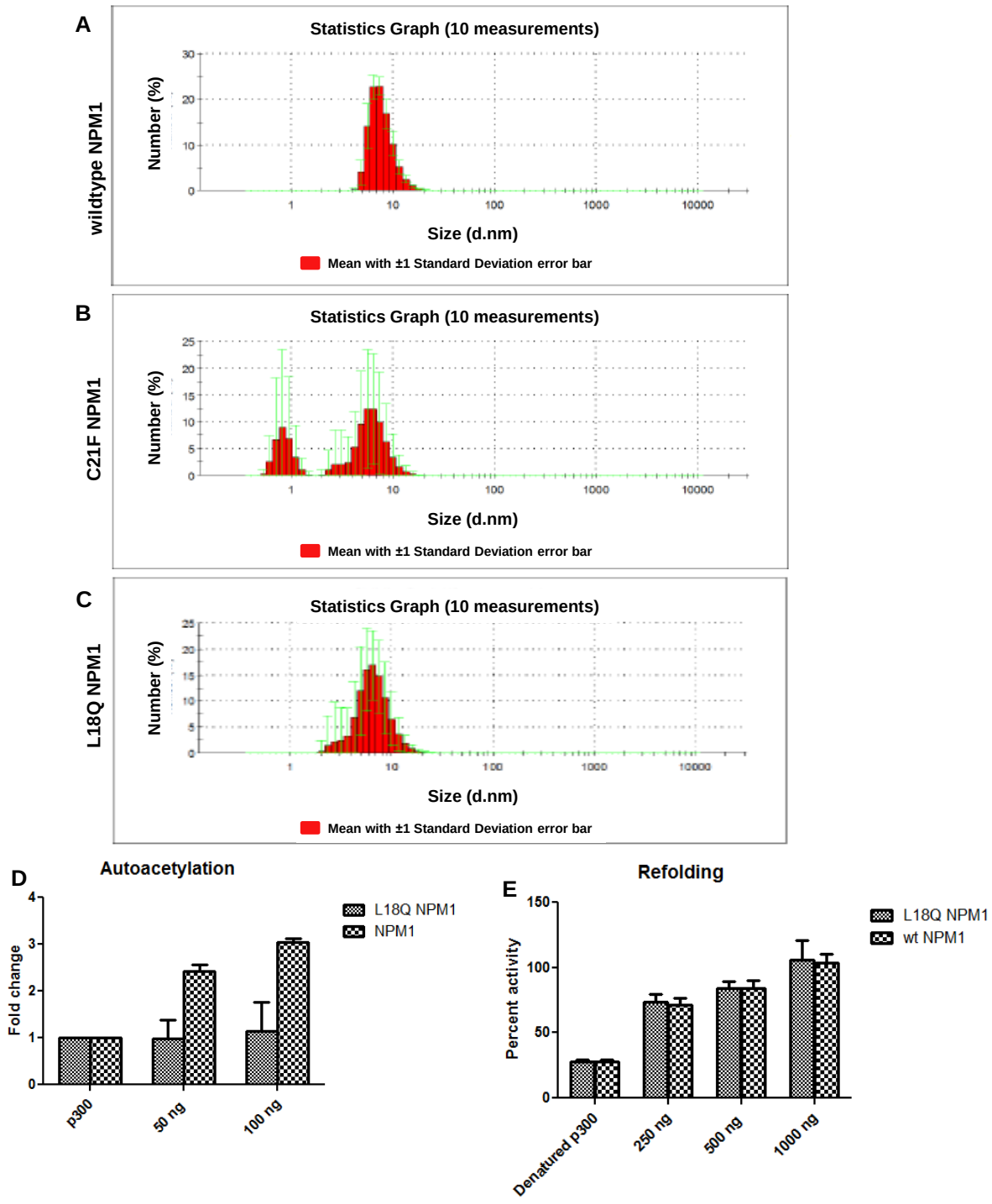

Figure 3.14: Higher concentrations are sufficient for oligomerization of the NPM1 mutants. Dynamic light scattering (DLS) to study the aggregation status of (A) NPM1 and NPM1 oligomerization-defective mutants (B) C21F NPM1 and (C) L18Q NPM1. The intensity statistics of 10 measurements each are plotted for NPM1, C21F and L18Q NPM1 at 2 µM. Shown are Z_{av} diameters for NPM1, C21F and L18Q NPM1, with error bars indicating S.D. The measurements were performed at 25 °C. Graphical representation of the (D) fold change in p300 autoacetylation levels and (E) heat denatured p300 activity rescue in the presence of the oligomerization-defective mutant L18Q NPM1 in comparison to wildtype NPM1. Shown are the mean ± SEM.

To confirm the importance of NPM1 oligomerization in the enhancement of p300 autoacetylation, oral cancer cell line AW13516 were treated with a small molecule inhibitor of NPM1, NSC348884. The dose of concentrations of the NSC348884 compound was first tested in the oral cancer cell line, AW13516, to determine the optimal compound concentration where the formation of NPM1 oligomerization is maximally abolished. It was observed that 2 μM of the compound was sufficient for the deoligomerization of NPM1; beyond this concentration no appreciable increase in deoligomerization was observed (Figure 3.15)

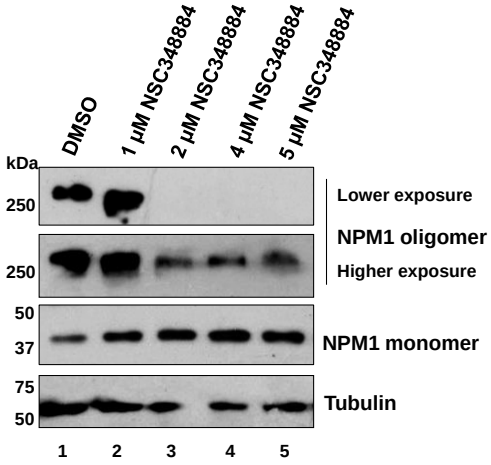

Figure 3.15: Deoligomerization of NPM1 in cells using the small molecule inhibitor, NSC348884. AW13516 cells were treated with either DMSO (control) or different concentrations of the NSC348884 compound at the concentrations indicated. The status of NPM1 was analyzed by western. Tubulin levels serve as the loading control.

To establish whether NPM1 oligomerization is important for the induction of p300 autoacetylation, AW13516 cells were treated with 5.0 μM concentration of NSC348884 compound. The effect of NPM1 deoligomerization on the status of p300 autoacetylation was probed by immunofluorescence. A significant reduction in autoacetylated p300 ($p<0.0001$) was observed in the compound treated cells in comparison to the control (DMSO treated) cells (Figure 3.16A). To confirm that the decrease observed was indeed at the autoacetylation levels and not at the protein level of p300, the levels of p300 protein was also probed by immunofluorescence, in the inhibitor treated cells versus the control cells. The overall levels of p300 appeared to be unaltered (Figure 3.16B). This experiment indicated the importance of NPM1 oligomerization in the regulation of p300 in cells.

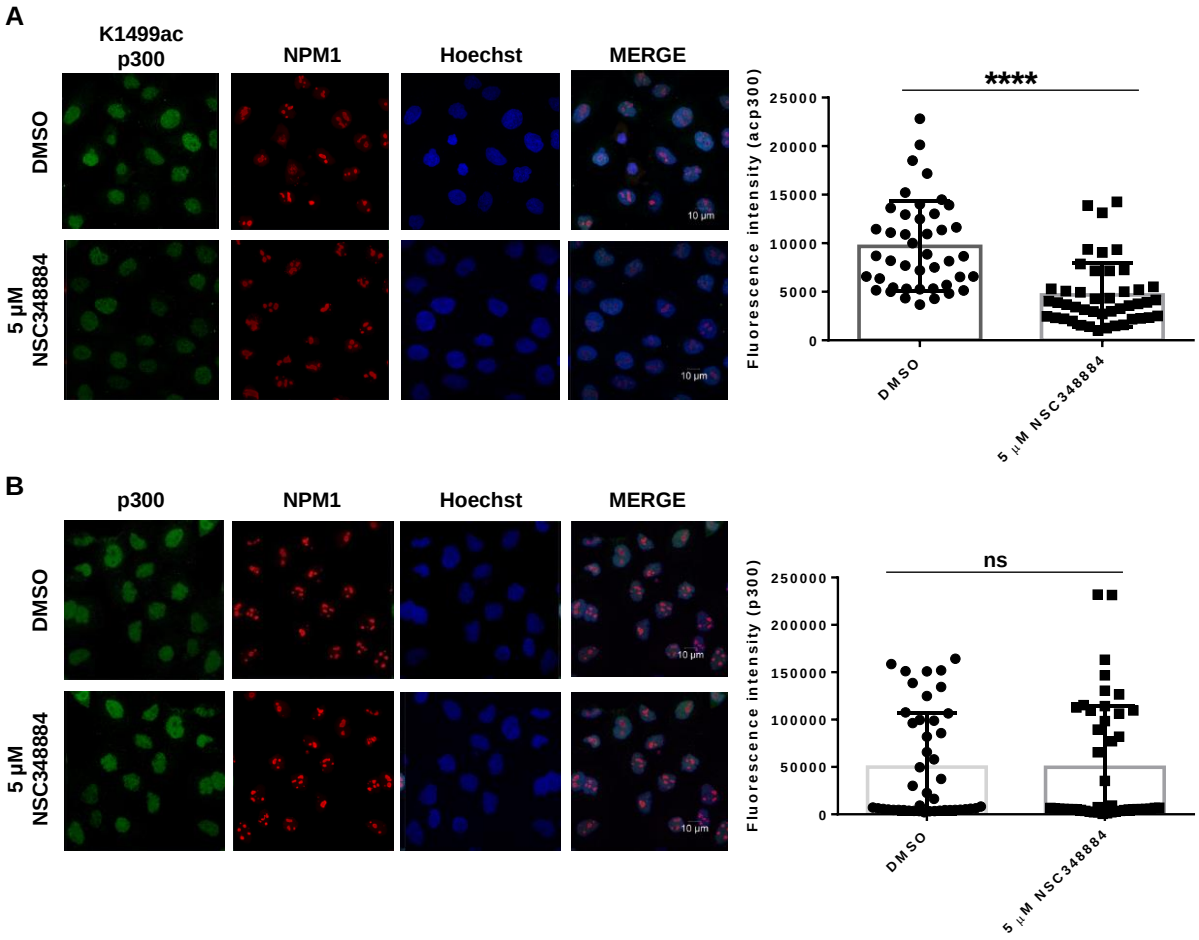

Figure 3.16: NPM1 oligomerization is important for the induction of p300 autoacetylation in cells. AW13516 cells were treated with DMSO or 5 µM NSC348884. Co-immunofluorescence was performed to determine the levels of (A) autoacetylated (K1499ac) and NPM1, (B) p300 and NPM1. The nuclei were counter stained with Hoechst. The mean fluorescence intensities ± SD were plotted alongside, statistical analysis was performed using two-tailed unpaired t-test (****,p<0.0001, ns, not significant), n=50 from two independent biological repeats.

3.8. The model of NPM1-mediated enhancement of p300 autoacetylation

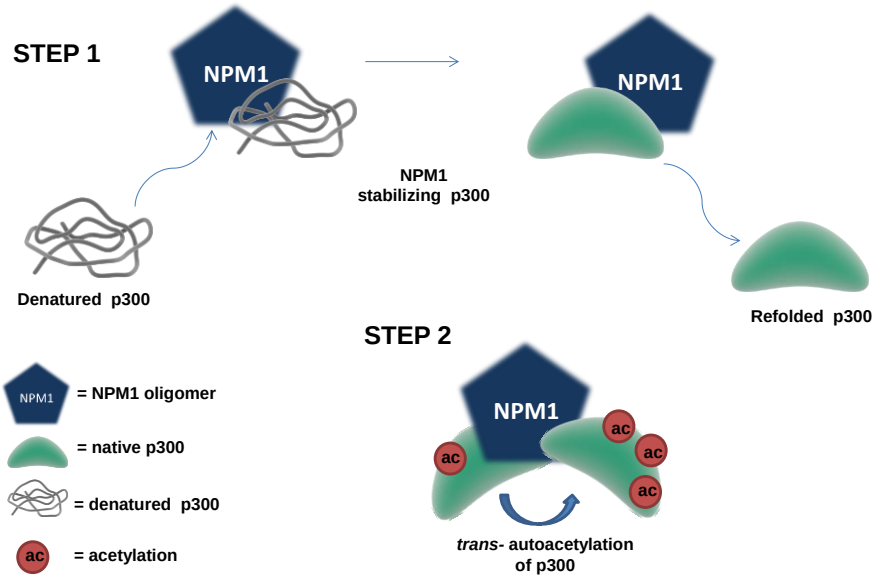

Figure 3.17: A 2-Step Model describing the probable mechanism of NPM1-mediated induction of p300 autoacetylation.

A model for the mode of NPM1-mediated induction of autoacetylation can be predicted from the experimental data obtained. NPM1-induced p300 autoacetylation appears to be a 2-step process which can be explained in the following way:

Step 1: The activity rescue experiments (Figure 3.5) suggest that NPM1 can stabilize the denatured structure of p300 and rescue its activity. Furthermore, by tracing the intrinsic tryptophan fluorescence of p300 in the presence of NPM1, it appeared that NPM1 could refold the otherwise intrinsically disordered conformation of p300 (Figure 3.8 and 3.11). These experiments proved that NPM1 is a chaperone for p300 and through this chaperone function NPM1 can modulate the activity of p300.

Step 2: The ability to modulate the structure of p300 is important for the enhancement of p300 activity, suggesting that the p300 conformation attained in the presence of NPM1 may facilitate intermolecular autoacetylation. But the interesting aspect is that the ability of NPM1 to induce autoacetylation is dependent on its oligomeric status (Figure 3.13-3.16). Thus, the oligomeric form of NPM1 may be an effective inducer of autoacetylation because of the two probable reasons: (i) the oligomeric NPM1 is important for its chaperone activity and (ii) it

can be speculated that the oligomeric form of NPM1 may interact with more than one molecule of p300, thereby enhancing the chances of *trans*-autoacetylation (Figure 3.17).

3.9. Summary

In all, it is evident that NPM1 is a specific inducer of p300 autoacetylation and activity. The mechanism of factor-induced p300 autoacetylation seems to be associated with the ability of the inducer, in this case NPM1, to stabilize the intrinsically disordered conformation of p300. Earlier studies involving p300 have shown that the promiscuity of p300 towards binding a wide variety of proteins stems from its structural plasticity. But only a subset of interacting partners can also induce structural alterations in the enzyme. Interestingly, in a previous study it was revealed that the estrogen receptor (ER) coactivator, SRC-3, could induce p300 HAT activity. The authors speculated that it could be due to the induced alteration in p300 conformation when it is present in the ER-SRC3-p300 complex (Yi et al., 2015). Similarly, this study reveals that the ability of NPM1 to modulate p300 structure may play a pivotal role in NPM1-mediated enhancement of p300 autoacetylation and catalytic activity.

This phenomenon is of physiological relevance, as it is seen under pathological and stress conditions such as cancers, NPM1 is overexpressed and localizes to the nucleoplasm (Shandilya et al., 2009). In oral cancer, NPM1 localizes to the nucleoplasm, where it encounters p300, resulting in the hyperactivation of the enzyme through the induction of autoacetylation. Since the maintenance of acetylation levels is important for cellular homeostasis, the dysregulation of p300 catalytic activity by NPM1 may lead to the deregulation of global gene expression contributing to the manifestation of oral cancer.

Chapter 4

Tumor Suppressor p53-mediated Allosteric Activation of p300

The screening of various physiological relevent p300 substrates and interactors led to the discovery of a novel inducer of p300 autoacetylation. This chapter presents extensive experimental evidence to establish that the tumor suppressor, p53, as a bona fide modulator of p300 catalytic activity, through the enhancement of p300 autoacetylation. p53 can specifically induce the autoacetylation of p300, while exhibiting negligible effect on KATs of other families. In cells, the overexpression of p53 resulted in the concomitant enhancement of p300 autoacetylation.. Therefore, to gain mechanistic insights into the regulation of p300 by this factor, Cryo-Electron Microscopy was employed to reveal the structural aspects of the p300-inducer complex. Elucidation of the mechanistic details discloses a conformational switch in the epigenetic enzyme, p300, from an inactive to a catalytically active form. To couple the regulation of p300 autoacetylation to chromatin targeting, investigation of the genome-wide occupancy of acetylated p300 was performed under inducer-mediated signaling pathways, which has revealed a unique gene network operating through this master epigenetic enzyme.

4.1. p53 is a specific inducer of p300 autoacetylation

The *trans*-autoacetylation of p300 enhances its lysine acetyltransferase activity. A few p300-interacting proteins, most of which are its substrates, can induce the autoacetylation and thereby the catalytic activity of p300. The molecular mechanisms of this activation are largely unknown. The association between p300 and p53 is well established. p300 is a co-activator for p53-mediated transcription (Lill et al., 1997). p300 acetylates p53 on 7 lysine residues present in the DNA binding domain and majorly in the C-terminal domain. p300-mediated acetylation was shown to enhance p53 DNA binding (Gu and Roeder, 1997). Apart from this, accumulation of acetylated p53 was also observed during cellular stresses (Reed and Quelle, 2014; Sakaguchi et al., 1998). p53 acetylation has been studied extensively with respect to its DNA binding properties and tumor suppressive functions such as cell cycle arrest, apoptosis, senescence and ferroptosis (Bieging et al., 2014; Jiang et al., 2015). p53,

interacts with p300 in its tetrameric form, through its bipartite transactivation domain AD1 and AD2, while p300 interacts through several domains namely, TAZ1, KIX, TAZ2 and IBiD (Krois et al., 2016; Teufel et al., 2007). Since the interplay between p53 and p300 is essential for p53 signaling pathways (Lee et al., 1998), the ability of p53 to regulate p300 activity could also contribute to the downstream execution of the p53 network. Since the direct interaction between p53 and p300 is essential for p53 signaling pathways, the possibility that p53 could regulate the catalytic activity of p300 which may contribute to the downstream execution of the p53 network was investigated. To test this possibility, an *in vitro* acetyltransferase assay for p300 autoacetylation was performed in the presence and absence of p53. It was observed that p53 specifically induces the autoacetylation of 20 nM p300 in a concentration-dependent manner (ranging from 40 nM to 160 nM) while exhibiting a negligible effect on the autoacetylation of the other two classes of KATs, PCAF and Tip60 (Figure 4.1A). An approximate 4.5 fold enhancement in the presence of 160 nM p53 (4:1 ratio of p53 tetramers to p300) was obtained. Since p53 forms a stable tetramer and p53 interacts with p300 as a tetramer, it may be speculated p53 interacts with p300 as a tetramer during induction of p300 autoacetylation. Therefore, only when p53 is present in a 1:1 ratio of tetrameric p53 to p300, a significant induction in the levels of p300 autoacetylation is observed, whereas under the suboptimal concentration of (40 nM) p53 where the ratio of tetrameric p53 to p300 is 0.5:1, only a negligible increase in the autoacetylation over the control could be observed. Moreover, since p53 is a substrate of most major nuclear KATs, including p300/CBP, PCAF (KAT2B), TIP60 (KAT5), MOZ (KAT6A) and MOF (KAT8), the specificity exhibited by p53 towards the enhancement of p300 autoacetylation over PCAF and Tip60 encouraged the hypothesis that the induction of p300 by p53 is not occurring only through transient enzyme-substrate interaction. The autoacetylation of KATs including p300 enhances its acetyltransferase activity. Since p300 acetylates a plethora of substrates, the induction of p300 autoacetylation by the transient substrate-enzyme interaction was investigated. For this, three different substrates of p300, p47 (N-terminal truncated (Δ40p53) isoform of p53), Positive Coactivator 4 (PC4) and p50 (subunit of NFκB) were tested. It was found that these substrates do not induce the autoacetylation of p300 effectively (Figure 4.1B-D), contrasting to what was observed in the case of p53. In the case of p47, it may be speculated that the 40 amino acid deletion from the N-terminal region of p53, decreases its affinity for p300, thereby reducing its ability to induce p300 autoacetylation. These results

indicate that the specific stable interactions between the inducer and p300 are essential for the induction of autoacetylation.

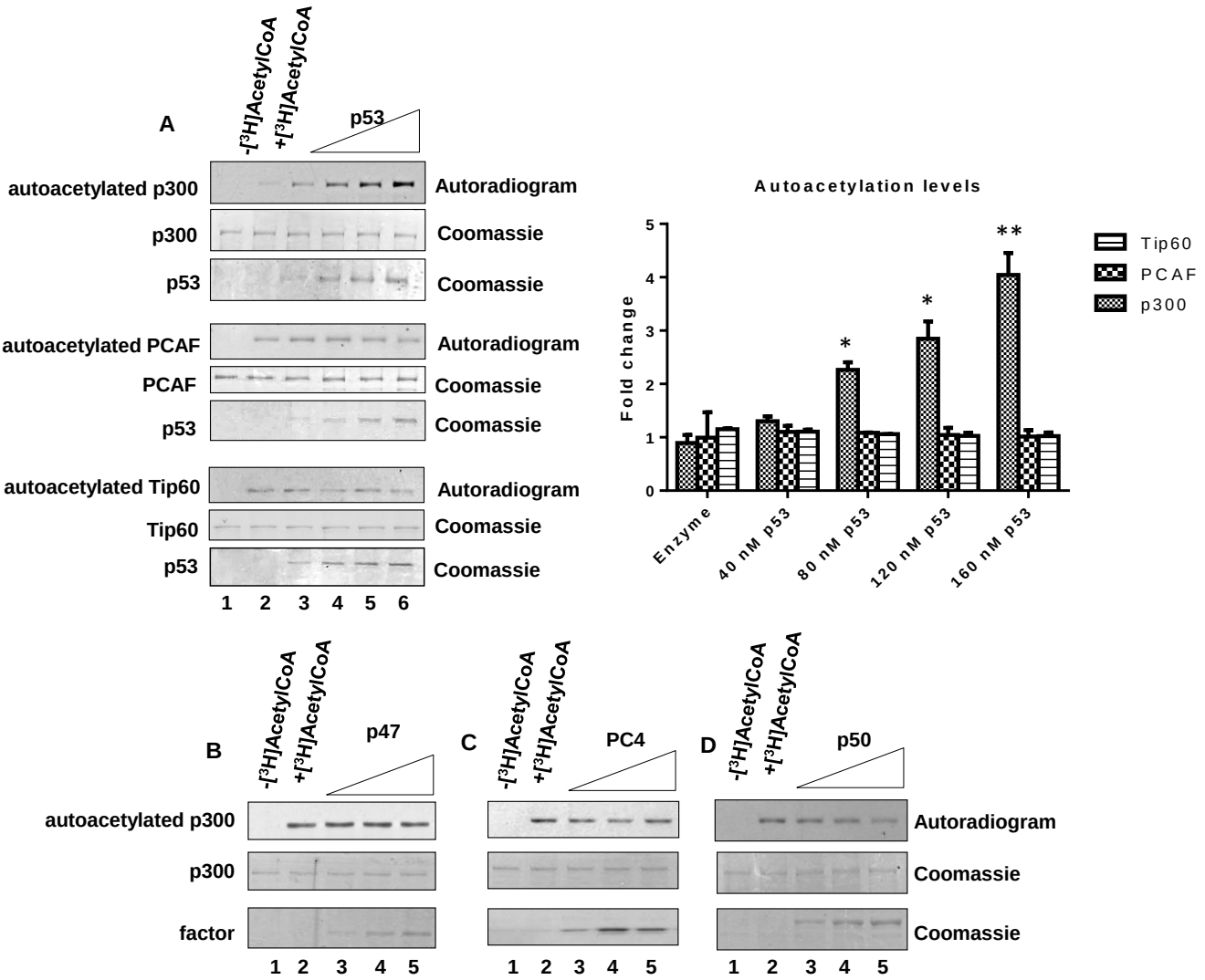

Figure 4.1: The tumor suppressor p53 specifically enhances autoacetylation of p300. (A) An in vitro acetyltransferase assay was performed to determine the levels of autoacetylation of different lysine acetyltransferases (KAT) in the presence of recombinant p53. The autoradiograms indicate the levels of p300, PCAF and Tip60 autoacetylation respectively; while the Coomassie stained protein panels show the loading control. The mean fold change of the levels of autoacetylation of each KAT, measured by the relative band intensities, have been plotted ± SD, statistical analysis was performed using two-tailed unpaired t-test (*, $p<0.05$, **, $p<0.01$). An in vitro acetyltransferase assay was performed to determine the levels of p300 autoacetylation in the presence of different p300 substrates (B) p47, (C) PC4 and (D) p50.

4.2. Overexpression of p53 enhances p300 autoacetylation levels in cells

p53 appears to be a potent inducer of p300 autoacetylation *in vitro*. To test whether this phenomenon holds true in the cellular context, p53 was ectopically expressed in p53 $^{-/-}$ H1299 cells. The transient transfection efficiency was around 50% and the cells expressing p53 were detected using the pan-p53 specific monoclonal antibody (DO-1). To determine the effect of p53 on the levels of p300 autoacetylation, the levels of p300 autoacetylation in cells expressing p53 were examined using an autoacetylation-specific antibody (K1499ac p300) (Thompson et al., 2004). The fluorescence intensity of p300 autoacetylation in p53-expressing cells was quantified and compared to the p300 autoacetylation in untransfected cells. A significant increase ($p<0.001$) in p300 autoacetylation was observed in presence of p53. As expected, there was a correlation between the expression of p53 and enhancement of p300 autoacetylation (Figure 4.2A).

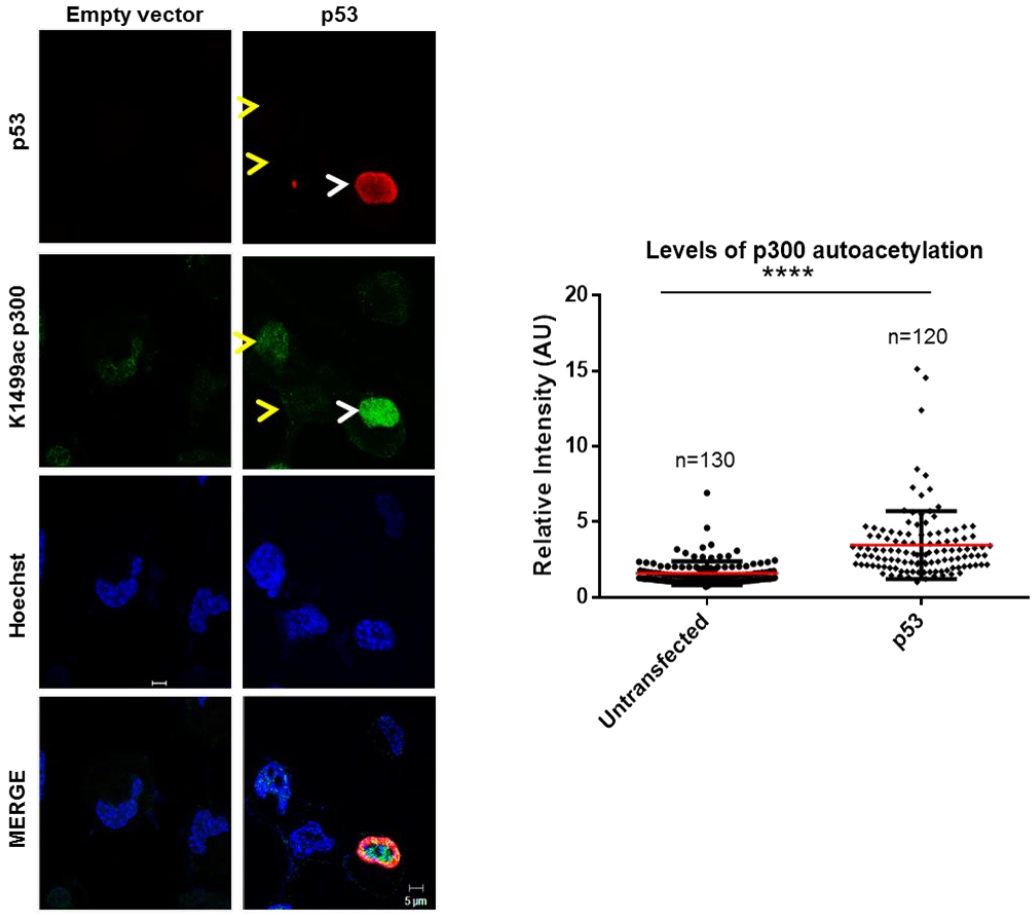

Figure 4.2: p53 regulates p300 autoacetylation in cells. The levels of K1499ac p300 and p53 were assessed in untrasfected versus p53 transfected cells in p53 null H1299 cell line by immunofluorescence. Fluorescence intensity of K1499ac (autoacetylated) p300 in untransfected versus p53 transfected cells have been quantified (represented as mean ± SD) and statistical analysis was performed using two-tailed unpaired t-test (****, $p<0.001$).

4.3. p53 stabilization by Nutlin3 enhances p300 autoacetylation

Although the previous results were indicative of the effect of p53 on p300 autoacetylation in cells, the role of endogenous p53 on p300 autoacetylation needed to be elucidated. In a resting cell, p53 protein levels are maintained at negligible levels through the concerted effort of E3 ligases, especially the MDM2 E3 ligase-mediated pathway resulting in the ubiquitination and proteasomal degradation of p53. Upon genotoxic stresses, several kinases especially the ATM/ ATR kinases phophsorylate and activate p53. p53 phosphorylation reduces its affinity for MDM2. Stabilized p53 then translocates to the nucleus and elicits a tumor-suppressive transcriptional program. During oncogenic stress, ARF tumor suppressor pathway is activated, which also inhibits MDM2, allowing p53 protein levels to further stabilize. Interestingly, MDM2 is also a target gene of p53 and constitutes a negative feedback loop to regulate p53 levels once the DNA damage response is resolved (Figure 4.3).

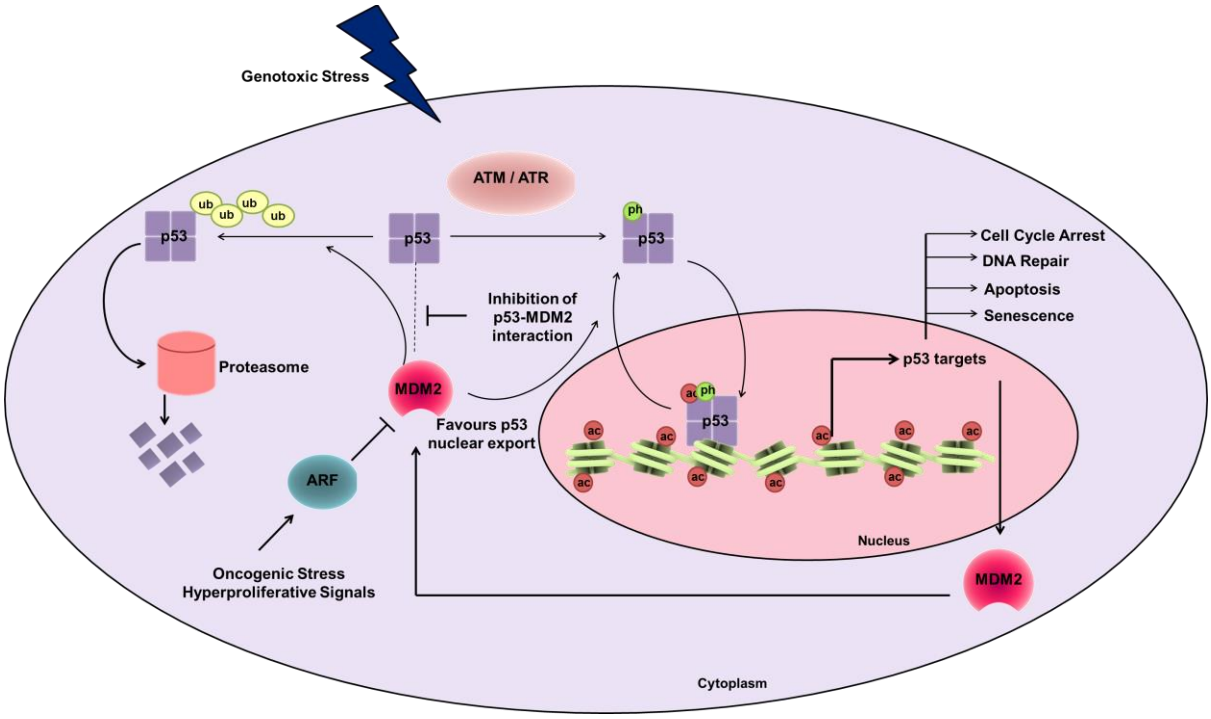

Figure 4.3: Canonical p53 signaling pathways in the cell. In a resting cell, p53 protein levels are maintained at a minimal level majorly through the ubiquitination and proteasomal degradation of p53 through the MDM2 E3 ligase-mediated pathway. Upon genotoxic stresses, p53 is phosphorylated and activated by several kinases, especially the ATM/ ATR kinases. The negative regulator of p53, MDM2 cannot bind to the phosphorylated p53, which can now enter the nuclear and transcribe its downstream effector genes. During oncogenic stress, ARF tumor suppressor pathway is activated, which inhibits MDM2, allowing p53 protein levels to stabilize. Interestingly, MDM2 is also a target gene of p53 and constitutes a negative feedback loop to regulate p53 levels once the DNA damage response is resolved. Small molecule inhibitors of the p53-MDM2 interaction, such as Nutlin-3a and RITA can

effectively stabilize p53 and can elicit the p53-mediated tumor suppressive signaling network (Issaeva et al., 2004; Vassilev et al., 2004). Adapted from (Bieging et al., 2014; Chène, 2003).

Therefore, in these set of experiments, the endogenous wildtype p53 levels were stabilized in HepG2 cells using the MDM2 antagonist, Nutlin-3a (Vassilev et al., 2004) (Figure 4.3). DNA damaging agents were not used, since they trigger a cascade of pathways and dissecting the contribution of p53 in the activation of p300 would be difficult. Even though Nutlin3 too has pleiotropic effects, it majorly stimulates the p53 pathway in cells. The levels of p300 autoacetylation in the Nutlin-3a-treated HepG2 cells were determined by immunoblotting analysis as well as immunofluorescence staining. The cells with stabilized p53 had significantly higher levels of autoacetylated p300 in comparison to the DMSO-treated or untreated counterpart (Figure 4.4 A,B). The fluorescence intensity of p300 autoacetylation was significantly ($p<0.001$) enhanced in cells treated with Nutlin-3a. A mild toxicity was observed upon treatment with 10 μM Nutlin-3a which may account for the marginal reduction in p300 autoacetylation observed at 10 μM Nutlin-3a treatment, as compared to 5 μM Nutlin-3a (Figure 4.4 B)

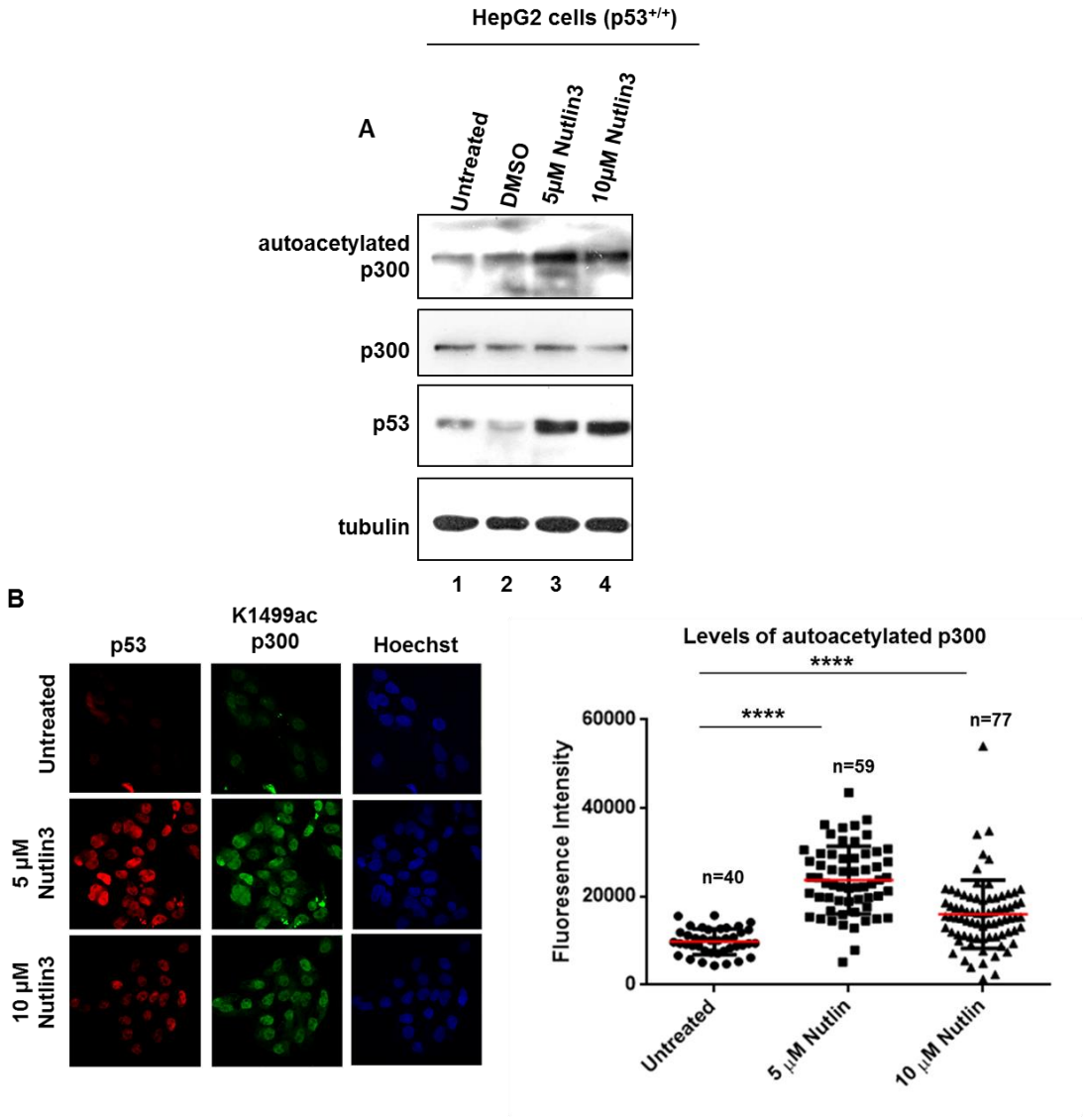

Figure 4.4: Nutlin3 activates p300 through p53 stabilization. (A) HepG2 cells were treated with DMSO (vehicle control) or Nutlin3 as indicated (Lane 2-5), levels of ac-p300, p300, p53 were analyzed by immunoblotting. Alpha-tubulin levels were considered as the loading control. (B) HepG2 cells were treated with Nutlin3 for 24 hours and the levels of autoacetylated p300 and p53 were assessed by co-immunofluorescence. The mean fluorescence intensities were plotted ± SD (of 3 biological repeats), statistical analysis was performed using two-tailed unpaired t-test (****,p<0.0001).

4.4. p53 can activate p300 acetyltransferase activity *in vitro* and in cells

To investigate the effect of p53-mediated induction of p300 autoacetylation, an *in vitro* histone acetyltransferase assay was performed, using recombinant histones as the substrate. In agreement with the autoacetylation assay, an approximate 3-fold increase in p300 histone acetyltransferase at the molar ratio of 1:2 for p300: p53 was observed. Notably, an approximate 4.5 fold increase in p300 activity in the presence of p53 suggested that p53 can positively modulate the p300 KAT activity through the induction of autoacetylation (Figure 4.5A). Further increase in the p53 concentration did not affect the HAT activity beyond 4.5 fold (Figure 4.5A).

Next, to conclude whether p53 could enhance p300 activity in cell, HepG2 cells were treated with Nutlin-3a and the levels of histone acetylation were determine by western blotting analysis. The levels histone acetylation also appeared to be higher in HepG2 cells treated with Nutlin-3a (Figure 4.5B). It was speculated that this increase in histone acetylation may be a direct consequence of p53-mediated activation of p300 acetyltransferase activity. Therefore, to attribute the enhancement in histone acetylation to the p53-mediated effect, the p53-null H1299 cells were treated with Nutlin-3 and probed for the levels of different histone acetylation marks in treated cells versus control cells (Figure 4.5C). Interestingly, it was found that the histone acetylation levels do not show any appreciable alteration in the Nutlin-3-treated H1299 cells thereby signifying the importance of p53 in the activation of p300. In conjunction with these results, an earlier report showed that Nutlin-3a could induce the levels of p53 acetylation and histone acetylation in the human AML cell line MOLM-13 cell line which expresses wildtype p53 (Haaland et al., 2014). Therefore, it is plausible that the effect of Nutlin-3a on lysine acetylation levels may be through p53-mediated enhancement of p300 autoacetylation and acetyltransferase activity.

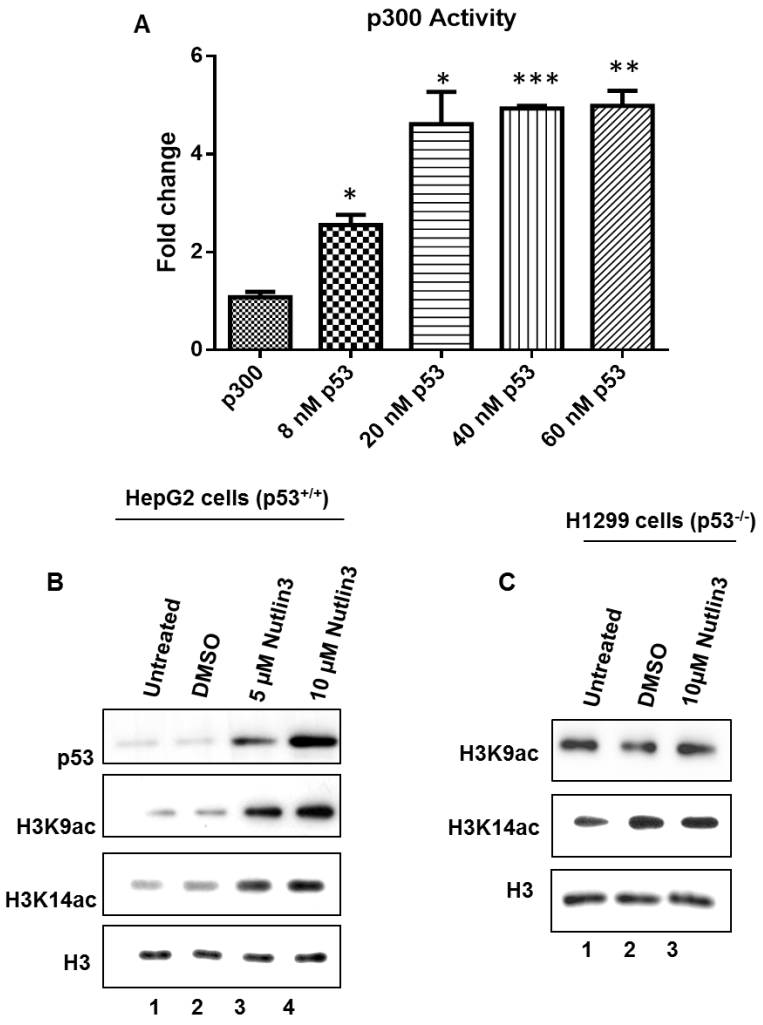

Figure 4.5: p53 enhances p300 acetyltransferase activity. (A) Enhancement of p300 activity in the presence of increasing concentrations of p53 as indicated was determined by filter binding assay. The mean fold change was plotted ± SD, statistical analysis was performed using two-tailed unpaired t-test (*, $p<0.05$; **, $p<0.01$; ***,$p<0.001$). HepG2 cells (B) and H1299 cells (C) were treated with DMSO (vehicle control) or Nutlin3 as indicated. Histone acetylation levels were analyzed by immunoblotting using H3K9ac and H3K14ac antibodies. Total histone H3 levels were used as the loading control. Untreated cells were used as a control.

4.5. p53 does not regulate p300 at the transcriptional level

p53 is a transcription factor, therefore to rule out the possibility that p300 may be transcriptionally regulated by p53 rather than post-translationally modulated, the p300 transcript levels were compared between cells treated with Nutlin-3 and vehicles control cells. Interestingly no alteration in p300 transcript levels in the presence of p53 (Figure 4.6A), whereas p21 (a p53 response gene) transcripts altered significantly upon Nutlin-3a treatment. A Tet-ON cell line expressing doxycycline-inducible p53 was created in the

H1299 background. Upon inducing the expression of p53 by doxycycline, the transcript levels of both p300 and p21 were determined by qPCR. Again, consistent with the previous results, p300 transcript levels remained unchanged while p21 expression was stimulated by the treatment of doxycycline (Figure 4.6B). These results indicate that p53 can modulate p300 activity in the cellular context through the induction of its autoacetylation.

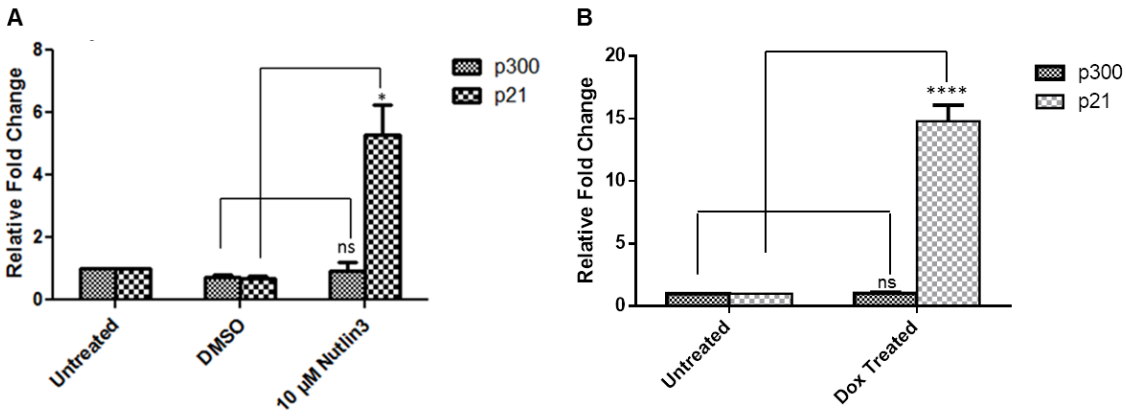

Figure 4.6: p53 does not regulate p300 at the transcriptional level. The relative transcript levels of p300 and p21 (p53-responsive gene) were determined by qRT-PCR (mean ± SD) in (A) Hepg2 cells treated with Nutlin3 and (B) H1299 doxycycline-inducible p53 expression cells treated with 1mg/ml doxycycline (Dox). Unpaired two-tailed t-test statistical analysis was performed (ns, non-significant; *, $p<0.05$; ****,$p<0.0001$). Actin transcript level was used as the internal control.

4.6. Direct interaction between p53 and p300 is required for the catalytic activation of p300

To elucidate the mechanistic details of p53-mediated activation of p300, the importance of the direct interaction between p53 and p300 was investigated. p53 makes direct contact with p300 through four important residues, (L22, W23, W53, F54) present on its transactivation domain. Mutations of these residues severely compromises p53 transactivation (Teufel et al., 2007). Upon DNA damage p53 is phosphorylated by several kinases, and this phosphorylated form of p53 binds to its coactivator p300 with higher affinity (Lambert et al., 1998; Lee et al., 2010a). Interestingly, the number of phosphorylation sites on p53 N-terminal has an additive effect on its affinity for CBP/p300 (Lee et al., 2009; Lee et al., 2010a). Here a triple-phospho-mimic peptide (S15E, T18E, S20E), comprising of the first 39 amino acid residues of the p53 TAD1 was employed to obstruct the interaction between p53 and p300 (Polley et al., 2008). Using a filter binding assay-based strategy, the importance of p53-p300 interaction was scored by the levels of p300-mediated histone acetylation as in Figure 4.5A. As expected, the

peptides and p53 alone do not bind to the p81 phosphocellulose filters (Figure 4.7A, Lane 1-3) therefore validating that the scintillation measurement was only from the tritium-labelled acetylated histones bound to the filters. The basal activity of p300 in the absence of any inducer was considered as 100% activity (Figure 4.7A, Lane 4) and the peptides alone could not alter the activity of p300, signifying that any change in histone acetylation observed thereafter would be the direct consequence of p300-p53 interaction (Figure 4.7A, Lane 5,6). In the presence of 4 nM p53, a 3-fold increase in the histone acetylation was observed (Figure 4.7A, Lane 7). The presence of scrambled peptide (Figure 4.7A, Lane 9) did not alter the p53-mediated induction of p300 activity, but the triple phospho-mimic p53 peptides (3E pep) could effectively reduce histone acetylation levels (Figure 4.7A, Lane 8). These results indicate that the 3E phospho-mimic p53 peptide could effectively interfere with the p53-p300 interaction, presumably leading to reduced p300 autoacetylation and activity, which was indicated by a significant reduction in histone acetylation levels (Figure 4.7A, Lane 8). While the scrambled peptide exhibited a negligible effect on p53-mediated p300 activation, ensuring that the decrease observed in the case of the phospho-mimic peptide is actually due to the disruption of p53-p300 axis and not a non-specific effect of the peptides. Furthermore, to check whether these peptides were effective even in cells, HepG2 cells were first treated with Nutlin-3 to stabilize the levels of p53. Following this, the cells were then treated with different concentrations of the 3E phospho-mimic p53 peptide as indicated in Figure 3B. The levels of p53 increased on Nutlin3 treatment and the peptide treatment did not alter p53 protein levels. Therefore, indicating that the peptides do alter the p53 protein levels in the cells and the observed alteration in histone acetylation would be a direct consequence of the disruption of p53-p300 interaction. Consistent with the previous observation, the H2AK5 acetylation increased on p53 stabilization with Nutlin3 (Figure 4.7B, Lane 3; Figure 4.5B, Lanes 3 and 4). But upon the treatment with the interfering peptide, the levels of H2AK5 acetylation gradually reduced in a concentration-dependent manner (Figure 4.6B, Lanes 4-6).

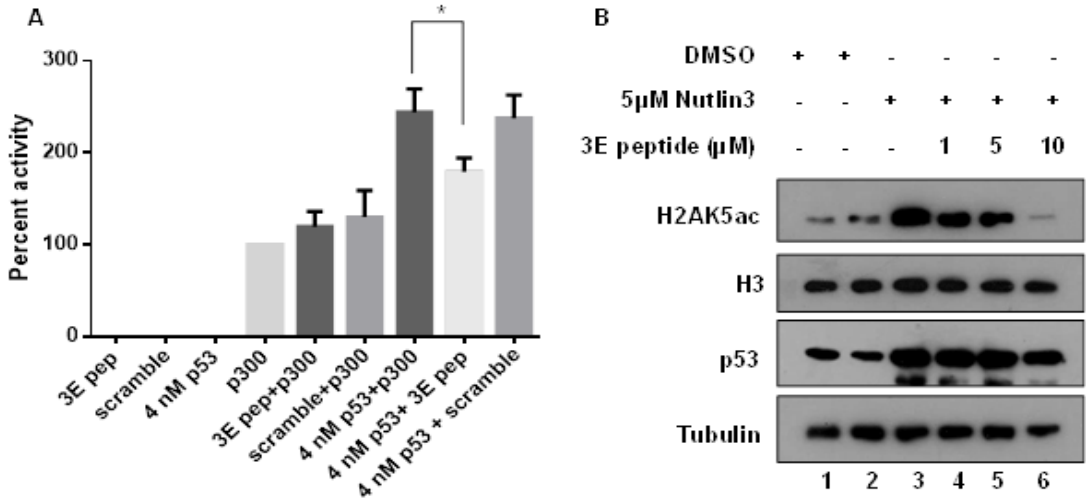

Figure 4.7: Disruption of p300 – p53 interaction by peptides reduces p300 activity. (A) Results of filter binding assay indicate that the phosphomimic p53 N-terminal peptide can effectively reduce the activity of p300 by interfering with its interaction to p53. (B) HepG2 cells treated with Nutlin3 or Nutlin3 and p53 phosphomimic peptide as indicated, levels of H2AK5ac, H3, p53 and tubulin were analyzed by immunoblotting.

4.7. Cryo-Electron Microscopy to elucidate the mechanism of p53-mediated enhancement of p300 autoacetylation

The results of the biochemical and cell-based assays designate that p53-interaction can induce p300 autoacetylation and enhance its catalytic activity. The most plausible expectation was that the p53 binding stimulates p300 activity through a structural switch, resulting in an active p300 conformation. Cryo-electron microscopy (cryo-EM) was employed to visualize the p53 tetramer-bound p300 complex structure. The cryo-EM structure was solved in collaboration with Dr. Jayati Sengupta, Indian Institute of Chemical Biology (IICB), Kolkata and Prof. Siddhartha Roy, Bose Institute Kolkata.

Predictions of this elusive 'active' p300 conformation has been made in a previous study by Delvecchio *et al.* through the crystal structure study of the p300 core domain (Delvecchio et al., 2013). In their study, the p300 core-catalytic domain structure consisting of the Bromo-RING-PHD-HAT domains, was resolved to a resolution of 2.8 Å. The authors elucidated the inhibitory role of a novel non-canonical RING domain which partially occludes the HAT domain from substrate binding. Based on this structure the authors put forth a model where they predict that p300 which is otherwise in an 'inactive' conformation requires trans-autoacetylation upon which the RING domain is displaced from the active site, exposing the substrate binding groove for efficient substrate acetylation.

In this study, it is important to elucidate the structural events that occur in the p300 protein upon p53 binding. Hence, to obtain a snap-shot of the structural conformation of p300 in complex with p53, cryo-electron microscopy was employed. 3-dimensional reconstruction from the cryo-EM electron density maps of p300 alone (Figure 4.8 A, B) and p300 in complex with tetrameric p53 (Figure 4.8 C, D) obtained at 13.5 Å and 15.7 Å, respectively. The intrinsically disordered linker regions spanning between the multiple globular domains of p300 constitutes almost 60% of its protein sequence (~1400 amino acids) (Dyson and Wright, 2016), therefore the molecular mass calculated from the size of the enclosed volume in the p300 density map (using 0.82 D/Å3 as protein density) was lesser than the theoretical molecular mass of p300 (264.161 kDa). When the free p300 density map is superimposed on the p300-p53 complex map, it was clear that the free p300 protein is more compact in comparison to the p300 in complex with p53 (Figure 4.8E). From the complex density map, the density corresponding to p53 tetramer can be segmented computationally using the cluster segmentation procedure implemented in SPIDER (Frank et al., 1996; Sachse et al., 2007) (Figure 4.8F). Interestingly the overall topology of the complex resembled the model predicted by Teufel *et al*, for the p300 – p53 tetramer complex, where it was proposed that one p300 molecule wraps around a p53 tetramer, forming several contacts through its multiple domains (Teufel et al., 2007).

There is a striking ‘trunk-link’ protuberance in the complex density map which resembles the bromodomain structure (PDB: 3I3J) (Filippakopoulos et al., 2012). Even though no crystal structure for the full length p300 is available, structures of the individual globular domains are available (PDB: 3BIY, 3IO2, 4BHW, 3I3J). Therefore, based on the available crystal structure data, each domain was logically assigned to the identifiable density regions in the electron density maps.

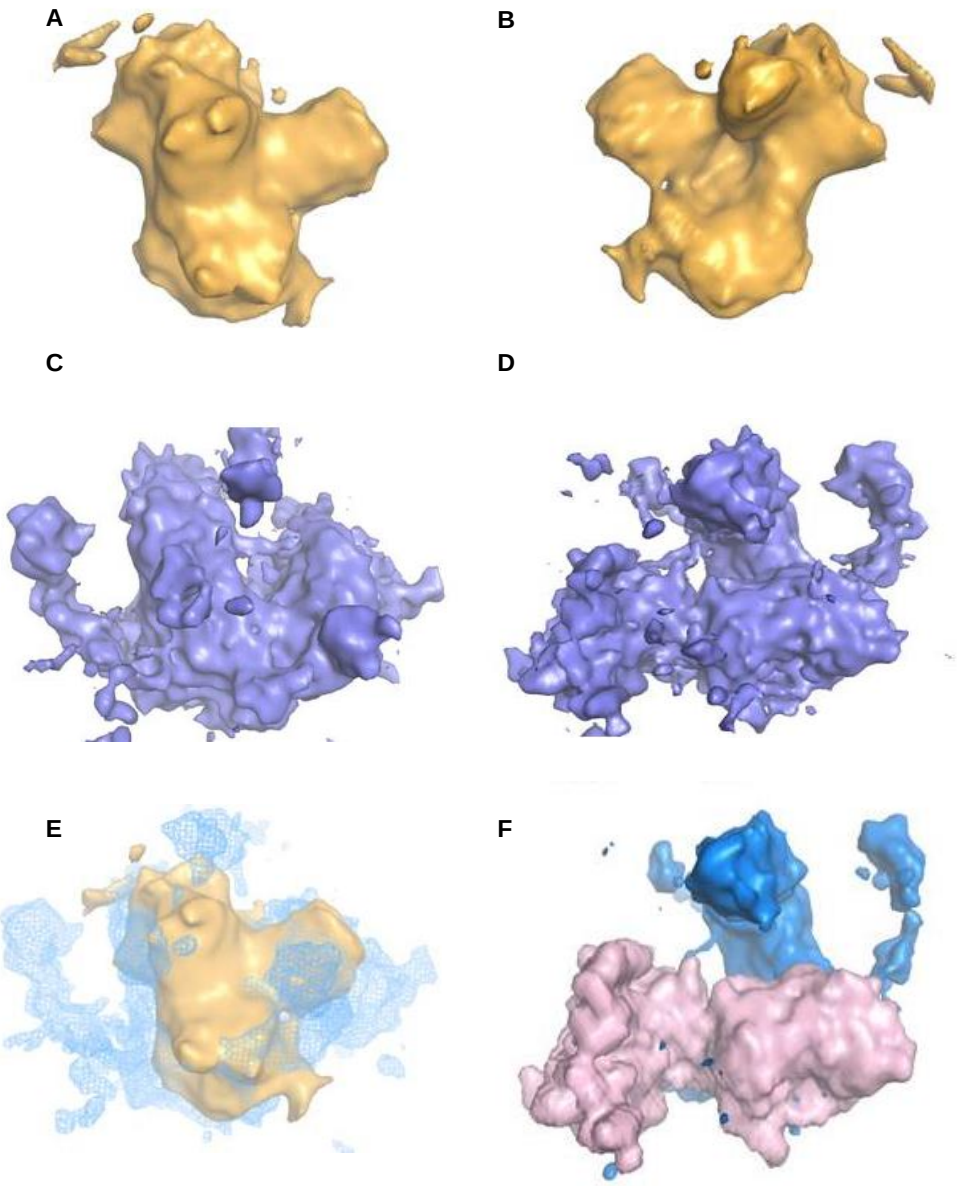

Figure 4.8: Cryo-EM reveals conformation alteration in p300 structure upon p53 binding. 3D reconstruction of p300 alone (A) back view and (B) front view, at 13.5 Å resolution. 3D reconstruction of p300 and p53 complex (C) back view and (D) front view at 15.7 Å resolution. (E) Overlay of p300 alone conformation and the p300-p53 density map. (F) 3D reconstruction of p300-p53 complex demarcating p53 (mauve) and p300 (blue).

The catalytic core domain of p300 (combined subdomains: bromodomain-PHD -RING – HAT), is located at the centre of the protein density, and is preceded by the N-terminal domains, NRID, TAZ1 and KIX domains and is followed by the C-terminal domains, ZZ, TAZ2 and IBiD domains (Fig. 4.9A).

To interpret the free p300 protein in molecular terms, each individual domain was identified onto the free p300 density map. Consistent with the earlier study, it appears that the central core domains (Bromo-RING-PHD-HAT) of p300 are closely packed (Figure 4.9B). The

previously solved crystal structure shows a 'kink' between the bromodomain and HAT domain, while the RING and PHD domains are loosely packed onto the HAT domain via long disordered linkers (PDB: 4BHW), presumably in an 'inactive' conformation (Delvecchio et al., 2013).

The free p300 density map was fitted with the crystal structure of the central domain using Chimera (CC= 0.82). The central density is occupied by the HAT and bromodomain while the RING and PHD domains occupy the outer rims of the region. In the cryo-structure, the position of the RING domain is slightly different with respect to the reported crystal structure although here too the RING structure partially occludes the HAT domain (Figure 4.9B).

The crystal structure of p300 HAT domain (PDB: 3BIY) reveals insights its broad substrate specificity. In the cryo-EM structure obtained, the HAT domain modelled is identical with the reported HAT structure, and even though the auto-inhibitory loop was omitted from the crystal structure, it can be fitted into the substrate-binding pocket in the cryo-EM structure, which is consistent with the proposed model of p300 autoacetylation (Liu et al., 2008; Thompson et al., 2004).

The cylindrical feature in the density map next to the bromodomain, towards the N-terminal, was attributed to the KIX domain (Figure 4.9A and B). The distance of the KIX domain from the bromo-HAT domain density was ~35Å, while the RING and PHD domain remain packed onto the structure (Figure 4.9B). The triangular density observed at the rear end of the HAT domain was assigned to the TAZ1 domain, and it appear that the TAZ1 domain acts as a 'latch', holding onto the HAT domain in a 'closed' conformation (Figure 4.9B). From the cryo-EM structure of free p300 it is revealed that the 'autoinhibited' conformation of the central core catalytic domains of p300 is stabilized by the N-terminal domains (KIX and TAZ1).

The remaining unoccupied density was attributed to the C-terminal domains. Due to the limitations of the current resolution of the map, it is difficult to fit in perfectly the crystal structures of the C-terminal domains (ZZ, TAZ2 and IBiD). So they were placed sequentially in the unoccupied density map. The cross-correlation coefficient (CC) of the overall fitted p300 model and the density map (Figure 4.9B) is 0.86.

Following a similar strategy, the domains were assigned to the p300-p53 complex density map. In contrast to the free p300 'closed' structure, it is observed that the complex map manifested a more 'open' conformation (Figure 4.9C). In the fitted structure it is observed

that the 'kink' between the HAT and the bromodomain is significantly larger, which is probably due the opening up of the overall conformation. The densities that were previously corresponding to the RING and PHD domains in the free p300 structure are missing from the complex density map, leaving only weak densities to the top of the bromodomain, suggesting that the RING-PHD domains have been displaced upon p53 binding (Figure 4.9D). Since the densities of these domains were weaker, it suggested that these domains are more flexible in the p53-bound form. To further corroborate to the evidence of an 'open' structure, it is seen that the 'kink' angle between the bromodomain and the HAT domain was much wider in comparison to the free p300, such that the domains could not be fitted together and were fitted separately using Chimera. The bromodomain is fitted into the central protuberance present in the density map, similar to the free p300 density map, while the HAT domain occupies the central body of the density in a rotated conformation (Figure 4.9B and 4.9C). The TAZ1 domain is fitted adjacent to the KIX domain, in a manner which is clearly different from the free p300 conformation. A 'loop-like' density is observed at the rear of the HAT domain, which could be the presence of the lysine-rich auto-inhibitory loop. This loop was place inside the density map, upon the rotation of the HAT domain.

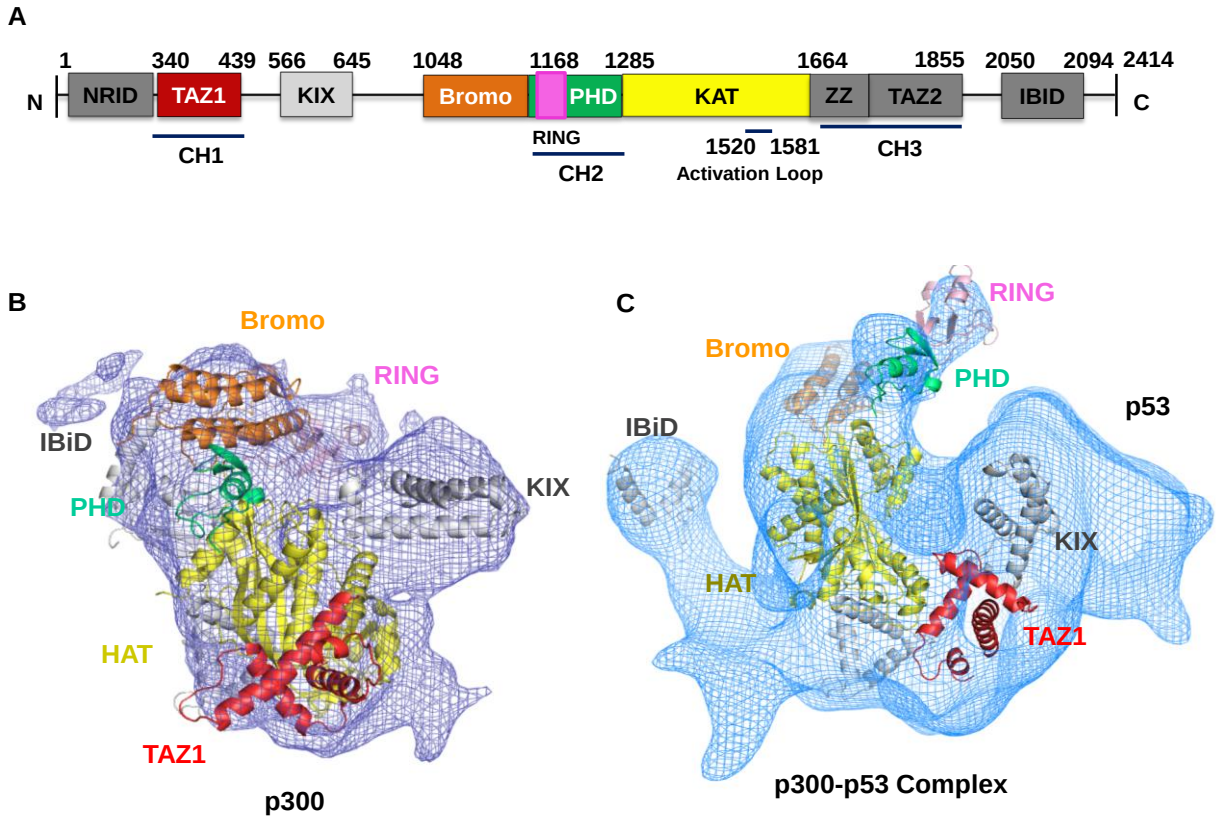

Figure 4.9: Rearrangement of p300 domains upon p53 binding. (A) Linear arrangement of domains in p300 color coded as the ribbon domain crystal structures fitted into the

electron density maps depicted in (B) and (D). 3D domain arrangement of (B) p300 alone and (C) p300-p53 complex fitted into the respective electron density maps.

4.8. The allosteric binding of p53 leads to the activation of p300 acetyltransferase activity

In the cryo-EM map of the p300-p53 complex, distinct features of the p53 tetramers are identifiable. Previous EM structures report a closed conformation of DNA-bound p53 tetramer, with the tetramerization domains placed on top and the closely packed DNA binding domain placed below (Kitayner et al., 2006; Melero et al., 2011; Tidow et al., 2007). In contrast to the closed DNA-bound p53 tetramer structures (~6-8 nm) reported previously (Melero et al., 2011; Tidow et al., 2007), the p53 in the complex structure adopts a distorted conformation with centrally connected side-lobes (~10 nm) in the complex density map (Figure 4.9A). The crystal structures of the dimers and tetramers are available (PDB: 2ADY, 2AC0, 2AHI, 2ATA). The side-lobes are non-symmetrically oriented in the complex structure, the core DNA binding domain dimers were docked in each of the lobes using Chimera. The unstructured N-terminal transactivation domains can be accommodated in the unoccupied density of the complex adjacent to p300. The clustered tetramerization domains can be found in a shallow groove like feature in the central density (Figure 4.10). The overall topology matches the previously reported cryo-EM structure of the p53 tetramer (Okorokov et al., 2006). The p53 dimers that interact with the KIX and TAZ1 domains of p300 are tilted towards the N-terminal of the p300 protein, since the N-terminal domains contain longer unstructured stretches in comparison to the C-terminal end. In the earlier p300-p53 interaction model proposed, one molecule of p300 encloses a p53 tetramer by interaction with p53 TAD1/2 through its TAZ1 and KIX domains on the N-terminal and TAZ2 and IBiD domains on it C-terminal end (Teufel et al., 2007). Strikingly similar to this model, the cryo-EM quaternary structure reveals that p300 interacts through its TAZ1, KIX and TAZ2 domains. The interaction through the IBiD domain is rather weaker suggesting higher conformational dynamics in this interaction.

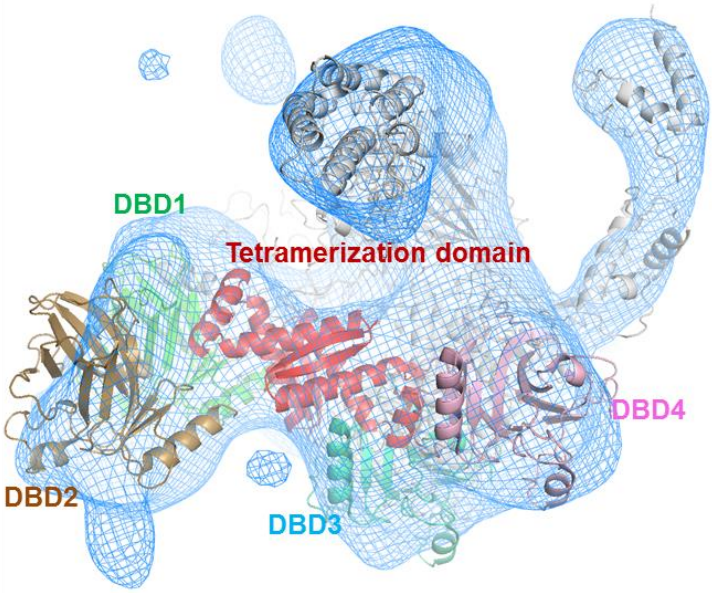

Figure 4.10: The allosteric binding of p53. Tetrameric p53 structure fittered into the p300-p53 complex electron density map. p53 tetramerization and DNA binding domains (DBD1-4) are indicated.

Comparing the structures of free p300 and p300 in complex with p53, insights into the mode of p300 regulation by p53 can be deciphered. From the complex structure it can be speculated that once p53 with p300 interacts through the KIX and TAZ2 domains (which flank the catalytic core domain), the RING and PHD domains are displaced to accommodate p53 (Figure 4.11). The TAZ1 which was acting as a 'latch', holding the HAT domain in place (as seen in the free p300 structure; Figure 4.9A) is now displaced, allowing the bromodomain and HAT domain to move away from the N-terminal (distance between KIX and bromo-HAT is 75Å in the complex structure) thereby resulting in an 'open', active and accessible conformation (Figure 4.9B). This indicates that the lys-rich autoinhibitory loop is exposed to *trans*-autoacetylation. Therefore, the allosteric binding of p53 creates a conformational alteration in p300 which can now explain the activation of the enzyme in the presence of p53. The previously predicted 'active' conformation of p300 has now been visualized through the cryo-EM studies of the p300-p53 complex.

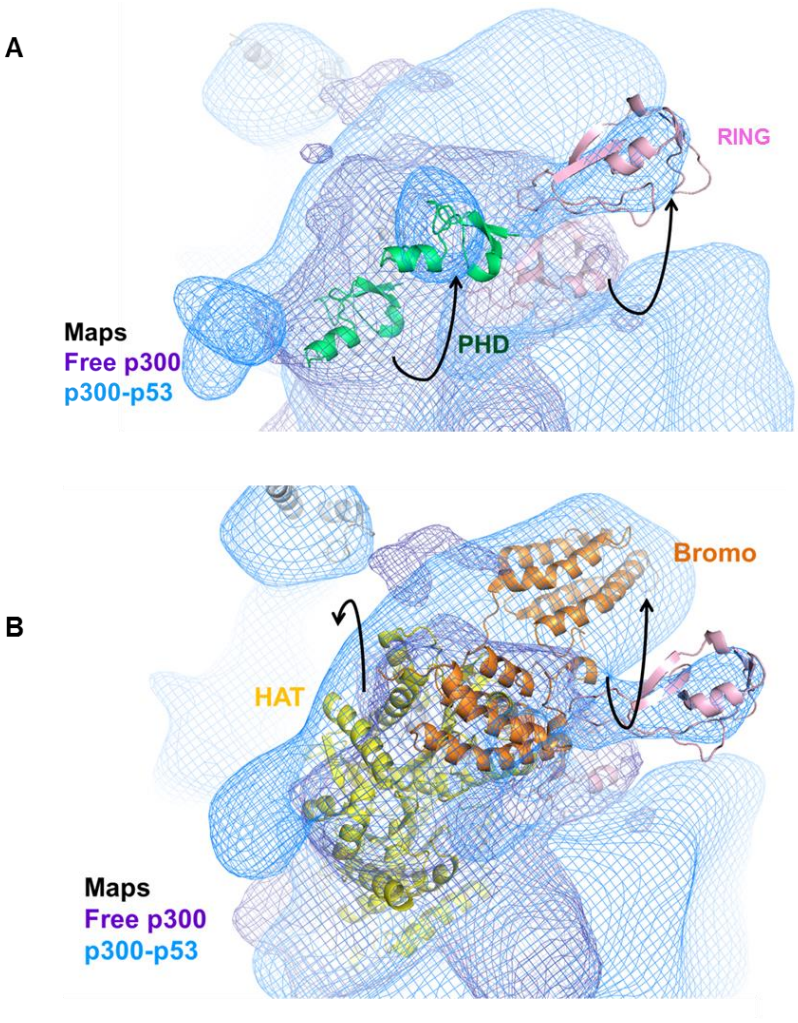

Figure 4.11: The allosteric binding of p53 induces structural alteration in p300. The superimposition of the p300 alone electron density map (purple) onto the p300-p53 complex electron density map reveals the relative reorientation of the (B) CH2 domain (PHD and RING domains) and the (C) HAT and bromodomain, upon p53 binding.

4.9. Global recruitment of autoacetylated p300 upon p53 activation

The cryo-EM structure corroborated with the biochemical results, revealing further insights into the enhancement of p300 autoacetylation by p53. Therefore, to further elucidate the importance of factor-mediated induction of autoacetylation in the physiological context, the genome-wide distribution of autoacetylated p300 (acp300) was investigated in the presence of p53 and compared it to the global chromatin occupancy of p300. The transcription coactivators CBP/p300 are integral components of cellular transcription ‘hubs’. Therefore, the factors p300 associates with not only dictates its substrate specificity but also the effective downstream transcriptional cascades (Lee et al., 1998; Perissi et al., 1999; Ravi et al., 1998). To elucidate the physiological significance of p53-mediated induction of p300

autoacetylation, a Tet-ON inducible system for p53 expression was created in the p53 null H1299 cells. The expression of p53 on doxycycline treatment was determined at the protein levels as well the RNA level (Figure 4.12A,B). In these cells, p300-specific histone acetylation mark H3K18ac was upregulated in the expressing p53 in comparison to the untreated cells (Figure 4.12A). This indicated that when p53 is inducibly expressed in the Tet-ON cell line, it can effectively induce p300-mediated histone acetylation. Furthermore, the transcript levels of p53-target genes were enhanced, whereas the expression of p53-non target genes such as GAPDH remained unaltered. Here too it is observed that p300 transcript levels are unchanged upon p53 expression, reiterating the fact the p300 is not regulated at the transcription level (Figure 4.12B). To further confirm that the inducible system has functional p53-downstream pathways upon doxycycline-treatment, a gene-expression microarray was performed and the pathway analysis revealed that p53 genes and networks were upregulated upon doxycycline treatment (genes with a fold change ≥ 2 and $p<0.01$ were analyzed) (4.12 C,D).

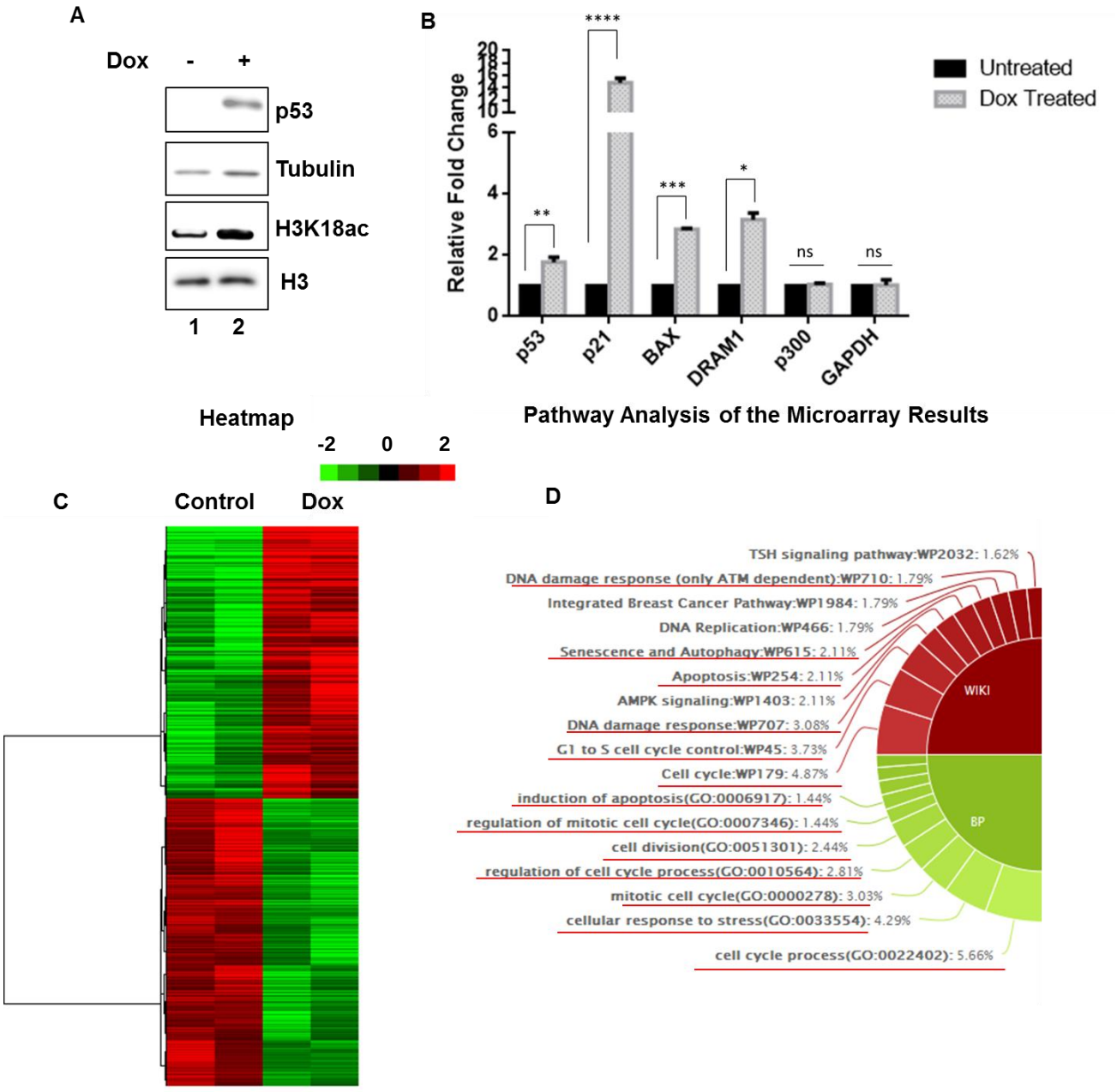

Figure 4.12: Characterization of doxycycline-inducible p53 expressing H1299 cell line. (A) Doxycycline-inducible p53 expression H1299 cell line to determine the levels of p53, H3K18ac, tubulin, and H3 upon doxycycline treatement. (B) RT-qPCR to determine relative expression levels of p53-target and non-target genes. (C) Heatmap and (D) Pathway analysis of the RNA microarray analysis performed on the doxycycline-inducible p53 expression H1299 cell line.

In the p53-inducible H1299 cell line, ChIP-seq for p300 and autoacetylated p300 (acp300) was performed. Differential peaks were called for the genome-wide enrichment of p300 and acp300 in the presence of p53 (+dox condition) over the control (-dox condition). The distribution pattern of p300 and acp300 therefore revealed the recruitment of the coactivator (either through direct or indirect interaction) by p53.The peak distributions of p300 and

acp300 chromatin enrichment were plotted. Distinct genomic distributions were observed for p300 and acp300; p300 appeared to occupy regions distal from the TSS (Figure 4.13A) and acp300 appeared to bind both the promoter proximal regions as well as the distal regions (Figure 4.13B).

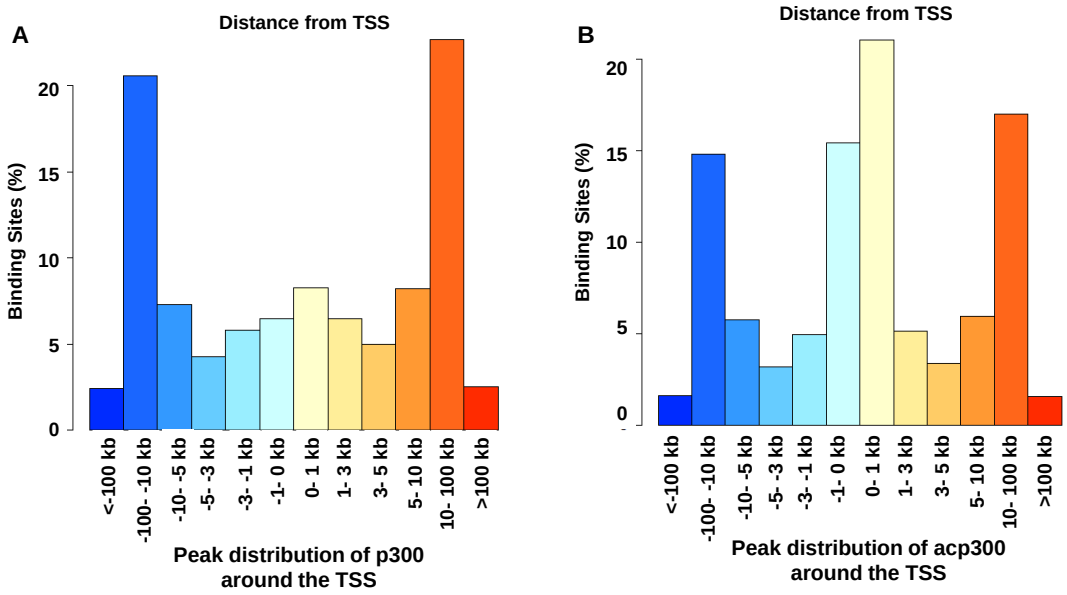

Figure 4.13: Distribution of p300 and autoacetylated p300 (acp300) peaks upon p53 expression in the H1299 cell line. Histograms representing the peak distribution of (A) p300 and (acp300) around the Transcription Start Site (TSS) upon p53 expression.

The p300 and acp300 peaks obtained were divided into two group, promoter proximal peaks which were peaks 5 kb ± TSS and distal peaks which >5 kb from TSS (Figure 4.14 A,B). The enrichment patterns indicated a distinct preference for acp300 occupancy for the promoter proximal regions, while only a weak enrichment pattern was observed for p300, reinforcing the fact that it may be the autoacetylated form of p300 which is actively associated with transcription initiation (Figure 4.14 A,C). The abundance of acp300 at the promoters also correlated with RNA Pol II enrichment, and the active promoter mark like H3K27ac (Figure 4.13A). The enrichment pattern clearly indicates a role of acp300 in gene transcription regulation. A reverse pattern was obtained for the distal elements. Here, acp300 binding patterns appeared to be opposite to the enrichment patterns obtained for active enhancer marks such as H3K4me1 and H3K27ac. Nevertheless, a good overlap between the enrichment of p300 and the enhancer marks was observed at the distal regions. This data indicates a specific role for acp300 over the entire pool of p300 existing in a cell.

Interestingly, the autoacetylated p300 probably plays an important role in the transcription pre-initiation complex (PIC) assembly and disassembly. This finding is in tune with the previous report from Black et al, where it was shown that autoacetylation of p300 was required for PIC assembly and transcription initiation (Black et al., 2006). The data is also in congruence with the previous studies that have shown the preferential occupancy of p300 at enhancers. p300 is a marker of tissue-specific enhancers and is ubiquitously associated with multiprotein assemblies at enhancers (Figure 4.14B). Of the 34,141 peaks identified for acp300, 2044 peaks overlap with p300 occupancy (Figure 4.14D). The differential occupancy of acp300 and p300 on the promoters of genes expressed upon stimulation of p53 was investigated. The coactivator occupancy was integrated with the microarray expression analysis of the differentially expressed genes in the Tet-ON p53 expression system revealing a greater overlap between the p53-driven transcription and acp300 (534 genes) recruitment in comparison to p300 (253 genes). The common genes (211 genes) which were enriched for both acp300 and p300 were further analyzed. Intriguingly, pathway analysis (p-value ≤ 0.05) for the acp300 unique genes enriched for several metabolic pathways in addition to the canonical p53-signaling and transcription-related pathways (Table 4.1). The ChIP-seq data for RNA Pol II, H3K27ac and H3K4me1 was retrieved from Data Bank of Japan (DDBJ), accession number: DRA001860 (http://dbtss.hgc.jp/) (Suzuki et al., 2014).

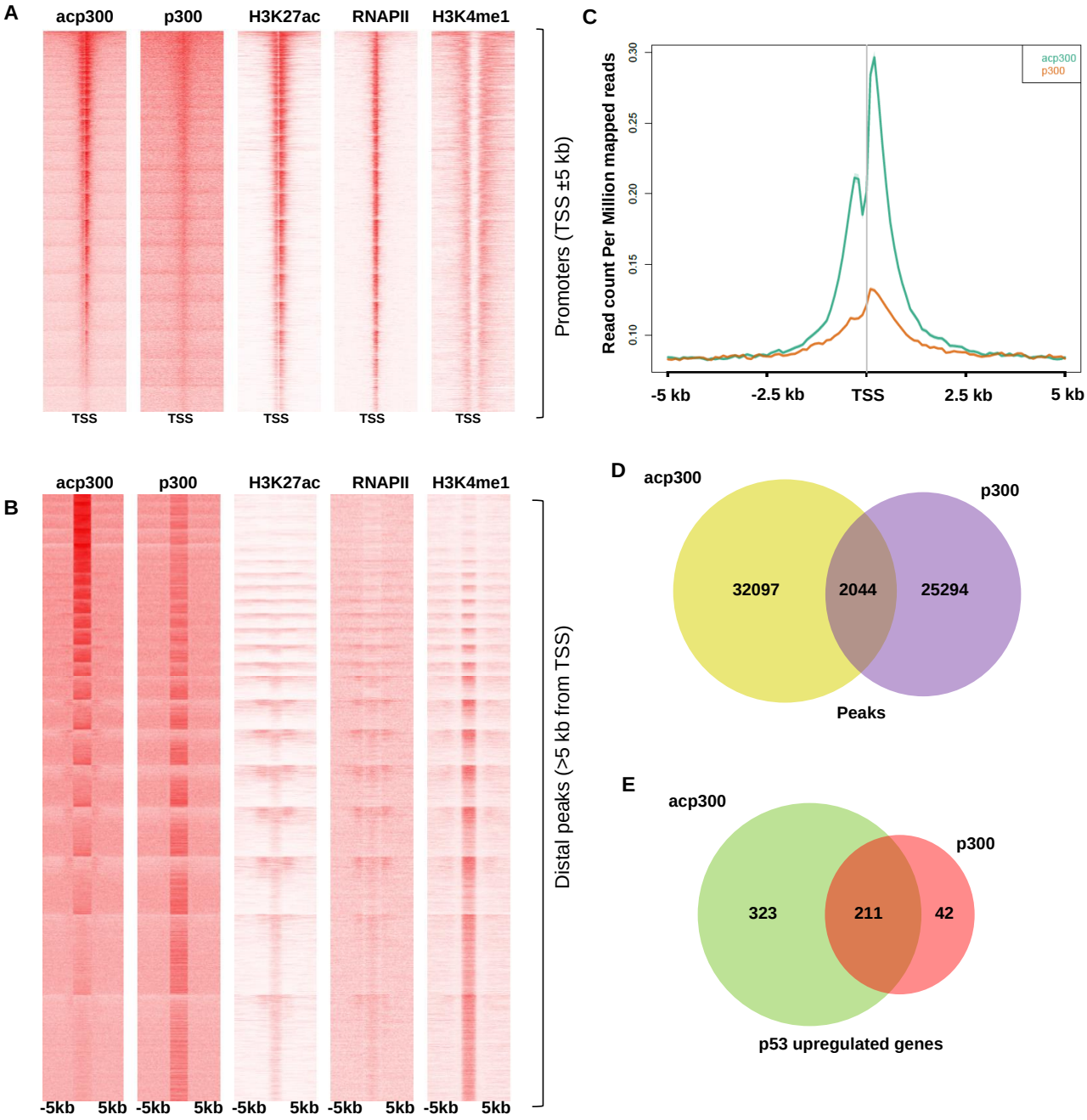

Figure 4.14: Global recruitment of autoacetylated p300 by p53-induction. Heatmaps depicting the enrichment of acp300, p300, H3K27ac, RNA Polymerase II (RNAPII), and H3K4me1 at (A) promoters (TSS±5 kb) and (B) distal elements (>5 kb from TSS). (C) Comparison of the average ChIP-seq enrichment per 50 bp bin of p300 (orange line) and acp300 (cyan line) at the promoters (TSS±5 kb). (D) Venn Diagram showing the peaks intersecting between p300 and acp300, (E) Venn diagram showing the overlap between the up-regulated genes enriched at the promoters with both acp300 and p300 and genes unique to each set.

Term	No. of genes	p-value
endoplasmic reticulum membrane	**28**	**0.00049052**
Apoptosis	**7**	**0.00090694**
Mitochondrion	**30**	**0.00123927**
endoplasmic reticulum	**26**	**0.00131164**
Transit peptide	**18**	**0.00172177**
extrinsic apoptotic signaling pathway via death domain receptors	**5**	**0.00322367**
mitochondrion	**34**	**0.00578275**
Ribonucleoprotein	**11**	**0.00971273**
GTP-binding	**12**	**0.01009015**
Serine/threonine-protein kinase	**13**	**0.01049547**
Acyltransferase	**8**	**0.01105162**
tumor necrosis factor-mediated signaling pathway	**7**	**0.01246378**
ER to Golgi vesicle-mediated transport	**8**	**0.01554622**
integrator complex	**3**	**0.01696651**
Transferase	**36**	**0.01702659**
Citrate cycle (TCA cycle)	**4**	**0.01714417**
response to lipopolysaccharide	**8**	**0.01757149**
snRNA processing	**3**	**0.01812607**
activation of cysteine-type endopeptidase activity involved in apoptotic signaling pathway	**3**	**0.01812607**

Table 4.1: Pathway analysis (KEGG and GO) of up-regulated genes unique to acp300 genome-wide occupancy.

The enrichment of acp300 and p300 at p53-responsive promoters was visualized using the Integrative Genomics Viewer (Robinson et al., 2011). In agreement with the enrichment heatmaps (Figure 4.14), a similar trend was observed at individual promoters. At p53-target genes, such a BBC3 (PUMA), GDF15 and TP53INP1, acp300 peaks coincided with the promoter mark H3K27ac (Figure 4.15 A-C).

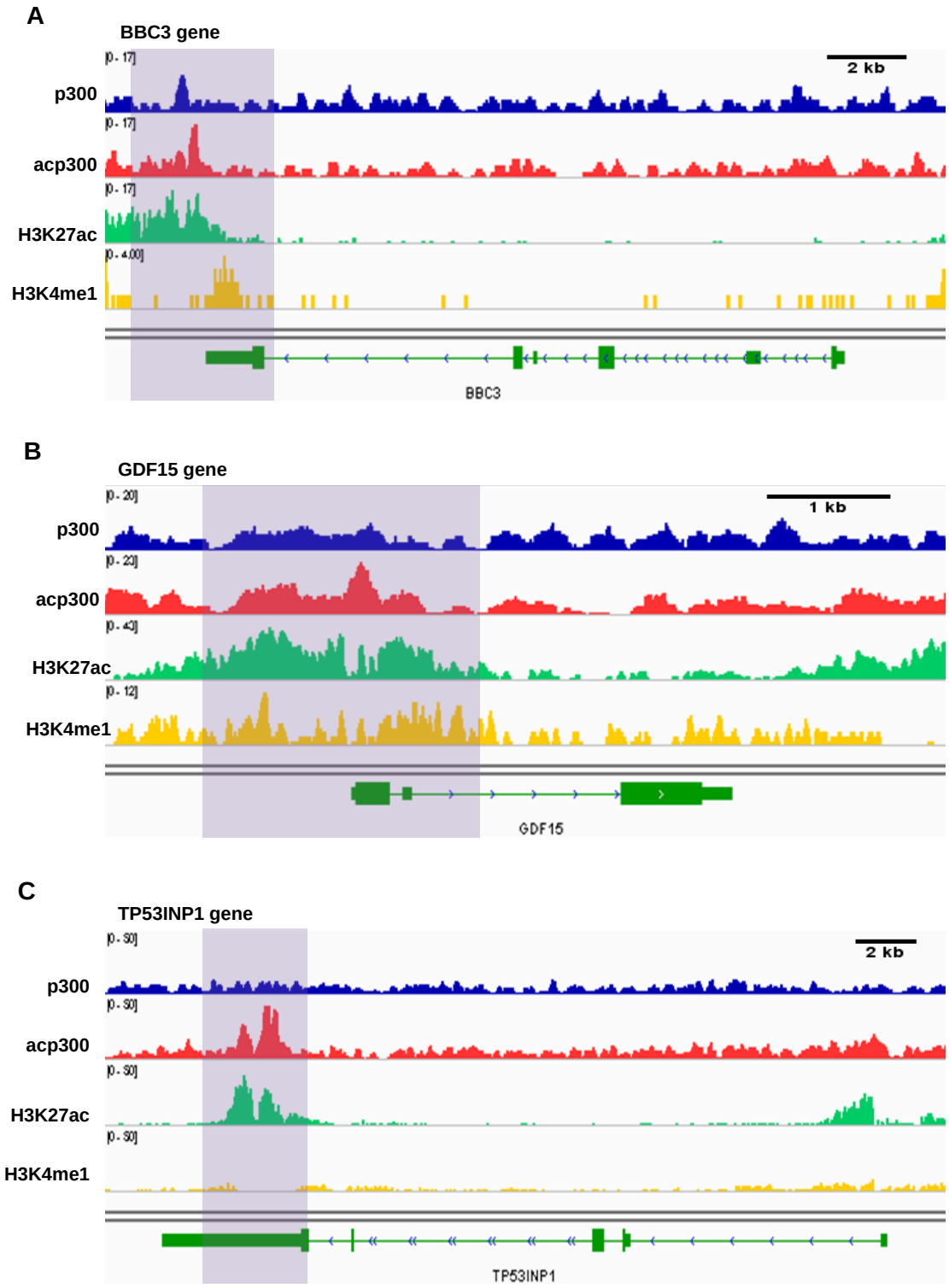

Figure 4.15: Acp300 occupancy on p53-target promoters. Track visualization of p300, acp300, H3K27ac, and H3K4me1 occupancy on p53-response gene promoters: (A) BBC3 gene, (B) GDF15 gene, and (C) TP53INP1 gene. Heatmaps depicting the enrichment of (A) autoacetylated p300 (acp300) peaks and (B p300 peaks ±5 kb around TSS on common genes. (C) Read density profiles of p300 and acp300 (D) Pathway analysis (GO and KEGG) of the common genes between p300 and acp300. Track visualization was done using the Integrative Genomics Viewer (IGV) genome browser software (Robinson et al., 2011).

The enrichment of p300 and acp300 was then visualized on p53-non-target genes, GAPDH and JADE1. No differential peaks were observed (dox-treated over control) (Figure 4.16 A,B). Next, by ChIP-qPCR the enrichment of acp300 and p300 at p53-responsive gene promoters and p53-non-responsive gene promoters were further verified under two conditions: (i) when p53 is at negligible levels (untreated) and (ii) when p53 is overexpressed (doxycycline-treated). Interestingly, upon the overexpression of p53, a surge in the recruitment of autoacetylated p300 at the p21 promoter was observed, while only a modest increase in p300 was observed (Figure 4.16 C,E). Moreover, the recruitment of p300 and autoacetylated p300 on the GAPDH promoter (p53-non-responsive) showed no preference for the presence of p53 (Figure 4.16 D,F).

These experiments provide evidences that once p53 has induced p300 catalytic activity through autoacetylation, it preferentially interacts (or remains in complex) with autoacetylated p300 and recruits it to the promoters of its downstream target genes.

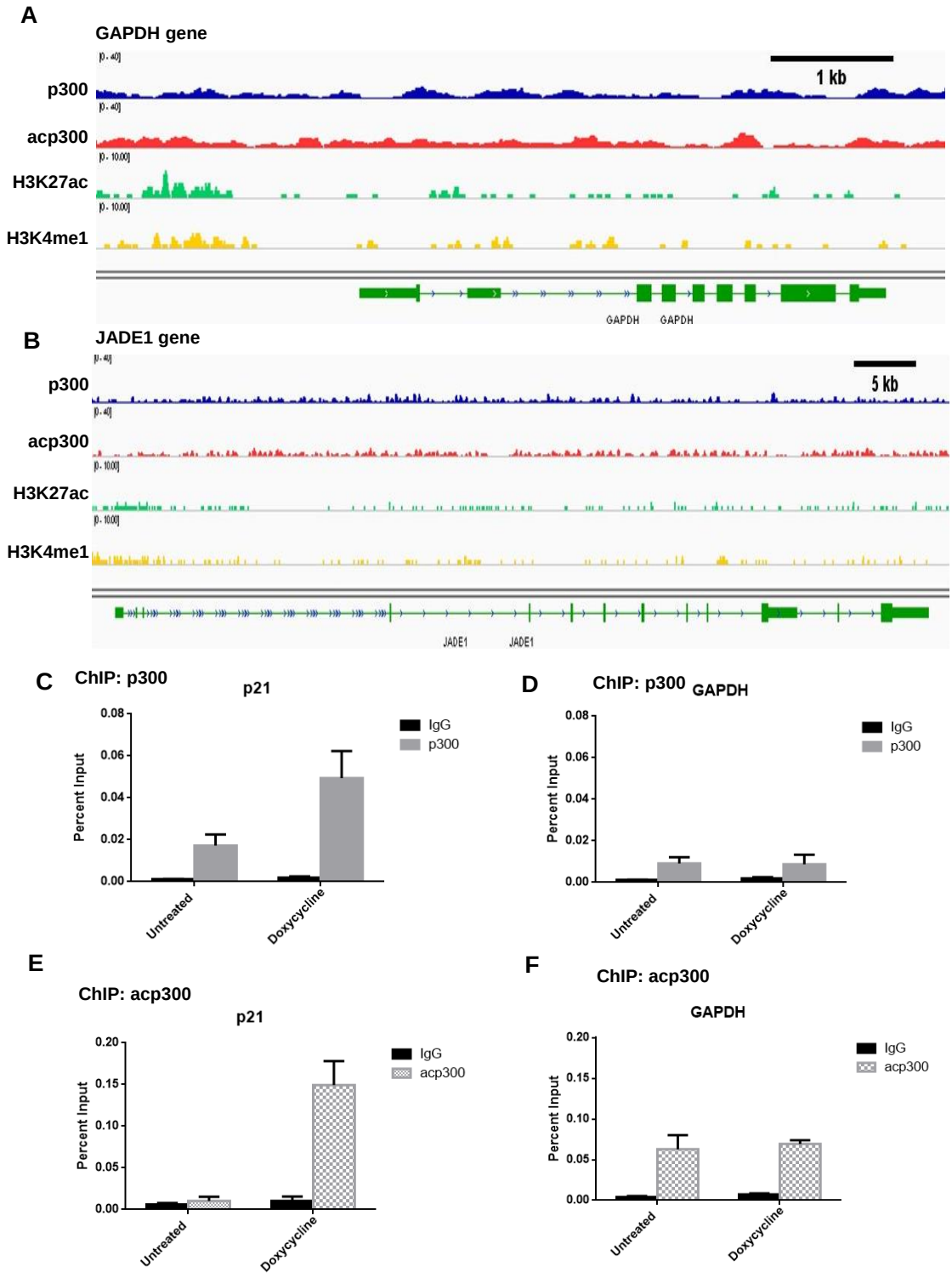

Figure 4.16: Comparison of p300 and acp300 occupancy in p53-responsive and non-responsive gene promoters. Track visualization, using IGV software, of p300, acp300, H3K27ac, and H3K4me1 occupancy on p53-non-target gene promoters: (A) GAPDH gene, (B) JADE1 gene. ChIP-qPCR to show the differential enrichment of p300 (C,D) and acp300 (E,F) at the p21 gene promoter (p53-target) (C,E) and GAPDH gene promoter (D,F) in p53 absence (untreated) and p53 presence (Doxycycline).

4.10. Physiological significance of p53-mediated enhancement of p300 autoacetylation

It can be postulated that once p53 is stabilized in the cell, it associates with its ubiquitously-expressed co-activator, p300. This association triggers an allosteric conformational switch in p300, exposing its lysine-rich autoinhibitory loop in its HAT domain for *trans*-autoacetylation. Once p300 is autoacetylated in *trans*, it is catalytically fully activated. This active, 'open' form of p300 is subsequently enriched onto the p53-target gene regulatory regions on the chromatin via the interaction with p53. Autoacetylated p300 then acetylates histone tails at these loci, opening chromatin, and subsequently assembles the transcription machinery complex resulting in enhanced transcription p53-downstream gene-network (Figure 4.17).

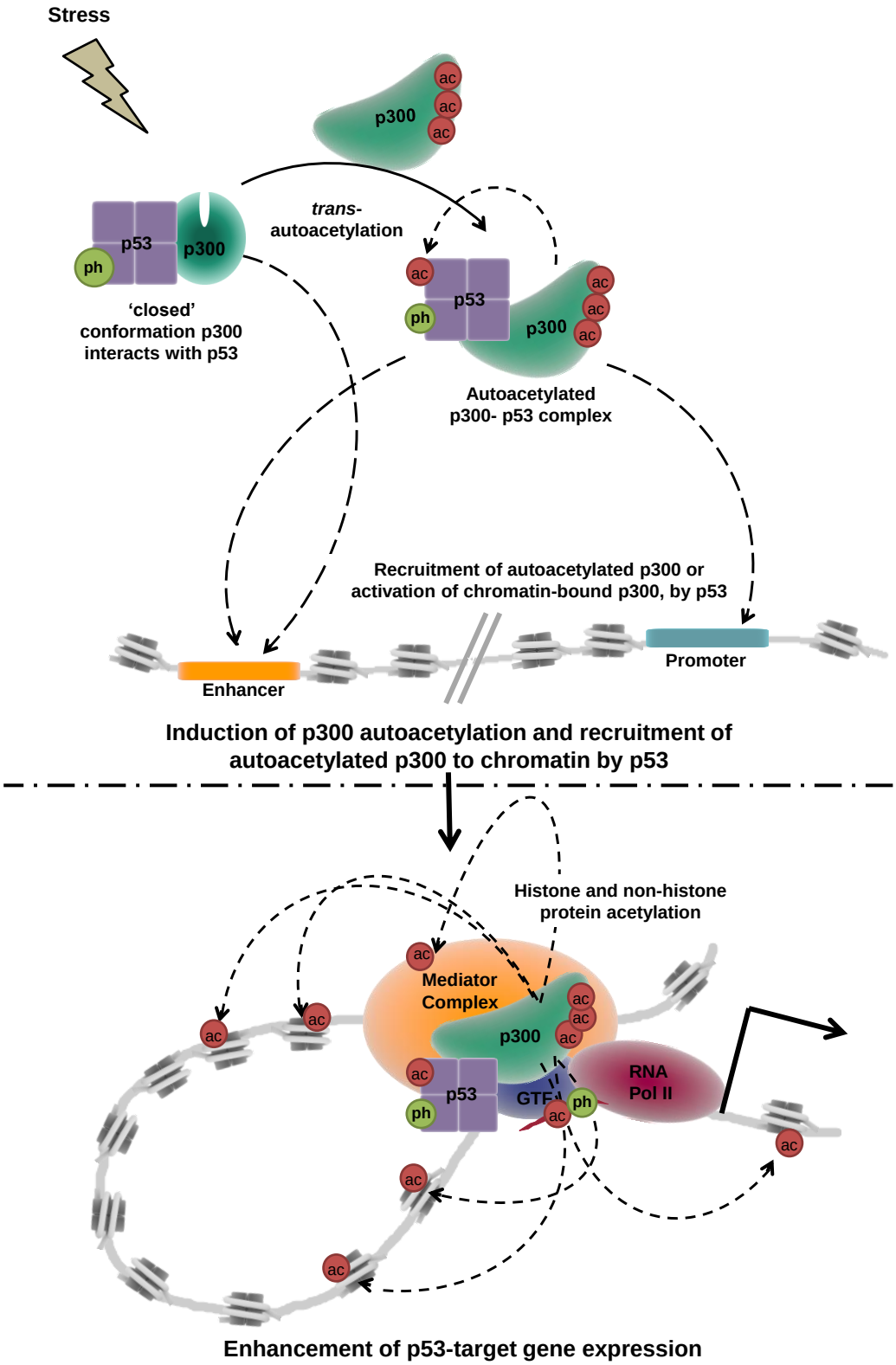

Figure 4.17: Physiological significance of p53-mediated induction of p300 autoacetylation. When p53 is stabilized upon genotoxic stress, it associated with p300 in the nucleus, leading to a conformational dynamics which results in the activation of the enzyme, presumably through *trans*-autoacetylation. It is the autoacetylated form of p300 which is recruited to gene regulatory elements through p53 interaction. p300 can now

acetylate histones leading to decompaction of chromatin and enhancement of p53-downstream gene expression.

4.11. Summary

This study has provided experimental evidence to establish p53 as a bona fide modulator of p300 autoacetylation. The preferential induction of p300 autoacetylation over other acetyltransferases by p53 exhibits the specificity of p53-mediated induction of p300 acetylation, and proves that the induction of autoacetylation is not a by-product of enzyme-substrate interaction. Moreover, p53 could modulate the levels of histone acetylation through the induction of p300 autoacetylation, signifying that the tumor suppressor p53 can alter the epigenetic landscape through the regulation of p300 acetyltransferase activity. The direct interaction between p53 and p300 was found to be essential for the induction of p300 activity. Earlier structural studies have shown that p300 core catalytic domain obtains a compact spatial conformation. In the 'inactive' conformation, which is also corroborated by the cryo-EM structure done in this study, the RING domain forms an obstruction to substrate-binding by occluding the substrate-binding groove of the HAT domain which is buried inside the compact structure (Delvecchio et al., 2013). In the p53-p300 complex, however, a distinct alteration in p300 conformation was observed. In this structure, the inhibitory RING domain was displaced away from the substrate-binding pocket of p300 HAT domain, in a conformation which can be termed as 'open' or 'active'. Through cryo-EM structural studies, it could be demonstrated that the 'open' conformation of p300 precedes the induction of autoacetylation, which is pre-requisite for the full activation of p300 enzymatic activity. Therefore, this data implicates that the ability of an effector to modulate the conformational state of p300 can have a direct impact p300 acetyltransferase activity. The ChIP-seq analysis of autoacetylated p300 (acp300) genome occupancy upon p53 induction, further gave an insight into gene specificity and gene expression cascades triggered by effector (p53)-mediated induction of p300 autoacetylation.

Chapter 5

Role of mutant p53 in the induction of p300 autoacetylation

The missense p53 mutant is a driving force in the establishment of malignancies. Depending on the site of the mutation, these missense mutations can impart unique Loss-of-function or Gain-of-function properties to the p53 protein. In this chapter, the role of mutant p53 in the induction of p300 autoacetylation has been investigated. Even though each missense mutant is a different protein with distinct GOF properties, a majority of them appear to modulate p300 autoacetylation levels in vitro as well as in cells. Interestingly, experimental evidence suggests that p300 may play a pivotal role in the p53-driven cancers. This study uncovers how differential regulation of p300 activity, through the modulation of its autoacetylation by inducers, may contribute to p300 dysfunction in disease conditions.

5.1. Gain-of-Function mutants of p53 are potent inducers of p300 autoacetylation *in vitro*

Another realm of p53 biology is the pathological impact of p53 gain-of-function mutants. The inactivation of the p53 gene is observed in over 50% of cancers. Of the mutations occurring on the p53 gene, 97% map to the DNA binding domain, often conferring functions to the protein which it would otherwise not exhibit. Moreover, earlier experimental data has established p53 as a potent inducer of p300. Since p53 mutants are key factors in cancer proliferation, invasion and metastasis, whether these mutants can harness the activity of p300 through the induction of autoacetylation, would be an interesting angle in p53-driven cancers. Mutant p53 can be broadly classified into three categories depending on the location of the mutation and the structure attributes imparted by the mutation. The three categories are (i) Conformational p53 mutants, these mutants are characteristic of exhibiting structural features distinct from the wildtype p53 protein; (ii) DNA contact mutants, these mutants do not exhibit a severe structural perturbation and have a conformation similar to the wildtype p53. In these mutants, the mutation disrupts the protein interface in contact with DNA, thereby partially or fully abrogating the sequence-specific DNA binding property of p53. (iii) The third class of p53 mutants are the tetramerization defective mutants. These mutations occur in

the tetramerization domain which are causal for the destabilizing of the functional p53 tetramers. A list of mutants used in this study is presented in Table 5.1.

Serial No.	Mutant	Dominant Negative p53/p73/p63	DNA binding	Domain of mutation/ region	Interacting partners	Properties/ class of genes affected	Localization
Conformational Mutants							
1.	**R175H**	DN (p53, p63, p73)	no	DBD, Loop 2	NF-Y, Sp1, VDR, Top BP1,PML, p63, p73	Proliferation, ECM, chemoresistance, metabolism, GTPase, cytoskeleton, RNA stability	Nuclear> cytoplasmic
2.	**V143A**	DN (p53, p73)	partial	DBD, β-Strand 3	Ets-1, TopBP1, p73	Proliferation	Nuclear> cytoplasmic
3.	**R249S**	DN	no	DBD, Loop 3	Sp1, TopBP1	Chemoresistance	cytoplasmic
DNA Contact Mutants							
4.	**R273H**	DN (p53, p63)	no	DBD, β-Strand 2	Sp1, SREBP-2, TopBP1, MRE11, PML, p63	Proliferation, chemoresistance,metabolism,ECM,GTPase ,cytoskeleton,RNA stability, M-phase,Centromere, mRNA processing	Nuclear
5.	**D281G**	DN p53,p73	no	DBD, α-Helix 2	Ets-1	ECM, limitless replication TERT	Nuclear
6.	**R280K**	DN Aggregates	no	DBD, α-Helix 2	SREBP-2, Pin1	Proliferation, metabolism, GTPase activity, cytoskeleton, M phase, centromere, mRNA processing	Cytoplasmic + nuclear
7.	**R248W**	Partial	no	DBD, Loop 3	TopBP1, MRE11, p63, p53	Proliferation, chemoresistance	Nuclear> cytoplasmic
8.	**L194F**	DN, p53, p63, p73	No	DBD, β-Strand 6			Cytoplasmic + nuclear
Tetramerization mutants							
9.	**G334V**	Co-aggregation amyloid formation	partial	TD (strand-helix junction)			-
10.	**R337H**	No	yes	TD			Cytoplasmic + nuclear
11.	**L344A**	Monomer/Dimer	partial	TD (alpha helix)			Nuclear

Table 5.1: Characteristic details of the p53 mutants used in this study. (Information Source: the International Agency for Research on Cancer [IARC] database, http://www-

p53.iarc.fr). (DBD: DNA binding Domain, TD: Tetramerization Domain, DN: Dominant negative)

In an *in vitro* acetyltransferase assay, different hotspot mutants of p53 were tested for their ability to induce p300 autoacetylation. In the assay, three conformational mutants of p53 (R175H, V143A, and R249S) and two DNA contact mutants of p53 (R273H and R248W) were used. Interestingly, all the GOF mutants appeared to enhance p300 autoacetylation *in vitro* which was comparable to the enhancement observed in the presence of wildtype p53 (Figure 5.1).

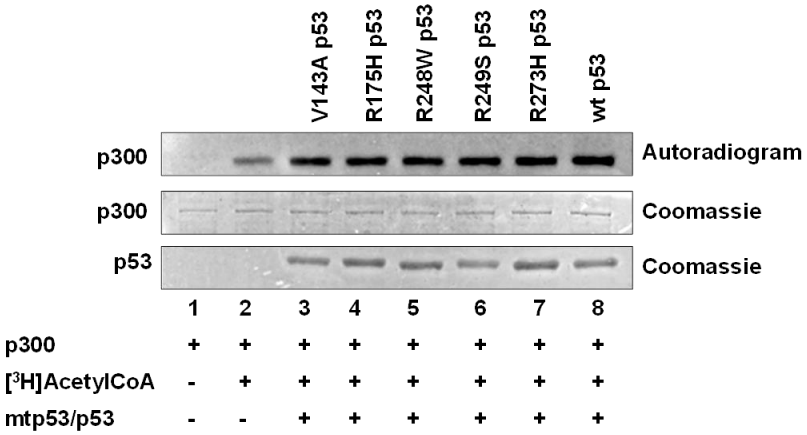

Figure 5.1: Gain-of-function p53 mutants enhance p300 autoacetylation. An *in vitro* HAT assay was performed to determine the levels of autoacetylation of p300 in the presence of recombinant GOF p53 mutants and wildtype p53. The autoradiograms indicate the levels of p300 autoacetylation; while the Coomassie Brilliant Blue stained protein panels serve as the loading.

5.2. Screening different classes of Gain-of-Function mutants of p53 for their ability to induce p300 autoacetylation in cells

Biochemical *in vitro* assays using hotspot mutants demonstrated that these mutants could efficiently enhance the levels of p300 autoacetylation. As a confirmation of this observation, GOF mutants of the classes, conformation and DNA contact, were screened in a cellular assay where the alteration in the levels of p300 autoacetylation was monitored through immunofluorescence. Gain-of-function mutants of p53 were ectopically expressed in a p53-null background and their ability to induce autoacetylation was scored based on the increase in the fluorescence intensity of p300 autoacetylation staining relative to the untransfected cells.

All the DNA contact mutants tested were competent in inducing the autoacetylation levels of p300 (Figure 5.2). Among the conformational mutants V143A and R249S were effective inducers of p300 autoacetylation, but the global conformational mutant, R175H failed to alter the levels of p300 autoacetylation in cells (Figure 5.3). Interestingly, the R175H mutant was an effective autoacetylation inducer *in vitro* (Figure 5.1). The difference observed may be presumably due to the inability to make functional contact with p300 in cell, due to its severely distorted structure. Overall, it is evident that most of the GOF mutants of p53 retain their ability to induce p300 autoacetylation in the cellular context as well.

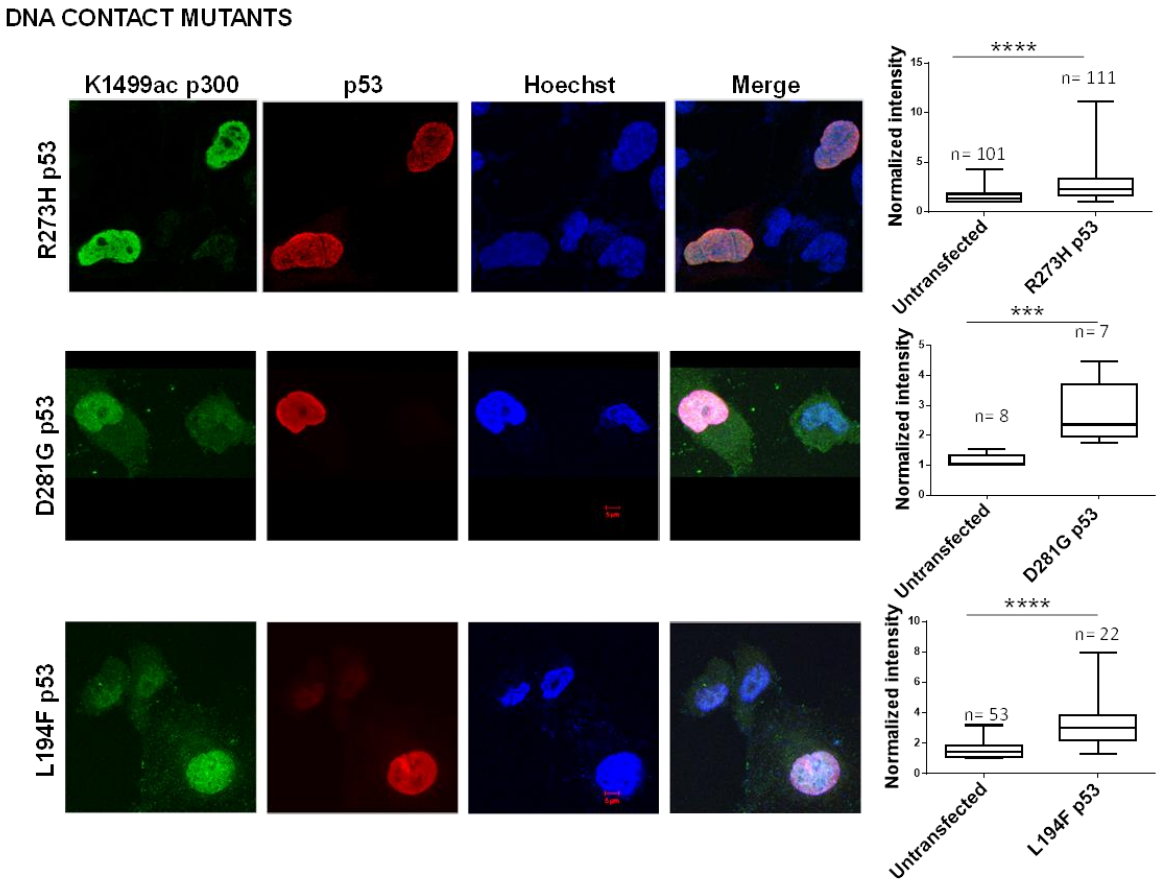

Figure 5.2: DNA contact GOF p53 mutants modulates p300 autoacetylation in cells. p53 null H1299 cells were transfected with R273H, D281G and L194F p53 mutants, as indicated. The levels of K1499ac p300 and mutant p53 were determined in untrasfected versus mutant p53 transfected cells in p53 null H1299 cell line by immunofluorescence. Fluorescence intensity of K1499ac (autoacetylated) p300 in untransfected versus p53 transfected cells have been quantified (represented as mean ± SD).

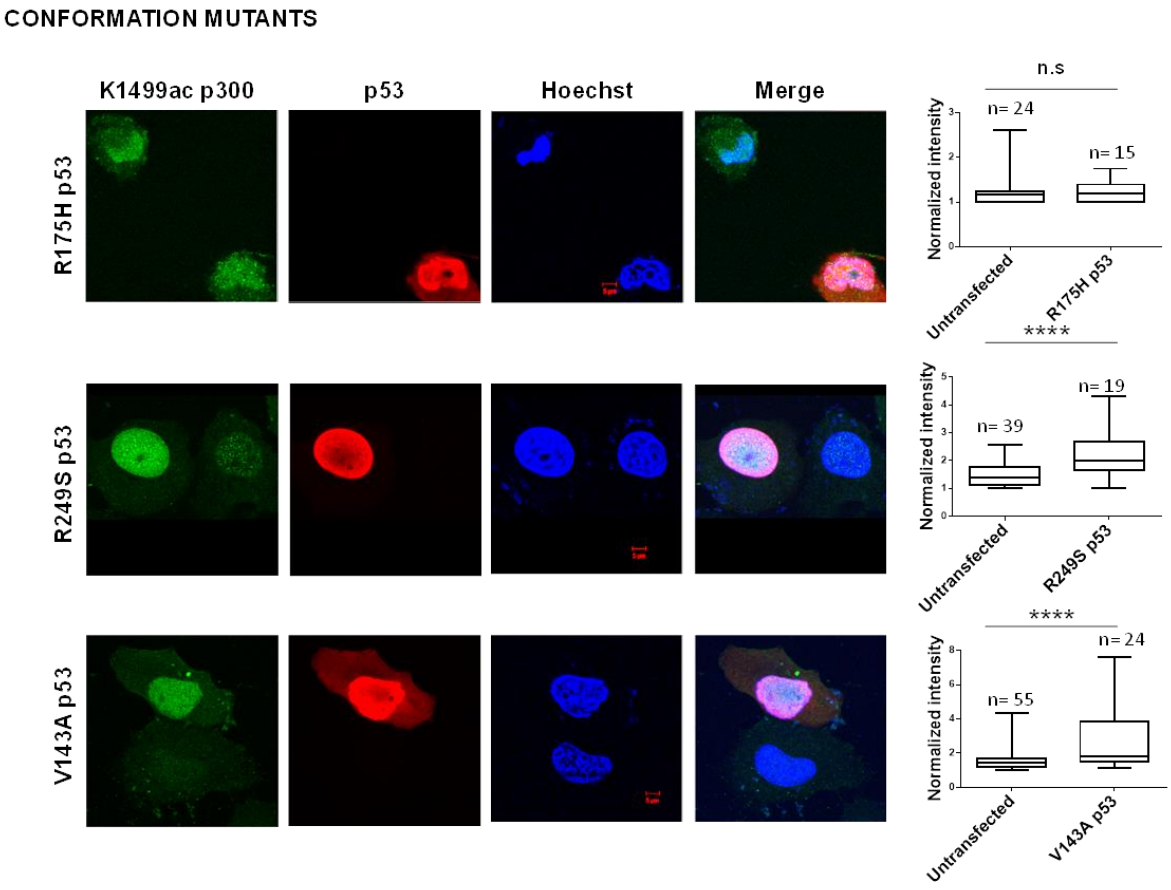

Figure 5.3: Conformational GOF p53 mutants regulates p300 autoacetylation in cells. p53 null H1299 cells were transfected with R175H, R249S and V143A p53 mutants, as indicated. The levels of K1499ac p300 and mutant p53 were determined in untrasfected versus mutant p53 transfected cells in p53 null H1299 cell line by immunofluorescence. Fluorescence intensity of K1499ac (autoacetylated) p300 in untransfected versus p53 transfected cells have been quantified (represented as mean ± SD).

5.3. The Gain-of-Function mutant R273H p53 modulates p300 autoacetylation and activity

The conversion of the wildtype p53 protein to a GOF mutant drastically alters the physical and functional properties of the protein therefore the retention of the p300 autoacetylation inducer function is an intriguing revelation in p53-driven disease biology. To understand the pathophysiological relevance of GOF mutant p53-mediated enhancement of p300 autoacetylation, the R273H p53 mutant, which has one of the highest incidences in cancers (6.7%), was chosen for further investigation.

To establish that R273H p53 mutant could alter the levels of p300 autoacetylation alone without affecting the overall p300 protein levels, immunofluorescence was performed in H1299 cells ectopically expressing R273H p53. As observed in the earlier

immunofluorescence staining, the autoacetylation of p300 increased drastically in the presence of R273H (Figure 5.4B, upper panel) while exhibiting negligible change in the overall p300 protein levels (Figure 5.4B, lower panel). This experiment reinforces the fact that, similar to wildtype p53, the GOF R273H mutant too, modulates p300 only at the autoacetylation level and does not appear to affect p300 protein stability. As established earlier, that increased KAT activity is a direct consequence of p300 autoacetylation, the levels of different p300-specific histone marks were checked, after ectopically expressing the mutant R273H and wildtype p53 as a control. It is evident from the western blotting analysis, that histone acetylation on H2AK5 and H3K9 were upregulated in cells transfected with the mutant and wildtype p53 in comparison to the vector transfected cells (Figure 5.4C).

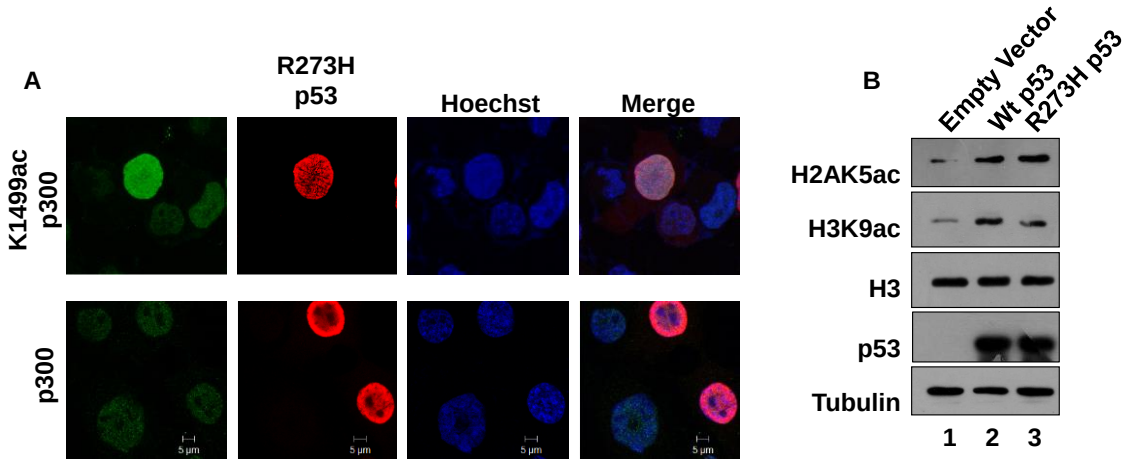

Figure 5.4: GOF mutant R273H modulates p300 autoacetylation and activity. (A) p53 null H1299 cells were transfected with R273H p53 mutant. The levels of K1499ac p300 (top panel, green), p300 (bottom panel, green) and mutant p53 red were determined by immunofluorescence. (B) Western blotting analysis to determine the levels of p300-specific histone acetylation levels.

5.4. R273H p53 mutant interaction with p300 is important for the p53 mutant-driven tumorigenesis

To investigate whether the R273H mutant-mediated induction of p300 autoacetylation had role in the regulating the tumorigenic potential of the mutant, an inducible Tet-ON cell line for R273H p53 expression was created. Earlier experiments have established that the direct interaction of p53 with p300 is essential for the induction of p300 autoacetylation. Therefore, the aim of the experiment was to test whether the direct interaction of p300 interaction the p53 mutant R273H played a role in the GOF of this mutant. For this purpose a wound healing assay was designed, where the cells were treated with doxycycline to induce the expression

of R273H p53 and the untreated cells served as the experiment controls. Under both conditions, ie., R273H presence and absence, the cells were treated with either the p53-p300 interfering phosphomimic p53 peptide (3E peptide) and the control scrambled peptide. It should be noted that this assay can account for the closure of the scratch/ wound, but cannot distinguish between the contribution of proliferation and migration. Upon doxycycline treatment the wound created in the control cells healed faster, suggesting that the R273H p53 mutant expressed indeed exhibited GOF propertied, marked by higher proliferation and migration. The cells treated with the scrambled peptide showed similar closure time as the control cells, signifying that the scrambled peptide did not have any apparent pleiotropic effect. Interestingly, the cells treated with the 3E peptide phosphomimic p300-p53 interfering peptide migrated and proliferated slower than the control cells, implicating a possible role of p300 interaction in the tumorigenic potential of R273H p53 (Figure 5.5A). Moreover, the delay in wound closure observed upon the 3E peptide treatment was comparable to the untreated (doxycycline negative) cells, suggesting that the peptide treatment may have abrogated the effect of the p53 mutant expression. Furthermore, in the doxycycline negative cells the control, 3E peptide, and scrambled peptide-treated cells migrated and proliferated at similar rates suggesting that the effect observed upon 3E peptide treatment in the doxycycline treated cells had a direct correlation with the presence of mutant p53 (Figure 5.5B). These results implicate the direct role of p300 (and possible p300 autoacetylation) in the induction of R273H tumorigenic functions, creating a positive feedback loop between the two proteins. Western blotting analysis was done with the cells used in the assay to ascertain the expression status of R273H p53 in the presence and absence of doxycycline treatment (Figure 5.5C). Since in the above experiment the mutant R273H was artificially expressed in H1299 cells, it was important to demonstrate a similar phenomenon in a cancerous cell line with the endogenous R273H mutant expression. Therefore, a similar wound healing assay was performed in the AW13516 oral cancer cell line which expresses high levels of the R273H p53 mutant. Similar to the previous experiment, 3E peptide drastically impaired the rate of wound closure (Figure 5.6, middle panel, 12 hours) in comparison to the untreated and scrambled peptide treated controls (Figure 5.6, top and bottom panels, 12 hours).

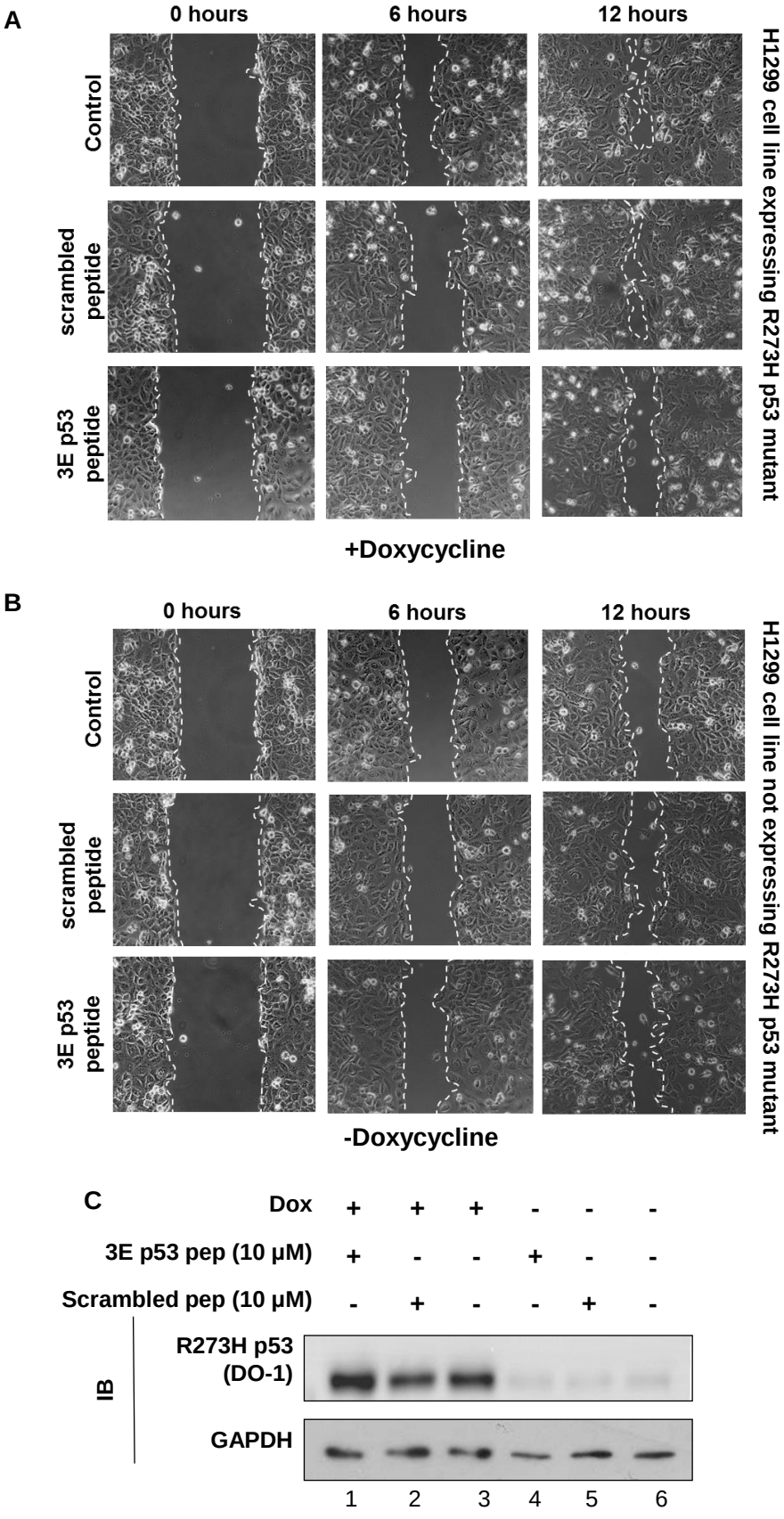

Figure 5.5: Disruption of R273H p53- p300 interaction compromises R273H p53 Gain-of-Function in cancer cells. (A) Representative images (of two biological repeats) of a

wound healing assay performed in doxycycline-inducible R273H p53 H1299 cells. The cells were treated with either phosphomimic p53 peptide or scrambled peptide as indicated under (A) doxycycline induced R273H expressing condition or (B) doxycycline absent condition. (C) Immunoblots to determine the expression of mutant p53 in cells under the different condition of the experiment.

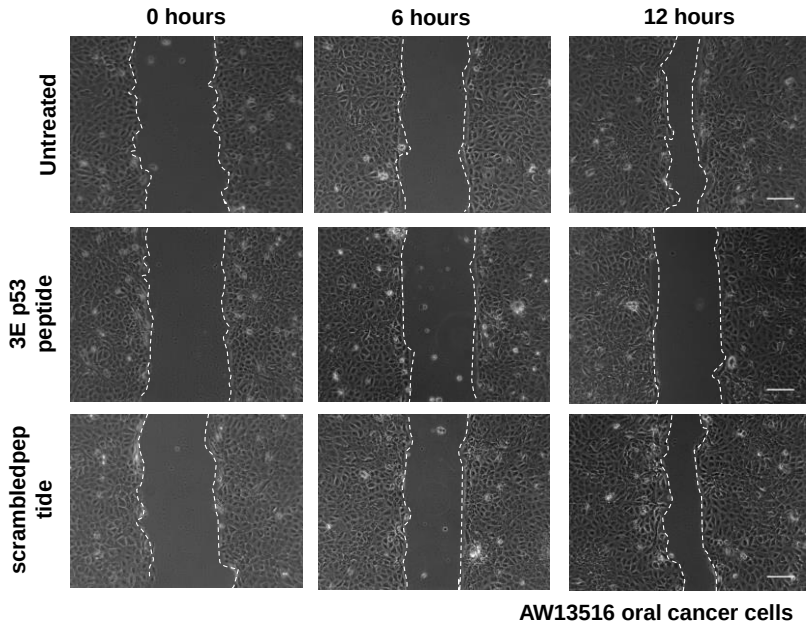

Figure 5.6: Disruption of R273H p53- p300 interaction compromises R273H p53 Gain-of-Function in cancer cells. (A) Representative images (of two biological repeats) of a wound healing assay performed in AW13516 oral cancer cells expressing p53 mutant, R273H. Scale bar represents 100 µm.

5.5. The Loss-of-Function tetramerization-defective mutants do not alter p300 autoacetylation levels

It has been shown earlier that p53 proteins that cannot form tetramers, lose their ability to interact with p300 (Itahana et al., 2009). It is fair to assume that the physical interaction of p53 and p300 is a key requisite for the induction of p300 autoacetylation. Therefore, to confirm this, tetramerization defective mutants were transfected into H1299 cells and the levels of autoacetylated p300 was probed by immunofluorescence. It was found that the p53 tetramerization mutants failed to enhance p300 autoacetylation in the H1299 cells (Figure 5.7).

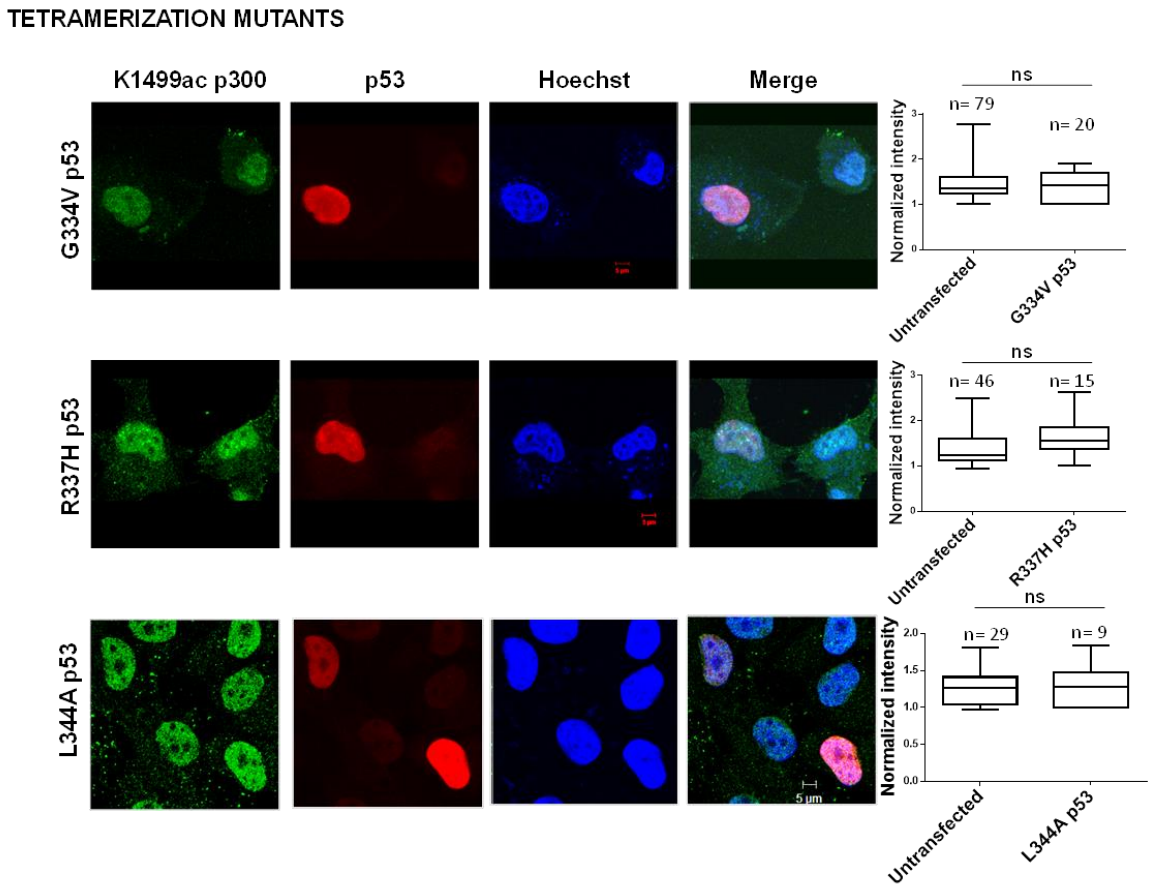

Figure 5.7: Tetramerization-defective p53 mutants fail to enhance p300 autoacetylation in cells. p53 null H1299 cells were transfected with G344A, R337H and L344A p53 mutants, as indicated. The levels of K1499ac p300 and mutant p53 were determined in untrasfected versus mutant p53 transfected cells in p53 null H1299 cell line by immunofluorescence. Fluorescence intensity of K1499ac (autoacetylated) p300 in untransfected versus p53 transfected cells have been quantified (represented as mean ± SD).

5.6. The expression status of mutant p53 and autoacetylated p300 in Oral cancer.

Previous studies have revealed that p300 autoacetylation and histone hyperacetylation may be responsible for the deregulation of gene expression in cancers (Arif et al., 2010b; Seligson et al., 2005). Therefore, to further understand the significance and consequence of p53-mediated p300 autoacetylation, p300, autoacetylated p300, p300-mediated histone acetylation at H3K18 and p53 protein levels were investigated in tumor and normal tissue from oral cancer patients, by immunohistochemistry. As expected, the samples with lower p53 levels have corresponding lower levels of autoacetylated p300 while samples with high levels of p53 have higher staining for autoacetylated p300 (Figure 5.8).

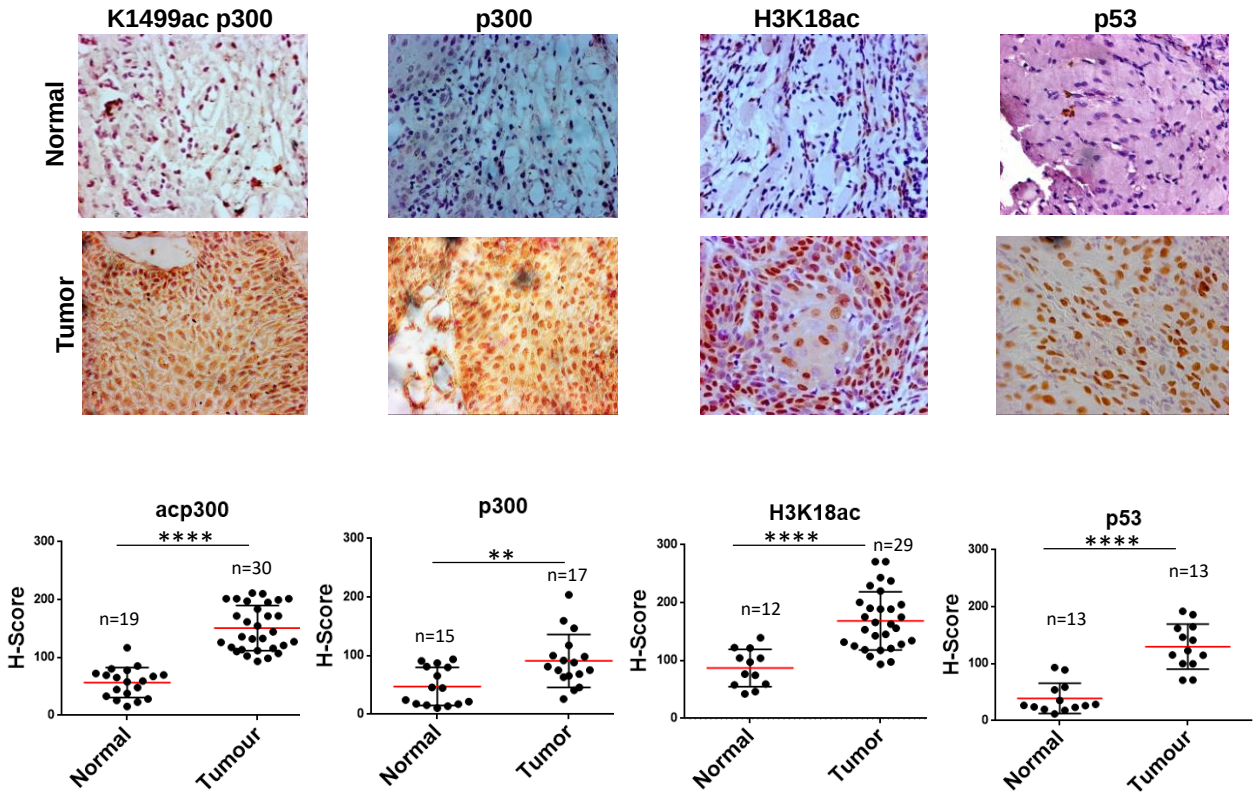

Figure 5.8: Immunohistochemistry to access the levels of p300, autoacetylated (K1499ac) p300, H3K18ac and p53 in OSCC tumor tissue versus the normal tissue. The intensity of the IHC staining was quantified by H-scoring and plotted alongside. The mean H-score was plotted ± SD, statistical analysis was performed using unpaired two-tailed t-test (****, p<0.0001; **, p<0.01).

5.7. Summary

The p53 gene acquires several mutations which abolish its tumor suppressive functions and confer oncogenic gain-of-function properties which contribute to tumorigenesis. Since p53 was discovered as a potent inducer of p300 autoacetylation, this section of the study investigates the role of mutant p300 in the induction of p300 autoacetylation and the probable implications in tumorigenesis. Three classes of p53 mutants, namely, conformational, DNA-binding and tetramerization mutants were screened for their ability to induce p300 autoacetylation. It is known that each missense mutation in the p53 protein attributes unique properties to the protein. Interestingly, it was observed that most GOF mutants belonging to the class of conformational and DNA binding mutants were capable of enhancing p300 autoacetylation. Further investigation of the effect of a hotspot DNA contact mutant, R273H, could increase the global levels of histone acetylation through the enhancement of p300 autoacetylation. Moreover, the p300 protein levels did not alter upon R273H p53 expression,

indicating that the effect on histone acetylation could be a direct consequence of the induction of p300 autoacetylation. Furthermore, using the p53 phosphomimic peptide to disrupt the interaction between R273H p53 and p300 revealed that the interaction between p300 and mutant p53 could play a significant role in the mutant p53-mediated tumorigenesis. This data indicates that GOF mutant p53 may execute its downstream oncogenic functions through the modulation of p300/CBP autoacetylation and function. This data also suggests that p300 may play an important role in mutant p53-driven cancers.

Chapter 6

Discussion

This chapter reflects on the major findings of the current study. Here the results of the thesis will be crtically examined in the light of the known literature and background, emphasizing on the highlights and the probable outcomes of the study.

6.1. Mechanism, function, and consequences of NPM1-mediated induction of p300 autoacetylation

To elucidate the molecular mechanisms involved in factor-induced p300 autoacetylation, an established inducer, NPM1 was chosen for this study. The histone chaperone NPM1 possesses the ability to modulate the catalytic activity of p300 through the enhancement of its autoacetylation. In the oral cancer patient tumor samples, a distinct upregulation in NPM1, autoacetylated p300 and H3K18ac was observed in tumor samples compared to the adjacent normal tissue. The overall p300 expression was also observed to be upregulated in the tumor tissue, although the increase appeared to be lesser in comparison to the autoacetylated p300. A positive correlation was established between the levels of autoacetylated p300 and the expression of NPM1, in oral cancer patient tumor tissue samples (Figure 3.2). From the disease perspective, it may be speculated that NPM1 can alter the histone acetylation patterns in oral cancer through the regulation of p300 autoacetylation. The alteration in the epigenetic landscape may be critical for the manifestation of the disease. The key to deciphering the mechanism of NPM1-mediated induction of p300 autoacetylation lies in the physical properties of these proteins. The in-depth analysis of the findings of this chapter is discussed in the following sub-sections.

6.1.1. NPM1 is a molecular chaperone for p300

The aim of the study was to gain in-sights into the mechanism of factor-induced enhancement of p300 autoacetylation. Therefore, to examine the mechanistic details of NPM1-mediated induction of p300 autoacetylation, the key structural features of both these proteins needed to be taken into account. p300 is a large protein of 264 kDa, containing multiple domains linked by intrinsically disordered regions. The astounding feature of this protein is its ability to interact with over 400 cellular proteins. This is possible due to the flexible nature of this protein. NPM1 on the other hand is a well-established histone chaperone. Previous studies

have revealed the preference of NPM1 for denatured proteins (Szebeni and Olson, 1999). Therefore, the possibility of NPM1 being a molecular chaperone for p300 has been explored in this study. The highlights of this part of the study are that the histone chaperone NPM1 can protect p300 from thermal denaturation and can effectively rescue the activity of heat denatured p300 (Figure 3.5A,B). The intrinsic tryptophan fluorescence studies further confirm the role of NPM1 chaperone activity in the stabilization of the intrinsically disordered structure of p300. Interestingly, the data suggests that once NPM1 has formed a stable complex with p300, it can alter the structure of p300, such that it may attain a conformation which is conducive to the induction of intermolecular autoacetylation and consequently its activity (Figure 3.8, 3.11). Furthermore, domain deletions of NPM1 implicated a possible role of the C-terminal domain in the induction of p300 autoacetylation, and the chaperone activity of NPM1. Earlier studies have demonstrated that the basic/aromatic C-terminal domain is important for several NPM1 function, most notably its histone chaperone activity (Figure 3.12).

6.1.2. Oligomeric form of NPM1 is important for the induction of p300 autoacetylation

Another interesting facet of the NPM1 protein is its ability to form stable decamers. NPM1 is functional in its oligomeric conformation, *in vitro* as well as *in vivo*. In this study, different oligomerization-defective mutants were used. Interestingly, the NPM1 mutants that fail form oligomers also fail to enhance the autoacetylation of p300 (Figure 3.13). It should be noted that these mutations did not abolish oligomerization completely. They could still form some NPM1 oligomers, albeit almost negligible in comparison to the NPM1 wildtype protein. These mutants were created by introducing missense mutations at the dimer interface. Even though at lower protein concentrations the oligomers were destabilized, above a critical concentration the proteins appeared to form higher order aggregates as detected through the DLS experiments (Figure 3.14A). The nature of these aggregates are yet unknown, but they appeared to retain the ability of NPM1 to rescue p300 activity at higher molar concentrations. To investigate the importance of NPM1 oligomerization on the induction of p300 autoacetylation in cells, a small molecule inhibitor of NPM1 oligomerization, NSC348884 was used. Oral cancer cells AW13516 were treated with NSC348884 and the levels of p300 autoacetylation was detected by immunofluorescence. A decrease in p300 autoacetylation was observed in cells treated with NSC348884 whereas the overall levels of p300 remained unaltered. Thus, the treatment of oral cancer cells AW13516 with NSC348884 further proved the importance of NPM1 oligomerization on p300 autoacetylation. The reduction observed in

p300 autoacetylation levels but not in the p300 protein levels confirmed that the functional, oligomeric NPM1 is a key cellular factor for the enhancement of p300 autoacetylation (Figure 3.16).

6.2. p53-mediated Allosteric Activation of p300

In the second part of the study, the role of p53 in the induction of p300 autoacetylation was investigated. p300 is a transcriptional coactivator of the tumor suppressor protein p53, and it binds to the p53 tetramer through four domains, Taz1/cysteine–histidine-rich region 1 (CH1), KIX, Taz2/CH3 and IBiD (Teufel et al., 2007). p53 is also a substrate of p300 (Gu and Roeder, 1997). The importance of p53 acetylation has been implicated in its DNA binding ability and tumor suppressive functions such as cell cycle arrest, apoptosis, senescence and ferroptosis (Bieging et al., 2014; Jiang et al., 2015). However, whether p53 can modulate the activity of p300 was yet to be disclosed. In this study, it is observed that among the different acetyltransferases that acetylate p53, it is only p300 which is activated by p53, through the enhancement of its autoacetylation. The cryo-EM structure analysis of p53-p300 complex elegantly demonstrates the possible structural rearrangement of p300 structure upon p53 interaction, which may result in a conformation which is more conducive for intermolecular autoacetylation. A genome-wide investigation of the recruitment of autoacetylated p300 to the chromatin upon p53-mediated induction was performed, which reveals p53 preferentially recruits autoacetylated p300 over p300 onto its downstream genes' promoters.

6.2.1. p53 is a p300-specific inducer of autoacetylation

The biochemical assays have shown that p53 is a potent inducer of p300 autoacetylation and activity. Interestingly, even though being a substrate of 3 families of KATs, p53 shows a clear preference towards p300 activation over PCAF and Tip60 (Figure 4.1A). The specificity of p53 towards p300 may be due the extensive interactions the two proteins make in a complex. Since p300 has a relatively flexible structure, it is clear that p53 can induce structural alterations in p300 leading to enhancement of its HAT activity. Importantly, p53 can enhance p300 autoacetylation and p300-mediated histone acetylation in cells (Figure 4.2), suggesting that p53 can modulate the activity of p300 in cells and can target this activation to the alteration of histone acetylation landscape and may alter gene expression globally.

6.2.2. Tetrameric p53 binds to p300 and triggers a conformational switch in p300

This is the first study to look into the p300-p53 complex structure using cryo-EM. Here the effector-induced allosteric activation of p300 upon p53 binding has been established through the structural studies. In a previous study, Thompson *et al.* proposed a model in which the lysine-rich loop residing in the HAT domain interacts with the electronegative patch present in the catalytic site, thereby hindering efficient substrate binding by acting as a pseudosubstrate (Thompson et al., 2004). It was proposed that upon *trans*-autoacetylation, the positive charges on the loop are neutralized, allowing its displacement from the active site, consequently leading to the activation of the enzyme (Karanam et al., 2006; Thompson et al., 2004). This model was revised by Delvecchio *et al*, who proposed that the additional effect of the domains flanking the catalytic domain play an important role in the regulation of p300 acetyltransferase activity. Their study revealed the inhibitory effect of a non-canonical RING domain on the activity of p300, which appears to occlude the HAT domain (Delvecchio et al., 2013). In congruence with the crystal structure of the core catalytic domain (bromodomain-PHD-RING-HAT), the cryo-EM structure of full-length p300 has revealed a 'closed' auto-inhibited conformation of p300. Interestingly, in the mechanism proposed, the RING domain displacement from the active site and trans-autoacetylation were necessary for the commencement of substrate acetylation. Again, consistent with this model, the cryo-EM structure of the p53-p300 complex demonstrates the presence of a switch in the conformation of p300 from an auto-inhibited 'closed' conformation to an accessible, 'open' conformation (Figure 4.9). This is the first study to visualize the conformational switching in the epigenetic enzyme p300. It is observed that upon binding to p53, there is a domain rearrangement leading to the displacement of the RING domain, this step precedes *trans*-autoacetylation. The 'open' conformation of p300 maybe more accessible to autoacetylation in *trans*. The reaction of intermolecular autoacetylation of p300 follows fourth order kinetics with respect to HAT domain concentrations and proceeds in a highly cooperative manner *in vitro* (Karanam et al., 2006). Since p300 is present in multiprotein complexes in cells, the interaction with different factors can modulate the enzymes in terms of both substrate-specificity as well as activity (Bedford et al., 2010; Dyson and Wright, 2016; Perissi et al., 1999). Therefore, the availability of an 'open' or 'closed' conformation of p300 could be dependent on the factors it associates with, which may alter the kinetics of p300 autoacetylation in the cellular context.

6.2.3. p53-induced autoacetylated p300 contribution in global gene regulation

p300 autoacetylation can control its catalytic activity, but the dynamics of p300 autoacetylation under physiological stimuli is not fully understood. p300 is recruited to gene promoters by several transcription factors where it can assemble transcription complexes to facilitate gene expression. The structural studies, previous and the current work have proved that p300 alone is catalytically "inactive". In addition to this, autoacetylation of p300 has been proposed to induce distinct structural changes which are critical for its activity. Black *et al.* have shown that the presence of p300 at the PIC exhibits an inhibitory effect of transcription *in vitro*. The acetylCoA-dependent catalytic switch in p300 activity, leads to the acetylation of chromatin and the dissociation from the PIC. Interestingly, the dissociation of p300 from the complex enhances the binding of TFIID to the transcription machinery assembly, culminating in increased transcriptional output. The release of p300 from the complex was attributed to the possible conformational switch in the p300 structure upon autoacetylation (Black et al., 2006). It is clear from this study that the autoacetylation of p300 is essential for maximal transcription to proceed. It is evident that the recruitment and dissociation of p300 from the basal transcriptional machinery is critical in this process. Since this study was established *in vitro*, many intriguing questions remain unanswered. For example, as concluded by the authors that p300 is recruited in its inactive form, it is not clear how the first event of autoacetylation may have occurred. It is plausible that there may be other steric effects of chromatin recruitment which may trigger the feed-forward loop of *trans*-autoacetylation. Moreover, there are several examples of factors modulating p300 autoacetylation, it is intriguing to fit these modulators into the proposed model. Additionally, the study does not give a complete understanding of the chromatin occupancy of p300 autoacetylation in response to stimuli (Mellert and McMahon, 2009). Subsequent studies have explored the contextual global enrichment of p300/CBP. Ceschin *et al.* have shown that CBP is methylated at multiple sites by the protein arginine methyltransferase, CARM1. The arginine methylation of CBP stimulated CBP activity through the induction of CBP autoacetyation. Interestingly, it was found that the CARM1-mediated methylation of CBP was required for estrogen-dependent recruitment to estrogen-regulated gene targets. The authors highlighted the contextual recruitment of methylated CBP upon a stimulus (estradiol treatment). Using polyclonal antibodies recognizing specific CBP methylation species, it was noted that each methylated class of CBP possessing differential HAT activity, form a distinct transcriptional niche, thereby diversifying the estrogen receptor response (Ceschin et al.,

2011). The contextual recruitment of p300 was noted in another study done in the MCF7 cell line, where it was observed that in a resting cell, p300 appeared to show a preference towards neural lineage gene promoters, whereas upon estradiol treatment the enrichment of p300 shifted towards estrogen-regulated gene targets (Wang and Li, 2016). In a recent report, CBP has been shown to interact with RNAs. At active enhancers, CBP interacts with enhancer RNAs, which bind to the CBP catalytic domain, inducing CBP autoacetylation. The resultant enhancement in CBP activity leads to increased histone acetylation and expression of target genes (Bose et al., 2017). In the present thesis work, the differential occupancy of p300 and autoacetylated p300 (acp300) was investigated upon p53 activation. The ChIP-seq analysis revealed that p300 binding patterns were in congruence with the previously reported trend for the coactivator; a high percentage of p300 recruitment was observed at putative enhancers upon p53 induction. Earlier studies have revealed that the homologous coactivators p300 and CBP are markers for active enhancers during developments and exhibit redundancy in their chromatin enrichment (Ramos et al., 2010). A strong correlation between p300 binding and H3K4me1 (an active enhancer mark) was observed at the distal genomic peaks, while only a weak p300 enrichment was observed at the TSS of genes (Figure 4.14A,B). Surprisingly, a contrary observation was made in the case of acp300. Upon autoacetylation in the presence of p53, p300 appears to show a strong preference for the TSS, which is in agreement with the recruitment model discussed earlier. The binding of acp300 associated strongly with RNA Pol II occupancy and the promoter acetylation mark H3K27ac (Figure 4.14A). Furthermore, a converse binding pattern was seen at the distal regions, which was reciprocal to the binding of p300 and H3K4me1 (Figure 4.14B). This suggests that acp300 is indeed involved in the assembly of the basal transcription machinery at the promoter proximal regions of genes (Figure 4.14A). Notably, the integration of the ChIPseq data with the gene expression microarray analysis revealed that the enrichment of acp300 was a better determinant of p53-mediated gene expression over the presence of p300 (Figure 4.14E). This result is in agreement with previous studies where p300 has been shown to occupy transcriptionally silent regions or the chromatin, whereas the co-occupancy of p300 with its histone acetylation mark H3K27ac is observed at transcriptionally active genes (Holmqvist and Mannervik, 2013). At p53 responsive genes, the acp300 peaks coincide with the H3K27ac peaks at the promoters, whereas the p53 non-responsive genes showed no such pattern, suggesting that the enrichment of acp300 is a marker of active transcription (Figure 4.15-4.16A,B). This was confirmed by the ChIP-qPCR results, where a strong induction in acp300 enrichment was

observed upon doxycycline treatment (p53 expression) at the CDKN1A (p21) promoter while the GAPDH promoter did not exhibit any difference in the recruitment of acp300 upon p53 activation (doxycycline treatment) (Figure 4.16C-F). Through the current study it can be speculated that the ability to induce structural alterations in p300, leading to enhancement of its acetyltransferase activity, may be a key deciding factor in p300 chromatin recruitment and downstream transcriptional programs. The chromatin IP data suggests that the phenomenon of factor-induced p300 autoacetylation may play a pivotal role in the integration of stimulus-driven transcriptional pathways, where the recruitment of the catalytically active form of p300 may trigger a quick transcriptional response to the internal and external signaling cues. In this study, it is the p53-driven pathway that stimulates a burst in autoacetylated p300 levels and alteration of the epigenetic landscape, which may be essential for the p53 signaling pathways. The dynamics of p300 autoacetylation in stimulus-driven gene expression is still not well understood. It may be proposed that upon a stimulus, such as stress, p53 recruits p300 to its target gene promoters. The interaction with p53 leads to a conformational switch in p300 from the inactive form to the open form, enhancing *trans*-autoacetylation of p300. The conformational switch in p300, however, leads to its expulsion from the PIC, an event which is proposed to be essential for transcription initiation (Black et al., 2006). Once the autoacetylated p300 is expelled from the PIC, the fate of the enzyme is largely unknown. It may be speculated that upon dissociation, p300 is deacetylated by SIRT2 (Black et al., 2008) to the inactive conformation, or the active p300 can now acetylate other substrates, or it may be degraded once the stress response is terminated (Figure 6.1).

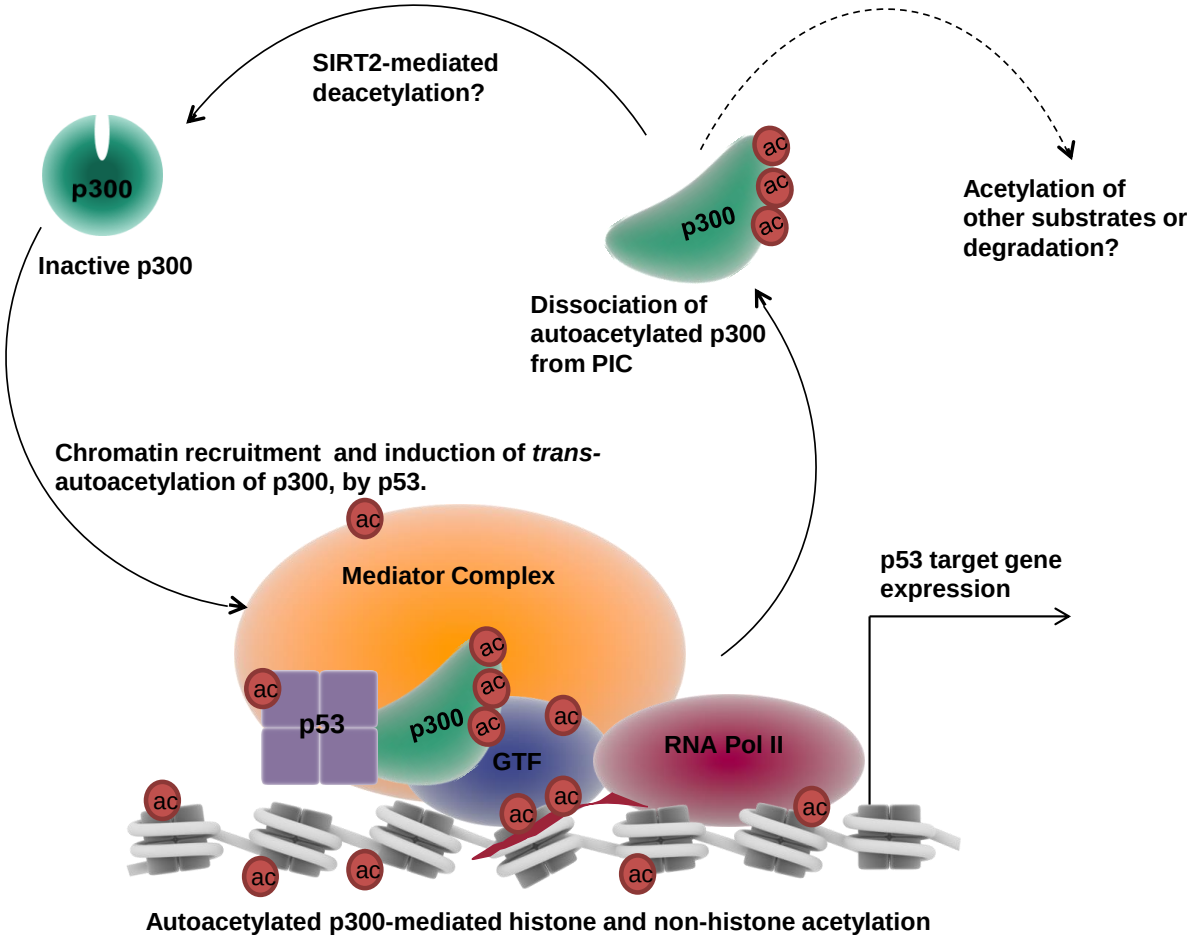

Figure 6.1: Dynamics of p300 autoacetylation in transcription. Inactive p300 interacts with p53 and is recruited to the chromatin. p300 facilitates the assembly of the basal transcription complex. P53-induced autoacetylation of p300 activated p300 to its maximum catalytic potential. Activated p300 then acetylates the associated transcription-related proteins (Mediator complex, general transcription factors (GTF) and RNA polymerase II (RNA Pol II)) and the promoter-proximal histones. Upon autoacetylation, the conformational alteration in p300 leads to its dissociation for the Pre-initiation complex (PIC). The dissociated autoacetylated p300 may either acetylate other targets, be deacetylated by SIRT2 leading to its conversion to the inactive form, or be degraded.

6.3. Role of mutant p53 in the induction of p300 autoacetylation

The inactivation of the p53 gene is observed in over 50% of cancers. Mutations occurring on the p53 gene, especially mapping to the DBD, often confer functions to the protein which it would otherwise not exhibit. Missense mutations of p53 not only abrogate the tumor suppressive functions of p53 but also contribute unique oncogenic functions which may contribute to tumor proliferation, invasion, and metastasis. These GOF mutants of p53 are speculated to be key players in tumorigenesis, but a universal molecular mode of action has been elusive. A previous study has implicated the hyperacetylation of histones and

autoacetylated p300 to disease progression. Mutant p53 has also been associated with altering the epigenetic landscape to form that is conducive to tumor progression. The earlier part of the work established p53 as a potent inducer for p300 autoacetylation. Since p53 itself appears to alter the distribution of autoacetylated p300 over p300 leading to p53-response gene expression, it was intriguing to find out whether the GOF mutants can adopt the ability of enhancement of p300 catalytic activity and autoacetylation and utilize this phenomenon to promote tumorigenesis through the deregulation of this important epigenetic enzyme.

6.3.1. Gain-of-Function mutants of p53 are potent inducers of p300 autoacetylation

Fascinatingly, the Gain-of-function mutants of p53 retained the ability to induce p300 autoacetylation. The cell-based screening of p53 mutants revealed a few interesting observations: (i) All the DNA contact mutants tested in this assay were positive regulators of p300 autoacetylation. This may be expected since the overall structure of the p53 mutant does not alter drastically from the wildtype p53. In the previous result section, the mechanistic details of p53-mediated enhancement of p300 autoacetylation revealed the importance of the interaction between p53 and p300 in the modulation of p300 structure and activity. It may be assumed that in the DNA contact mutants, these specific interactions between p300 and p53 are not perturbed, thereby allowing these GOF mutants to effectively enhance p300 autoacetylation. (ii) In contrast to the DNA contact mutants, the conformational mutants exhibit a characteristic distortion in the native p53 structure. Therefore, it was interesting to observe that a few of these mutants also retained the ability to induce p300 autoacetylation. Since p53 interacts with p300 through its bipartite TAD which is intrinsically disordered, the mutants which exhibit local distortion, such as, R249S, may still retain the required structural features important of this interaction. (iii) The global conformational mutant, R175H, failed to induce p300 autoacetylation in cells but was effective in the *in vitro* autoacetylation assay. The exact reason for this observation is unknown, yet it may be speculated that in a confined system such as the *in vitro* reaction, the R175H mutant may interact with p300, may be non-specifically though its severely disordered structure, but in the cellular context, the two proteins may not be able to make sufficient contact to induce the autoacetylation of p300.

6.3.2. p300 is essential for mutant p53-driven tumorigenesis

Several p53 missense mutants possess the ability to induce p300 autoacetylation. The R273H mutant could also alter global acetylation levels, presumably by the catalytic activation of p300 through the induction of autoacetylation. If the p53 mutant can indeed alter the epigenetic landscape through the modulation of p300, then the disruption of p300-mutant p53 interaction may serve as a novel target in cancer therapeutics. Using peptides that disrupt the interaction between p53 and p300, p300 autoacetylation can be regulated in cells. It was observed that the interaction of R273H p53 and p300 was important for the tumorigenic functions of this mutant. These results are indicative of the importance of p300/autoacetylated p300 in the mutant p53-driven cancers (Figure 6.2). It may prove to be a useful therapeutic approach in anti-cancer drug development.

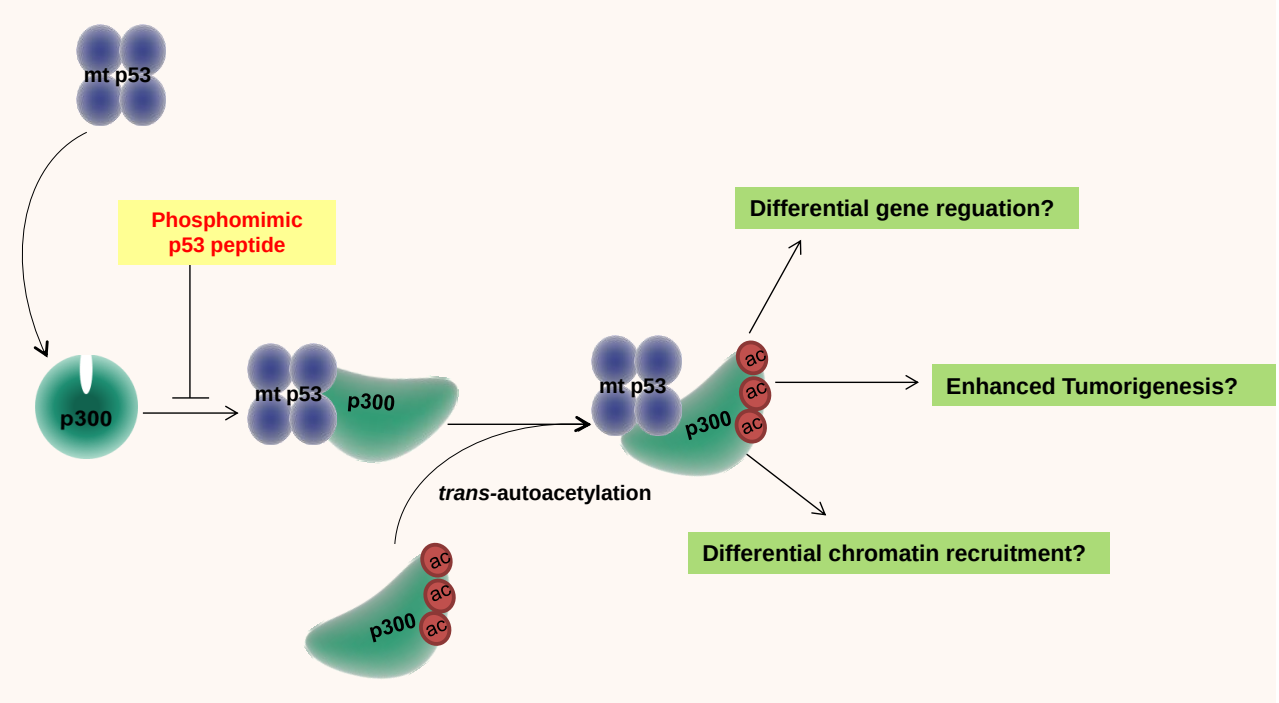

Figure 6.2: Importance of p300 autoacetylation in mutant p53-driven cancers. Induction of p300 autoacetylation by GOF mutant p53 may lead to several consequences, such as differential chromatin recruitment and differential gene expression which may culminate in enhanced tumorigenesis. Interaction between p300 and mutant p53 can be a potential therapeutic target in p300-dependent mutant p53-driven cancers.

Future Perspectives of this Study

The differential regulation of factor-induced p300 autoacetylation in response to different signaling pathways is yet to be deciphered. There are many questions still unanswered, for example, do these factors induce autoacetylation at distinct lysine residues on the autoinhibitory loop? Does differential factor-induced autoacetylation of p300 dictate its interactome? Does differentially autoacetylated p300 have distinct acetylomes? Does contextually regulated autoacetylated p300 have distinct histone acetylation signatures? These aspects of p300 autoacetylation are yet to be explored, but by expanding the current understanding of the mechanisms of factor-induced enhancement of p300 autoacetylation, the modes of regulation and deregulation of this master epigenetic enzyme can be further elucidated.

The mechanisms of p300 autoacetylation regulation may be conserved in CBP as well. It would also be intriguing to investigate the differences in the regulation of p300 and CBP autoacetylation, and whether there are any environmental cues or context under which their autoacetylation and activity is differentially modulated. It is also known that p300 and CBP differ significantly during development and differentiation. They also possess distinct substrate specificities *in vivo*. Therefore, the probability of discovering an inducer of autoacetylation which is exclusive to either p300 or CBP is quite likely.

Furthermore, studying the altered histone acetylation marks and their cross-talk with histone and non-histone post translational modifications, under diseased conditions like cancers, would give an insight into the complex and possibly predictive “epigenetic language”. This would provide a better understanding of the underlying epigenetic events involved in the manifestation of the disease. A better understanding of the regulation of p300, an important epigenetic enzyme, can also aid in the development of epigenetic therapeutics targeting specific modules of p300 function, such as interfering molecules which can disrupt the interaction between p300 and autoacetylation inducers or small molecule enhancing p300 autoacetylation and activity.

Chapter 7

Summary

In this chapter the major findings of the present study will be summarized.

The present thesis work has focused on the regulation and deregulation of p300 autoacetylation. The aim of the work was to elucidate the molecular mechanisms of factor-induced enhancement of p300 autoacetylation by considering a known factor, the histone chaperone NPM1 and a newly discovered factor, p53, the guardian of the genome. NPM1-mediated induction of autoacetylation is specific to p300 and it is evident that the oligomerization and chaperone activity of NPM1 is critical for the enhancement of *trans*-autoacetylation. The inherent chaperone activity of NPM1 appears to stabilize the intrinsically disordered regions of p300, while it may be speculated that the oligomerization of NPM1 is critical for triggering the cooperative, feed-forward loop of intermolecular p300 autoacetylation, by interacting with two or more molecules of p300. Drawing parallels to these results, similar observations were made in the case of the tumor-suppressor, p53. p53 too, is a specific inducer of p300 autoacetylation. Moreover, p53 can induce structural alterations in p300 which is essential for the induction of *trans*-autoacetylation. Similar to NPM1, p53 is also active as a multimer, which again appears to be critical for the induction of p300 autoacetylation. Tetramerization-defective mutants of p53 lose their ability to enhance p300 autoacetylation. To understand the implications of p53-mediated induction of p300 autoacetylation at the genomic scale, ChIP-seq analysis of acp300 and p300 was done, upon p53 activation. The ChIP-seq analysis of autoacetylated p300 upon p53 activation revealed that the autoacetylated form of p300 is distinctly found at active promoters. Furthermore, the induction of acp300 upon p53 induction indicates that the dynamics of autoacetylation and deacetylation of p300 may play a pivotal role in the stimulation of signal-mediated gene expression pathways. Under different physiological conditions, the contextual regulation of p300 autoacetylation is quite apparent, but to appreciate the role of deregulated hyper-activated, autoacetylated p300, the context of oral cancer was investigated further. The connection between hyperacetylation and p300 autoacetylation has been previously established (Arif et al., 2010b), in this backdrop, the various factors that may influence or deregulate p300 autoacetylation were investigated. A positive correlation between NPM1 expression and autoacetylated p300 was found in the oral cancer tumor tissue samples.

Moreover, GOF mutants of p53, which have a high incidence in oral cancer, also appeared to modulate the levels of p300 autoacetylation. Through a screen of these p53 mutants, it was found that most GOF p53 mutants retained the ability to induce the autoacetylation of p300. Furthermore, the direct interaction between p300 and mutant p53 was also observed to be critical for the tumorigenic potential of these GOF mutants. Overall, through this work, the mechanisms and implications of factor-induced enhancement of p300 autoacetylation has been established.

Overall Significance of the study

I. A correlation between overexpressed NPM1 and the hyperactive, autoacetylated form of p300 in the oral cancer patient samples has been established through this study. The study has demonstrated that NPM1 is a specific inducer of p300 autoacetylation and can enhance p300 catalytic activity.

   Experimental evidences prove that NPM1 is a novel molecular chaperone of p300. It has been observed that NPM1 can rescue the activity of thermal denatured p300 and can refold the intrinsically disordered structure of p300, shown by the intrinsic fluorescence experiments. Moreover, the functional oligomeric form of NPM1 is essential for the induction of p300 autoacetylation.

II. This study has established the unique function of the tumor suppressor protein, p53 as a new inducer of p300 autoacetylation and activity. p53 can enhance p300 autoacetylation and p300-mediated histone acetylation in cells. The direct interaction between p53 and p300 is required for the enhancement of p300 autoacetylation and catalytic activity. This is the first study to examine the structure of the p300-p53 complex through Cryo-Electron Microscopy. An effector-induced allosteric activation of p300 upon p53 binding was observed. It is therefore, the first study to visualize the “active” conformation of p300. It is also the first study to investigate the global chromatin occupancy and the global functional consequences of autoacetylated p300 through ChIP-seq analysis. This study suggests the importance of autoacetylated p300 in an inducible gene expression program.

III. The study establishes the function of p53 GOF mutants as enhancers of p300 autoacetylation, through which they directly modulate the activity of this epigenetic enzyme. The GOF mutants-mediated enhancement of p300 autoacetylation and activity maybe a novel pathway through which they exert their tumorigenic potential.

Disruption of p300-mutant p53 function maybe a novel target for therapeutic intervention.

In summary, through this study the mechanisms and physiological importance of factor-mediated modulation of p300 autoacetylation and the global effect on the epigenetic landscape and transcriptional programs under various cellular contexts has been established.

Appendix I: OSCC Patient Samples Details

	Patient ID	Site of Tumor	Histological Features	Stage (TNM)
1	5642	Left lower gingiva buccal sulcus	Well differentiated squamous	T2N1Mx
2	6651	Left Buccal Mucosa	Well differentiated squamous	T2N1Mx
3	16983	Carcinoma left GBS	Well differentiated squamous	T2N1Mx
4	62265	Right Buccal Mucosa	Moderately differentiated	T4aN2Mx
5	77147	Right Buccal Mucosa	Section studies from lymph node	T2N1Mx
6	89014	Left Buccal Mucosa	Well differentiated squamous	T1N0Mx
7	100925	Left Buccal Mucosa	Well differentiated squamous	T1N0Mx
8	102262	Left Buccal Mucosa	Well differentiated squamous	T1N0Mx
9	208989	Right Buccal Mucosa	Well differentiated squamous	
10	242458	Left lower alveolus	Well differentiated squamous	T4aN0Mx
11	247143	Left Buccal Mucosa	Verrucous carcinoma left buccal lesion	T3N1Mx
12	251012	Left Buccal Mucosa	Moderately differentiated Squamous	pT1N1Mx
13	251027	Left Buccal Mucosa	Well differentiated squamous	pT1N1Mx
14	262411	Left Buccal Mucosa Biopsy	Squamous cell carcinoma	T3N0Mx
15	263289	Left Alveolus	Squamous cell carcinoma	
16	268662	Left Buccal Mucosa	Well differentiated squamous	TwN0Mx
17	295366	Left Buccal Mucosa	Moderately differentiated	T4aN1Mx
18	908855	Left buccal mucosa	Well differentiated squamous	T2N0Mx
19	917486	Left buccal mucosa	Well to Moderately differentiated	T1N0Mx
20	920669	Right Buccal mucosa	Moderately differentiated	T1N2bMx
21	922107	Left Buccal mucosa	Well differentiated squamous	T2N0Mx
22	924178	Carcinoma Floor of Mouth	Well differentiated squamous	T3N1Mx
23	930713	Carcinoma Floor of Mouth	Well differentiated squamous	
24	955865	Left retromolar trigon	Well differentiated keratinizing	T4aN2bMx
25	957783	Left Buccal Mucosa	Well differentiated keratinizing	T2N2aMx
26	957786	Left buccal mucosa +retromolar trigon	Moderately differentiated	T4aN2aMx
27	961721	Right Buccal mucosa	Well differentiated squamous	T4aN2bMx
28	962579	Right Gingiva Buccal Sulcus	Well differentiated squamous	T2N2bMx
29	1003917	Left gingiva buccal sulcus	Well differentiated squamous	T4aN0Mx
30	1004604	Malignancy left lower GBS	Well differentiated squamous	T4N2bMx
31	1015497	Left buccal mucosa	Well differentiated squamous	T2N2bMx
32	1018358	Left buccal mucosa	Moderately differentiated	pT3N1M0

Appendix II: List of Abbreviations and Acronyms

AF9 ALL1-Fused gene from chromosome 9 protein

AIL Auto-inhibitory Loop

AML Acute Myeloid Leukemia

APC Anaphase Promoting Complex

AR Androgen Receptor

ARF Alternative Reading Frame

ATM Ataxia Telangiectasia Mutated

ATR Ataxia telangiectasia and Rad3 related

BrD Bromodomain

cAMP Cyclic Adenosine Monophosphate

CARM1 Coactivator-Associated Arginine Methyltransferase 1

CD Circular Dichroism

CDK1 Cyclin-Dependent Kinase 1

cDNA complementary DNA

CH1/2/3 Cysteine-Histidine rich domain 1/2/3

ChIP Chromatin Immunoprecipitation

CI Confidence Interval

CID CBP/p300 interacting domain

CRD1 Cell Cycle Regulatory domain 1

CREB cAMP Response Element Binding Protein

CREBBP/CBP CREB binding protein

CSP Carbon Nanosphere

CTCL Cutaneous T Cell Lymphoma

CTPB N-(4-chloro-3-trifluoromethyl-phenyl)-2-ethoxy-6-pentadecyl-benzamide

DAB 3,3′-Diaminobenzidine

DBD DNA-Binding Domain

DDX24 DEAD-Box Helicase 24

DLS Dynamic Light Scattering

DMSO Dimethyl Sulfoxide

DNA Deoxyribonucleic acid

DNMT DNA methyltransferase

DSB Double stand break

E1A Early Region 1A

ERK1/2 Extracellular signal-regulated kinase 1/2

ERα Estrogen Receptor α

Esa1 Essential Sas2-related acetyltransferase 1

EtBr Ethidium bromide

FDA Food and Drug Administration USA

FDR False Discovery Rate

GAPDH Glyceraldehyde 3-phosphate dehydrogenase

Gcn5 General Control Non-derepressible 5

GNAT Gcn5-related N-acetylatransferase

GO Gene Ontology

GOF Gain of Function

GOI Gene Of Interest

GRIP Glutamate receptor-interacting protein

GTF General Transcription Factor

HAT Histone Acetyltransferase

HBO1 HAT bound to ORC

HCC Hepatocellular Carcinoma

Hda1 Histone deacetylase 1

HIF1α Hypoxia-inducible factor 1α

HIRA HIR(histone regulator) protein family

HMG High Mobility Goup

HNSCC Head and Neck Squamous Cell Carcinoma

HPV Human Papilloma Virus

HRP Horseradish peroxidase

IBiD Interferon-Binding Domain

IgG Immunoglobulin G

IHC Immunohistochemistry

IL Interleukin

IR Ionizing Radiation

KAT Lysine (K) Acetyltransferase

KATa Lysine Acetyltransferase Activator

KATi Lysine Acetyltransferase Inhibitor

KDAC Lysine Deacetylase

KEGG Kyoto Encyclopedia of Genes and Genomes

KIX Kinase-inducible domain Interacting Domain

KLH Keyhole Limpet Hemocyanin

LB Luria Broth

LFS Li-Fraumeni Syndrome

LOH Loss of Heterozygosity

LPS Lipopolysaccharides

MAML1 Mastermind-like protein 1

MAPK Mitogen-activated protein kinases

MATIIα Methionine adenosyltransferase Iiα

MDM2 Murine Double Minute 2

MDR1 Multi Drug Resistance

MLL Mixed-lineage Leukemia

M-MLV Moloney-Murine Leukemia Virus

MMP Matrix Metalloproteinase

MOF Males absent On First

MORF MOZ-related factor

MOZ Monocytic Leukaemia Zinc-finger protein

MSL Male-specific Lethal

MYBB1A MYB Binding Protein 1A

Myf5 Myogenic factor 5

MyoD Myogenic Differentiation 1

MYST MOZ, Ybf2, Sas2, TIP60

NAD Nicotinamide Adenine Dinucleotide

NAM Nicotinamide

NCBD Nuclear Coactivator Binding Domain

NDG Nearest Downstream Gene

NES Nucear Exit Signal

NFκB Nuclear factor κB

Ni-NTA Nickel-Nitrilotriacetic Acid

NLS Nuclear Localization Signal

NO Nitric Oxide

NO38 38kD Nucleolar Protein

NoLS Nucleolus Localization Signal

NOS Nitric Oxide Synthase

NPM1 Nucleophosmin

NRID Nuclear Receptor Interaction Domain

NSCLC Non-Small Cell Lung Carcinoma

NSL Non-specific Lethal

ORC1 Origin Recognition Complex 1

OSCC Oral Squamous Cell Carcinoma

PAD4 Protein arginine deiminase 4

PC4 Positive Coactivator

PCAF p300/CBP-associated factor

PDB Protein Database

PHD Plant Homeodomain

PKA/C Protein Kinase A/C

PML Promyelocytic leukemia

PMSF Phenylmethanesulfonyl Fluoride

PRMT1 Protein Arginine Methyltransferase

PTCL Peripheral T-Cell Lymphoma

PTM Post Translational Modification

PVDF Polyvinylidene Fluoride

RelA Rel-like domain-containing proteins

RIN RNA integrity number

RING Really Interesting New Gene

RITA Reactivation of p53 and Induction of Tumor cell Apoptosis

RNA Ribonucleic Acid

ROS Reactive Oxygen Species

rRNA Ribosomal Ribonucleic Acid

RTS Rubinstein Taybi Syndrome

Rtt109 Regulator of Ty1 transposition protein 109

RUNX1 Runt-related transcription factor 1

SAHA Suberoylanilide Hydroxamic Acid

Sas Something about silencing

SDS Sodium Dodecyl Sulfate

SDS-PAGE Sodium Dodecyl Sulfate Polyacrylamide Gel Electrophoresis

SIK2 Salt-inducible Kinase 2

SILAC Stable-Isotope Labeling by Amino acid in Cell culture

Sir2 Silent Information Regulator 2

SIRT1 Sirtuin 1

SKP2 S-phase Kinase-associated Protein 2

STAT3 Signal Transducer and Activator of Transcription 3

SUMO Small Ubiquitin-like Modifier

SV40 Simian Vacuolating Virus 40

TAD Transactivation Domain

TAF TBP-associated factors

TBP TATA-box Binding Protein

TEMED N,N,N',N'-tetramethylethylenediamine

Tip60 HIV1 Tat interacting protein

TSS Transcription Start Site

UBD Ubiquitin-Binding Domain

VEGF Vascular endothelial growth factor

WTX Wilms tumor gene on X chromosome

YEATS YNK7, ENL, AF-9, TFIIF small subunit

Publications

Kaypee S, Ghosh R, Sahadevan SA, Sengupta J, Roy S, Kundu TK. **p53-mediated Allosteric Activation of p300 Autoacetylation.** *(Communicated)*

Kaypee S, Sahadevan SA, Sudarshan D, Patil S, Senapati P, Dasgupta D, Kundu TK. **Oligomers of Human Histone Chaperone NPM1 alters p300/KAT3B Folding to Induce Autoacetylation.** *(Communicated)*

Kaypee S, Sahadevan SA, Patil S, Ghosh P, Roy S, Kundu TK. **The Role of p300 Autoacetylation in Mutant p53-driven Cancers.** *(Manuscript under preparation)*

Kaypee S, Sudarshan D, Shanmugam MK, Mukherjee D, Sethi G, Kundu TK. **Aberrant lysine acetylation in tumorigenesis: Implications in the development of therapeutics.** *Pharmacol Ther.* 2016 Jun;162:98-119. PMID: 26808162

Naiya G, **Kaypee S**, Kundu TK, Roy S. **A Constrained Helical Peptide Against S100A4 Inhibits Cell Motility in Tumor Cells.** *Chem Biol Drug Des.* 2015 Oct;86(4):945-50. PMID: 25763457

Kaypee S, Mandal S, Chatterjee S and Kundu TK. **Emerging Epigenetic Therapies: Lysine Acetyltransferase Inhibitors.** *Epigenetic Cancer Therapy (Book).* 2015. Academic Press.

Wu M, Kim SH, Datta I, Levin A, Dyson G, Li J, **Kaypee S**, Swamy MM, Gupta N, Kwon HJ, Menon M, Kundu TK, Reddy GP. **Hydrazinobenzoylcurcumin inhibits androgen receptor activity and growth of castration-resistant prostate cancer in mice.** *Oncotarget.* 2015 Mar 20;6(8):6136-50. PMID: 25704883

Vasudevarao MD*, Mizar P*, Kumari S*, Mandal S, Siddhanta S, Swamy MM, **Kaypee S**, Kodihalli RC, Banerjee A, Naryana C, Dasgupta D, Kundu TK. **Naphthoquinone-mediated inhibition of lysine acetyltransferase KAT3B/p300, basis for non-toxic inhibitor synthesis.** *J Biol Chem.* 2014 Mar 14;289(11):7702-17. PMID: 24469461

*authors contributed equally

Ray SS*, Halder S*, **Kaypee S**, Bhattacharyya D. **HD-RNAS: An Automated Hierarchical Database of RNA Structures.** *Front Genet.* 2012 Apr 18;3:59. PMID: 22529851

*authors contributed equally

Bibliography

Ait-Si-Ali, S., Polesskaya, A., Filleur, S., Ferreira, R., Duquet, A., Robin, P., Vervish, A., Trouche, D., Cabon, F., and Harel-Bellan, A. (2000). CBP/p300 histone acetyl-transferase activity is important for the G1/S transition. Oncogene *19*, 2430-2437.

Ait-Si-Ali, S., Ramirez, S., Barre, F.X., Dkhissi, F., Magnaghi-Jaulin, L., Girault, J.A., Robin, P., Knibiehler, M., Pritchard, L.L., Ducommun, B., *et al.* (1998). Histone acetyltransferase activity of CBP is controlled by cycle-dependent kinases and oncoprotein E1A. Nature *396*, 184-186.

Akimaru, H., Chen, Y., Dai, P., Hou, D.X., Nonaka, M., Smolik, S.M., Armstrong, S., Goodman, R.H., and Ishii, S. (1997a). Drosophila CBP is a co-activator of cubitus interruptus in hedgehog signalling. Nature *386*, 735-738.

Akimaru, H., Hou, D.X., and Ishii, S. (1997b). Drosophila CBP is required for dorsal-dependent twist gene expression. Nat Genet *17*, 211-214.

Albaugh, B.N., Arnold, K.M., Lee, S., and Denu, J.M. (2011). Autoacetylation of the histone acetyltransferase Rtt109. J Biol Chem *286*, 24694-24701.

Allfrey, V.G., Faulkner, R., and Mirsky, A.E. (1964). ACETYLATION AND METHYLATION OF HISTONES AND THEIR POSSIBLE ROLE IN THE REGULATION OF RNA SYNTHESIS. Proc Natl Acad Sci U S A *51*, 786-794.

Arany, Z., Sellers, W.R., Livingston, D.M., and Eckner, R. (1994). E1A-associated p300 and CREB-associated CBP belong to a conserved family of coactivators. Cell *77*, 799-800.

Arif, M., Senapati, P., Shandilya, J., and Kundu, T.K. (2010a). Protein lysine acetylation in cellular function and its role in cancer manifestation. Biochim Biophys Acta *1799*, 702-716.

Arif, M., Vedamurthy, B.M., Choudhari, R., Ostwal, Y.B., Mantelingu, K., Kodaganur, G.S., and Kundu, T.K. (2010b). Nitric oxide-mediated histone hyperacetylation in oral cancer: target for a water-soluble HAT inhibitor, CTK7A. Chem Biol *17*, 903-913.

Attardi, L.D., and Jacks, T. (1999). The role of p53 in tumour suppression: lessons from mouse models. Cell Mol Life Sci *55*, 48-63.

Bach, M., Grigat, S., Pawlik, B., Fork, C., Utermöhlen, O., Pal, S., Banczyk, D., Lazar, A., Schömig, E., and Gründemann, D. (2007). Fast set-up of doxycycline-inducible protein expression in human cell lines with a single plasmid based on Epstein-Barr virus replication and the simple tetracycline repressor. FEBS J *274*, 783-790.

Baker, S.J., Fearon, E.R., Nigro, J.M., Hamilton, S.R., Preisinger, A.C., Jessup, J.M., vanTuinen, P., Ledbetter, D.H., Barker, D.F., Nakamura, Y., *et al.* (1989). Chromosome 17 deletions and p53 gene mutations in colorectal carcinomas. Science *244*, 217-221.

Balasubramanyam, K., Swaminathan, V., Ranganathan, A., and Kundu, T.K. (2003). Small molecule modulators of histone acetyltransferase p300. J Biol Chem *278*, 19134-19140.

Bannister, A.J., and Kouzarides, T. (1995). CBP-induced stimulation of c-Fos activity is abrogated by E1A. Embo j *14*, 4758-4762.

Bannister, A.J., and Kouzarides, T. (1996). The CBP co-activator is a histone acetyltransferase. Nature *384*, 641-643.

Bannister, A.J., Oehler, T., Wilhelm, D., Angel, P., and Kouzarides, T. (1995). Stimulation of c-Jun activity by CBP: c-Jun residues Ser63/73 are required for CBP induced stimulation in vivo and CBP binding in vitro. Oncogene *11*, 2509-2514.

Barlev, N.A., Liu, L., Chehab, N.H., Mansfield, K., Harris, K.G., Halazonetis, T.D., and Berger, S.L. (2001). Acetylation of p53 activates transcription through recruitment of coactivators/histone acetyltransferases. Mol Cell *8*, 1243-1254.

Bartholdi, D., Roelfsema, J.H., Papadia, F., Breuning, M.H., Niedrist, D., Hennekam, R.C., Schinzel, A., and Peters, D.J. (2007). Genetic heterogeneity in Rubinstein-Taybi syndrome: delineation of the phenotype of the first patients carrying mutations in EP300. J Med Genet *44*, 327-333.

Bedford, D.C., Kasper, L.H., Fukuyama, T., and Brindle, P.K. (2010). Target gene context influences the transcriptional requirement for the KAT3 family of CBP and p300 histone acetyltransferases. Epigenetics *5*, 9-15.

Bedford, M.T., and Clarke, S.G. (2009). Protein arginine methylation in mammals: who, what, and why. Mol Cell *33*, 1-13.

Ben David, Y., Prideaux, V.R., Chow, V., Benchimol, S., and Bernstein, A. (1988). Inactivation of the p53 oncogene by internal deletion or retroviral integration in erythroleukemic cell lines induced by Friend leukemia virus. Oncogene *3*, 179-185.

Bernstein, B.E., Mikkelsen, T.S., Xie, X., Kamal, M., Huebert, D.J., Cuff, J., Fry, B., Meissner, A., Wernig, M., Plath, K., *et al.* (2006). A bivalent chromatin structure marks key developmental genes in embryonic stem cells. Cell *125*, 315-326.

Bieging, K.T., Mello, S.S., and Attardi, L.D. (2014). Unravelling mechanisms of p53-mediated tumour suppression. Nat Rev Cancer *14*, 359-370.

Black, J.C., Choi, J.E., Lombardo, S.R., and Carey, M. (2006). A mechanism for coordinating chromatin modification and preinitiation complex assembly. Mol Cell *23*, 809-818.

Black, J.C., Mosley, A., Kitada, T., Washburn, M., and Carey, M. (2008). The SIRT2 deacetylase regulates autoacetylation of p300. Mol Cell *32*, 449-455.

Blough, R.I., Petrij, F., Dauwerse, J.G., Milatovich-Cherry, A., Weiss, L., Saal, H.M., and Rubinstein, J.H. (2000). Variation in microdeletions of the cyclic AMP-responsive element-binding protein gene at chromosome band 16p13.3 in the Rubinstein-Taybi syndrome. Am J Med Genet *90*, 29-34.

Bordoli, L., Netsch, M., Lüthi, U., Lutz, W., and Eckner, R. (2001). Plant orthologs of p300/CBP: conservation of a core domain in metazoan p300/CBP acetyltransferase-related proteins. Nucleic Acids Res *29*, 589-597.

Borer, R.A., Lehner, C.F., Eppenberger, H.M., and Nigg, E.A. (1989). Major nucleolar proteins shuttle between nucleus and cytoplasm. Cell *56*, 379-390.

Bose, D.A., Donahue, G., Reinberg, D., Shiekhattar, R., Bonasio, R., and Berger, S.L. (2017). RNA Binding to CBP Stimulates Histone Acetylation and Transcription. Cell *168*, 135-149.e122.

Bricambert, J., Miranda, J., Benhamed, F., Girard, J., Postic, C., and Dentin, R. (2010). Salt-inducible kinase 2 links transcriptional coactivator p300 phosphorylation to the prevention of ChREBP-dependent hepatic steatosis in mice. J Clin Invest *120*, 4316-4331.

Brownell, J.E., and Allis, C.D. (1996). Special HATs for special occasions: linking histone acetylation to chromatin assembly and gene activation. Curr Opin Genet Dev *6*, 176-184.

Calnan, D.R., and Brunet, A. (2008). The FoxO code. Oncogene *27*, 2276-2288.

Capell, B.C., and Berger, S.L. (2013). Genome-wide epigenetics. The Journal of investigative dermatology *133*, e9.

Carty, M., Zamparo, L., Sahin, M., González, A., Pelossof, R., Elemento, O., and Leslie, C.S. (2017). An integrated model for detecting significant chromatin interactions from high-resolution Hi-C data. Nat Commun *8*, 15454.

Ceschin, D.G., Walia, M., Wenk, S.S., Duboé, C., Gaudon, C., Xiao, Y., Fauquier, L., Sankar, M., Vandel, L., and Gronemeyer, H. (2011). Methylation specifies distinct estrogen-induced binding site repertoires of CBP to chromatin. Genes Dev *25*, 1132-1146.

Chan, H.M., Krstic-Demonacos, M., Smith, L., Demonacos, C., and La Thangue, N.B. (2001). Acetylation control of the retinoblastoma tumour-suppressor protein. Nat Cell Biol *3*, 667-674.

Chan, H.M., and La Thangue, N.B. (2001). p300/CBP proteins: HATs for transcriptional bridges and scaffolds. J Cell Sci *114*, 2363-2373.

Chan, W.Y., Liu, Q.R., Borjigin, J., Busch, H., Rennert, O.M., Tease, L.A., and Chan, P.K. (1989). Characterization of the cDNA encoding human nucleophosmin and studies of its role in normal and abnormal growth. Biochemistry *28*, 1033-1039.

Chang, J.H., Lin, J.Y., Wu, M.H., and Yung, B.Y. (1998). Evidence for the ability of nucleophosmin/B23 to bind ATP. Biochem J *329 (Pt 3)*, 539-544.

Chatterjee, S., Mizar, P., Cassel, R., Neidl, R., Selvi, B.R., Mohankrishna, D.V., Vedamurthy, B.M., Schneider, A., Bousiges, O., Mathis, C., *et al.* (2013). A novel activator of CBP/p300 acetyltransferases promotes neurogenesis and extends memory duration in adult mice. J Neurosci *33*, 10698-10712.

Chatterjee, S., Senapati, P., and Kundu, T.K. (2012). Post-translational modifications of lysine in DNA-damage repair. Essays in biochemistry *52*, 93-111.

Chen, L.F., Mu, Y., and Greene, W.C. (2002). Acetylation of RelA at discrete sites regulates distinct nuclear functions of NF-kappaB. Embo j *21*, 6539-6548.

Chen, M.K., Cai, M.Y., Luo, R.Z., Tian, X., Liao, Q.M., Zhang, X.Y., and Han, J.D. (2015). Overexpression of p300 correlates with poor prognosis in patients with cutaneous squamous cell carcinoma. Br J Dermatol *172*, 111-119.

Chen, Y., Sprung, R., Tang, Y., Ball, H., Sangras, B., Kim, S.C., Falck, J.R., Peng, J., Gu, W., and Zhao, Y. (2007a). Lysine propionylation and butyrylation are novel post-translational modifications in histones. Mol Cell Proteomics *6*, 812-819.

Chen, Y.J., Wang, Y.N., and Chang, W.C. (2007b). ERK2-mediated C-terminal serine phosphorylation of p300 is vital to the regulation of epidermal growth factor-induced keratin 16 gene expression. J Biol Chem *282*, 27215-27228.

Chevillard-Briet, M., Trouche, D., and Vandel, L. (2002). Control of CBP co-activating activity by arginine methylation. EMBO J *21*, 5457-5466.

Choudhary, C., Kumar, C., Gnad, F., Nielsen, M.L., Rehman, M., Walther, T.C., Olsen, J.V., and Mann, M. (2009). Lysine acetylation targets protein complexes and co-regulates major cellular functions. Science *325*, 834-840.

Chrivia, J.C., Kwok, R.P., Lamb, N., Hagiwara, M., Montminy, M.R., and Goodman, R.H. (1993). Phosphorylated CREB binds specifically to the nuclear protein CBP. Nature *365*, 855-859.

Chène, P. (2003). Inhibiting the p53-MDM2 interaction: an important target for cancer therapy. Nat Rev Cancer *3*, 102-109.

Colombo, E., Alcalay, M., and Pelicci, P.G. (2011). Nucleophosmin and its complex network: a possible therapeutic target in hematological diseases. Oncogene *30*, 2595-2609.

Costanzo, A., Merlo, P., Pediconi, N., Fulco, M., Sartorelli, V., Cole, P.A., Fontemaggi, G., Fanciulli, M., Schiltz, L., Blandino, G., *et al.* (2002). DNA damage-dependent acetylation of p73 dictates the selective activation of apoptotic target genes. Mol Cell *9*, 175-186.

Creaven, M., Hans, F., Mutskov, V., Col, E., Caron, C., Dimitrov, S., and Khochbin, S. (1999). Control of the histone-acetyltransferase activity of Tip60 by the HIV-1 transactivator protein, Tat. Biochemistry *38*, 8826-8830.

Dai, P., Akimaru, H., Tanaka, Y., Hou, D.X., Yasukawa, T., Kanei-Ishii, C., Takahashi, T., and Ishii, S. (1996). CBP as a transcriptional coactivator of c-Myb. Genes Dev *10*, 528-540.

Dancy, B.M., and Cole, P.A. (2015). Protein lysine acetylation by p300/CBP. Chem Rev *115*, 2419-2452.

de Wit, E., and de Laat, W. (2012). A decade of 3C technologies: insights into nuclear organization. Genes Dev *26*, 11-24.

Debes, J.D., Sebo, T.J., Lohse, C.M., Murphy, L.M., Haugen, D.A., and Tindall, D.J. (2003). p300 in prostate cancer proliferation and progression. Cancer research *63*, 7638-7640.

DeLeo, A.B., Jay, G., Appella, E., Dubois, G.C., Law, L.W., and Old, L.J. (1979). Detection of a transformation-related antigen in chemically induced sarcomas and other transformed cells of the mouse. Proc Natl Acad Sci U S A *76*, 2420-2424.

Delvecchio, M., Gaucher, J., Aguilar-Gurrieri, C., Ortega, E., and Panne, D. (2013). Structure of the p300 catalytic core and implications for chromatin targeting and HAT regulation. Nat Struct Mol Biol *20*, 1040-1046.

Demarest, S.J., Martinez-Yamout, M., Chung, J., Chen, H., Xu, W., Dyson, H.J., Evans, R.M., and Wright, P.E. (2002). Mutual synergistic folding in recruitment of CBP/p300 by p160 nuclear receptor coactivators. Nature *415*, 549-553.

Deng, Q., Li, Y., Tedesco, D., Liao, R., Fuhrmann, G., and Sun, P. (2005). The ability of E1A to rescue ras-induced premature senescence and confer transformation relies on inactivation of both p300/CBP and Rb family proteins. Cancer research *65*, 8298-8307.

Deng, W.G., and Wu, K.K. (2003). Regulation of inducible nitric oxide synthase expression by p300 and p50 acetylation. Journal of immunology *171*, 6581-6588.

Devaiah, B.N., Case-Borden, C., Gegonne, A., Hsu, C.H., Chen, Q., Meerzaman, D., Dey, A., Ozato, K., and Singer, D.S. (2016). BRD4 is a histone acetyltransferase that evicts nucleosomes from chromatin. Nat Struct Mol Biol *23*, 540-548.

Diab, A., Zickl, L., Abdel-Wahab, O., Jhanwar, S., Gulam, M.A., Panageas, K.S., Patel, J.P., Jurcic, J., Maslak, P., Paietta, E., *et al.* (2013). Acute myeloid leukemia with translocation t(8;16) presents with features which mimic acute promyelocytic leukemia and is associated with poor prognosis. Leukemia research *37*, 32-36.

Donehower, L.A., Harvey, M., Slagle, B.L., McArthur, M.J., Montgomery, C.A., Butel, J.S., and Bradley, A. (1992). Mice deficient for p53 are developmentally normal but susceptible to spontaneous tumours. Nature *356*, 215-221.

Dulac, C. (2010). Brain function and chromatin plasticity. Nature *465*, 728-735.

Dumbar, T.S., Gentry, G.A., and Olson, M.O. (1989). Interaction of nucleolar phosphoprotein B23 with nucleic acids. Biochemistry *28*, 9495-9501.

Dutnall, R.N., Tafrov, S.T., Sternglanz, R., and Ramakrishnan, V. (1998). Structure of the histone acetyltransferase Hat1: a paradigm for the GCN5-related N-acetyltransferase superfamily. Cell *94*, 427-438.

Dutta, S., Akey, I.V., Dingwall, C., Hartman, K.L., Laue, T., Nolte, R.T., Head, J.F., and Akey, C.W. (2001). The crystal structure of nucleoplasmin-core: implications for histone binding and nucleosome assembly. Mol Cell *8*, 841-853.

Dyson, H.J., and Wright, P.E. (2016). Role of Intrinsic Protein Disorder in the Function and Interactions of the Transcriptional Coactivators CREB-binding Protein (CBP) and p300. J Biol Chem *291*, 6714-6722.

Eckner, R., Ewen, M.E., Newsome, D., Gerdes, M., DeCaprio, J.A., Lawrence, J.B., and Livingston, D.M. (1994). Molecular cloning and functional analysis of the adenovirus E1A-associated 300-kD protein (p300) reveals a protein with properties of a transcriptional adaptor. Genes Dev *8*, 869-884.

Espinosa, J.M., and Emerson, B.M. (2001). Transcriptional regulation by p53 through intrinsic DNA/chromatin binding and site-directed cofactor recruitment. Mol Cell *8*, 57-69.

Feuerstein, N., Chan, P.K., and Mond, J.J. (1988). Identification of numatrin, the nuclear matrix protein associated with induction of mitogenesis, as the nucleolar protein B23. Implication for the role of the nucleolus in early transduction of mitogenic signals. J Biol Chem *263*, 10608-10612.

Filippakopoulos, P., Picaud, S., Mangos, M., Keates, T., Lambert, J.P., Barsyte-Lovejoy, D., Felletar, I., Volkmer, R., Müller, S., Pawson, T., *et al.* (2012). Histone recognition and large-scale structural analysis of the human bromodomain family. Cell *149*, 214-231.

Frank, J., Radermacher, M., Penczek, P., Zhu, J., Li, Y., Ladjadj, M., and Leith, A. (1996). SPIDER and WEB: processing and visualization of images in 3D electron microscopy and related fields. J Struct Biol *116*, 190-199.

Freed-Pastor, W.A., and Prives, C. (2012). Mutant p53: one name, many proteins. Genes Dev *26*, 1268-1286.

Fu, M., Rao, M., Wang, C., Sakamaki, T., Wang, J., Di Vizio, D., Zhang, X., Albanese, C., Balk, S., Chang, C., *et al.* (2003). Acetylation of androgen receptor enhances coactivator binding and promotes prostate cancer cell growth. Molecular and cellular biology *23*, 8563-8575.

Fu, M., Wang, C., Reutens, A.T., Wang, J., Angeletti, R.H., Siconolfi-Baez, L., Ogryzko, V., Avantaggiati, M.L., and Pestell, R.G. (2000). p300 and p300/cAMP-response element-binding protein-associated factor acetylate the androgen receptor at sites governing hormone-dependent transactivation. The Journal of biological chemistry *275*, 20853-20860.

Garcia-Jimenez, C., Garcia-Martinez, J.M., Chocarro-Calvo, A., and De la Vieja, A. (2014). A new link between diabetes and cancer: enhanced WNT/beta-catenin signaling by high glucose. Journal of molecular endocrinology *52*, R51-66.

Garcia-Wilson, E., and Perkins, N.D. (2005). p21WAF1/CIP1 regulates the p300 sumoylation motif CRD1 through a C-terminal domain independently of cyclin/CDK binding. Cell Cycle *4*, 1113-1119.

Geng, H., Liu, Q., Xue, C., David, L.L., Beer, T.M., Thomas, G.V., Dai, M.S., and Qian, D.Z. (2012). HIF1alpha protein stability is increased by acetylation at lysine 709. J Biol Chem *287*, 35496-35505.

George, P., Bali, P., Annavarapu, S., Scuto, A., Fiskus, W., Guo, F., Sigua, C., Sondarva, G., Moscinski, L., Atadja, P., *et al.* (2005). Combination of the histone deacetylase inhibitor LBH589 and the hsp90 inhibitor 17-AAG is highly active against human CML-BC cells and AML cells with activating mutation of FLT-3. Blood *105*, 1768-1776.

Ghizzoni, M., Boltjes, A., Graaf, C., Haisma, H.J., and Dekker, F.J. (2010). Improved inhibition of the histone acetyltransferase PCAF by an anacardic acid derivative. Bioorg Med Chem *18*, 5826-5834.

Giles, R.H., Dauwerse, H.G., van Ommen, G.J., and Breuning, M.H. (1998). Do human chromosomal bands 16p13 and 22q11-13 share ancestral origins? Am J Hum Genet *63*, 1240-1242.

Girdwood, D., Bumpass, D., Vaughan, O.A., Thain, A., Anderson, L.A., Snowden, A.W., Garcia-Wilson, E., Perkins, N.D., and Hay, R.T. (2003). P300 transcriptional repression is mediated by SUMO modification. Mol Cell *11*, 1043-1054.

Goldberg, A.D., Allis, C.D., and Bernstein, E. (2007). Epigenetics: a landscape takes shape. Cell *128*, 635-638.

Grisendi, S., Bernardi, R., Rossi, M., Cheng, K., Khandker, L., Manova, K., and Pandolfi, P.P. (2005). Role of nucleophosmin in embryonic development and tumorigenesis. Nature *437*, 147-153.

Grisendi, S., Mecucci, C., Falini, B., and Pandolfi, P.P. (2006). Nucleophosmin and cancer. Nat Rev Cancer *6*, 493-505.

Grummitt, C.G., Townsley, F.M., Johnson, C.M., Warren, A.J., and Bycroft, M. (2008). Structural consequences of nucleophosmin mutations in acute myeloid leukemia. J Biol Chem *283*, 23326-23332.

Grönroos, E., Hellman, U., Heldin, C.H., and Ericsson, J. (2002). Control of Smad7 stability by competition between acetylation and ubiquitination. Mol Cell *10*, 483-493.

Gu, W., and Roeder, R.G. (1997). Activation of p53 sequence-specific DNA binding by acetylation of the p53 C-terminal domain. Cell *90*, 595-606.

Guha, M., Srinivasan, S., Guja, K., Mejia, E., Garcia-Diaz, M., Johnson, F.B., Ruthel, G., Kaufman, B.A., Rappaport, E.F., Glineburg, M.R., *et al.* (2016). HnRNPA2 is a novel histone acetyltransferase that mediates mitochondrial stress-induced nuclear gene expression. Cell Discov *2*, 16045.

Haaland, I., Opsahl, J.A., Berven, F.S., Reikvam, H., Fredly, H.K., Haugse, R., Thiede, B., McCormack, E., Lain, S., Bruserud, O., *et al.* (2014). Molecular mechanisms of nutlin-3 involve acetylation of p53, histones and heat shock proteins in acute myeloid leukemia. Mol Cancer *13*, 116.

Hansson, M.L., Popko-Scibor, A.E., Saint Just Ribeiro, M., Dancy, B.M., Lindberg, M.J., Cole, P.A., and Wallberg, A.E. (2009). The transcriptional coactivator MAML1 regulates p300 autoacetylation and HAT activity. Nucleic Acids Res *37*, 2996-3006.

Hara, M.R., Agrawal, N., Kim, S.F., Cascio, M.B., Fujimuro, M., Ozeki, Y., Takahashi, M., Cheah, J.H., Tankou, S.K., Hester, L.D., *et al.* (2005). S-nitrosylated GAPDH initiates apoptotic cell death by nuclear translocation following Siah1 binding. Nat Cell Biol *7*, 665-674.

Hara, M.R., Cascio, M.B., and Sawa, A. (2006). GAPDH as a sensor of NO stress. Biochim Biophys Acta *1762*, 502-509.

Hara, M.R., and Snyder, S.H. (2006). Nitric oxide-GAPDH-Siah: a novel cell death cascade. Cell Mol Neurobiol *26*, 527-538.

Hecht, A., Vleminckx, K., Stemmler, M.P., van Roy, F., and Kemler, R. (2000). The p300/CBP acetyltransferases function as transcriptional coactivators of beta-catenin in vertebrates. The EMBO journal *19*, 1839-1850.

Hingorani, K., Szebeni, A., and Olson, M.O. (2000). Mapping the functional domains of nucleolar protein B23. J Biol Chem *275*, 24451-24457.

Hisaoka, M., Nagata, K., and Okuwaki, M. (2014). Intrinsically disordered regions of nucleophosmin/B23 regulate its RNA binding activity through their inter- and intra-molecular association. Nucleic Acids Res *42*, 1180-1195.

Holmqvist, P.H., and Mannervik, M. (2013). Genomic occupancy of the transcriptional co-activators p300 and CBP. Transcription *4*, 18-23.

Hornbeck, P.V., Kornhauser, J.M., Tkachev, S., Zhang, B., Skrzypek, E., Murray, B., Latham, V., and Sullivan, M. (2012). PhosphoSitePlus: a comprehensive resource for investigating the structure and function of experimentally determined post-translational modifications in man and mouse. Nucleic acids research *40*, D261-270.

Hou, X., Li, Y., Luo, R.Z., Fu, J.H., He, J.H., Zhang, L.J., and Yang, H.X. (2012). High expression of the transcriptional co-activator p300 predicts poor survival in resectable non-small cell lung cancers. European journal of surgical oncology : the journal of the European Society of Surgical Oncology and the British Association of Surgical Oncology *38*, 523-530.

Hsu, D.S., Wang, H.J., Tai, S.K., Chou, C.H., Hsieh, C.H., Chiu, P.H., Chen, N.J., and Yang, M.H. (2014). Acetylation of snail modulates the cytokinome of cancer cells to enhance the recruitment of macrophages. Cancer Cell *26*, 534-548.

Huang, B., Yang, X.D., Zhou, M.M., Ozato, K., and Chen, L.F. (2009). Brd4 coactivates transcriptional activation of NF-kappaB via specific binding to acetylated RelA. Molecular and cellular biology *29*, 1375-1387.

Huang, W.C., and Chen, C.C. (2005). Akt phosphorylation of p300 at Ser-1834 is essential for its histone acetyltransferase and transcriptional activity. Mol Cell Biol *25*, 6592-6602.

Ikenoue, T., Inoki, K., Zhao, B., and Guan, K.L. (2008). PTEN acetylation modulates its interaction with PDZ domain. Cancer Res *68*, 6908-6912.

Inoue, Y., Itoh, Y., Abe, K., Okamoto, T., Daitoku, H., Fukamizu, A., Onozaki, K., and Hayashi, H. (2007). Smad3 is acetylated by p300/CBP to regulate its transactivation activity. Oncogene *26*, 500-508.

Isharwal, S., Miller, M.C., Marlow, C., Makarov, D.V., Partin, A.W., and Veltri, R.W. (2008). p300 (histone acetyltransferase) biomarker predicts prostate cancer biochemical recurrence and correlates with changes in epithelia nuclear size and shape. Prostate *68*, 1097-1104.

Ishihama, K., Yamakawa, M., Semba, S., Takeda, H., Kawata, S., Kimura, S., and Kimura, W. (2007). Expression of HDAC1 and CBP/p300 in human colorectal carcinomas. J Clin Pathol *60*, 1205-1210.

Issaeva, N., Bozko, P., Enge, M., Protopopova, M., Verhoef, L.G., Masucci, M., Pramanik, A., and Selivanova, G. (2004). Small molecule RITA binds to p53, blocks p53-HDM-2 interaction and activates p53 function in tumors. Nat Med *10*, 1321-1328.

Itahana, Y., Ke, H., and Zhang, Y. (2009). p53 Oligomerization is essential for its C-terminal lysine acetylation. J Biol Chem *284*, 5158-5164.

Iyer, N.G., Ozdag, H., and Caldas, C. (2004). p300/CBP and cancer. Oncogene *23*, 4225-4231.

Jang, E.R., Choi, J.D., Jeong, G., and Lee, J.S. (2010). Phosphorylation of p300 by ATM controls the stability of NBS1. Biochem Biophys Res Commun *397*, 637-643.

Jang, E.R., Choi, J.D., and Lee, J.S. (2011). Acetyltransferase p300 regulates NBS1-mediated DNA damage response. FEBS Lett *585*, 47-52.

Jiang, L., Kon, N., Li, T., Wang, S.J., Su, T., Hibshoosh, H., Baer, R., and Gu, W. (2015). Ferroptosis as a p53-mediated activity during tumour suppression. Nature *520*, 57-62.

Karanam, B., Jiang, L., Wang, L., Kelleher, N.L., and Cole, P.A. (2006). Kinetic and mass spectrometric analysis of p300 histone acetyltransferase domain autoacetylation. The Journal of biological chemistry *281*, 40292-40301.

Karmodiya, K., Anamika, K., Muley, V., Pradhan, S.J., Bhide, Y., and Galande, S. (2014). Camello, a novel family of Histone Acetyltransferases that acetylate histone H4 and is essential for zebrafish development. Sci Rep *4*, 6076.

Kaypee, S., Mandal, S., Chatterjee, S., and Kundu, T.K. (2015). Emerging Epigenetic Therapies: Lysine Acetyltransferase Inhibitors. Lysine Acetyltransferase Inhibitors. In Epigenetic Cancer Therapy, S. Gray, ed. (Academic Press).

Kaypee, S., Sudarshan, D., Shanmugam, M.K., Mukherjee, D., Sethi, G., and Kundu, T.K. (2016). Aberrant lysine acetylation in tumorigenesis: Implications in the development of therapeutics. Pharmacol Ther *162*, 98-119.

Kelly, T.J., Qin, S., Gottschling, D.E., and Parthun, M.R. (2000). Type B histone acetyltransferase Hat1p participates in telomeric silencing. Mol Cell Biol *20*, 7051-7058.

Kiernan, R., Bres, V., Ng, R.W., Coudart, M.P., El Messaoudi, S., Sardet, C., Jin, D.Y., Emiliani, S., and Benkirane, M. (2003). Post-activation turn-off of NF-kappa B-dependent transcription is regulated by acetylation of p65. The Journal of biological chemistry *278*, 2758-2766.

Kim, W.J., Rivera, M.N., Coffman, E.J., and Haber, D.A. (2012). The WTX tumor suppressor enhances p53 acetylation by CBP/p300. Mol Cell *45*, 587-597.

Kishimoto, M., Kohno, T., Okudela, K., Otsuka, A., Sasaki, H., Tanabe, C., Sakiyama, T., Hirama, C., Kitabayashi, I., Minna, J.D., *et al.* (2005). Mutations and deletions of the CBP gene in human lung cancer. Clin Cancer Res *11*, 512-519.

Kitagawa, M., Lee, S.H., and McCormick, F. (2008). Skp2 suppresses p53-dependent apoptosis by inhibiting p300. Mol Cell *29*, 217-231.

Kitayner, M., Rozenberg, H., Kessler, N., Rabinovich, D., Shaulov, L., Haran, T.E., and Shakked, Z. (2006). Structural basis of DNA recognition by p53 tetramers. Mol Cell *22*, 741-753.

Kouzarides, T. (2007). Chromatin modifications and their function. Cell *128*, 693-705.

Kraus, W.L., Manning, E.T., and Kadonaga, J.T. (1999). Biochemical analysis of distinct activation functions in p300 that enhance transcription initiation with chromatin templates. Mol Cell Biol *19*, 8123-8135.

Krivtsov, A.V., and Armstrong, S.A. (2007). MLL translocations, histone modifications and leukaemia stem-cell development. Nature reviews Cancer *7*, 823-833.

Krois, A.S., Ferreon, J.C., Martinez-Yamout, M.A., Dyson, H.J., and Wright, P.E. (2016). Recognition of the disordered p53 transactivation domain by the transcriptional adapter zinc finger domains of CREB-binding protein. Proc Natl Acad Sci U S A *113*, E1853-1862.

Kruse, J.P., and Gu, W. (2009). Modes of p53 regulation. Cell *137*, 609-622.

Kulashreshtha, M., Mehta, I.S., Kumar, P., and Rao, B.J. (2016). Chromosome territory relocation during DNA repair requires nuclear myosin 1 recruitment to chromatin mediated by ϒ-H2AX signaling. Nucleic Acids Res *44*, 8272-8291.

Kumar, B.R., Swaminathan, V., Banerjee, S., and Kundu, T.K. (2001). p300-mediated acetylation of human transcriptional coactivator PC4 is inhibited by phosphorylation. The Journal of biological chemistry *276*, 16804-16809.

Kumazawa, T., Nishimura, K., Kuroda, T., Ono, W., Yamaguchi, C., Katagiri, N., Tsuchiya, M., Masumoto, H., Nakajima, Y., Murayama, A., *et al.* (2011). Novel nucleolar pathway connecting intracellular energy status with p53 activation. J Biol Chem *286*, 20861-20869.

Kundu, T.K., Palhan, V.B., Wang, Z., An, W., Cole, P.A., and Roeder, R.G. (2000). Activator-dependent transcription from chromatin in vitro involving targeted histone acetylation by p300. Mol Cell *6*, 551-561.

Kung, A.L., Rebel, V.I., Bronson, R.T., Ch'ng, L.E., Sieff, C.A., Livingston, D.M., and Yao, T.P. (2000). Gene dose-dependent control of hematopoiesis and hematologic tumor suppression by CBP. Genes Dev *14*, 272-277.

Lambert, P.F., Kashanchi, F., Radonovich, M.F., Shiekhattar, R., and Brady, J.N. (1998). Phosphorylation of p53 serine 15 increases interaction with CBP. J Biol Chem *273*, 33048-33053.

Lane, D.P. (1992). Cancer. p53, guardian of the genome. Nature *358*, 15-16.

Lane, D.P., and Crawford, L.V. (1979). T antigen is bound to a host protein in SV40-transformed cells. Nature *278*, 261-263.

Lee, C.W., Arai, M., Martinez-Yamout, M.A., Dyson, H.J., and Wright, P.E. (2009). Mapping the interactions of the p53 transactivation domain with the KIX domain of CBP. Biochemistry *48*, 2115-2124.

Lee, C.W., Ferreon, J.C., Ferreon, A.C., Arai, M., and Wright, P.E. (2010a). Graded enhancement of p53 binding to CREB-binding protein (CBP) by multisite phosphorylation. Proc Natl Acad Sci U S A *107*, 19290-19295.

Lee, C.W., Sørensen, T.S., Shikama, N., and La Thangue, N.B. (1998). Functional interplay between p53 and E2F through co-activator p300. Oncogene *16*, 2695-2710.

Lee, H.H., Kim, H.S., Kang, J.Y., Lee, B.I., Ha, J.Y., Yoon, H.J., Lim, S.O., Jung, G., and Suh, S.W. (2007). Crystal structure of human nucleophosmin-core reveals plasticity of the pentamer-pentamer interface. Proteins *69*, 672-678.

Lee, J.S., Smith, E., and Shilatifard, A. (2010b). The language of histone crosstalk. Cell *142*, 682-685.

Lee, Y.H., Bedford, M.T., and Stallcup, M.R. (2011). Regulated recruitment of tumor suppressor BRCA1 to the p21 gene by coactivator methylation. Genes Dev *25*, 176-188.

Lee, Y.H., Coonrod, S.A., Kraus, W.L., Jelinek, M.A., and Stallcup, M.R. (2005). Regulation of coactivator complex assembly and function by protein arginine methylation and demethylimination. Proc Natl Acad Sci U S A *102*, 3611-3616.

Levine, A.J., and Oren, M. (2009). The first 30 years of p53: growing ever more complex. Nat Rev Cancer *9*, 749-758.

Levy, L., Wei, Y., Labalette, C., Wu, Y., Renard, C.A., Buendia, M.A., and Neuveut, C. (2004). Acetylation of beta-catenin by p300 regulates beta-catenin-Tcf4 interaction. Molecular and cellular biology *24*, 3404-3414.

Li, A.G., Piluso, L.G., Cai, X., Gadd, B.J., Ladurner, A.G., and Liu, X. (2007). An acetylation switch in p53 mediates holo-TFIID recruitment. Molecular cell *28*, 408-421.

Li, F.P., and Fraumeni, J.F. (1969a). Rhabdomyosarcoma in children: epidemiologic study and identification of a familial cancer syndrome. J Natl Cancer Inst *43*, 1365-1373.

Li, F.P., and Fraumeni, J.F. (1969b). Soft-tissue sarcomas, breast cancer, and other neoplasms. A familial syndrome? Ann Intern Med *71*, 747-752.

Li, M., Luo, R.Z., Chen, J.W., Cao, Y., Lu, J.B., He, J.H., Wu, Q.L., and Cai, M.Y. (2011). High expression of transcriptional coactivator p300 correlates with aggressive features and poor prognosis of hepatocellular carcinoma. Journal of translational medicine *9*, 5.

Li, T., Kon, N., Jiang, L., Tan, M., Ludwig, T., Zhao, Y., Baer, R., and Gu, W. (2012). Tumor suppression in the absence of p53-mediated cell-cycle arrest, apoptosis, and senescence. Cell *149*, 1269-1283.

Li, Z., Boone, D., and Hann, S.R. (2008). Nucleophosmin interacts directly with c-Myc and controls c-Myc-induced hyperproliferation and transformation. Proc Natl Acad Sci U S A *105*, 18794-18799.

Liao, Z.W., Zhou, T.C., Tan, X.J., Song, X.L., Liu, Y., Shi, X.Y., Huang, W.J., Du, L.L., Tu, B.J., and Lin, X.D. (2012). High expression of p300 is linked to aggressive features and poor prognosis of nasopharyngeal carcinoma. J Transl Med *10*, 110.

Lill, N.L., Grossman, S.R., Ginsberg, D., DeCaprio, J., and Livingston, D.M. (1997). Binding and modulation of p53 by p300/CBP coactivators. Nature *387*, 823-827.

Lindström, M.S. (2011). NPM1/B23: A Multifunctional Chaperone in Ribosome Biogenesis and Chromatin Remodeling. Biochem Res Int *2011*, 195209.

Liu, L., Chen, B., Qin, S., Li, S., He, X., Qiu, S., Zhao, W., and Zhao, H. (2010). A novel histone deacetylase inhibitor Chidamide induces apoptosis of human colon cancer cells. Biochem Biophys Res Commun *392*, 190-195.

Liu, X., Liu, Z., Jang, S.W., Ma, Z., Shinmura, K., Kang, S., Dong, S., Chen, J., Fukasawa, K., and Ye, K. (2007). Sumoylation of nucleophosmin/B23 regulates its subcellular localization, mediating cell proliferation and survival. Proc Natl Acad Sci U S A *104*, 9679-9684.

Liu, X., Wang, L., Zhao, K., Thompson, P.R., Hwang, Y., Marmorstein, R., and Cole, P.A. (2008). The structural basis of protein acetylation by the p300/CBP transcriptional coactivator. Nature *451*, 846-850.

Lopez-Atalaya, J.P., Gervasini, C., Mottadelli, F., Spena, S., Piccione, M., Scarano, G., Selicorni, A., Barco, A., and Larizza, L. (2012). Histone acetylation deficits in lymphoblastoid cell lines from patients with Rubinstein-Taybi syndrome. J Med Genet *49*, 66-74.

Luger, K., Mader, A.W., Richmond, R.K., Sargent, D.F., and Richmond, T.J. (1997). Crystal structure of the nucleosome core particle at 2.8 A resolution. Nature *389*, 251-260.

Lundblad, J.R., Kwok, R.P., Laurance, M.E., Harter, M.L., and Goodman, R.H. (1995). Adenoviral E1A-associated protein p300 as a functional homologue of the transcriptional co-activator CBP. Nature *374*, 85-88.

Maggi, L.B., Kuchenruether, M., Dadey, D.Y., Schwope, R.M., Grisendi, S., Townsend, R.R., Pandolfi, P.P., and Weber, J.D. (2008). Nucleophosmin serves as a rate-limiting nuclear export chaperone for the Mammalian ribosome. Mol Cell Biol *28*, 7050-7065.

Malkin, D., Li, F.P., Strong, L.C., Fraumeni, J.F., Nelson, C.E., Kim, D.H., Kassel, J., Gryka, M.A., Bischoff, F.Z., and Tainsky, M.A. (1990). Germ line p53 mutations in a familial syndrome of breast cancer, sarcomas, and other neoplasms. Science *250*, 1233-1238.

Melero, R., Rajagopalan, S., Lázaro, M., Joerger, A.C., Brandt, T., Veprintsev, D.B., Lasso, G., Gil, D., Scheres, S.H., Carazo, J.M., *et al.* (2011). Electron microscopy studies on the quaternary structure of p53 reveal different binding modes for p53 tetramers in complex with DNA. Proc Natl Acad Sci U S A *108*, 557-562.

Mellert, H.S., and McMahon, S.B. (2009). Biochemical pathways that regulate acetyltransferase and deacetylase activity in mammalian cells. Trends Biochem Sci *34*, 571-578.

Miller, R.W., and Rubinstein, J.H. (1995). Tumors in Rubinstein-Taybi syndrome. Am J Med Genet *56*, 112-115.

Mitchell, J.A., and Fraser, P. (2008). Transcription factories are nuclear subcompartments that remain in the absence of transcription. Genes Dev *22*, 20-25.

Mujtaba, S., He, Y., Zeng, L., Yan, S., Plotnikova, O., Sachchidanand, Sanchez, R., Zeleznik-Le, N.J., Ronai, Z., and Zhou, M.M. (2004). Structural mechanism of the bromodomain of the coactivator CBP in p53 transcriptional activation. Molecular cell *13*, 251-263.

Munshi, N., Merika, M., Yie, J., Senger, K., Chen, G., and Thanos, D. (1998). Acetylation of HMG I(Y) by CBP turns off IFN beta expression by disrupting the enhanceosome. Mol Cell *2*, 457-467.

Murano, K., Okuwaki, M., Hisaoka, M., and Nagata, K. (2008). Transcription regulation of the rRNA gene by a multifunctional nucleolar protein, B23/nucleophosmin, through its histone chaperone activity. Mol Cell Biol *28*, 3114-3126.

Nakajima, H., Kim, Y.B., Terano, H., Yoshida, M., and Horinouchi, S. (1998). FR901228, a potent antitumor antibiotic, is a novel histone deacetylase inhibitor. Exp Cell Res *241*, 126-133.

Nguyen, D.X., Baglia, L.A., Huang, S.M., Baker, C.M., and McCance, D.J. (2004). Acetylation regulates the differentiation-specific functions of the retinoblastoma protein. EMBO J *23*, 1609-1618.

Nishimura, Y., Ohkubo, T., Furuichi, Y., and Umekawa, H. (2002). Tryptophans 286 and 288 in the C-terminal region of protein B23.1 are important for its nucleolar localization. Biosci Biotechnol Biochem *66*, 2239-2242.

Nora, E.P., Goloborodko, A., Valton, A.L., Gibcus, J.H., Uebersohn, A., Abdennur, N., Dekker, J., Mirny, L.A., and Bruneau, B.G. (2017). Targeted Degradation of CTCF Decouples Local Insulation of Chromosome Domains from Genomic Compartmentalization. Cell *169*, 930-944.e922.

Ogryzko, V.V., Schiltz, R.L., Russanova, V., Howard, B.H., and Nakatani, Y. (1996). The transcriptional coactivators p300 and CBP are histone acetyltransferases. Cell *87*, 953-959.

Oike, Y., Takakura, N., Hata, A., Kaname, T., Akizuki, M., Yamaguchi, Y., Yasue, H., Araki, K., Yamamura, K., and Suda, T. (1999). Mice homozygous for a truncated form of CREB-binding protein exhibit defects in hematopoiesis and vasculo-angiogenesis. Blood *93*, 2771-2779.

Okorokov, A.L., Sherman, M.B., Plisson, C., Grinkevich, V., Sigmundsson, K., Selivanova, G., Milner, J., and Orlova, E.V. (2006). The structure of p53 tumour suppressor protein reveals the basis for its functional plasticity. EMBO J *25*, 5191-5200.

Okuwaki, M. (2008). The structure and functions of NPM1/Nucleophsmin/B23, a multifunctional nucleolar acidic protein. J Biochem *143*, 441-448.

Okuwaki, M., Iwamatsu, A., Tsujimoto, M., and Nagata, K. (2001a). Identification of nucleophosmin/B23, an acidic nucleolar protein, as a stimulatory factor for in vitro replication of adenovirus DNA complexed with viral basic core proteins. J Mol Biol *311*, 41-55.

Okuwaki, M., Matsumoto, K., Tsujimoto, M., and Nagata, K. (2001b). Function of nucleophosmin/B23, a nucleolar acidic protein, as a histone chaperone. FEBS Lett *506*, 272-276.

Okuwaki, M., Sumi, A., Hisaoka, M., Saotome-Nakamura, A., Akashi, S., Nishimura, Y., and Nagata, K. (2012). Function of homo- and hetero-oligomers of human nucleoplasmin/nucleophosmin family proteins NPM1, NPM2 and NPM3 during sperm chromatin remodeling. Nucleic Acids Res *40*, 4861-4878.

Ozdağ, H., Batley, S.J., Försti, A., Iyer, N.G., Daigo, Y., Boutell, J., Arends, M.J., Ponder, B.A., Kouzarides, T., and Caldas, C. (2002). Mutation analysis of CBP and PCAF reveals rare inactivating mutations in cancer cell lines but not in primary tumours. Br J Cancer *87*, 1162-1165.

Parthun, M.R., Widom, J., and Gottschling, D.E. (1996). The major cytoplasmic histone acetyltransferase in yeast: links to chromatin replication and histone metabolism. Cell *87*, 85-94.

Pasheva, E., Sarov, M., Bidjekov, K., Ugrinova, I., Sarg, B., Lindner, H., and Pashev, I.G. (2004). In vitro acetylation of HMGB-1 and -2 proteins by CBP: the role of the acidic tail. Biochemistry *43*, 2935-2940.

Pattabiraman, D.R., McGirr, C., Shakhbazov, K., Barbier, V., Krishnan, K., Mukhopadhyay, P., Hawthorne, P., Trezise, A., Ding, J., Grimmond, S.M., *et al.* (2014). Interaction of c-Myb with p300 is required for the induction of acute myeloid leukemia (AML) by human AML oncogenes. Blood *123*, 2682-2690.

Perissi, V., Dasen, J.S., Kurokawa, R., Wang, Z., Korzus, E., Rose, D.W., Glass, C.K., and Rosenfeld, M.G. (1999). Factor-specific modulation of CREB-binding protein acetyltransferase activity. Proc Natl Acad Sci U S A *96*, 3652-3657.

Plumb, J.A., Finn, P.W., Williams, R.J., Bandara, M.J., Romero, M.R., Watkins, C.J., La Thangue, N.B., and Brown, R. (2003). Pharmacodynamic response and inhibition of growth of human tumor xenografts by the novel histone deacetylase inhibitor PXD101. Mol Cancer Ther *2*, 721-728.

Poizat, C., Puri, P.L., Bai, Y., and Kedes, L. (2005). Phosphorylation-dependent degradation of p300 by doxorubicin-activated p38 mitogen-activated protein kinase in cardiac cells. Mol Cell Biol *25*, 2673-2687.

Polley, S., Guha, S., Roy, N.S., Kar, S., Sakaguchi, K., Chuman, Y., Swaminathan, V., Kundu, T., and Roy, S. (2008). Differential recognition of phosphorylated transactivation domains of p53 by different p300 domains. J Mol Biol *376*, 8-12.

Prinos, P., Lacoste, M.C., Wong, J., Bonneau, A.M., and Georges, E. (2011). Mutation of cysteine 21 inhibits nucleophosmin/B23 oligomerization and chaperone activity. Int J Biochem Mol Biol *2*, 24-30.

Qi, W., Shakalya, K., Stejskal, A., Goldman, A., Beeck, S., Cooke, L., and Mahadevan, D. (2008). NSC348884, a nucleophosmin inhibitor disrupts oligomer formation and induces apoptosis in human cancer cells. Oncogene *27*, 4210-4220.

Qin, Y., Chen, W., Xiao, Y., Yu, W., Cai, X., Dai, M., Xu, T., Huang, W., Guo, W., Deng, W., *et al.* (2015). RFPL3 and CBP synergistically upregulate hTERT activity and promote lung cancer growth. Oncotarget *6*, 27130-27145.

Qiu, Y., Zhao, Y., Becker, M., John, S., Parekh, B.S., Huang, S., Hendarwanto, A., Martinez, E.D., Chen, Y., Lu, H., *et al.* (2006). HDAC1 acetylation is linked to progressive modulation of steroid receptor-induced gene transcription. Mol Cell *22*, 669-679.

Ramos, Y.F., Hestand, M.S., Verlaan, M., Krabbendam, E., Ariyurek, Y., van Galen, M., van Dam, H., van Ommen, G.J., den Dunnen, J.T., Zantema, A., *et al.* (2010). Genome-wide assessment of differential roles for p300 and CBP in transcription regulation. Nucleic Acids Res *38*, 5396-5408.

Ramsay, R.G., and Gonda, T.J. (2008). MYB function in normal and cancer cells. Nat Rev Cancer *8*, 523-534.

Ravi, R., Mookerjee, B., van Hensbergen, Y., Bedi, G.C., Giordano, A., El-Deiry, W.S., Fuchs, E.J., and Bedi, A. (1998). p53-mediated repression of nuclear factor-kappaB RelA via the transcriptional integrator p300. Cancer Res *58*, 4531-4536.

Rebel, V.I., Kung, A.L., Tanner, E.A., Yang, H., Bronson, R.T., and Livingston, D.M. (2002). Distinct roles for CREB-binding protein and p300 in hematopoietic stem cell self-renewal. Proc Natl Acad Sci U S A *99*, 14789-14794.

Reed, S.M., and Quelle, D.E. (2014). p53 Acetylation: Regulation and Consequences. Cancers (Basel) *7*, 30-69.

Richon, V.M., Emiliani, S., Verdin, E., Webb, Y., Breslow, R., Rifkind, R.A., and Marks, P.A. (1998). A class of hybrid polar inducers of transformed cell differentiation inhibits histone deacetylases. Proc Natl Acad Sci U S A *95*, 3003-3007.

Robinson, J.T., Thorvaldsdóttir, H., Winckler, W., Guttman, M., Lander, E.S., Getz, G., and Mesirov, J.P. (2011). Integrative genomics viewer. Nat Biotechnol *29*, 24-26.

Roelfsema, J.H., and Peters, D.J. (2007). Rubinstein-Taybi syndrome: clinical and molecular overview. Expert Rev Mol Med *9*, 1-16.

Roth, J.F., Shikama, N., Henzen, C., Desbaillets, I., Lutz, W., Marino, S., Wittwer, J., Schorle, H., Gassmann, M., and Eckner, R. (2003). Differential role of p300 and CBP acetyltransferase during myogenesis: p300 acts upstream of MyoD and Myf5. EMBO J *22*, 5186-5196.

Rotter, V. (1983). p53, a transformation-related cellular-encoded protein, can be used as a biochemical marker for the detection of primary mouse tumor cells. Proc Natl Acad Sci U S A *80*, 2613-2617.

Roussel, P., and Hernandez-Verdun, D. (1994). Identification of Ag-NOR proteins, markers of proliferation related to ribosomal gene activity. Exp Cell Res *214*, 465-472.

Rubinstein, J.H., and Taybi, H. (1963). Broad thumbs and toes and facial abnormalities. A possible mental retardation syndrome. Am J Dis Child *105*, 588-608.

Sabari, B.R., Tang, Z., Huang, H., Yong-Gonzalez, V., Molina, H., Kong, H.E., Dai, L., Shimada, M., Cross, J.R., Zhao, Y., *et al.* (2015). Intracellular crotonyl-CoA stimulates transcription through p300-catalyzed histone crotonylation. Mol Cell *58*, 203-215.

Sachse, C., Chen, J.Z., Coureux, P.D., Stroupe, M.E., Fändrich, M., and Grigorieff, N. (2007). High-resolution electron microscopy of helical specimens: a fresh look at tobacco mosaic virus. J Mol Biol *371*, 812-835.

Saint Just Ribeiro, M., Hansson, M.L., and Wallberg, A.E. (2007). A proline repeat domain in the Notch co-activator MAML1 is important for the p300-mediated acetylation of MAML1. Biochem J *404*, 289-298.

Sakaguchi, K., Herrera, J.E., Saito, S., Miki, T., Bustin, M., Vassilev, A., Anderson, C.W., and Appella, E. (1998). DNA damage activates p53 through a phosphorylation-acetylation cascade. Genes & development *12*, 2831-2841.

Sandberg, M.L., Sutton, S.E., Pletcher, M.T., Wiltshire, T., Tarantino, L.M., Hogenesch, J.B., and Cooke, M.P. (2005). c-Myb and p300 regulate hematopoietic stem cell proliferation and differentiation. Dev Cell *8*, 153-166.

Santos-Rosa, H., Valls, E., Kouzarides, T., and Martínez-Balbás, M. (2003). Mechanisms of P/CAF auto-acetylation. Nucleic Acids Res *31*, 4285-4292.

Schwartz, C., Beck, K., Mink, S., Schmolke, M., Budde, B., Wenning, D., and Klempnauer, K.H. (2003). Recruitment of p300 by C/EBPbeta triggers phosphorylation of p300 and modulates coactivator activity. EMBO J *22*, 882-892.

Seligson, D.B., Horvath, S., Shi, T., Yu, H., Tze, S., Grunstein, M., and Kurdistani, S.K. (2005). Global histone modification patterns predict risk of prostate cancer recurrence. Nature *435*, 1262-1266.

Selvi, B.R., Jagadeesan, D., Suma, B.S., Nagashankar, G., Arif, M., Balasubramanyam, K., Eswaramoorthy, M., and Kundu, T.K. (2008). Intrinsically fluorescent carbon nanospheres as a nuclear targeting vector: delivery of membrane-impermeable molecule to modulate gene expression in vivo. Nano Lett *8*, 3182-3188.

Sen, N., Hara, M.R., Kornberg, M.D., Cascio, M.B., Bae, B.I., Shahani, N., Thomas, B., Dawson, T.M., Dawson, V.L., Snyder, S.H., *et al.* (2008). Nitric oxide-induced nuclear GAPDH activates p300/CBP and mediates apoptosis. Nat Cell Biol *10*, 866-873.

Shaikh, T.R., Gao, H., Baxter, W.T., Asturias, F.J., Boisset, N., Leith, A., and Frank, J. (2008). SPIDER image processing for single-particle reconstruction of biological macromolecules from electron micrographs. Nat Protoc *3*, 1941-1974.

Shandilya, J., Senapati, P., Dhanasekaran, K., Bangalore, S.S., Kumar, M., Kishore, A.H., Bhat, A., Kodaganur, G.S., and Kundu, T.K. (2014). Phosphorylation of multifunctional nucleolar protein nucleophosmin (NPM1) by aurora kinase B is critical for mitotic progression. FEBS Lett *588*, 2198-2205.

Shandilya, J., Swaminathan, V., Gadad, S.S., Choudhari, R., Kodaganur, G.S., and Kundu, T.K. (2009). Acetylated NPM1 localizes in the nucleoplasm and regulates transcriptional activation of genes implicated in oral cancer manifestation. Mol Cell Biol *29*, 5115-5127.

Shi, D., Dai, C., Qin, J., and Gu, W. (2016). Negative regulation of the p300-p53 interplay by DDX24. Oncogene *35*, 528-536.

Shi, Y., and Mello, C. (1998). A CBP/p300 homolog specifies multiple differentiation pathways in Caenorhabditis elegans. Genes Dev *12*, 943-955.

Shikama, N., Lutz, W., Kretzschmar, R., Sauter, N., Roth, J.F., Marino, S., Wittwer, J., Scheidweiler, A., and Eckner, R. (2003). Essential function of p300 acetyltransferase activity in heart, lung and small intestine formation. EMBO J *22*, 5175-5185.

Shogren-Knaak, M., Ishii, H., Sun, J.M., Pazin, M.J., Davie, J.R., and Peterson, C.L. (2006). Histone H4-K16 acetylation controls chromatin structure and protein interactions. Science *311*, 844-847.

Simonsson, M., Heldin, C.H., Ericsson, J., and Grönroos, E. (2005). The balance between acetylation and deacetylation controls Smad7 stability. J Biol Chem *280*, 21797-21803.

Sobulo, O.M., Borrow, J., Tomek, R., Reshmi, S., Harden, A., Schlegelberger, B., Housman, D., Doggett, N.A., Rowley, J.D., and Zeleznik-Le, N.J. (1997). MLL is fused to CBP, a histone acetyltransferase, in therapy-related acute myeloid leukemia with a t(11;16)(q23;p13.3). Proc Natl Acad Sci U S A *94*, 8732-8737.

Spector, D.L., Ochs, R.L., and Busch, H. (1984). Silver staining, immunofluorescence, and immunoelectron microscopic localization of nucleolar phosphoproteins B23 and C23. Chromosoma *90*, 139-148.

Srivastava, S., Zou, Z.Q., Pirollo, K., Blattner, W., and Chang, E.H. (1990). Germ-line transmission of a mutated p53 gene in a cancer-prone family with Li-Fraumeni syndrome. Nature *348*, 747-749.

Sterner, R., Vidali, G., and Allfrey, V.G. (1979). Studies of acetylation and deacetylation in high mobility group proteins. Identification of the sites of acetylation in HMG-1. J Biol Chem *254*, 11577-11583.

Sun, B., Guo, S., Tang, Q., Li, C., Zeng, R., Xiong, Z., Zhong, C., and Ding, J. (2011). Regulation of the histone acetyltransferase activity of hMOF via autoacetylation of Lys274. Cell Res *21*, 1262-1266.

Sun, T., Li, X., Zhang, P., Chen, W.D., Zhang, H.L., Li, D.D., Deng, R., Qian, X.J., Jiao, L., Ji, J., *et al.* (2015). Acetylation of Beclin 1 inhibits autophagosome maturation and promotes tumour growth. Nat Commun *6*, 7215.

Suzuki, A., Makinoshima, H., Wakaguri, H., Esumi, H., Sugano, S., Kohno, T., Tsuchihara, K., and Suzuki, Y. (2014). Aberrant transcriptional regulations in cancers: genome, transcriptome and epigenome analysis of lung adenocarcinoma cell lines. Nucleic Acids Res *42*, 13557-13572.

Swaminathan, V., Kishore, A.H., Febitha, K.K., and Kundu, T.K. (2005). Human histone chaperone nucleophosmin enhances acetylation-dependent chromatin transcription. Mol Cell Biol *25*, 7534-7545.

Szebeni, A., and Olson, M.O. (1999). Nucleolar protein B23 has molecular chaperone activities. Protein Sci *8*, 905-912.

Szklarczyk, D., Franceschini, A., Wyder, S., Forslund, K., Heller, D., Huerta-Cepas, J., Simonovic, M., Roth, A., Santos, A., Tsafou, K.P., *et al.* (2015). STRING v10: protein-protein interaction networks, integrated over the tree of life. Nucleic Acids Res *43*, D447-452.

Takeuchi, A., Shiota, M., Tatsugami, K., Yokomizo, A., Tanaka, S., Kuroiwa, K., Eto, M., and Naito, S. (2012). p300 mediates cellular resistance to doxorubicin in bladder cancer. Mol Med Rep *5*, 173-176.

Tang, G., Peng, L., Baldwin, P.R., Mann, D.S., Jiang, W., Rees, I., and Ludtke, S.J. (2007). EMAN2: an extensible image processing suite for electron microscopy. J Struct Biol *157*, 38-46.

Tang, Y., Holbert, M.A., Wurtele, H., Meeth, K., Rocha, W., Gharib, M., Jiang, E., Thibault, P., Verreault, A., Verrault, A., *et al.* (2008). Fungal Rtt109 histone acetyltransferase is an unexpected structural homolog of metazoan p300/CBP. Nat Struct Mol Biol *15*, 738-745.

Teufel, D.P., Freund, S.M., Bycroft, M., and Fersht, A.R. (2007). Four domains of p300 each bind tightly to a sequence spanning both transactivation subdomains of p53. Proc Natl Acad Sci U S A *104*, 7009-7014.

Thompson, P.R., Kurooka, H., Nakatani, Y., and Cole, P.A. (2001). Transcriptional coactivator protein p300. Kinetic characterization of its histone acetyltransferase activity. J Biol Chem *276*, 33721-33729.

Thompson, P.R., Wang, D., Wang, L., Fulco, M., Pediconi, N., Zhang, D., An, W., Ge, Q., Roeder, R.G., Wong, J., *et al.* (2004). Regulation of the p300 HAT domain via a novel activation loop. Nat Struct Mol Biol *11*, 308-315.

Tidow, H., Melero, R., Mylonas, E., Freund, S.M., Grossmann, J.G., Carazo, J.M., Svergun, D.I., Valle, M., and Fersht, A.R. (2007). Quaternary structures of tumor suppressor p53 and a specific p53 DNA complex. Proc Natl Acad Sci U S A *104*, 12324-12329.

Tillinghast, G.W., Partee, J., Albert, P., Kelley, J.M., Burtow, K.H., and Kelly, K. (2003). Analysis of genetic stability at the EP300 and CREBBP loci in a panel of cancer cell lines. Genes Chromosomes Cancer *37*, 121-131.

Trievel, R.C., Rojas, J.R., Sterner, D.E., Venkataramani, R.N., Wang, L., Zhou, J., Allis, C.D., Berger, S.L., and Marmorstein, R. (1999). Crystal structure and mechanism of histone acetylation of the yeast GCN5 transcriptional coactivator. Proc Natl Acad Sci U S A *96*, 8931-8936.

Tu, A.W., and Luo, K. (2007). Acetylation of Smad2 by the co-activator p300 regulates activin and transforming growth factor beta response. J Biol Chem *282*, 21187-21196.

Turnell, A.S., Stewart, G.S., Grand, R.J., Rookes, S.M., Martin, A., Yamano, H., Elledge, S.J., and Gallimore, P.H. (2005). The APC/C and CBP/p300 cooperate to regulate transcription and cell-cycle progression. Nature *438*, 690-695.

Unnikrishnan, A., Gafken, P.R., and Tsukiyama, T. (2010). Dynamic changes in histone acetylation regulate origins of DNA replication. Nature structural & molecular biology *17*, 430-437.

Uttarkar, S., Dukare, S., Bopp, B., Goblirsch, M., Jose, J., and Klempnauer, K.H. (2015). Naphthol AS-E Phosphate Inhibits the Activity of the Transcription Factor Myb by Blocking the Interaction with the KIX Domain of the Coactivator p300. Mol Cancer Ther *14*, 1276-1285.

Vassilev, L.T., Vu, B.T., Graves, B., Carvajal, D., Podlaski, F., Filipovic, Z., Kong, N., Kammlott, U., Lukacs, C., Klein, C., *et al.* (2004). In vivo activation of the p53 pathway by small-molecule antagonists of MDM2. Science *303*, 844-848.

Vervoorts, J., Luscher-Firzlaff, J.M., Rottmann, S., Lilischkis, R., Walsemann, G., Dohmann, K., Austen, M., and Luscher, B. (2003). Stimulation of c-MYC transcriptional activity and acetylation by recruitment of the cofactor CBP. EMBO Rep *4*, 484-490.

Vo, N., and Goodman, R.H. (2001). CREB-binding protein and p300 in transcriptional regulation. The Journal of biological chemistry *276*, 13505-13508.

Vousden, K.H., and Prives, C. (2009). Blinded by the Light: The Growing Complexity of p53. Cell *137*, 413-431.

Waddington, C.H. (1942). The Epigenotype. Endeavour *1*, 18–20.

Wang, C., Fu, M., Angeletti, R.H., Siconolfi-Baez, L., Reutens, A.T., Albanese, C., Lisanti, M.P., Katzenellenbogen, B.S., Kato, S., Hopp, T., *et al.* (2001). Direct acetylation of the estrogen receptor alpha hinge region by p300 regulates transactivation and hormone sensitivity. The Journal of biological chemistry *276*, 18375-18383.

Wang, D., Umekawa, H., and Olson, M.O. (1993). Expression and subcellular locations of two forms of nucleolar protein B23 in rat tissues and cells. Cell Mol Biol Res *39*, 33-42.

Wang, J., and Chen, J. (2010). SIRT1 regulates autoacetylation and histone acetyltransferase activity of TIP60. J Biol Chem *285*, 11458-11464.

Wang, L., Huang, G., Zhao, X., Hatlen, M.A., Vu, L., Liu, F., and Nimer, S.D. (2009). Post-translational modifications of Runx1 regulate its activity in the cell. Blood Cells Mol Dis *43*, 30-34.

Wang, L., Tang, Y., Cole, P.A., and Marmorstein, R. (2008). Structure and chemistry of the p300/CBP and Rtt109 histone acetyltransferases: implications for histone acetyltransferase evolution and function. Curr Opin Struct Biol *18*, 741-747.

Wang, Q.E., Han, C., Zhao, R., Wani, G., Zhu, Q., Gong, L., Battu, A., Racoma, I., Sharma, N., and Wani, A.A. (2013). p38 MAPK- and Akt-mediated p300 phosphorylation regulates its degradation to facilitate nucleotide excision repair. Nucleic Acids Res *41*, 1722-1733.

Wang, R., Cherukuri, P., and Luo, J. (2005a). Activation of Stat3 sequence-specific DNA binding and transcription by p300/CREB-binding protein-mediated acetylation. J Biol Chem *280*, 11528-11534.

Wang, S.A., Hung, C.Y., Chuang, J.Y., Chang, W.C., Hsu, T.I., and Hung, J.J. (2014). Phosphorylation of p300 increases its protein degradation to enhance the lung cancer progression. Biochim Biophys Acta *1843*, 1135-1149.

Wang, W., Budhu, A., Forgues, M., and Wang, X.W. (2005b). Temporal and spatial control of nucleophosmin by the Ran-Crm1 complex in centrosome duplication. Nat Cell Biol *7*, 823-830.

Wang, X., and Li, S. (2016). [Corrigendum] Chromatin immunoprecipitation-sequencing predicts p300 binding sites in the MCF7 human breast cancer cell line. Int J Mol Med *38*, 675.

Wasylishen, A.R., Kalkat, M., Kim, S.S., Pandyra, A., Chan, P.K., Oliveri, S., Sedivy, E., Konforte, D., Bros, C., Raught, B., *et al.* (2014). MYC activity is negatively regulated by a C-terminal lysine cluster. Oncogene *33*, 1066-1072.

Weinberg, R.A. (1991). Tumor suppressor genes. Science *254*, 1138-1146.

Whyte, P., Williamson, N.M., and Harlow, E. (1989). Cellular targets for transformation by the adenovirus E1A proteins. Cell *56*, 67-75.

Wolf, D., and Rotter, V. (1984). Inactivation of p53 gene expression by an insertion of Moloney murine leukemia virus-like DNA sequences. Mol Cell Biol *4*, 1402-1410.

Xiao, X.S., Cai, M.Y., Chen, J.W., Guan, X.Y., Kung, H.F., Zeng, Y.X., and Xie, D. (2011). High Expression of p300 in Human Breast Cancer Correlates with Tumor Recurrence and Predicts Adverse Prognosis. Chin J Cancer Res *23*, 201-207.

Xiao, Y., Wang, J., Qin, Y., Xuan, Y., Jia, Y., Hu, W., Yu, W., Dai, M., Li, Z., Yi, C., *et al.* (2015). Ku80 cooperates with CBP to promote COX-2 expression and tumor growth. Oncotarget *6*, 8046-8061.

Xu, W., Chen, H., Du, K., Asahara, H., Tini, M., Emerson, B.M., Montminy, M., and Evans, R.M. (2001). A transcriptional switch mediated by cofactor methylation. Science *294*, 2507-2511.

Yan, G., Eller, M.S., Elm, C., Larocca, C.A., Ryu, B., Panova, I.P., Dancy, B.M., Bowers, E.M., Meyers, D., Lareau, L., *et al.* (2013). Selective inhibition of p300 HAT blocks cell cycle progression, induces cellular senescence, and inhibits the DNA damage response in melanoma cells. J Invest Dermatol *133*, 2444-2452.

Yan, Y., Harper, S., Speicher, D.W., and Marmorstein, R. (2002). The catalytic mechanism of the ESA1 histone acetyltransferase involves a self-acetylated intermediate. Nat Struct Biol *9*, 862-869.

Yang, C., Wu, J., Sinha, S.H., Neveu, J.M., and Zheng, Y.G. (2012). Autoacetylation of the MYST lysine acetyltransferase MOF protein. J Biol Chem *287*, 34917-34926.

Yang, H., Yan, B., Liao, D., Huang, S., and Qiu, Y. (2015a). Acetylation of HDAC1 and degradation of SIRT1 form a positive feedback loop to regulate p53 acetylation during heat-shock stress. Cell Death Dis *6*, e1747.

Yang, H.B., Xu, Y.Y., Zhao, X.N., Zou, S.W., Zhang, Y., Zhang, M., Li, J.T., Ren, F., Wang, L.Y., and Lei, Q.Y. (2015b). Acetylation of MAT IIα represses tumour cell growth and is decreased in human hepatocellular cancer. Nat Commun *6*, 6973.

Yang, X., Yu, W., Shi, L., Sun, L., Liang, J., Yi, X., Li, Q., Zhang, Y., Yang, F., Han, X., *et al.* (2011). HAT4, a Golgi apparatus-anchored B-type histone acetyltransferase, acetylates free histone H4 and facilitates chromatin assembly. Mol Cell *44*, 39-50.

Yang, X.J., and Seto, E. (2008). Lysine acetylation: codified crosstalk with other posttranslational modifications. Molecular cell *31*, 449-461.

Yao, T.P., Oh, S.P., Fuchs, M., Zhou, N.D., Ch'ng, L.E., Newsome, D., Bronson, R.T., Li, E., Livingston, D.M., and Eckner, R. (1998). Gene dosage-dependent embryonic development and proliferation defects in mice lacking the transcriptional integrator p300. Cell *93*, 361-372.

Yao, Z., Duan, S., Hou, D., Wang, W., Wang, G., Liu, Y., Wen, L., and Wu, M. (2010). B23 acts as a nucleolar stress sensor and promotes cell survival through its dynamic interaction with hnRNPU and hnRNPA1. Oncogene *29*, 1821-1834.

Yee, S.P., and Branton, P.E. (1985). Detection of cellular proteins associated with human adenovirus type 5 early region 1A polypeptides. Virology *147*, 142-153.

Yi, P., Wang, Z., Feng, Q., Pintilie, G.D., Foulds, C.E., Lanz, R.B., Ludtke, S.J., Schmid, M.F., Chiu, W., and O'Malley, B.W. (2015). Structure of a biologically active estrogen receptor-coactivator complex on DNA. Mol Cell *57*, 1047-1058.

Yokomizo, C., Yamaguchi, K., Itoh, Y., Nishimura, T., Umemura, A., Minami, M., Yasui, K., Mitsuyoshi, H., Fujii, H., Tochiki, N., *et al.* (2011). High expression of p300 in HCC predicts shortened overall survival in association with enhanced epithelial mesenchymal transition of HCC cells. Cancer Lett *310*, 140-147.

Yu, Y., Maggi, L.B., Brady, S.N., Apicelli, A.J., Dai, M.S., Lu, H., and Weber, J.D. (2006). Nucleophosmin is essential for ribosomal protein L5 nuclear export. Mol Cell Biol *26*, 3798-3809.

Yuan, L.W., Soh, J.W., and Weinstein, I.B. (2002). Inhibition of histone acetyltransferase function of p300 by PKCdelta. Biochim Biophys Acta *1592*, 205-211.

Yung, B.Y. (2007). Oncogenic role of nucleophosmin/B23. Chang Gung Med J *30*, 285-293.

Zhang, K., Faiola, F., and Martinez, E. (2005). Six lysine residues on c-Myc are direct substrates for acetylation by p300. Biochemical and biophysical research communications *336*, 274-280.

Zhang, Y., Qiu, J., Wang, X., and Xia, M. (2011). AMP-activated protein kinase suppresses endothelial cell inflammation through phosphorylation of transcriptional coactivator p300. Arterioscler Thromb Vasc Biol *31*, 2897-2908.

Zhao, S., Xu, W., Jiang, W., Yu, W., Lin, Y., Zhang, T., Yao, J., Zhou, L., Zeng, Y., Li, H., *et al.* (2010). Regulation of cellular metabolism by protein lysine acetylation. Science *327*, 1000-1004.

Zhu, J., Sammons, M.A., Donahue, G., Dou, Z., Vedadi, M., Getlik, M., Barsyte-Lovejoy, D., Al-awar, R., Katona, B.W., Shilatifard, A., *et al.* (2015). Gain-of-function p53 mutants co-opt chromatin pathways to drive cancer growth. Nature *525*, 206-211.

Zhuang, S. (2013). Regulation of STAT signaling by acetylation. Cellular signalling *25*, 1924-1931.